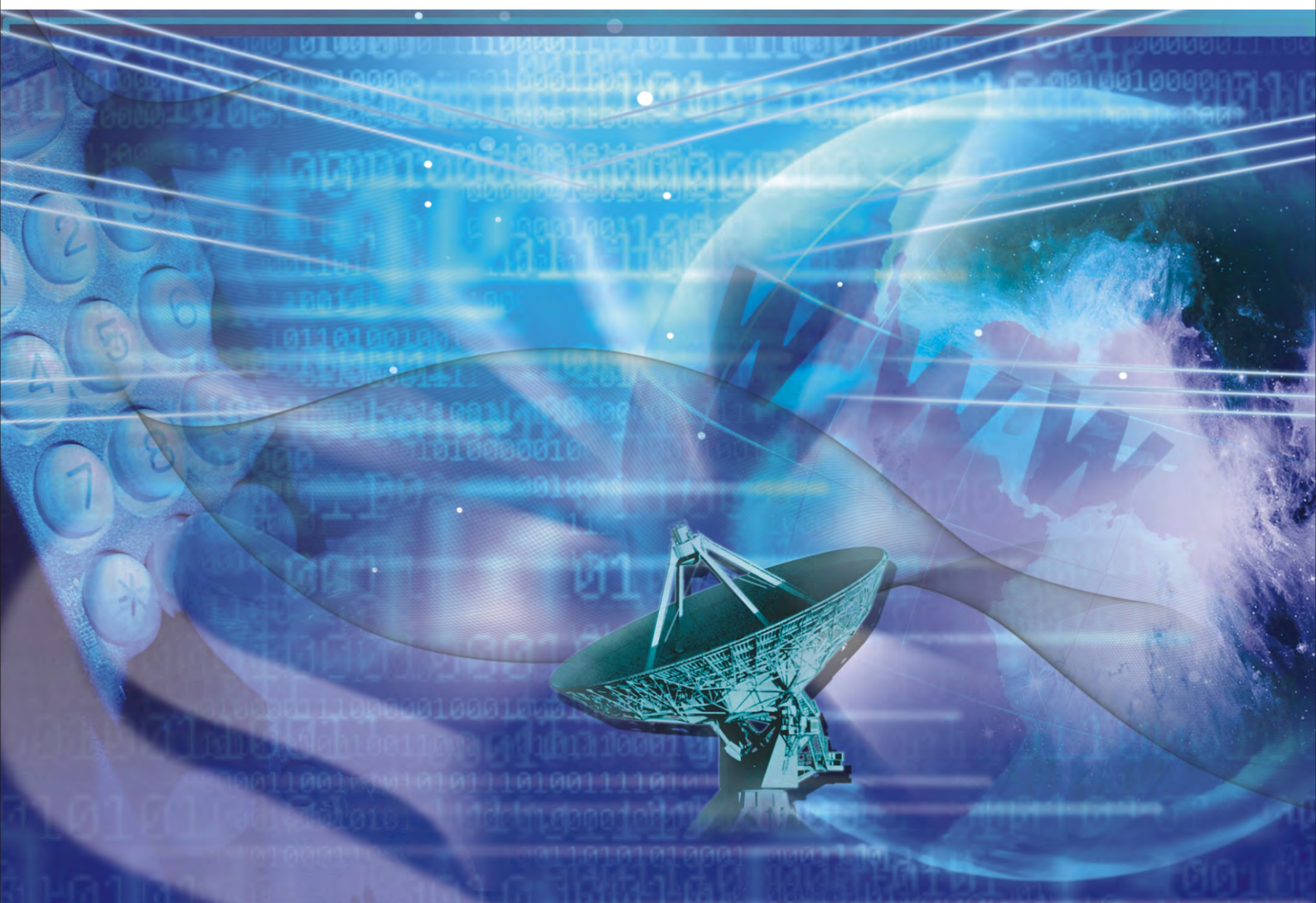


# International Journal of Communications, Network and System Sciences

ISSN: 1913-3715

Volume 3, Number 3, March 2010



# JOURNAL EDITORIAL BOARD

ISSN 1913-3715 (Print) ISSN 1913-3723 (Online)

<http://www.scirp.org/journal/ijcns/>

---

## Editors-in-Chief

**Prof. Huaibei Zhou**

Advanced Research Center for Sci. & Tech., Wuhan University, China

**Prof. Tom Hou**

Department of Electrical and Computer Engineering, Virginia Tech., USA

## Editorial Board

**Prof. Dharma P. Agrawal**

University of Cincinnati, USA

**Dr. Franca Delmastro**

National Research Council, Italy

**Prof. Klaus Doppler**

Nokia Research Center, Nokia Corporation, Finland

**Dr. Li Huang**

Stiching IMEC Nederland, Netherlands

**Prof. Chun Chi Lee**

Shu-Te University, Taiwan (China)

**Prof. Jaime Lloret Mauri**

Polytechnic University of Valencia, Spain

**Dr. Lim Nguyen**

University of Nebraska-Lincoln, USA

**Prof. Petar Popovski**

Aalborg University, Denmark

**Dr. Kosai Raoof**

University of Joseph Fourier, Grenoble, France

**Prof. Bimal Roy**

Indian Statistical Institute, India

**Prof. Heung-Gyoon Ryu**

Chungbuk National University, Korea (South)

**Prof. Shaharuddin Salleh**

University Technology Malaysia, Malaysia

**Prof. Rainer Schoenen**

RWTH Aachen University, Germany

**Dr. Lingyang Song**

Philips Research, Cambridge, UK

**Prof. Boris S. Verkhovskiy**

New Jersey Institute of Technology, USA

**Dr. Hassan Yaghoobi**

Mobile Wireless Group, Intel Corporation, USA

## Editorial Assistants

**Xiaoqian QI Li ZHU**

Scientific Research Publishing, USA

---

## Guest Reviewers

Resul Das

Jing Chen

Rashid A. Saeed

Der-Rong Din

Xi Chen

Marco Castellani

Zahir Hussain

Yen-Lin Chen

Mingxin Tan

Anjan Biswas

Burcin Ozmen

Sophia G. Petridou

Xiao-Hui Lin

Wei-Hung Lin

Abed Ellatif Samhat

Yudong Zhang

Yansong Wang

Zahir M. Hussain

X. Perramon

K. Thilagavathi

Krishanthmohan Ratnam

Hui-Kai Su

Haitao Zhao

Abed Ellatif Samhat

Zafer Iscan

Nicolas Burrus

Luiz Henrique Alves Monteiro

## TABLE OF CONTENTS

Volume 3    Number 3

March 2010

<b>Advances in MIMO Techniques for Mobile Communications—A Survey</b>	
F. Khalid, J. Speidel.....	213
<b>Complex Domain Wavelet-Based Denoising of Measured UHF Wireless Channel Power Delay Profiles</b>	
M. H. C. Dias, G. L. Siqueira.....	253
<b>On Cross-Layer Design of AMC Based on Rate Compatible Punctured Turbo Codes</b>	
F. Foukalas, E. Zervas.....	256
<b>Performance of Block Diagonalization Broadcasting Scheme for Multiuser MIMO System Operating in Presence of Spatial Correlation and Mutual Coupling</b>	
F. Wang, M. E. Bialkowski, X. Liu.....	266
<b>Short-Term Load Forecasting Using Soft Computing Techniques</b>	
D. K. Chaturvedi, S. A. Premdayal, A. Chandiok.....	273
<b>Spectrum Efficiency Improvement Based on the Cognitive Radio Management</b>	
J. Raiyn.....	280
<b>A Mobile Ad-Hoc Routing Algorithm with Comparative Study of Earlier Proposed Algorithms</b>	
P. K. Verma, T. Gupta, N. Rakesh, N. Nitin.....	289
<b>A New Global Asymptotic Stability Result of Delayed Neural Networks via Nonsmooth Analysis</b>	
Y. N. Gu, D. Y. Liu, W. J. Wu, J. W. Zhang.....	294
<b>Self-Organized Detection of Relationships in a Network</b>	
Q. A. Memon.....	303
<b>Scheduling Mobile Data Services in a Bluetooth Based Platform</b>	
X. Y. Liu, K. C. Yow.....	311
<b>Time Domain Signal Analysis Using Wavelet Packet Decomposition Approach</b>	
M. Y. Gokhale, D. K. Khanduja.....	321
<b>Indoor Radio Propagation Model Based on Dominant Path</b>	
Y. X. Zhao, M. F. Li, F. Shi.....	330

# **International Journal of Communications, Network and System Sciences (IJCNS)**

## **Journal Information**

### **SUBSCRIPTIONS**

The *International Journal of Communications, Network and System Sciences* (Online at Scientific Research Publishing, [www.SciRP.org](http://www.SciRP.org)) is published monthly by Scientific Research Publishing, Inc., USA.

#### **Subscription rates:**

Print: \$50 per issue.

To subscribe, please contact Journals Subscriptions Department, E-mail: [sub@scirp.org](mailto:sub@scirp.org)

### **SERVICES**

#### **Advertisements**

Advertisement Sales Department, E-mail: [service@scirp.org](mailto:service@scirp.org)

#### **Reprints (minimum quantity 100 copies)**

Reprints Co-ordinator, Scientific Research Publishing, Inc., USA.

E-mail: [sub@scirp.org](mailto:sub@scirp.org)

### **COPYRIGHT**

Copyright©2010 Scientific Research Publishing, Inc.

All Rights Reserved. No part of this publication may be reproduced, stored in a retrieval system, or transmitted, in any form or by any means, electronic, mechanical, photocopying, recording, scanning or otherwise, except as described below, without the permission in writing of the Publisher.

Copying of articles is not permitted except for personal and internal use, to the extent permitted by national copyright law, or under the terms of a license issued by the national Reproduction Rights Organization.

Requests for permission for other kinds of copying, such as copying for general distribution, for advertising or promotional purposes, for creating new collective works or for resale, and other enquiries should be addressed to the Publisher.

Statements and opinions expressed in the articles and communications are those of the individual contributors and not the statements and opinion of Scientific Research Publishing, Inc. We assume no responsibility or liability for any damage or injury to persons or property arising out of the use of any materials, instructions, methods or ideas contained herein. We expressly disclaim any implied warranties of merchantability or fitness for a particular purpose. If expert assistance is required, the services of a competent professional person should be sought.

### **PRODUCTION INFORMATION**

For manuscripts that have been accepted for publication, please contact:

E-mail: [ijcns@scirp.org](mailto:ijcns@scirp.org)

# Advances in MIMO Techniques for Mobile Communications—A Survey

Farhan Khalid, Joachim Speidel

*Institute of Telecommunications, University of Stuttgart, Stuttgart, Germany*

*Email: {khalid, speidel}@inue.uni-stuttgart.de*

*Received December 2, 2009; revised January 5, 2010; accepted February 6, 2010*

## Abstract

This paper provides a comprehensive overview of critical developments in the field of multiple-input multiple-output (MIMO) wireless communication systems. The state of the art in single-user MIMO (SU-MIMO) and multiuser MIMO (MU-MIMO) communications is presented, highlighting the key aspects of these technologies. Both open-loop and closed-loop SU-MIMO systems are discussed in this paper with particular emphasis on the data rate maximization aspect of MIMO. A detailed review of various MU-MIMO uplink and downlink techniques then follows, clarifying the underlying concepts and emphasizing the importance of MU-MIMO in cellular communication systems. This paper also touches upon the topic of MU-MIMO capacity as well as the promising convex optimization approaches to MIMO system design.

**Keywords:** Multiple-Input Multiple-Output (MIMO), Multiuser MIMO, Wireless Communications, Beamforming, Diversity, Precoding, Capacity

## 1. Introduction

Multiple-input multiple-output (MIMO) wireless systems employ multiple transmit and receive antennas to increase the transmission data rate through spatial multiplexing or to improve system reliability in terms of bit error rate (BER) performance using space-time codes (STCs) for diversity maximization [1]. MIMO systems exploit multipath propagation to achieve these benefits, without the expense of additional bandwidth. More recent MIMO techniques like the geometric mean decomposition (GMD) technique proposed in [2] aim at combining the diversity and data rate maximization aspects of MIMO in an optimal manner. These advantages make MIMO a very attractive and promising option for future mobile communication systems especially when combined with the benefits of orthogonal frequency-division multiplexing (OFDM) [3,4].

The capacity of an  $M \times N$  single-user MIMO (SU-MIMO) system with  $M$  transmit and  $N$  receive antennas, in terms of the spectral efficiency i.e. bits per second per Hz, is given by [1]

$$C = \log_2 \left[ \det \left( \mathbf{I}_N + \frac{\rho}{M} \mathbf{H} \mathbf{H}^H \right) \right] \quad (1)$$

where  $\mathbf{H}$  is the  $N \times M$  MIMO channel matrix and  $\rho$  is the

signal to noise ratio (SNR) at any receive antenna. Equation (1) assumes that the  $M$  information sources are uncorrelated and have equal power. Expressed in terms of the eigenvalues, Equation (1) can be written as [1]

$$C = \sum_{i=1}^m \log_2 \left( 1 + \frac{\rho}{M} \lambda_i \right) \quad (2)$$

where  $\lambda_i$  represent the nonzero eigenvalues of  $\mathbf{H} \mathbf{H}^H$  or  $\mathbf{H}^H \mathbf{H}$  for  $N \leq M$  and  $M < N$  respectively and  $m = \min(M, N)$ . Therefore, MIMO systems are capable of achieving several-fold increase in system capacity as compared to single-input single-output (SISO) systems by transmitting on the spatial eigenmodes of the MIMO channel.

Equation (2) also shows that the performance of MIMO systems is dependent on the channel eigenvalues. Very low eigenvalues indicate weak transmission channels which may make it difficult to recover the information from the received signals. Optimal power allocation based on the water-filling algorithm can be used to maximize the system capacity subject to a total transmit power constraint. Water-filling provides substantial capacity gain when the eigenvalue spread, i.e., the condition number  $\lambda_{max}/\lambda_{min}$  is sufficiently large.

The MIMO concept becomes even more attractive in multiuser scenarios where the network capacity can be increased by simultaneously accommodating several users

without the expense of valuable frequency resources.

This paper is arranged as follows: Section 2 provides an overview of the current wireless standards which support MIMO technologies. Sections 3 and 4 include detailed discussion and performance analysis of various important SU-MIMO and multiuser MIMO (MU-MIMO) techniques respectively that are proposed for the next generation wireless communication systems. In-depth description of several MU-MIMO uplink and downlink schemes is given in Section 4 followed by a brief discussion of the MU-MIMO capacity. Section 5 provides an overview of convex optimization which has become an important tool for designing optimal MIMO beamforming systems. Section 6 concludes this work and identifies the areas for future research.

## 2. Current Implementation Status

There has been a lot of research on MIMO systems and techniques. MIMO-OFDM WLAN products based on the IEEE 802.11n standard are already available. The IEEE 802.16 wireless MAN standard known as WiMAX also includes MIMO features. Fixed WiMAX services are being offered by operators worldwide. Mobile WiMAX networks based on 802.16e are also being deployed while 802.16m is under development. IEEE 802.20 mobile broadband wireless access (MBWA) standard is also being formulated which will have complete support for mobility including high-speed mobile users e.g., on train networks. For other applications like cellular mobile communications which supports both voice and data traffic, MIMO systems are yet to be deployed. However, the 3GPP's long term evolution (LTE) is under development and adopts MIMO-OFDM, orthogonal frequency-division multiple access (OFDMA) and single-carrier frequency-division multiple access (SC-FDMA) transmission schemes. The following text presents a more detailed discussion of the various technical aspects of these standards and technologies.

### 2.1. IEEE 802.11n Wi-Fi

The IEEE 802.11n WLAN standard incorporates MIMO-OFDM as a compulsory feature to enhance data rate. Initial target was to achieve data rates in excess of 100 Mb/s [5]. However, current WLAN devices based on 802.11n Draft 2.0 are capable of achieving throughput up to 300 Mb/s utilizing two spatial streams in a 40 MHz channel in the 5 GHz band [6].

Initially, there were two main proposals one from the WWiSE consortium and the other from the TGnSync consortium competing for adoption by the IEEE 802.11 TGn. However, another proposal by the Enhanced Wireless Consortium (EWC) was finally accepted as the first draft for IEEE 802.11n [7].

The IEEE 802.11n standard proposes the use of the legacy 20 MHz channel and also an optional 40 MHz channel. The available modulation schemes include BPSK, QPSK, 16-QAM and 64-QAM [5,6]. Convolutional coding with different code rates is specified and use of low-density parity-check (LDPC) codes is also supported [5,8]. The MIMO techniques adopted include both spatial multiplexing and diversity techniques. Open-loop MIMO (OL-MIMO) techniques which do not require channel state information (CSI) at the transmitter seem to have been preferred [9]. Non-iterative linear minimum mean square error (LMMSE) detection has primarily been considered so as to minimize the complexity associated with MIMO detection while ensuring reasonably good performance [10].

Spatial spreading mentioned in [11] is an open-loop MIMO spatial multiplexing technique where multiple data streams are transmitted such that the diversity is maximized for each of the streams. The MIMO diversity techniques introduced in the standard include space-time block coding (STBC) and cyclic shift diversity (CSD) which extend the range and reception of 802.11n devices. In addition, conventional receiver spatial diversity techniques like maximum ratio combining (MRC) are also specified. Transmit beamforming is also specified as an optional feature [6]. The Cisco Aironet 1250 series access point based on 802.11n draft 2.0 supports open-loop transmit beamforming [12].

802.11n draft 2.0 specifies a maximum of 4 spatial streams per channel. Thus, a maximum throughput of 600 Mb/s can be achieved by using 4 spatial streams in a 40 MHz channel. In addition to spatial multiplexing and doubled channel bandwidth, more efficient OFDM with shorter guard interval (GI) and new medium access control (MAC) layer enhancements (e.g. closed-loop rate adaptation [13]) have also contributed to the increased throughput of 802.11n [6].

### 2.2. IEEE 802.16 WiMAX

The IEEE 802.16 worldwide interoperability for microwave access (WiMAX) is a recently developed wireless MAN standard that employs MIMO spatial multiplexing and diversity techniques. In addition to fixed WiMAX, the IEEE 802.16e Mobile WiMAX standard has also been developed and was approved in December 2005 [14]. Fixed WiMAX networks have already been deployed around the world and Mobile WiMAX deployments have also started.

802.16e-2005 is basically an amendment to the 802.16-2004 standard for fixed WiMAX with addition of new features to support mobility. 802.16e specifies the 2–6 GHz frequency band for mobile applications and the 2–11 GHz band for fixed applications (The single-carrier WirelessMAN-SC PHY specification for fixed wireless

access however specifies the 10–66 GHz frequency band [15]). It also specifies a license-exempt band between 5–6 GHz. A cellular network structure is specified with support for handoffs and mobile users moving at vehicular speeds are also supported, thus enabling mobile wireless internet access [14,16].

In addition to single carrier transmission, the standard specifies OFDM transmission scheme with 128, 256, 512, 1024 or 2048 subcarriers. Both TDD and FDD duplexing is specified while the multiplexing/multiple access schemes include OFDMA in addition to burst TDM/TDMA. However, scalable OFDMA is specified in all mobile WiMAX profiles as the physical layer multiple access technique. The various channel bandwidths specified in the standard include 1.25, 1.75, 3.5, 5, 7, 10, 8.75, 10, 14 and 15 MHz. WiMAX supports adaptive modulation and coding schemes. The supported modulation schemes include BPSK, QPSK, 16-QAM and 64-QAM [14,16]. Optional 256-QAM support is provided in the WirelessMAN-SCa PHY [15]. Convolutional codes at rate 1/2, 2/3, 3/4 or 5/6 are specified as mandatory for both uplink and downlink. In addition, convolutional turbo codes, repetition codes, LDPC and concatenated Reed-Solomon convolutional code (RS-CC) are specified as optional. The supported data rates range from 1 Mb/s to 75 Mb/s [14,16].

IEEE 802.16e supports both open-loop and closed-loop MIMO. Open-loop MIMO techniques include spatial multiplexing (SM) and space-time coding (STC) [14,17,18]. 802.16e includes support for up to four spatial streams and therefore a maximum of  $4 \times 4$  MIMO configuration [14,18]. STC is based on the Alamouti scheme (also STBC) and is also called space-time transmit diversity (STTD). It is an optional feature and may be used to provide higher order transmit diversity on the downlink [14].

In closed-loop MIMO, full or partial CSI is available at the transmitter through feedback. Eigenvector steering is employed to approach full capacity of the MIMO channel and water filling can be used to maximize throughput by allocating power in an optimal manner [9,19]. IEEE 802.16e supports closed-loop MIMO precoding for SM and also closed-loop STC [14,17]. However, closed-loop MIMO is not yet supported in the latest WiMAX Forum Wave 2 profiles [18]. Another MIMO mode called “collaborative spatial multiplexing” is also specified where two subscriber stations (SS), each having a single antenna, use the same subchannel for uplink transmission in order to increase the throughput [14,15,17,20].

The adaptive antenna systems (AAS) supported in 802.16e also include closed-loop adaptive beamforming, which uses feedback from the SS to the base station (BS) to optimize the downlink transmission [14,15,18].

IEEE 802.16 Task Group m (TGm) has also been set up to develop the IEEE 802.16m standard which will

enable interoperability between WiMAX and 3GPP’s Long Term Evolution (LTE) standard for next generation mobile communications [21,22]. 802.16m is expected to support high-speed mobile wireless access (up to 350 km/h) and peak data rates of over 300 Mb/s using  $4 \times 4$  MIMO [22].

### 2.3. IEEE 802.20 MBWA

The IEEE 802.20 working group was established to draft the IEEE 802.20 Mobile Broadband Wireless Access (MBWA) standard which is also nicknamed as MobileFi. IEEE 802.20 proposes a complete cellular structure and is designed and optimized for mobile data services at speeds up to 250 km/h. However, it can also support voice services due to very low transmission latency of 10–30 ms (better than the 25–40 ms for 802.16e). User data rates in excess of 1 Mb/s can be supported at 250 km/h [23–25].

MBWA is designed to operate in the licensed bands below 3.5 GHz [24,25]. 2.5 MHz to 20 MHz of uplink/downlink transmission bandwidth can be allocated per cell [25]. For a bandwidth of 5 MHz, peak aggregate data rate of around 16 Mb/s can be supported in the downlink [23,24] which obviously would be much greater for higher bandwidths.

The transmission scheme is based on OFDM, with OFDMA used for downlink transmission while both OFDMA and code-division multiple access (CDMA) are specified for the uplink. Rotational OFDM is specified as an optional scheme. The standard supports both FDD and TDD operation. The supported modulation schemes include QPSK, 8-PSK, 16-QAM and 64-QAM. Support of hierarchical (layered) modulation involving the superposition of two modulation schemes is also included for broadcast and multicast services. The specified FEC coding schemes include convolutional codes, turbo codes and LDPC codes [25].

Various MIMO schemes are also supported. STTD (based on STBC) and SM are specified for SU-MIMO transmission, utilizing up to 4 transmit antennas. STTD is particularly important for high speed mobile access. Two different stream multiplexing schemes namely single codeword (SCW) and multiple codeword (MCW) may be employed for MIMO transmission. These schemes also support closed-loop MIMO downlink transmission with rank adaptation. Both schemes utilize linear precoding at the BS for transmit beamforming based on the feedback of a suitable precoding matrix from the user equipment’s (UE’s) codebook to the BS. The standard also supports MU-MIMO or space-division multiple access (SDMA) transmission in the downlink which involves multiuser scheduling and precoding at the BS depending upon the feedback of the preferred precoding matrix index and differential channel quality indicator

(CQI) reports from the UEs [25].

The IEEE 802.20 standard was supposed to be available in 2006 but was delayed due to lack of support from some of the key vendors and the political turmoil within the standards forum [23]. However, it was finally approved in June 2008 and made available by the end of August 2008 [25].

## 2.4. 3GPP LTE

The 3<sup>rd</sup> generation partnership project's (3GPP) long term evolution (LTE) project is aimed at developing a new mobile communications standard for gradual migration from 3G to 4G. LTE physical layer is almost near completion. It specifies an OFDM based system with support for MIMO. Downlink transmission is based on OFDMA while SC-FDMA is used for the uplink due to its low PAPR characteristics. It supports both TDD and FDD operation. A packet switching architecture is specified for LTE [26,27].

LTE supports scalable bandwidths of 1.25, 2.5, 5, 10 and 20 MHz. Peak data rates of 100 Mb/s and 50 Mb/s are supported in the downlink and the uplink respectively, in 20 MHz channel. The standard specifies full performance within a cell up to 5 km radius and slight degradation from 5–30 km. Operation up to 100 km may be possible. It also supports high-speed mobility with high performance at speeds up to 120 km/h while the E-UTRAN (Evolved Universal Terrestrial Radio Access Network i.e., LTE's RAN) should be able to maintain the connection up to 350 km/h, or even up to 500 km/h. LTE also specifies very low latency operation with control plane (C-plane) latency of < 50-100ms and user plane (U-plane) latency of < 10 ms [27,28].

The single-user MIMO techniques supported include STBC and SM. Closed-loop multiple codeword (MCW) SM with codebook based precoding and with support for cyclic delay diversity (CDD) is specified. A maximum of two downlink spatial streams are specified. LTE also supports MU-MIMO in the downlink as well as in the uplink. Closed-loop transmit diversity using MIMO beamforming with rank adaptation is also supported. The supported antenna configurations for the downlink include  $4 \times 2$ ,  $2 \times 2$ ,  $1 \times 2$  and  $1 \times 1$  whereas  $1 \times 2$  and  $1 \times 1$  configurations are supported in the uplink [27,29,30]. However, multiple UE antennas in the uplink may be supported in future.

## 3. Single-User MIMO Techniques

Various open-loop and closed-loop SU-MIMO techniques are discussed in the following text along with performance analysis and comparison. Some of the techniques mentioned herein have already been adopted for the current standards while other advanced methods are

likely candidates for the next generation wireless systems.

## 3.1. V-BLAST

The vertical Bell Laboratories Layered Space-Time (V-BLAST) [31] is one of the very first open-loop spatial multiplexing MIMO systems which has been practically demonstrated to achieve much higher spectral efficiencies than SISO systems, in rich scattering environments. In V-BLAST, a single data stream is demultiplexed into multiple substreams which are mapped on to symbols and then transmitted through multiple antennas. Inter-substream coding is not employed in V-BLAST, however channel coding can be applied to the individual substreams for reduction of bit error rate (BER). CSI in a V-BLAST system is available at the receiver only by means of channel estimation. **Figure 1** shows the simple block diagram of a V-BLAST system.

V-BLAST detection can be accomplished by using linear detectors like zero-forcing (ZF) or minimum mean square error (MMSE) detector along with symbol cancellation (also called successive interference cancellation). Symbol cancellation is a nonlinear technique which enhances the detection performance by subtracting the detected components of the transmit vector from the received symbol vector [31]. This technique, however, is prone to error propagation.

The QR decomposition of the MIMO channel matrix  $\mathbf{H}$  can be used to represent the ZF nulling in V-BLAST [2]. Assuming a frequency-flat fading MIMO channel, the corresponding sampled baseband received signal for a V-BLAST system with  $M$  transmit and  $N$  receive antennas ( $M \leq N$ ) is therefore given by

$$\begin{aligned} \mathbf{y} &= \mathbf{H}\mathbf{x} + \mathbf{n} \\ &= \mathbf{Q}\mathbf{R}\mathbf{x} + \mathbf{n} \end{aligned} \quad (3)$$

where  $\mathbf{Q}$  is an  $N \times M$  unitary matrix with orthonormal columns,  $\mathbf{R}$  is a  $M \times M$  upper triangular matrix,  $\mathbf{x}$  is the transmitted signal and  $\mathbf{n}$  represents the noise vector. The

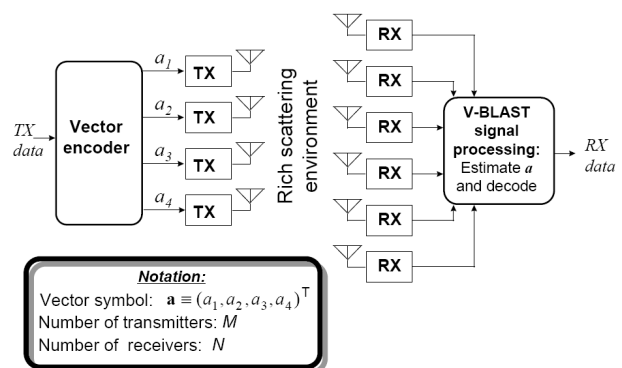


Figure 1. V-BLAST system block diagram [31].

discrete-time index is dropped to simplify notation. Multiplying both sides of Equation (3) by  $\mathbf{Q}^H$  gives

$$\tilde{\mathbf{y}} = \mathbf{R}\mathbf{x} + \tilde{\mathbf{n}} \quad (4)$$

The sequential signal detection in V-BLAST can be accomplished as follows [2]:

for  $i = M : -1 : 1$

$$\hat{x}_i = C\left[\left(\tilde{y}_i - \sum_{j=i+1}^M r_{ij}\hat{x}_j\right) / r_{ii}\right]$$

end

where  $C$  represents mapping to the nearest modulation symbol.

The results for an initial V-BLAST prototype mentioned in [31] yielded spectral efficiencies of 20–40 bps/Hz in indoor scenarios which is quite impressive. However, later has shown that V-BLAST also performs reasonably well in mobile scenarios and can be employed for MIMO-

OFDM systems as well and further improvements have been suggested in the literature. [32] proposes an extension of V-BLAST incorporating power and rate feedback which approaches closed-loop MIMO capacities. Equal power allocation with per-antenna rate control (PARC) produces the best results for the proposed system. PARC enables the transmitter to select the appropriate data rate and the associated modulation and coding scheme (MCS) for each transmit antenna based on the feedback of channel quality information from the receiver [33].

It presents a comparison between a modified V-BLAST system with limited feedback (including the modulation index and the number of streams to be used) and closed-loop MIMO (CL-MIMO) in [34]. CL-MIMO shows 15.1% throughput improvement for Rayleigh fading channel, 48.1% for spatially correlated channel and 104% for the case of a realistic channel model, at SNR of 25 dB. **Figure 2** shows these results.

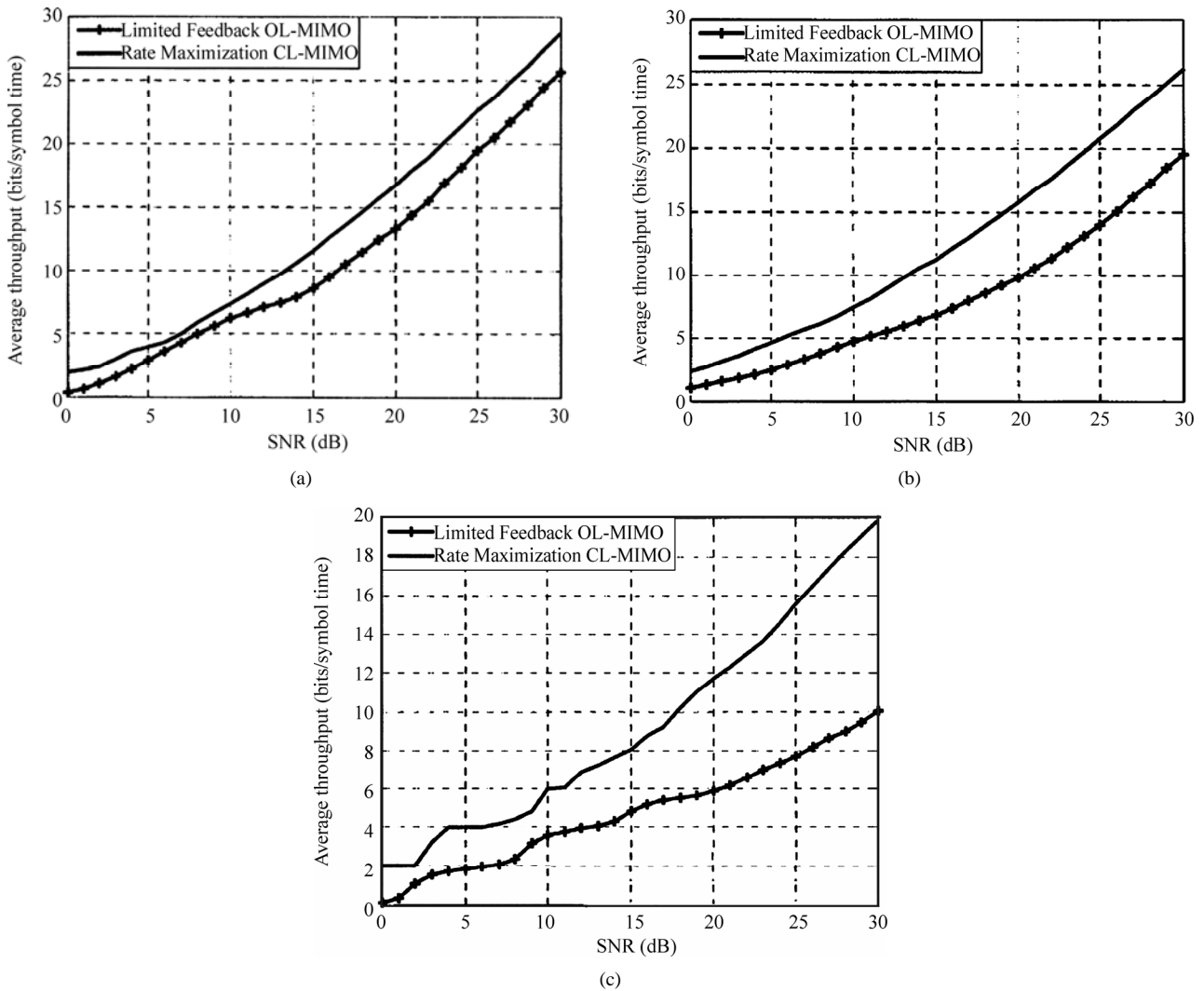


**Figure 2.** Throughput for (a) Rayleigh fading channel, (b) Spatial correlation channel and (c) Realistic channel model [34].

### 3.2. Spatial Multiplexing with Cyclic Delay Diversity

Spatial multiplexing (SM) can be combined with a simple diversity technique such as cyclic delay diversity (CDD) to obtain much better performance as compared to regular SM systems like V-BLAST. Such a system which combines SM and MIMO diversity is referred to as a joint diversity and multiplexing (JDM) system [35]. SM with CDD is also specified in the 3GPP LTE standard [30].

It proposes a cyclic delay assisted SM-OFDM (CDA-SM-OFDM) system which does not require any CSI at the transmitter, however complete CSI is required at the receiver [35]. **Figure 3** shows the transmitter and receiver block diagram.

The blocks denoted  $\Omega_1, \Omega_2, \dots, \Omega_\Delta$  perform the cyclic delay operation which involves cyclic shifting of the signal within each group of  $\Delta$  transmit antennas per SM branch. If there are  $P$  SM branches then the total number of transmit antennas is  $P\Delta$ . The receiver for CDA-SM-OFDM system is similar to V-BLAST.

CDD increases the channel frequency-selectivity since cyclic shifting of the OFDM signal and then adding those shifted signals linearly at the receiver inserts virtual echoes on the channel response. The resulting higher order frequency diversity can be exploited by any coded OFDM (COFDM) system [35].

**Figure 4** shows a comparison of the CDA-SM-OFDM system capacity with  $2 \times 2$  and  $4 \times 2$  SM-OFDM systems. Here it can be seen that the capacity of the CDA-SM-

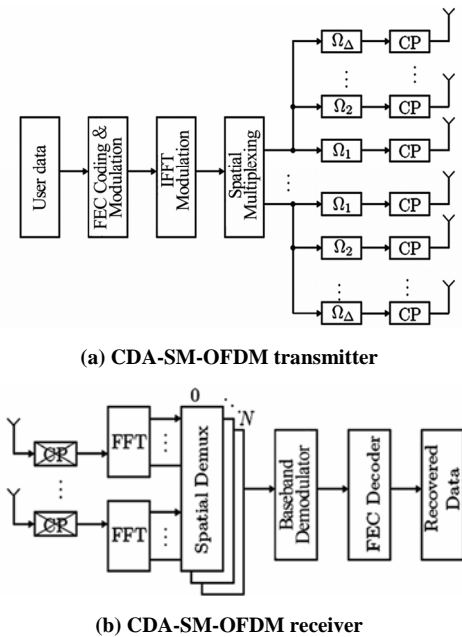


**Figure 3.** CDA-SM-OFDM system transmitter and receiver [35].

OFDM system lies between that for the two SM-OFDM systems. However, the capacities for the SM-OFDM systems are plotted for the ideal case i.e. with the best possible STC and channel coding schemes. It can also be seen that the outage capacity i.e. the capacity obtained below 10% of the times, for the CDA-SM-OFDM system is much higher than the  $2 \times 2$  SM-OFDM and closer to the  $4 \times 2$  SM-OFDM. Thus the system performance for the CDA-SM-OFDM system shows a significant increase just by employing a simple STC i.e. CDD.

It has also been shown in [35] that the eigenvalue spread for the CDA-SM-OFDM system is generally higher than both the SM-OFDM schemes and this means that eigen-beamforming can be employed for CDD based SM systems. In fact, the 3GPP LTE standard incorporates CDD based SM with precoding and specifies precoding matrices for small and large delay CDD [30].

**Figure 5** provides a comparison of the average spectral

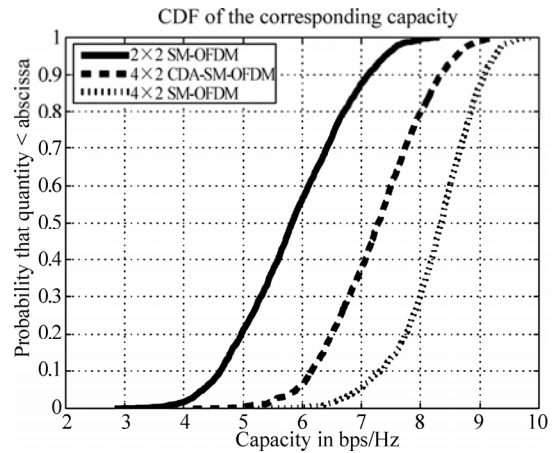


**Figure 4.** Comparison of system capacity for  $4 \times 2$  CDA-SM-OFDM system with  $2 \times 2$  and  $4 \times 2$  SM-OFDM system [35].

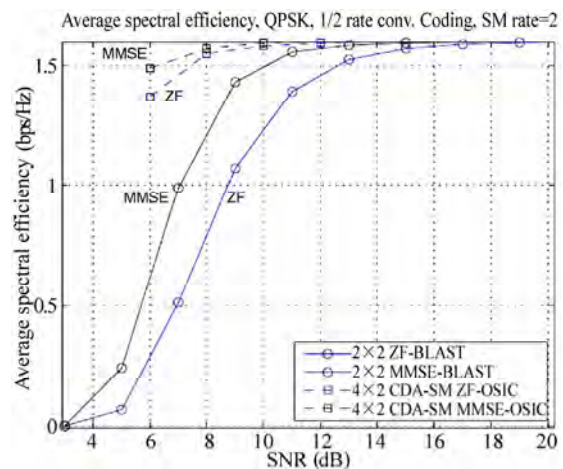


**Figure 5.** Average spectral efficiencies in bps/Hz [35].

efficiencies of  $2 \times 2$  SM-OFDM systems and  $4 \times 2$  CDA-SM-OFDM systems for a low user mobility indoor WLAN scenario. Here it can be seen that the  $4 \times 2$  CDA-SM-OFDM systems provide much higher spectral efficiencies at low SNR values.

### 3.3. Singular Value Decomposition Based MIMO Precoding

Singular value decomposition (SVD) based MIMO precoding is a closed-loop MIMO scheme where the precoding filter at the transmitter is designed by taking the SVD of the MIMO channel matrix  $\mathbf{H}$ .

[36] provides an analysis of the classical SVD based MIMO precoding scheme, SVD based precoding with ZF equalization, SVD based precoding with MMSE equalization and also an improved SVD based precoding technique. All of these schemes are analyzed with realistic channel knowledge at the transmitter. **Figure 6** shows the block diagram of the SVD based MIMO-OFDM transmitter and receiver.

#### 3.3.1. Classical SVD Precoding and Equalization

In SVD based techniques, the channel matrix  $\mathbf{H}$  of a MIMO system with  $N_t$  transmit antennas and  $N_r$  receive antennas, is decomposed as

$$\mathbf{H} = \mathbf{U}\mathbf{D}\mathbf{V}^H \tag{5}$$

where  $\mathbf{U} \in \mathbb{C}^{N_r \times N_r}$  and  $\mathbf{V} \in \mathbb{C}^{N_t \times N_t}$  are unitary matrices while  $\mathbf{D} \in \mathbb{R}^{N_t \times N_t}$  is a diagonal matrix consisting of the ordered singular values  $d_i$ .

The classical SVD approach utilizes matrix  $\mathbf{V}$  for precoding at the transmitter. The columns  $v_i$  of matrix  $\mathbf{V}$  are the eigenvectors of  $\mathbf{H}\mathbf{H}^H$ . The received signal is given by

$$\mathbf{r} = \mathbf{H}\mathbf{V}\mathbf{s} + \mathbf{n} \tag{6}$$

where  $\mathbf{s}$  is a vector of information symbols  $s_i$  and  $\mathbf{n}$  is the noise vector corresponding to an additive white Gaussian noise (AWGN) process with variance  $\sigma_n^2$  for each element. At the receiver, matrix  $\mathbf{U}^H$  is employed for equalization and the detected signal vector is given by

$$\begin{aligned} \mathbf{y} &= \mathbf{U}^H \mathbf{r} = \mathbf{U}^H \mathbf{H}\mathbf{V}\mathbf{s} + \mathbf{U}^H \mathbf{n} \\ &= \mathbf{U}^H \mathbf{U}\mathbf{D}\mathbf{V}^H \mathbf{V}\mathbf{s} + \mathbf{U}^H \mathbf{n} \\ \mathbf{y} &= \mathbf{D}\mathbf{s} + \mathbf{U}^H \mathbf{n} \end{aligned} \tag{7}$$

Each individual received signal can be written as

$$y_i = d_i s_i + n'_i \tag{8}$$

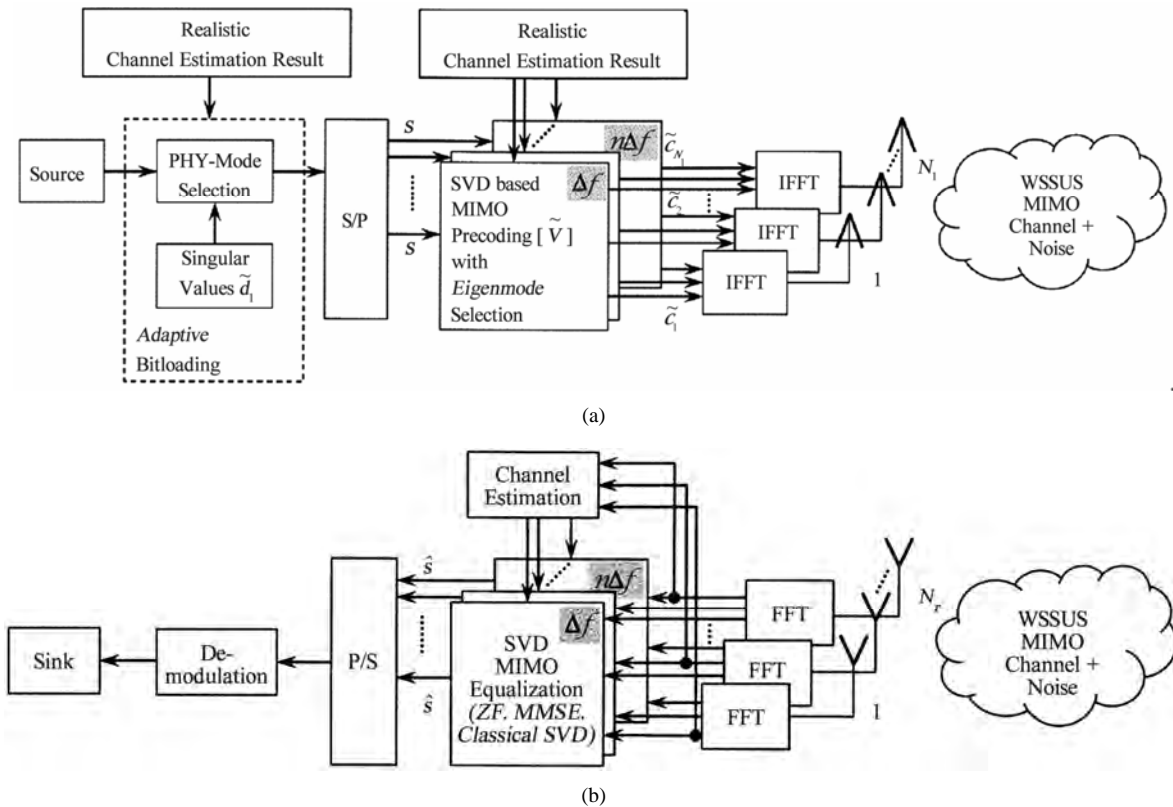


Figure 6. SVD based MIMO-OFDM system (a) Transmitter and (b) Receiver [36].

where  $n_i$  represents the  $i$ -th element of  $\mathbf{U}^H \mathbf{n}$ . The corresponding SISO SNR values are then given by

$$SNR_i = d_i^2 \frac{|s_i|^2}{2\sigma_n^2} \quad (9)$$

Equations (8) and (9) show that the singular values represent the MIMO processing gain for each of the eigenmodes. Therefore, SVD based MIMO precoding requires adaptive modulation and bit loading techniques for capacity maximization [36].

### 3.3.2. SVD Precoding with ZF Equalization

Linear ZF equalization can also be used at the receiver which is based on the inversion of the estimated MIMO channel matrix. ZF equalization requires the estimation of the product of  $\mathbf{H}\mathbf{V}$  at the receiver. Assuming ideal channel knowledge at the receiver, the detected signal can then be given by

$$\mathbf{y} = (\mathbf{H}\mathbf{V})^+ \mathbf{r} \quad (10)$$

$$= (\mathbf{H}\mathbf{V})^+ \mathbf{H}\mathbf{V}\mathbf{s} + (\mathbf{H}\mathbf{V})^+ \mathbf{n}$$

$$\mathbf{y} = \mathbf{s} + (\mathbf{U}\mathbf{D})^{-1} \mathbf{n} \quad (11)$$

where  $(\cdot)^+$  represents the pseudo inverse.

### 3.3.3. SVD Precoding with MMSE Equalization

MMSE equalization is based on minimizing the mean square error (MSE) between the transmitted and detected symbols. The minimum mean square error is given by

$$e = \min \left( \left\{ |\hat{s}_i - s_i|^2 \right\} \right) \quad (12)$$

where  $s_i$  is the transmitted symbol and  $\hat{s}_i$  represents the received symbol. The detected signal for SVD based MIMO MMSE equalization is given by

$$\mathbf{y} = \left[ K\sigma_n^2 \mathbf{I} + (\mathbf{H}\mathbf{V})^H (\mathbf{H}\mathbf{V}) \right]^{-1} (\mathbf{H}\mathbf{V})^H \mathbf{r} \quad (13)$$

with  $K = N_i$  utilized eigenmodes. As seen from Equation (13), MMSE MIMO equalization also requires the precoding matrix  $\mathbf{V}$  at the receiver.

### 3.3.4. Improved SVD Precoding Technique with Realistic Channel Knowledge

An improved SVD based MIMO precoding technique is also proposed in [36] which maximizes MIMO capacity while considering realistic channel knowledge at the transmitter rather than the ideal one. The MIMO capacity for realistic channel knowledge is given by

$$C_H = \sum_{i=1}^{N_i} \log_2 \left( 1 + \tilde{d}_i^2 \frac{|s_i|^2}{2\sigma_n^2} \right) \quad (14)$$

where  $\tilde{d}_i$  represent the singular values for the case of

realistic channel knowledge. The improved technique considers the  $K$  strongest eigenmodes for transmission with  $K < N_i$  if the following statement is fulfilled.

$$\sum_{i=1}^{N_i} \log_2 \left( 1 + \tilde{d}_i^2 \frac{|s_i|^2}{2\sigma_n^2} \right) \leq \sum_{i=1}^K \log_2 \left( 1 + \frac{N_i}{K} \tilde{d}_i^2 \frac{|s_i|^2}{2\sigma_n^2} \right) \quad (15)$$

The remaining eigenmodes which correspond to the  $N_i - K$  unused eigenvectors of the precoding matrix  $\tilde{\mathbf{V}}$  are not utilized.

### 3.3.5. Performance Comparison

Figure 7 shows the BER performance comparison of the classical SVD, ZF and MMSE equalization schemes for a  $4 \times 4$  MIMO-OFDM system. A curve for ideal ZF equalization is also provided for reference. It is clear from the comparison that MMSE equalization provides the best results with realistic channel estimation.

Figure 8 shows the performance comparison of the

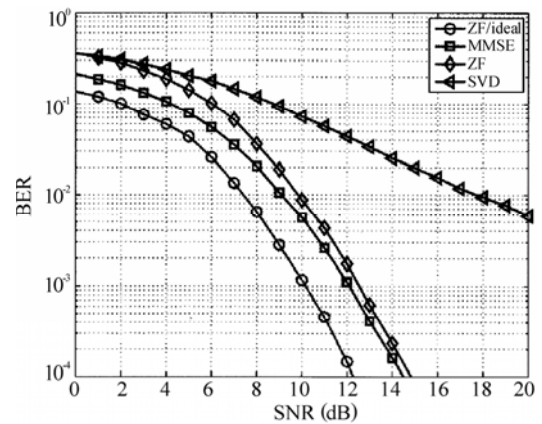


Figure 7. BER performance of uncoded  $4 \times 4$  SVD based MIMO systems [36].

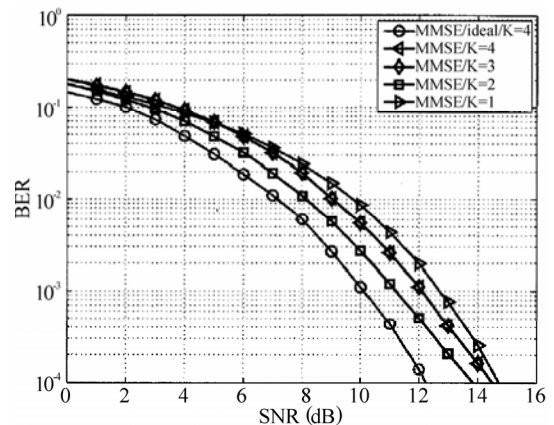


Figure 8. BER performance of an uncoded  $4 \times 4$  SVD based MIMO system with MMSE equalization [36].

MMSE equalization scheme with different values of  $K$  (utilized eigenmodes) for an uncoded  $4 \times 4$  MIMO system with realistic channel knowledge at the transmitter. The BER curve for the case of ideal channel knowledge is also provided. The MMSE equalization scheme provides the best performance for  $K = 2$  utilized eigenmodes selected according to Equation (15).

### 3.4. Geometric Mean Decomposition (GMD) Based MIMO

GMD based MIMO [2] is also a closed-loop joint transmitter design scheme which aims at optimally combining the benefits of MIMO diversity and spatial multiplexing. This technique utilizes the GMD of the MIMO channel matrix for precoder and equalizer design when the CSI is available at both the transmitter and the receiver. It is also applicable to MIMO-OFDM systems.

GMD calculation algorithm in [2] starts from the SVD of the channel matrix  $\mathbf{H}$  which is given according to Equation (5)

$$\mathbf{H} = \mathbf{U}\mathbf{D}\mathbf{V}^H$$

The GMD is then given by

$$\mathbf{H} = \mathbf{U}\mathbf{U}_R^H \mathbf{R}\mathbf{V}_R \mathbf{V}^H \triangleq \mathbf{Q}\mathbf{R}\mathbf{P}^H \quad (16)$$

where  $\mathbf{Q}$  and  $\mathbf{P}$  are semi-unitary matrices,  $\mathbf{P}$  being the linear precoder at the transmitter.  $\mathbf{R} \in \mathbb{R}^{K \times K}$  is an upper triangular matrix whose diagonal elements are the geometric mean of the  $K$  nonzero singular values of  $\mathbf{H}$ . The GMD scheme thus decomposes the MIMO channel into identical parallel subchannels which makes the symbol constellation selection and the overall system design much simpler. GMD can also be seen as an extended QR decomposition.

GMD MIMO can be implemented with the V-BLAST receiver and also with the zero-forcing dirty paper precoder (ZFDP). The V-BLAST technique has been discussed earlier in the text. The ZFDP technique also involves sequential nulling and cancellation but at the transmitter and utilizes CSI at the transmitter only.

The ZFDP scheme combines QR decomposition and “dirty paper” precoding. The QR decomposition for ZFDP is given by

$$\mathbf{H}^H = \tilde{\mathbf{Q}}\tilde{\mathbf{R}} \quad (17)$$

The sampled baseband received signal is then given by

$$\mathbf{y} = \tilde{\mathbf{R}}^H \tilde{\mathbf{Q}}^H \mathbf{x} + \mathbf{n} \quad (18)$$

Substituting  $\mathbf{x} = \tilde{\mathbf{Q}}\tilde{\mathbf{x}}$  we have

$$\mathbf{y} = \tilde{\mathbf{R}}^H \tilde{\mathbf{x}} + \mathbf{n} \quad (19)$$

Let  $\mathbf{s} \in \mathbb{C}^{K \times 1}$  be the transmitted symbol vector then

$\tilde{\mathbf{x}}$  should satisfy

$$\text{diag}\{\tilde{\mathbf{R}}\}\mathbf{s} = \tilde{\mathbf{R}}^H \tilde{\mathbf{x}} \quad (20)$$

where the left-hand side represents the element-wise multiplication of the diagonal elements of  $\tilde{\mathbf{R}}$  with the elements of  $\mathbf{s}$ . The solution to Equation (20) is then

$$\tilde{\mathbf{x}} = (\tilde{\mathbf{R}}^H)^{-1} \text{diag}\{\tilde{\mathbf{R}}\}\mathbf{s} \quad (21)$$

The ZFDP scheme, unlike V-BLAST, does not suffer from the error propagation problem. However, due to the matrix inversion in Equation (21) the norm of  $\tilde{\mathbf{x}}$  can be significantly amplified resulting in increased transmitter power consumption. This problem can be resolved by using the Tomlinson-Harashima precoder to restrict the transmit signal level within acceptable limits [2].

#### 3.4.1. Combining GMD with V-BLAST and ZFDP

The GMD-VBLAST scheme can be implemented beginning with the GMD of the channel matrix,  $\mathbf{H} = \mathbf{Q}\mathbf{R}\mathbf{P}^H$ . The information symbol vector  $\mathbf{s}$  is then encoded by the linear precoder  $\mathbf{P}$  resulting in the transmit signal  $\mathbf{x} = \mathbf{P}\mathbf{s}$ . The resulting signal at the receiver is then given by

$$\mathbf{y} = \mathbf{Q}\mathbf{R}\mathbf{s} + \mathbf{n} \quad (22)$$

which can be decoded simply by using the V-BLAST receiver. GMD-ZFDP scheme can also be implemented in a similar way. The resulting  $K$  independent and identical subchannels are given by

$$y_i = \bar{\lambda}_H x_i + n_i \quad ; i = 1, \dots, K \quad (23)$$

where  $\bar{\lambda}_H$  represent the subchannel gain and are in fact the identical diagonal elements of the matrix  $\mathbf{R}$  [2].

#### 3.4.2. Performance

Some simulation results from [2] depicting the performance of GMD based MIMO schemes are presented in the following text, assuming independent identically distributed (i.i.d) Rayleigh flat fading channels. **Figure 9** shows a comparison of the capacity of GMD-MIMO with other schemes for  $4 \times 4$  MIMO configuration. The informed transmitter (IT) curve corresponds to the Shannon channel capacity when CSI is available at both the transmitter and the receiver while the uninformed transmitter (UT) curve corresponds to the channel capacity when CSI is not available at the transmitter. MTM and MMD are both linear precoder design schemes for linear transceivers. MTM is based on the minimization of the trace of the MSE matrix while MMD minimizes the maximum diagonal elements of the MSE matrix resulting in near-optimal performance. Clearly, GMD outperforms both MTM and MMD at high SNR and approaches optimal capacity. The capacity loss of GMD at low SNR is due to

the ZF receiver. Based on GMD, the authors of [2] have also proposed another scheme called uniform channel decomposition (UCD) which can decompose a MIMO channel into identical subchannels in a strictly capacity lossless manner [37].

Figures 10 and 11 show the BER performance comparison of GMD-MIMO with ordered MMSE-VBLAST, MTM and MMD for  $2 \times 4$  and  $4 \times 4$  MIMO configurations respectively. GMD achieves much higher performance particularly at high SNR.

Figure 12 shows a performance comparison of GMD-VBLAST and GMD-ZFDP when combined with OFDM for ISI suppression. GMD-VBLAST results in performance loss of about 2 dB because of error propagation.

### 3.5. Turbo-MIMO Systems

Turbo-MIMO systems represent a class of MIMO com-

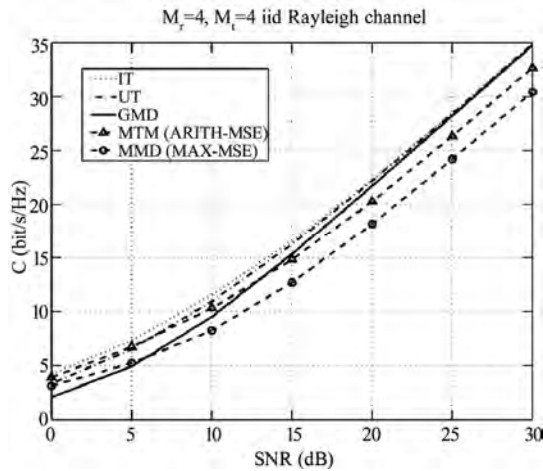


Figure 9. Average capacity for  $4 \times 4$  MIMO configuration [2].

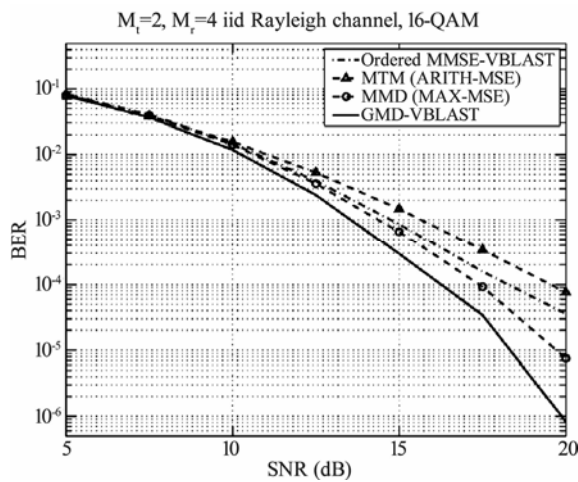


Figure 10. BER performance for  $2 \times 4$  MIMO configuration [2].

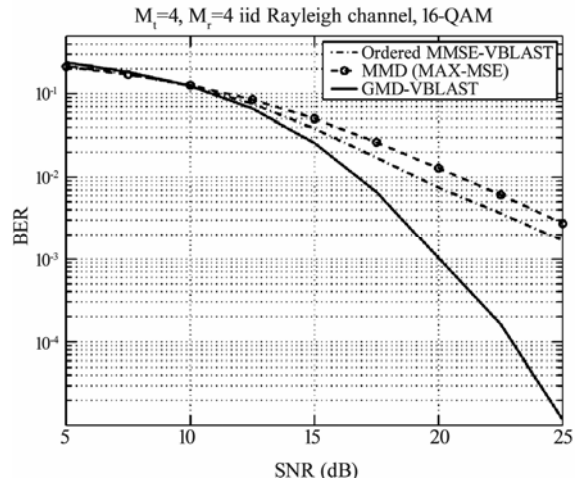


Figure 11. BER performance for  $4 \times 4$  MIMO configuration [2].

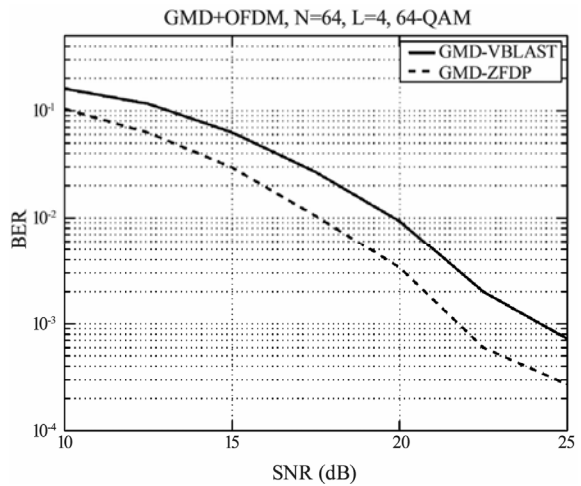


Figure 12. BER performance of GMD based MIMO-OFDM systems [2].

munication systems that combine the turbo-processing principle used in turbo coding with MIMO. These systems aim at attaining channel capacity close to the Shannon limit for MIMO channels with manageable complexity and can be implemented from diversity maximization or SM aspects [38].

A turbo-MIMO architecture known as TurboBLAST is presented in [39]. This MIMO system is based on random layered space-time (RLST) coding which is a combination of independent block-time coding and space-time interleaving. The receiver uses iterative turbo-processing for RLST decoding and estimation of the flat fading MIMO channel matrix. A similar turbo-MIMO system based on space-time bit-interleaved coded modulation (ST-BICM) is presented in [38]. ST-BICM codes are formed by concatenation of a turbo encoded sequence and ST interleaving.

**Figure 13** shows the block diagram of a ST-BICM MIMO system transmitter. The information bits are turbo encoded based on a linear forward error correction (FEC) code represented as the outer code. The encoded sequence is then bit-interleaved using a space-time pseudo-random interleaver denoted by  $\Pi$  in the figure. Each interleaved substream is then independently mapped onto  $M$ -ary PSK or QAM symbols and transmitted using a separate antenna. The inner code basically represents a linear space-time mapper which allows for a flexible MIMO design with optimal diversity order and multiplexing gain or a desired tradeoff between the two. STBCs can be used to obtain the maximum diversity order while a symbol multiplexer can be used if full multiplexing gain is desired [38].

**Figure 14** shows a double iterative decoding receiver for the ST-BICM MIMO system. It operates in two stages consisting of inner and outer iterative decoding loops. The inner and outer decoders are separated by an interleaver and a deinterleaver represented by  $\Pi$  and  $\Pi^{-1}$

respectively. This arrangement decorrelates the correlated outputs between the two stages. The decorrelator compensates for the interleaving operation at the transmitter. The two stages iteratively exchange information, producing a better estimate of the transmitted symbols after each iteration, until the receiver converges [38].

The inner decoder is in fact a MIMO detector, the optimal choice being the maximum a posteriori probability (MAP or APP) detector/decoder. However, due to the excessive computational complexity of APP detection, reduced-complexity near-optimal detectors like MMSE-SIC or reduced-complexity APP detectors e.g. the list-sphere detector (LSD), iterative tree search (ITS) and multilevel bit mapping ITS (MLM-ITS) detectors can be used.

The outer decoder consists of a channel turbo decoder with two decoding stages separated by an interleaver and a deinterleaver denoted by  $\alpha$  and  $\alpha^{-1}$  respectively in **Figure 14**. This arrangement forms the outer iterative decoding loop of the ST-BICM MIMO receiver [38].

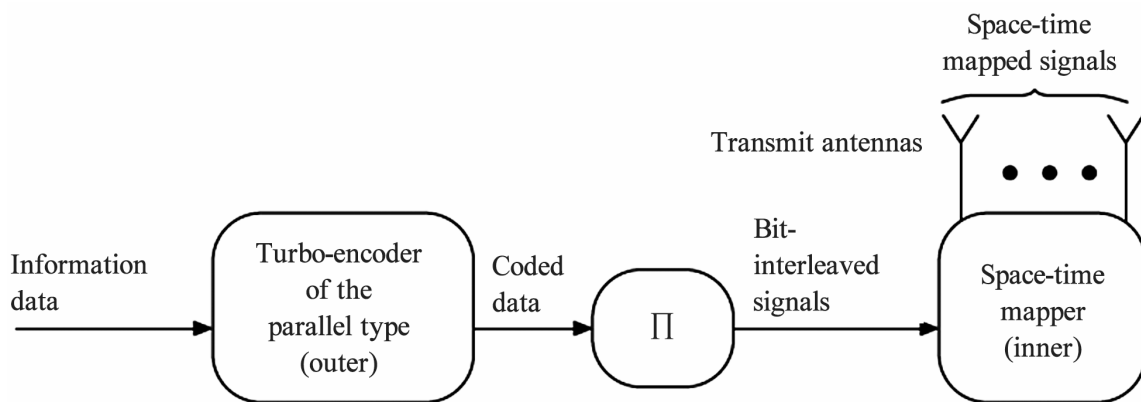


**Figure 13.** ST-BICM MIMO system transmitter [38].

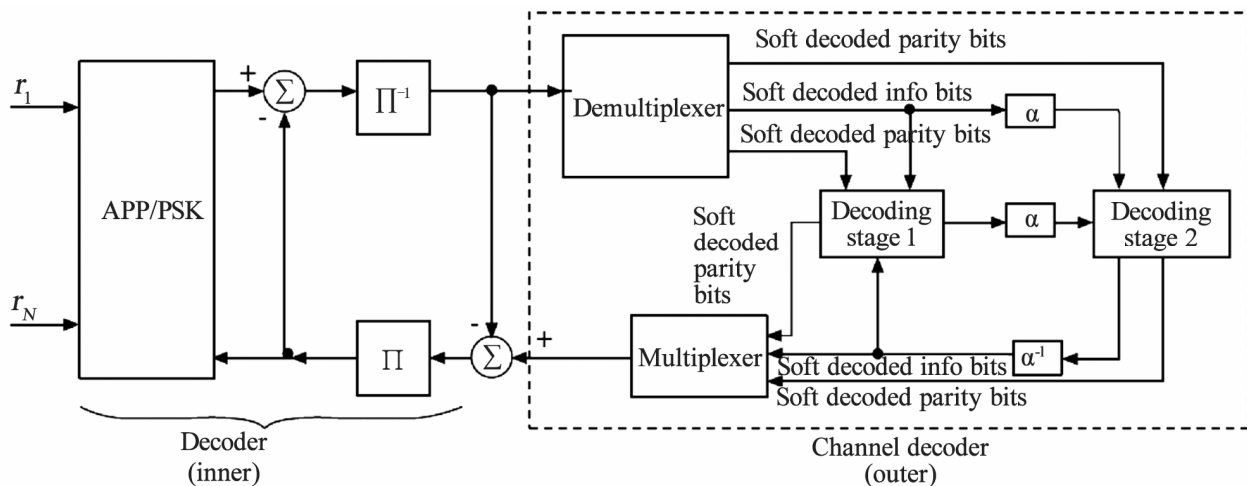


**Figure 14.** Receiver structure for the ST-BICM MIMO system [38].

**3.5.1. Performance**

**Figure 15** shows the BER performance of a simulated  $8 \times 8$  ST-BICM MIMO system using a rate-1/2, memory 2 turbo code as the outer channel code, with feed-forward and feedback generators 5 and 7 (octal) respectively. A block fading channel is assumed for the inner encoder which remains constant for a block size of 192 information bits with each block representing a statistically independent channel realization. A rich scattering Rayleigh MIMO model is used to select the elements of the MIMO channel matrix. 4 iterations are used in the inner decoder loop while 8 iterations are used in the outer channel decoder loop. The figure shows a comparison for different modulation schemes with MMSE-SIC and MLM-ITS inner detectors. The performance of MLM-ITS detection increases with larger list size  $M$  however, at the cost of increased complexity. The respective capacity limits for QPSK, 16-QAM and 64-QAM are also shown. At BER =  $10^{-5}$  and  $M = 64$ , The ST-BICM systems using QPSK, 16-QAM and 64-QAM operate 1, 4 and 6 dB away from their respective capacity limits [38].

**Figure 16** shows the BER performance of the ST-BICM system using MLM-ITS detector as the no. of iterations in the outer decoder increase from 1 to 5. Clearly the performance improves with the no. of iterations which pertains to only a linear increase in complexity. However, it can also be seen that the performance gain between successive iterations diminishes somewhat due to the feedback of correlated noise. Further increase in iterative gain can be achieved by using larger interleavers [38].

**3.6. Limited Feedback Strategies for Closed-loop MIMO Systems**

Certain closed-loop MIMO systems like the SVD and GMD based systems assume the availability of full CSI at the transmitter. Full CSI is available at the transmitter in a TDD system with duplex time less than the channel coherence time due to the reciprocity of the channel while in a FDD system a feedback channel for CSI is required thus consuming additional bandwidth. However, in practical scenarios the extra load resulting from large

CSI feedback is not desirable and may not even be possible e.g. in case of rapidly varying mobile channels. Furthermore, results have shown that performance close to that with full CSI can be achieved by using limited feedback strategies utilizing only a few bits of feedback. **Figure 17** shows the block diagram of a limited feedback MIMO system [40].

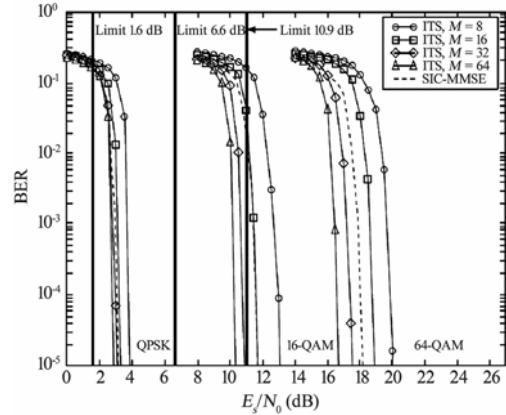


**Figure 15. BER performance of  $8 \times 8$  ST-BICM MIMO system with different modulation and inner detection schemes [38].**

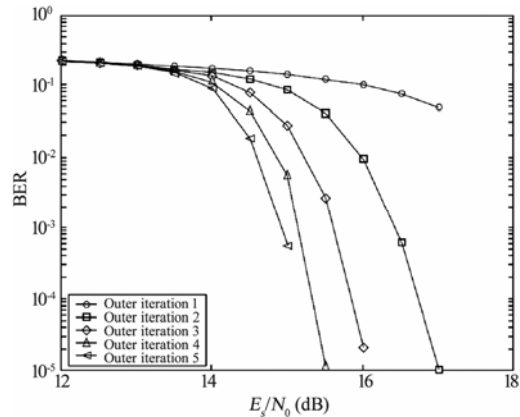


**Figure 16. BER performance of  $8 \times 8$  ST-BICM MIMO system with different no. of iteration in the outer decoder [38].**

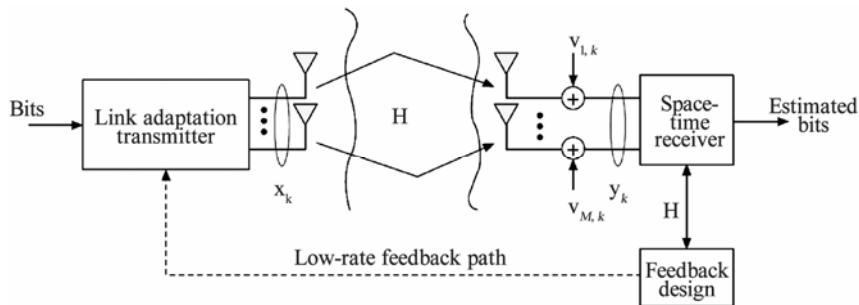


**Figure 17. Limited feedback closed-loop MIMO system [40].**

The feedback may be based on channel quantization or quantization of some properties of the transmitted signal. Channel quantization involves vector quantization (VQ) of the channel matrix  $\mathbf{H}$  as depicted in **Figure 18**. The quantized version of the MIMO channel can then be fed back to the transmitter. However, it has been observed that quantization of the entire channel may not be necessary and it may be sufficient to include only some part of the channel structure like the channel singular vectors. For example, the optimal precoding matrix for an i.i.d MIMO channel consists of the eigenvectors of the channel covariance matrix, as columns. The feedback overhead may be further reduced by using only a limited number of quantized weighting vectors or matrices for precoding. This collection of precoding matrices is known as a precoding codebook and is shared by the transmitter and the receiver. The feedback consists of bits representing a particular precoding matrix within the codebook [40,41].

A large codebook length for vector quantization schemes results in increased complexity at the receiver due to the exhaustive search required for selecting a precoding matrix. In such cases, when the codebook length and therefore the corresponding no. of feedback bits  $B$  is large, scalar quantization of the elements of the precoding matrix can be employed instead. However, for small values of  $B$ , scalar quantization may become too inaccurate. In such cases, performance of scalar quantization can be improved by using the *reduced rank* approach where the columns of the precoding matrix are constrained to lie within a subspace of dimension less than the no. of transmit antennas  $N_t$  [40].

**Figure 19** shows the symbol error rate (SER) performance of a simulated  $4 \times 5$  limited feedback MIMO beamformer with different feedback strategies. The system uses 16-QAM modulation for transmission and MRC at the receiver. Optimal BF in the figure represents the optimal beamformer with unquantized feedback and full CSI at the transmitter. Grassmannian BF (6-bit) represents signal adaptive beamforming using a 6-bit feedback VQ codebook and results in the best performance, lying within 0.7 dB of the optimal BF and approximately 1dB better than the 40-bit channel quantization which suffers from large quantization error. The 6-bit quantized reduced rank (RR) beamformer with dimension  $D = 3$ , performs close to the 40-bit channel quantization [40].

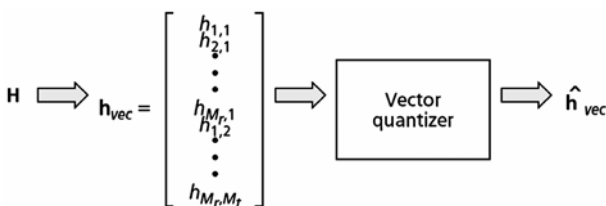


**Figure 18. Channel Quantization [40].**

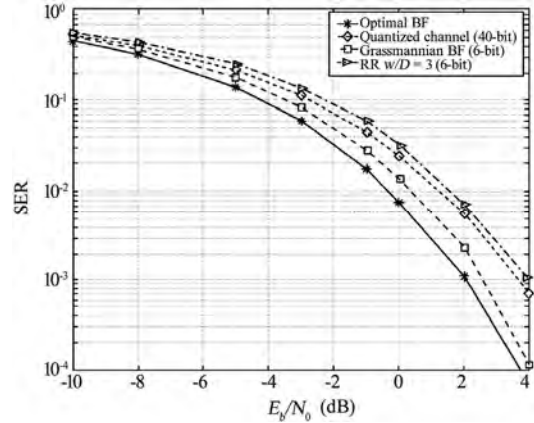


**Figure 19. Limited feedback beamformer performance for  $4 \times 5$  MIMO configuration [40].**

### 3.6.1. Link Adaptation without Precoding

In addition to the precoding matrix, other information e.g. the received signal to interference and noise ratio (SINR) may also be included in the feedback for link adaptation. However, some MIMO schemes like the modified V-BLAST schemes in [32,34] rely solely on this type of feedback without any precoding information.

Another example is the 2-codeword multiple codewords (2CW-MCW) scheme for FDD MIMO-OFDM cellular systems proposed in [41] that uses SINR feedback for each stream to select a suitable modulation and coding scheme (MCS) for each of the two simultaneously transmitted codewords. The two codewords are mapped onto 2 and 4 streams respectively for  $2 \times 2$  and  $4 \times 4$  antenna configurations. The mapping may either be fixed or adaptive. Adaptive mapping also makes use of the SINR feedback. Precoding is not used in this scheme resulting in reduced feedback overhead.

### 3.6.2. Partial Feedback Schemes

Partial feedback schemes for MIMO systems are based on the feedback of statistical channel information along with some instantaneous channel quality indicator (CQI) e.g. SNR, SINR etc. to the transmitter. A partial feedback scheme for MIMO-OFDM systems involving the decomposition of MIMO channel covariance matrix is presented in [42].

The covariance matrix  $\mathbf{R}$  is calculated from the estimated MIMO channel matrix  $\mathbf{H}$  (for the  $k$ -th subcarrier) at the receiver and is given by

$$\mathbf{R} = E\{\mathbf{H}^H \mathbf{H}\} \tag{24}$$

The matrix  $\mathbf{R}$  is then decomposed using SVD which is given by

$$\mathbf{R} = \mathbf{U}_{Stat} \mathbf{\Lambda}_{Stat} \mathbf{V}_{Stat}^H \tag{25}$$

where  $\mathbf{\Lambda}_{Stat}$  is a diagonal matrix containing the singular

values while  $\mathbf{U}_{Stat}$  and  $\mathbf{V}_{Stat}$  are unitary matrices. The feedback includes the matrix  $\mathbf{\Lambda}_{Stat}$  and the column vectors of  $\mathbf{V}_{Stat}$  for power allocation and spatial processing (precoding) at the transmitter [42].

Figure 20 shows the block diagram of a  $N_T \times N_R$  MIMO-OFDM system based on this partial feedback scheme which transmits  $N_S$  spatial streams using  $N_C$  OFDM subcarriers. The received signal vector for the  $k$ -th subcarrier is given by

$$\mathbf{y} = \mathbf{H}\mathbf{Q}\mathbf{A}\mathbf{x} \quad (26)$$

where  $\mathbf{x}$  is the transmit data vector,  $\mathbf{H}$  is the MIMO channel matrix for the  $k$ -th subcarrier,  $\mathbf{A}$  is a diagonal matrix with  $N_S$  diagonal elements determined by the matrix  $\mathbf{\Lambda}_{Stat}$  feedback for power allocation to the active spatial streams, and the  $N_T \times N_S$  matrix  $\mathbf{Q}$  represents a spatial processing transformation which maps the spatial streams to the transmit antennas. The  $\mathbf{Q}$  matrix is constructed from the vectors of  $\mathbf{V}_{Stat}$  received at the transmitter via feedback and is used to maximize the received energy for each transmitted spatial stream. This enables

maximum ratio transmission (MRT) and SVD beamforming along with tracking of spatial variations of the MIMO channel [42].

The MIMO channel covariance and the corresponding channel singular values do not vary rapidly with time even at vehicular speeds around 100 km/h [42]. This greatly reduces the feedback load on the system and makes this closed-loop MIMO-OFDM system suitable for mobile environments.

Figures 21 and 22 show the simulated frame error rate (FER) performance of the proposed MIMO-OFDM system in comparison with open-loop SM and perfect CSI feedback MIMO-OFDM systems, for  $2 \times 2$  and  $4 \times 4$  MIMO configurations respectively. The figures include FER performance curves for QPSK and 64-QAM modulation in a low speed mobile scenario using the ITU PB channel profile with vehicular speeds of 3 km/h. The OFDM scheme is based on 512-point FFT with 15 subchannels for data transmission each consisting of 20 continuous subcarriers, for a total bandwidth of 5 MHz. The frame duration is about 0.5ms. Turbo coding is employed for FEC and MMSE detection is used at the receiver.

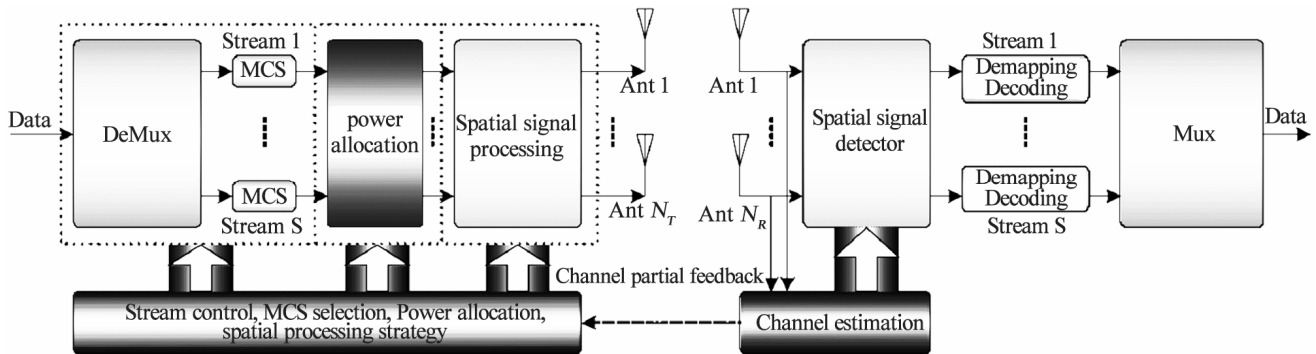


Figure 20. MIMO-OFDM system with partial feedback [42].

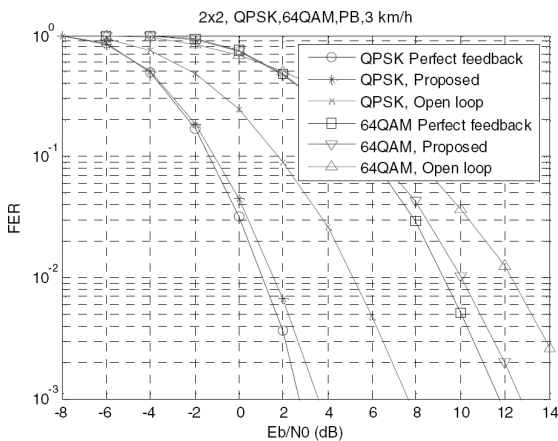


Figure 21. FER performance for coded  $2 \times 2$  MIMO configuration [42].

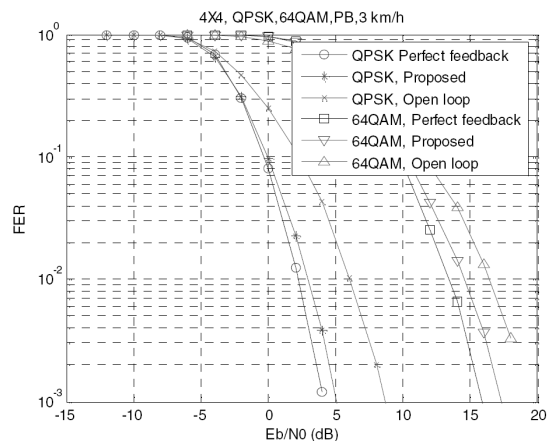


Figure 22. FER performance for coded  $4 \times 4$  MIMO configuration [42].

Equal power allocation is used for the open-loop SM system while water-filling is used for the closed-loop systems. Ideal channel knowledge is assumed at the receiver for all systems and antenna correlations are not considered [42].

As seen from the results, the proposed system operates quite close to the perfect CSI feedback system and shows substantial performance gain over the open-loop system. The small performance loss in comparison with the perfect feedback system is primarily due to the quantization error associated with limited feedback [42].

Efficient feedback reconstruction algorithms for improvement of the closed-loop transmit diversity scheme constituting the mode 1 of 3GPP's wideband code-division multiple access (WCDMA) 3G standard are presented in [43]. These algorithms efficiently reconstruct the beamforming weights at the transmitter while considering the effect of feedback error. Performance results for vehicular speeds up to 100 km/h are provided. The proposed techniques are applicable to closed-loop MIMO diversity systems and may possibly be extended to 4G systems.

In [44], the optimal MIMO precoder designs for frequency-flat and frequency-selective fading channels are presented, assuming partial CSI at the transmitter consisting of transmit and receive correlation matrices. The elements of transmit and receive correlation matrices are determined from the respective transmit and receive antenna spacing and angular spread. It is shown that from the capacity maximization perspective, the optimal precoder for a frequency-flat fading channel is an eigen-beamformer. On the other hand, the optimal precoder for a frequency-selective fading channel represented by  $L$  uncorrelated effective paths consists of  $P + L$  parallel eigen-beamformers where  $P$  is an arbitrary value depending on the no. of vectors in a transmission data block [44].

A closed-loop limited feedback MIMO scheme called multi-beam MIMO (MB-MIMO) is proposed in [45] for 3GPP LTE E-UTRA downlink. MB-MIMO employs multiple fixed beams at the base station (Node B) to transmit multiple data streams. The no. of beams and data streams to be used are adaptively selected using a codebook at the UE. The selected precoding vectors or beam indices constituting a precoding matrix are then fed back to the Node B. The MB-MIMO scheme can adaptively switch between MIMO SM and transmit beamforming (Tx-BF) modes. Tx-BF is used if a single beam is selected and SM is used if multiple beams are selected.

The proposed scheme eliminates the need for a hardware calibrator (HW-CAL) at Node B that was required for a previously proposed MB-MIMO implementation. HW-CAL compensates the phase variations caused by RF components and was needed to align the phase condition of each transmit antenna element for maximizing the transmit beamforming gain. The proposed scheme

uses a larger codebook based on an extended precoding matrix which includes phase terms that can be controlled to align the phase condition of the 4 node B antenna elements. This results in high beamforming gain even without HW-CAL. However, 4 additional bits or a total of 8 bits are required for feedback, which is still a small number.

### 3.7. MIMO over High-Speed Mobile Channels

Open-loop MIMO diversity techniques like STC and space frequency coding (SFC) are appropriate choices for high-speed mobile channels that vary rapidly with time. In such scenarios, maintaining a reliable link becomes the foremost priority rather than maximizing system throughput.

High-speed mobile channels undergo fast fading which may cause time variation of the fading channel within an OFDM symbol period. This results in the loss of subchannel orthogonality and leads to interchannel interference (ICI) due to the distribution of leakage signals over other OFDM subcarriers. The error floor associated with ICI increases with the speed of the mobile terminal [46].

An improved MIMO-OFDM technique for high-speed mobile access in cellular environments is proposed in [46]. This technique reduces ICI and provides diversity gain as well as noise averaging even for highly correlated channels. ICI is reduced by transmitting weighted data on adjacent subcarriers. The weights are selected such that the mean ICI power is minimized. The adopted weight selection procedure however results in suboptimal weights. Diversity gain in [46] is achieved by using space-frequency block coding (SFBC) which is based on Alamouti code but the coding is applied in frequency domain i.e. to OFDM subcarriers rather than to OFDM symbols in time domain [47]. **Figure 23** shows the data assignment scheme for the  $2 \times 1$  SFBC-OFDM system, without the weighting factors. The transmit data is assigned to subcarrier groups each consisting of two adjacent subcarriers, as shown in the figure.

Instead of SFBC, other diversity techniques such as STBC, space-frequency trellis coding (SFTC), maximal-

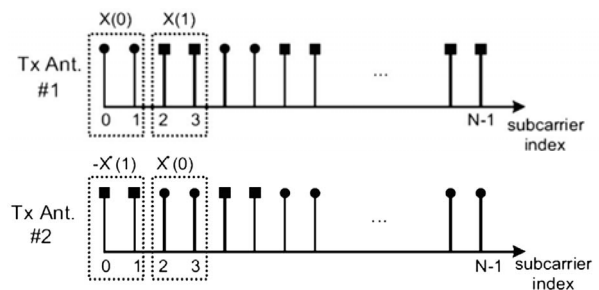


**Figure 23.** Data assignment scheme for ICI reduction in  $2 \times 1$  SFBC-OFDM system [46].

ratio receive combining (MRRCC) etc. can also be used. The proposed technique operates without CSI at the transmitter and does not require any pilot signals for channel tracking. However, it is suitable for OFDM systems with subcarrier group spacing less than the channel coherence bandwidth because the channel coefficients are assumed to be identical for adjacent subcarriers.

**Figure 24** shows the simulated BER performance of the proposed SFBC-OFDM scheme in comparison with conventional SFBC MIMO-OFDM schemes for  $2 \times 1$  antenna configuration using I-METRA MIMO channel model Case A for downlink transmission with mobile speed of 250 km/h. Case A corresponds to a frequency-flat Rayleigh fading channel with uncorrelated antennas. 25 MHz of downlink channel bandwidth is used at 2 GHz with 2048 OFDM subcarriers. Performance results for QPSK and 16-QAM are provided.

**Figure 25** shows the performance comparison using

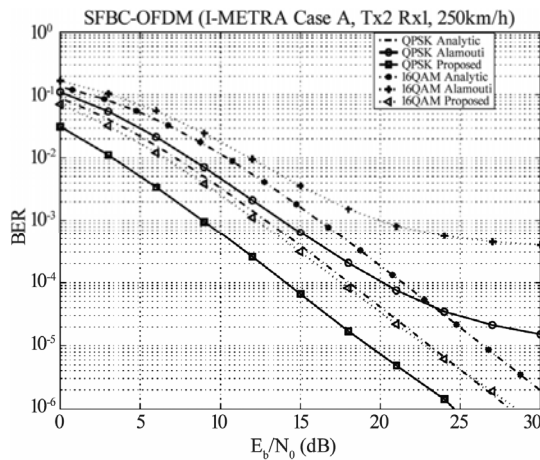


**Figure 24.** BER Performance of SFBC-OFDM systems using I-METRA Case A channel [46].

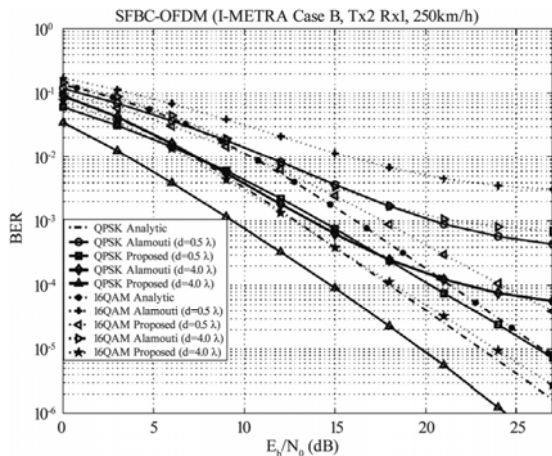


**Figure 25.** BER Performance of SFBC-OFDM systems using I-METRA Case B channel [46].

I-METRA Case B which corresponds to a frequency-selective fading channel with correlated transmit antennas in an urban macro cellular environment.

The proposed SFBC-OFDM scheme clearly outperforms the conventional SFBC-OFDM schemes in both cases. The conventional SFBC-OFDM scheme referred to as Alamouti in the figures is severely performance limited due to the error floor phenomenon resulting from ICI introduced by the high-speed mobile user at 250 km/h.

### 4. Multiuser MIMO

Multiuser MIMO (MU-MIMO) systems consist of multiple antennas at the BS and a single or multiple antennas at each UE. MU-MIMO enables space-division multiple access (SDMA) in cellular systems which increases the system capacity by exploiting the spatial dimension (i.e. the location of UEs) to accommodate more users within a cell. It also provides beamforming or array gain as well as diversity gain due to the use of multiple antennas. In case of multiple antennas at the UE, spatial multiplexing can also be employed to further enhance the spectral efficiency [48].

The uplink and the downlink of a MU-MIMO system represent two different problems which are discussed in the following text.

#### 4.1. The MU-MIMO Uplink

The MU-MIMO uplink channel is a MIMO multiple access channel (MIMO-MAC) [49] where the users simultaneously transmit data over the same frequency channel to the BS equipped with multiple antennas. The BS must separate the received user signals by means of array processing, multiuser detection (MUD), or some other method [48]. **Figure 26** shows various linear and nonlinear MUD schemes for MIMO-OFDM systems, some of which are discussed in the later sections.

##### 4.1.1. Classic SDMA-OFDM MUDs

An overview of some classic MUDs for MU-MIMO-OFDM is presented in [3]. The discussion is based on the

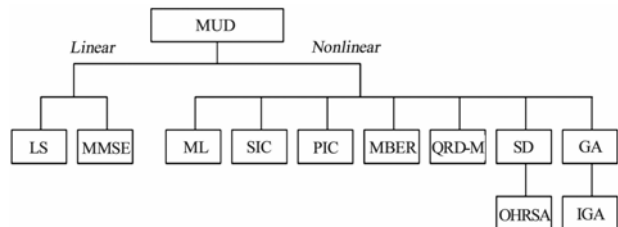


**Figure 26.** Various multiuser detectors (MUDs) for MIMO-OFDM systems [3].

uplink MIMO SDMA-OFDM system model of **Figure 27** where each of the  $L$  UEs uses a single transmit antenna while the BS is equipped with  $P$  antennas.

The complex-valued  $P \times 1$  received signal vector at the BS antenna array for the  $k$ -th subcarrier of the  $n$ -th OFDM symbol is given by

$$\mathbf{x} = \mathbf{H}\mathbf{s} + \mathbf{n} \tag{27}$$

where  $\mathbf{s}$  is the  $L \times 1$  transmitted signal vector,  $\mathbf{n}$  is the  $P \times 1$  AWGN noise vector and  $\mathbf{H}$  is the  $P \times L$  channel transfer function matrix consisting of  $L$  column vectors, each containing the transfer functions for a particular UE. Therefore,  $\mathbf{H}$  can be represented as

$$\mathbf{H} = [\mathbf{H}^{(1)}, \mathbf{H}^{(2)}, \dots, \mathbf{H}^{(L)}] \tag{28}$$

where

$$\mathbf{H}^{(l)} = [H_1^{(l)}, H_2^{(l)}, \dots, H_p^{(l)}]^T, \quad l = 1, \dots, L \tag{29}$$

is a  $P \times 1$  vector whose elements are the channel transfer functions for the transmission paths between the transmit antenna of the  $l$ -th UE and the  $P$  BS antennas.

It is assumed that the complex signal  $s^{(l)}$  transmitted by the  $l$ -th user has zero mean and variance  $\sigma_l^2$  while

the AWGN signal  $n_p$  has zero mean and variance  $\sigma_n^2$ .

The channel transfer functions  $H_p^{(l)}$  are assumed to be independent, stationary, complex Gaussian distributed processes with zero mean and unit variance.

The classic MUD schemes [3] are discussed in the following text.

1) *MMSE MUD*:

**Figure 28** shows the schematic diagram of a MMSE SDMA-OFDM MUD. The multiuser signals received at each BS antenna are multiplied by a complex-valued array weight  $w_p^{(l)}$  and then summed up. The superscript  $l$  represents a particular user which means that a separate set of weights is used for detection of each user's signal. The combiner output  $y(t)$  is subtracted from a user specific reference signal  $r(t)$  known at the BS and the UE, resulting in an error signal  $\epsilon(t)$ . The error signal is used for weight estimation according to the MMSE criterion. The steepest descent algorithm can be used in this regard for stepwise weight adjustment for each subcarrier of each user. The performance of the MMSE MUD improves as the no. of antennas  $P$  in the BS antenna array is increased and degrades when the no. of users increase.

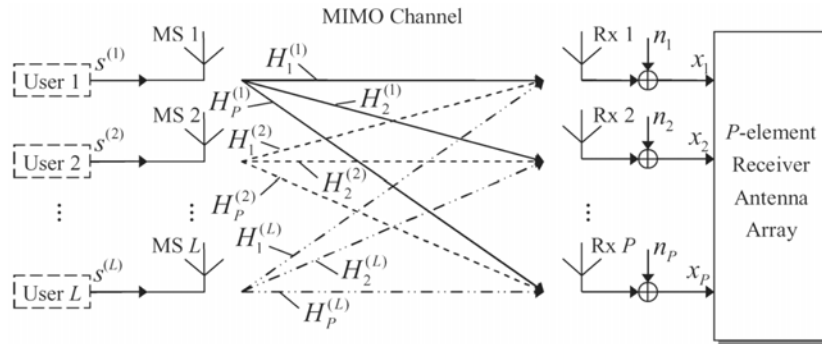


**Figure 27.** Uplink MIMO SDMA-OFDM system model with single antenna at each UE [3].

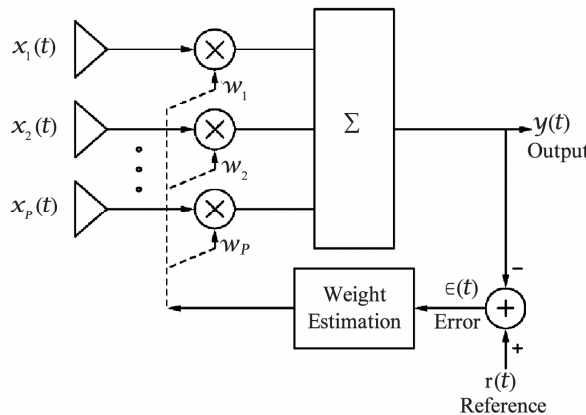


**Figure 28.** MMSE SDMA-OFDM MUD [3].

### 2) Successive Interference Cancellation (SIC) MUD:

The successive interference cancellation (SIC) MUD enhances the MMSE MUD using SIC. For each subcarrier, the detection order of the users is arranged according to their estimated total received signal power at the BS antenna array and the strongest user's signal with the least multiuser interference (MUI) is detected using the MMSE MUD. The detected user signal is then subtracted from the composite multiuser signal and the next strongest user is detected by the same procedure. This process continues till the detection is completed for all users. SIC results in high diversity gain at the MMSE combiner, which mitigates the effects of MUI as well as channel fading. The SIC MUD is also effective in near-far scenarios that result from inaccurate power control. However, it is prone to errors in power classification of user signals and also to interuser error propagation. **Figure 29** shows the BER performance comparison of MMSE MUD and SIC MUD ( $M$ -SIC with  $M = 2$ ) for an SDMA-OFDM scenario with four single-antenna UEs and a four-antenna BS antenna array using QPSK modulation. The indoor short wireless asynchronous transfer mode (SWATM) channel model is used.

### 3) Parallel Interference Cancellation (PIC) MUD:

The PIC MUD does not require any power classification of the received user signals. The detection procedure consists of two iterations for all subcarriers. In the first iteration, MMSE detection is used to estimate all user signals  $y^{(l)}$  from the received composite multiuser signal vector  $\mathbf{x}$ . In case of channel encoded transmission, all user signals must be decoded, sliced, channel encoded

again and also remodulated onto subcarriers. In the second detection iteration, signal vectors  $\tilde{\mathbf{x}}^{(l)}$  for all  $L$  users are reconstructed and an estimate  $\tilde{y}^{(k)}$  of each user signal is generated by subtracting the signal vectors  $\tilde{\mathbf{x}}^{(l)}$ ,  $l \neq k$  of all other users followed by MMSE combining. The estimated user signals are then channel decoded and sliced. The PIC MUD scheme is also vulnerable to interuser error propagation.

### 4) Maximum Likelihood (ML) MUD:

The ML MUD employs the ML detection principle to find the most likely transmitted user signals through an exhaustive search. It provides the optimal detection performance but also has the highest complexity of any other MUD. For an OFDM-SDMA system with  $L$  simultaneous users, the ML MUD produces the estimated  $L \times 1$  symbol vector  $\hat{\mathbf{s}}_{\text{ML}}$  consisting of the most likely transmitted symbols of the  $L$  users for a particular OFDM subcarrier, as given by

$$\hat{\mathbf{s}}_{\text{ML}} = \arg \min_{\mathbf{s} \in M^L} \|\mathbf{x} - \mathbf{H}\mathbf{s}\|^2 \quad (30)$$

where  $M^L$  is a set containing  $2^{mL}$  trial vectors,  $m$  being the no. of bits per symbol depending on the modulation scheme used resulting in  $2^m$  constellation points. Therefore, the computational complexity of the ML MUD increases exponentially with the no. of users  $L$  thus making it prohibitive for practical implementation.

### 5) Sphere Decoding (SD) aided MUD:

SD-aided MUDs use SD for reduced-complexity ML multiuser detection with near-optimal performance. SD reduces the ML search to within a hypersphere of a certain radius around the received signal. The radius of this search sphere determines the complexity of the MUD. Various SD algorithms have been proposed in literature like the complex-valued SD (CSD) and multistage SD (MSD) which significantly reduce the complexity by reducing the required search radius [3].

### 4.1.2. Layered Space-Time MUD

A V-BLAST based MUD scheme referred to as layered space-time MUD (LAST-MUD) is presented in [50] for CDMA uplink. This scheme is somewhat similar to the SIC MUD since V-BLAST detection also incorporates SIC.

**Figure 30** shows the layered space-time MU-MIMO system block diagram. Here the single antenna users are arranged in  $G$  groups each containing  $M$  users for a total of  $K = G \times M$ . The UEs within each group are treated as the multiple transmit antennas of a V-BLAST system. The users within each group share the same unique spreading code which distinguishes the groups from one another. Therefore, out of the  $K$  total spreading codes, only  $G$  are unique. The  $N \times K$  random spreading matrix consisting of  $K$  length  $N$  code vectors is denoted by

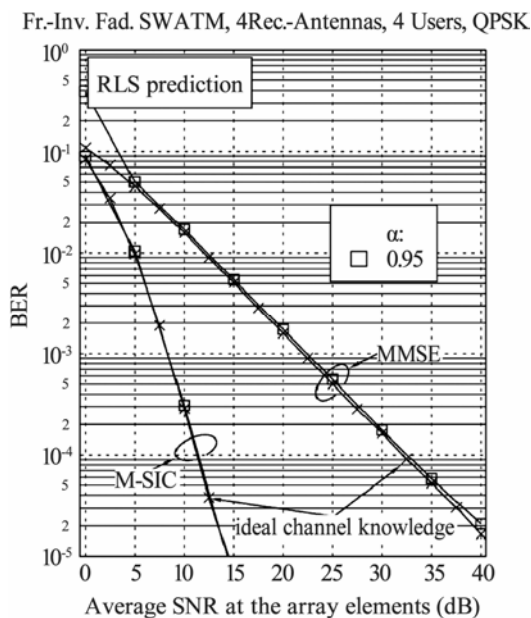


**Figure 29.** BER performance of MMSE MUD and SIC MUD [3].

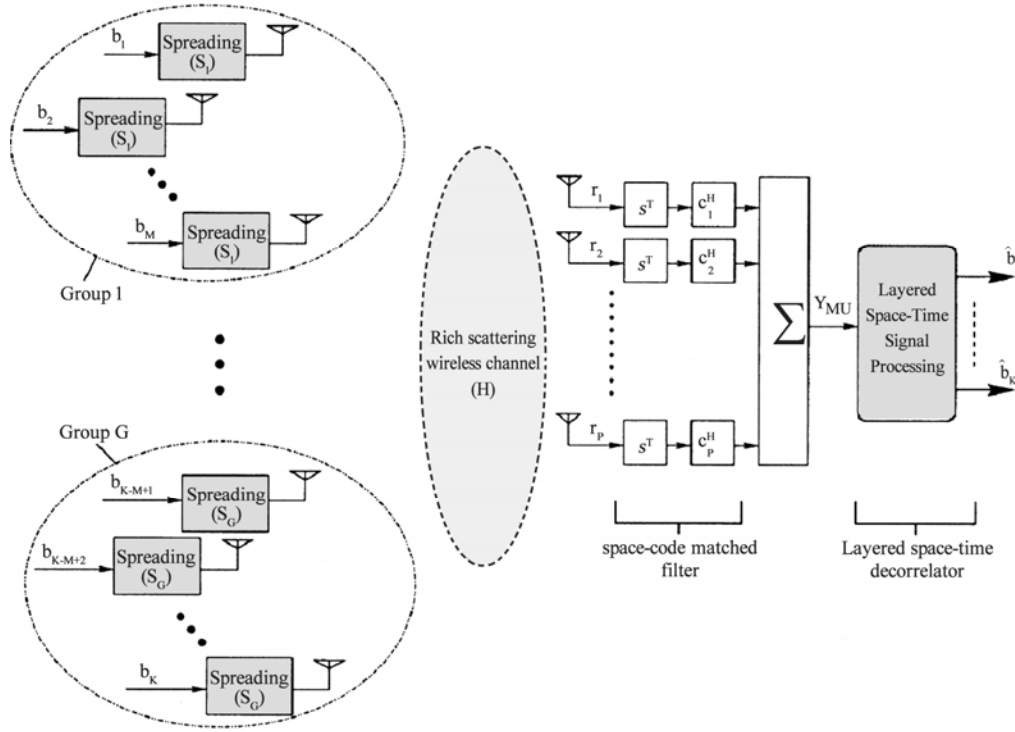


Figure 30. LAST MU-MIMO system [50].

$\mathbf{S} = [\mathbf{S}_1, \dots, \mathbf{S}_1, \mathbf{S}_2, \dots, \mathbf{S}_2, \dots, \mathbf{S}_G, \dots, \mathbf{S}_G]$ . The proposed system can also accommodate users with multiple antennas thus enabling spatial multiplexing for achieving high data rates. In that case each user with multiple transmit antennas will be considered as one group. The  $K \times 1$  transmitted symbol vector is represented as  $\mathbf{b} = [b_1, \dots, b_k]^T$  where each element represents the bit transmitted by a particular user. The channel between the users and the BS is considered to be a frequency-flat fading MIMO channel and is denoted by the channel matrix  $\mathbf{H} = [\mathbf{h}_1, \dots, \mathbf{h}_p]^T$  where  $\mathbf{h}_p$  is the  $K \times 1$  channel coefficient vector between all  $K$  users and the  $p$ -th BS antenna. The BS is equipped with a total of  $P$  antennas.

The  $N \times 1$  received baseband signal at the  $p$ -th BS antenna for a certain symbol period after chip-matched filtering is given by

$$\mathbf{r}_p = \mathbf{S}\mathbf{C}_p \mathbf{b} + \mathbf{n}_p \quad (31)$$

where  $\mathbf{C}_p = \text{diag}(\mathbf{h}_p)$  is the complex diagonal channel matrix for the  $p$ -th BS antenna and  $\mathbf{n}_p$  is the corresponding complex-valued AWGN noise vector with zero mean and variance  $\sigma^2$ . A frequency-flat fading MIMO channel is assumed as well as perfect channel estimation and symbol synchronization. The users are assumed to be

separated by a considerable distance so that the antennas of different users are not correlated. The channel estimation and symbol synchronization at the BS is also assumed to be ideal.

The BS employs space-code matched filtering to separate the different user groups. The  $K \times 1$  sufficient statistic vector  $\mathbf{Y}_{\text{MU}}$  is then fed to the layered space-time decorrelator which eliminates the remaining inter-user interference to produce the estimated symbol vector  $\hat{\mathbf{b}} = [\hat{b}_1, \dots, \hat{b}_k]$ . The vector  $\mathbf{Y}_{\text{MU}}$  is given by

$$\mathbf{Y}_{\text{MU}} = \sum_{p=1}^P \mathbf{C}_p^H \mathbf{S}^T \mathbf{r}_p = \tilde{\mathbf{R}}_{\text{MU}} \mathbf{b} + \tilde{\mathbf{n}} \quad (32)$$

where  $\tilde{\mathbf{R}}_{\text{MU}}$  is the  $K \times K$  space-code cross-correlation matrix,

$$\tilde{\mathbf{R}}_{\text{MU}} = \sum_{p=1}^P \mathbf{X}_p^H \mathbf{X}_p \quad (33)$$

with  $\mathbf{X}_p = \mathbf{S}\mathbf{C}_p$ . The  $K \times 1$  real Gaussian noise vector  $\tilde{\mathbf{n}}$  with covariance matrix  $\sigma^2 \mathbf{R}_{\text{MU}}$  is given by

$$\tilde{\mathbf{n}} = \sum_{p=1}^P \mathbf{X}_p^H \mathbf{n}_p \quad (34)$$

The detection algorithm is iterative and consists of three steps: 1) computation of the nulling vector, 2) user

signal estimation and 3) interference cancellation (SIC).

For the  $i$ -th iteration, the first step consists of calculating the pseudoinverse  $[\tilde{\mathbf{R}}_{\text{MU}}(i)]^+$  of  $\tilde{\mathbf{R}}_{\text{MU}}(i)$ . The user signals are then ranked according to their post detection SNRs (following the space-code matched filtering) and the user having the highest SNR, given by

$$k_i = \arg \max_{j \in \{k_i, \dots, k_{i-1}\}} \frac{\|b_j\|^2}{\sigma^2 [\tilde{\mathbf{R}}_{\text{MU}}(i)]_{(j,j)}^+} \quad (35)$$

is selected. The subscripts  $i$  and  $j$  in this equation denote the elements of an array, vector or matrix. The nulling vector for the selected user is  $\mathbf{w}_{k_i} = [\tilde{\mathbf{R}}_{\text{MU}}(i)]_{k_i}^+$ , i.e., the  $k_i$ -th column of  $[\tilde{\mathbf{R}}_{\text{MU}}(i)]^+$ . The slicer output is then given by

$$z_{k_i} = \mathbf{w}_{k_i}^T \mathbf{Y}_{\text{MU}}(i) \quad (36)$$

resulting in the estimated symbol  $\hat{b}_{k_i}$ . The final step is interference cancellation where the detected symbol is subtracted from the received signal vector resulting in the symbol vector for the next iteration  $i+1$ , given by

$$\mathbf{r}_p(i+1) = \mathbf{r}_p(i) - (\mathbf{X}_p(i))_{k_i} \hat{b}_{k_i} \quad (37)$$

where  $(\mathbf{X}_p(i))_{k_i}$  is the  $k_i$ -th column of  $\mathbf{X}_p(i)$ . Similarly,  $\mathbf{X}_p(i+1)$  and  $\tilde{\mathbf{R}}_{\text{MU}}(i+1)$  are obtained by striking out the  $k_i$ -th column of  $\mathbf{X}_p(i)$  and the  $k_i$ -th row and column of  $\tilde{\mathbf{R}}_{\text{MU}}(i)$  respectively.  $\mathbf{Y}_{\text{MU}}(i+1)$  is then given by

$$\mathbf{Y}_{\text{MU}}(i+1) = \sum_{p=1}^P \mathbf{X}_p(i+1)^H \mathbf{r}_p(i+1) \quad (38)$$

This process is repeated until all  $K$  user signals are detected. Two reduced complexity versions of LAST-MUD called serial layered space-time group multiuser detector (LASTG-MUD) and parallel LASTG-MUD are also presented in [50].

**Figure 31** shows the SER performance of the LAST-MUD scheme using 4-QAM modulation with 12 simultaneous users (single-antenna) and 6 BS antennas, as the no. of user groups is increased. Fixed spreading factor of  $N = 15$  is used. The performance improves as the users are distributed into more (smaller) groups since the no. of unique spreading codes also increases. For  $G = 1$ , the performance is equivalent to V-BLAST and represents the worst case.

**Figure 32** shows the SER performance as the no. of users is increased by adding more user groups with  $M =$

4 users per group. The LAST-MUD scheme provides substantial increase in network capacity by accommodating a large no. of simultaneous users with good SER performance.

#### 4.1.3. SMMSE SIC MUD

A MUD scheme for MIMO-OFDM systems referred to as successive MMSE receive filtering with SIC (SMMSE SIC) is presented in [51]. The MMSE SIC MUD suffers from performance loss in scenarios with multiple closely spaced antennas located at the same UE. The proposed scheme tackles this problem by successively calculating the rows of the receive matrix at the BS for each of the UE transmit antennas, followed by SIC thus transforming the uplink MU-MIMO channel into a set of parallel SU-MIMO channels.

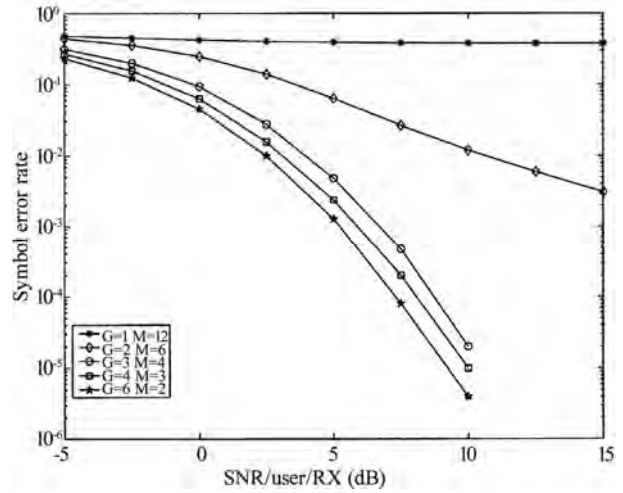


**Figure 31.** Grouping effect on SER performance of LAST-MUD [50].

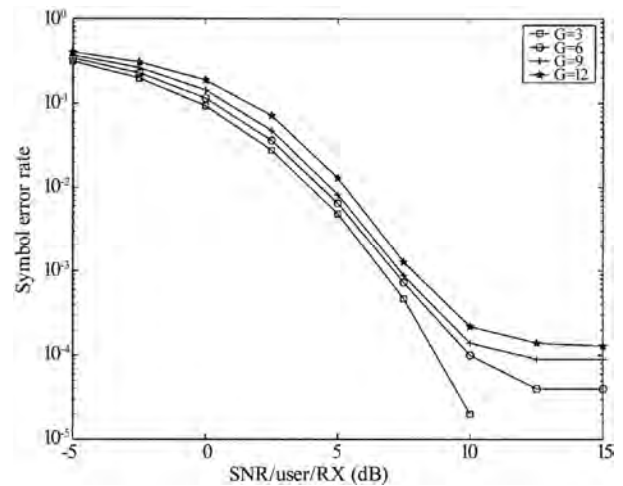


**Figure 32.** SER performance of LAST-MUD with increasing number of users [50].

**Figure 33** shows the MU-MIMO uplink employing SMMSE SIC detection. The system consists of  $K$  simultaneous users, each equipped with  $M_{T_i}$  transmit antennas for  $i=1, \dots, K$  and therefore, a total of  $M_T = \sum_{i=1}^K M_{T_i}$  transmit antennas. The BS has  $M_R$  receive antennas.  $s_i$  and  $r_i$  represent the  $i$ -th user data vector and the receive vector respectively whereas  $D_i$  and  $F_i$  are the respective UE transmit matrix and the BS receive matrix. The MIMO channel matrix is represented as

$$\mathbf{H} = [\mathbf{H}_1 \mathbf{H}_2 \dots \mathbf{H}_K] \quad (39)$$

where  $\mathbf{H}_i \in \mathbb{C}^{M_R \times M_{T_i}}$  is the MIMO channel matrix between user  $i$  and the BS for  $i = 1, \dots, K$ . The  $M_R \times M_T$  receive filter matrix at the BS is given by

$$\mathbf{F} = [\mathbf{F}_1 \mathbf{F}_2 \dots \mathbf{F}_K] \quad (40)$$

where  $\mathbf{F}_i \in \mathbb{C}^{M_{T_i} \times M_R}$  corresponds to the  $i$ -th user. Each row of  $\mathbf{F}_i$  corresponds to one of the  $M_{T_i}$  transmit antennas at the UE.

The proposed algorithm successively calculates the rows of each  $\mathbf{F}_i$  using the MMSE criterion such that the users are ordered according to their respective total MSE in ascending order (starting with the minimum MSE). The total MSE of user  $i$  is obtained by summing up the MSE corresponding to each of its individual transmit antennas. Following the receive filtering by the receive filter matrix  $\mathbf{F}$ , SIC is performed to eliminate the MUI. This process has the effect of transforming the multiuser uplink channel into a set of parallel  $M_{T_i} \times M_{T_i}$  SU-MIMO channels represented as  $\mathbf{F}_i \mathbf{H}_i$ .

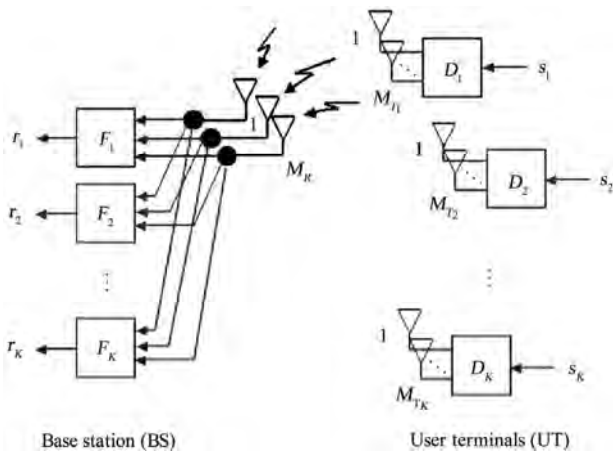


**Figure 33.** Block diagram of SMMSE SIC MUD based MU-MIMO system [51].

The SMMSE SIC detection in [51] has been considered for STBC based MIMO transmission i.e. the Alamouti scheme and also for dominant eigenmode transmission (DET). The open-loop Alamouti scheme provides MIMO diversity without the need for any CSI at the UEs. On the other hand, DET requires full CSI at both the transmitter and the receiver, which means that the UE transmit matrices  $D_i$  need to be computed at the BS and then fed forward to the UEs. However, beside the full diversity gain equal to that of STBC, DET also provides the maximum array gain by transmitting over the strongest eigenmode of the MIMO channel [49,51,52].

**Figure 34** shows the BER performance of SMMSE SIC Alamouti in comparison with V-BLAST. The impact of channel estimation errors is also shown. The simulated MIMO-OFDM system consists of 6 BS antennas and 3 UEs equipped with 2 antennas each, denoted as  $6 \times \{2, 2, 2\}$  MU-MIMO configuration. The MIMO channel  $\mathbf{H}$  is assumed to be frequency selective with the power delay profile defined by IEEE 802.11n-D for non-line-of-sight (NLOS) conditions. The channel model for each user's channel  $\mathbf{H}_i$  takes into account the antenna correlation at the BS. However, the antennas at each UE are considered to have low spatial correlation assuming large angular spread at the user. A total of 64 OFDM subcarriers are used with subcarrier spacing of 150 kHz. The user data is encoded using a 1/2 rate convolutional code. 4-QAM modulation is used for each subcarrier of SMMSE SIC Alamouti system while BPSK is used for V-BLAST so that the data rate remains the same for both systems.

Clearly, the SMMSE SIC Alamouti system outperforms V-BLAST by a large margin particularly when the channel estimation errors are taken into account.

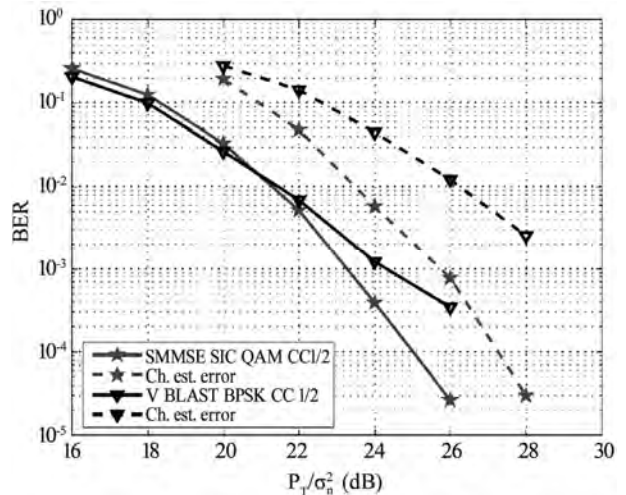


**Figure 34.** BER performance of SMMSE SIC Alamouti and V-BLAST for  $6 \times \{2, 2, 2\}$  configuration [51].

**Figure 35** shows the performance gain of SMMSE SIC DET over SMMSE SIC Alamouti. SMMSE SIC DET shows substantial gains in the high SNR region and these become more significant as the no. of users in the system increases.

**4.1.4. Turbo MUD**

An iterative Turbo MMSE MUD scheme is presented in [53] for single-carrier (SC) space-time trellis-coded (STTC) SDMA MIMO systems in frequency-selective fading channels. This scheme can jointly detect multiple UE transmit antennas while cancelling the MUI from undetected users along with co-channel interference (CCI) and ISI through soft cancellation. Unknown co-channel interference (UCCI) from other interferers not known to the system is also considered. It is also shown that the no. of BS antennas required to achieve the corresponding lower performance bound of single-user detection is equal to the no. of users rather than the total no. of transmit antennas. The receiver derivations in [53] are provided for  $M$ -PSK modulation but can be extended to QAM as well.

**Figure 36** shows the system model while the UE transmitter block diagram is given in **Figure 37**. The system has a total of  $K + K_I$  simultaneous users, each indexed by  $k = 1, \dots, K, K + 1, \dots, K_I$  where the first  $K$  are the users to be detected at the BS while the remaining  $K_I$  are unknown interfering users representing the source of UCCI. Each UE is equipped with  $N_T$  transmit antennas. However, the system can also support unequal no. of antennas at the UEs. Each UE encodes the bit sequence  $c_k(i)$  for  $i = 1, \dots, BN_T$  using a rate  $k_0 / N_T$  STTC code, where  $B$  represents the frame length in symbols. The encoded sequences  $b_k(i) \in \mathbb{Q}$ ,  $i = 1, \dots, BN_T$  are

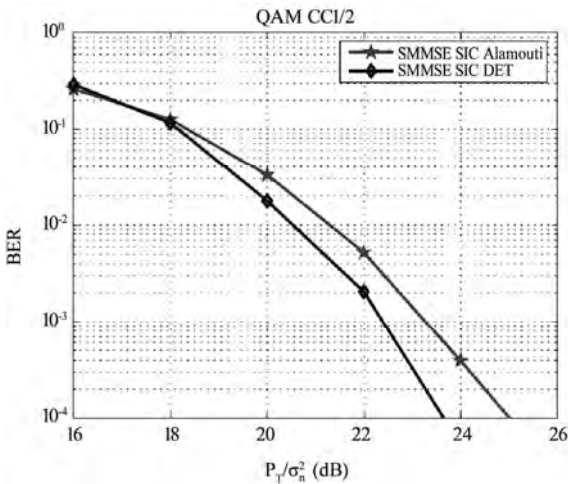


**Figure 35. BER performance of SMMSE SIC Alamouti and SMMSE SIC DET for  $6 \times \{2, 2, 2\}$  configuration [51].**

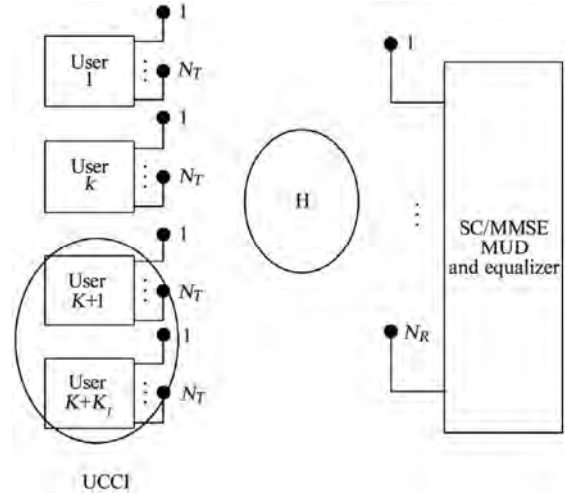


**Figure 36. System model of Turbo MUD based STTC MU-MIMO system [53].**

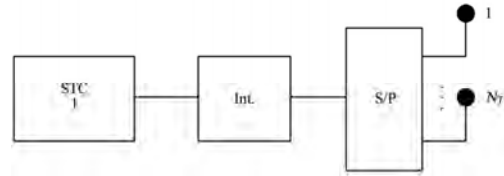


**Figure 37. UE transmitter block diagram [53].**

grouped into  $B$  blocks of  $N_T$  symbols, where  $\mathbb{Q} = \{\alpha_1, \dots, \alpha_{2^b}\}$  represents the modulation alphabet of  $M$ -PSK, and then interleaved by user-specific permutation of blocks of length  $N_T$  within a frame, such that the positions within each block remain unchanged. This interleaving process preserves the rank properties of the STTC code. User-specific training sequences of length  $TN_T$  are then attached at the start of the interleaved sequences. After serial-to-parallel (S/P) conversion of the entire frame, the resulting sequences  $b_k^{(n)}(i)$  for  $n = 1, \dots, N_T$ ,  $i = 1, \dots, B + T$  are transmitted over the frequency-selective MIMO channel using the  $N_T$  transmit antennas.

The transmit signals from all users are received at the  $N_R$  BS receive antennas. The space-time sampled received signal vector  $\mathbf{y}(i) \in \mathbb{C}^{N_R \times 1}$  at time instant  $i$  is given by

$$\mathbf{y}(i) = \underbrace{\mathbf{H}\mathbf{u}(i)}_{\text{desired}} + \underbrace{\mathbf{H}_I\mathbf{u}_I(i)}_{\text{UCCI}} + \underbrace{\mathbf{n}(i)}_{\text{noise}}, \quad i = 1, \dots, T + B \quad (41)$$

which can also be represented as

$$\mathbf{y}(i) = [\mathbf{r}^T(i + L - 1), \dots, \mathbf{r}^T(i)]^T \quad (42)$$



From the second iteration onward, the soft feedback vector  $\bar{\mathbf{u}}(i)$  from the APP (also MAP) SISO decoding is used to obtain the covariance matrix estimate

$$\hat{\mathbf{R}} = \frac{1}{T} \sum_{i=1}^T (\mathbf{y}(i) - \hat{\mathbf{H}}\mathbf{u}(i))(\mathbf{y}(i) - \hat{\mathbf{H}}\mathbf{u}(i))^H + \frac{1}{B} \sum_{i=T+1}^{T+B} (\mathbf{y}(i) - \hat{\mathbf{H}}\bar{\mathbf{u}}(i))(\mathbf{y}(i) - \hat{\mathbf{H}}\bar{\mathbf{u}}(i))^H. \quad (48)$$

Vector  $\bar{\mathbf{u}}(i)$  consists of the sequences  $\bar{b}_k^{(n)}(i)$  calculated using the *a posteriori* probability  $P_{\text{SISO}}^{\text{APP}}$ . The signals  $b_k^{(n)}(i)$ ,  $n=1, \dots, n_0$  for user  $k$  are jointly detected using a linear MMSE MUD which filters the signal vector

$$\mathbf{y}_k^{(l)} = \mathbf{y}(i) - \mathbf{H}\mathbf{u}_k^{(l)}(i), \quad i = T+1, \dots, B+T \quad (49)$$

where the vector  $\mathbf{u}_k^{(l)}(i)$  is calculated using the *extrinsic* probability  $P_{\text{SISO}}^{\text{ext}}$  obtained after APP SISO decoding and  $(\cdot)^{(l)}$  denotes the first set of  $n_0$  antennas for user  $k$ . The weighting matrix  $\mathbf{W}_k^{(l)}(i)$  for the MMSE MUD satisfies the criterion,

$$[\mathbf{W}_k^{(l)}(i), \mathbf{A}_k^{(l)}(i)] = \arg \min_{\mathbf{W}, \mathbf{A}} \|\mathbf{W}^H \mathbf{y}_k^{(l)}(i) - \mathbf{A}^H \boldsymbol{\beta}_k^{(l)}(i)\|^2 \quad (50)$$

subject to the constraint  $[\mathbf{A}]_{j,j} = 1$ ,  $j=1, \dots, n_0$  to avoid the trivial solution  $[\mathbf{W}_k^{(l)}(i), \mathbf{A}_k^{(l)}(i)] = [\mathbf{0}, \mathbf{0}]$ . The vector  $\boldsymbol{\beta}_k^{(l)}(i) \in \mathbb{C}^{n_0 \times 1}$  is given by

$$\boldsymbol{\beta}_k^{(l)}(i) = [b_k^{(1)}(i), \dots, b_k^{(n_0)}(i)]^T. \quad (51)$$

The corresponding output  $\mathbf{z}_k^{(l)}(i) \in \mathbb{C}^{n_0 \times 1}$  of the MMSE MUD is given by

$$\mathbf{z}_k^{(l)}(i) = \mathbf{W}_k^{(l)}(i) \mathbf{y}_k^{(l)}(i) = \boldsymbol{\Omega}_k^{(l)}(i) \boldsymbol{\beta}_k^{(l)}(i) + \boldsymbol{\psi}_k^{(l)}(i) \quad (52)$$

where the matrix  $\boldsymbol{\Omega}_k^{(l)}(i) \in \mathbb{C}^{n_0 \times n_0}$  consists of the equivalent channel gains after filtering and  $\boldsymbol{\psi}_k^{(l)}(i) \in \mathbb{C}^{n_0 \times 1}$  is the filtered AWGN vector. The MMSE MUD outputs  $\mathbf{z}_k^{(\gamma)}(i)$  along with the parameters  $\boldsymbol{\Omega}_k^{(\gamma)}(i)$  and  $\boldsymbol{\psi}_k^{(\gamma)}(i)$  for all antenna sets  $\gamma=1, \dots, N_T/n_0$  of user  $k$ , are passed on to the APP SISO detector which calculates the *extrinsic* probabilities for SISO decoding. This iterative procedure is continued for all antenna sets of the remaining users until all users are detected. The complexity of this receiver is primarily associated with the MMSE and APP blocks and is on the order of  $\mathcal{O}\{\max(L^3 N_R^3, 2^{k_0 n_0})\}$ .

Two special cases of the proposed receiver architecture are considered in [53]. Receiver 1, with  $n_0 = 1$ , detects the transmit antennas of user  $k$  one by one. This receiver type has the lowest complexity since the complexity depends exponentially on  $n_0$ . Receiver 2, with  $n_0 = N_T$ , jointly detects all  $N_T$  transmit antennas of user  $k$  and has the highest complexity.

The simulated SER and FER performance of the two receiver types vs. per-antenna  $E_s/N_0$  is shown in **Figure 39** and **Figure 40**, for a particular user referred to as user 1. Performance comparison with optimal joint ML

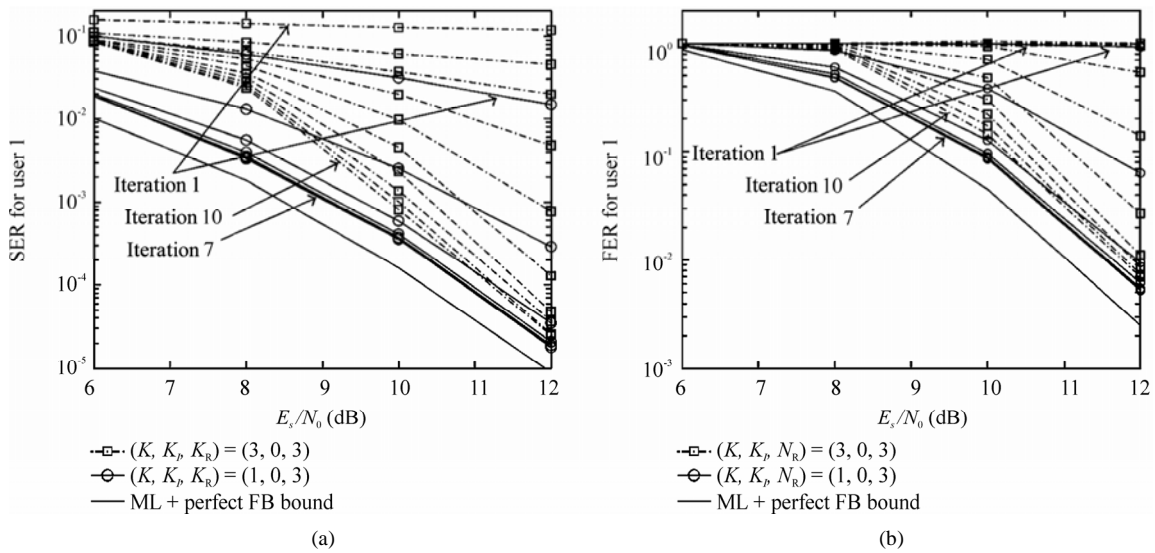


**Figure 39.** Receiver 1's (a) SER and (b) FER performance,  $(K, K_p, N_R) = (3, 0, 3)$  and  $(1, 0, 3)$ ,  $N_T = 2$  [53].

detection of all  $N_T$  antennas of user 1 followed by MAP SISO decoding assuming perfect feedback (FB), is also provided. The results are provided for 1 and 10 iterations for  $(K, K_I, N_R) = (3, 0, 3)$  and for 1 and 7 iterations for  $(K, K_I, N_R) = (1, 0, 3)$  with  $N_T = 2$  transmit antennas per user.  $K$ ,  $K_I$  and  $N_R$  represent the no. of desired users, unknown interferers (UCCI) and BS receive antennas. QPSK modulation is used for transmission and frequency-selective fading is assumed with  $L = 5$  uncorrelated Rayleigh distributed paths. For a sufficient no. of iterations, both receivers perform reasonably

close to the ML receiver, particularly in the high SNR region. Receiver 2 shows slightly better performance than receiver 1.

**Figure 41** shows the SER and FER performance of the two receivers for  $(K, K_I, N_R) = (2, 1, 3)$  with  $N_T = 2$  transmit antennas per desired user and a single transmit antenna for the unknown interferer (UCCI) i.e.  $N_I = 1$ . Two cases of signal-to-UCCI interference ratio (SIR) are considered. For SIR = 3 dB, the signal transmitted from UCCI's antenna is assumed to have the same power as that of the signal from one antenna of the desired user whereas, for SIR = 0 dB, UCCI's antenna transmits at

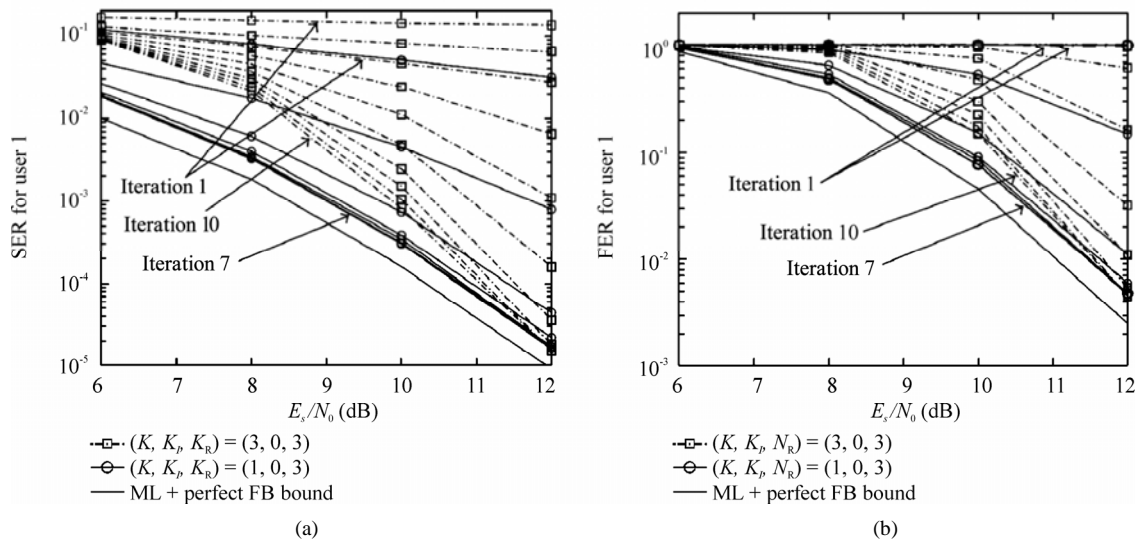


**Figure 40.** Receiver 2's (a) SER and (b) FER performance,  $(K, K_I, N_R) = (3, 0, 3)$  and  $(1, 0, 3)$ ,  $N_T = 2$  [53].

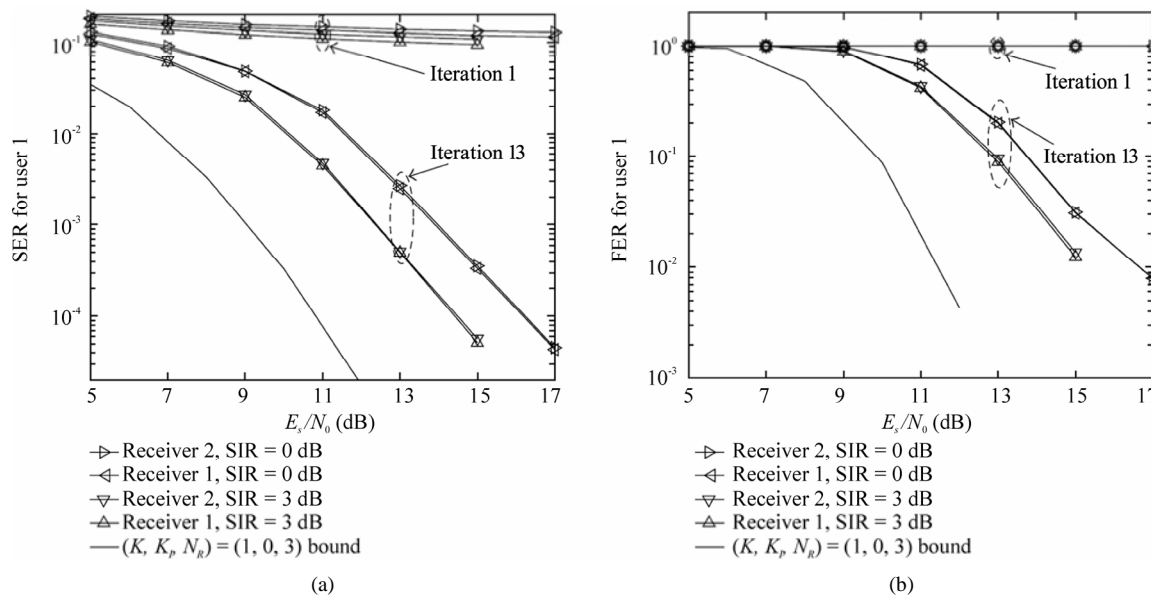


**Figure 41.** Receiver 1's and 2's (a) SER and (b) FER performance,  $(K, K_I, N_R) = (2, 1, 3)$ ,  $N_T = 2$ ,  $N_I = 1$  [53].

twice the transmit power of a desired user’s antenna. The performance of both receivers is obviously better for the 3 dB SIR case. However, the UCCI has a considerable impact on performance and more iterations are needed to achieve a reasonably low SER or FER. The performance will degrade further in case of multiple UCCI antennas and also as the UCCI sources i.e. the no. of unknown interferers increase.

**4.1.5. Genetic Algorithm (GA) Assisted MUDs**

Genetic algorithms (GAs) are based on the theory of evolution’s concept of survival of the fittest, where the genes from the fittest individuals of a species are passed on to the next generation through the process of “natural selection”. When applied to MUDs, an “individual” represents the  $L$ -dimensional MUD weight vector corresponding to the  $L$  users. These MUD weights are then optimized using GA by genetic operations of “mating” and “mutation” to get a new generation of individuals i.e. the MUD weights. The initial “population” (MUD weights) is typically obtained from the MMSE solution which is retained throughout the GA search process as an alternate solution in case of poor convergence [3].

Considering the SDMA-OFDM system model of **Figure 27** with a single transmit antenna at each UE and  $P$  receive antennas at the BS, the ML-based decision metric or objective function (OF) for a GA-assisted MUD corresponding to the  $p$ -th receive antenna can be written as

$$\Omega_p(\tilde{\mathbf{s}}) = |x_p - \mathbf{H}_p \tilde{\mathbf{s}}|^2 \tag{53}$$

where  $x_p$  is the received symbol corresponding to the  $p$ -th BS antenna for a specific OFDM subcarrier and

$\mathbf{H}_p$  is the  $p$ -th row of the channel transfer function matrix  $\mathbf{H}$ . The estimated symbol vector of the  $L$  users corresponding to the  $p$ -th BS antenna is then given by

$$\hat{\mathbf{s}}_{\text{GA}_p} = \arg \left\{ \min_{\tilde{\mathbf{s}}} \left[ \Omega_p(\tilde{\mathbf{s}}) \right] \right\} \tag{54}$$

The combined decision metric for the  $P$  receive antennas can therefore be written as

$$\Omega(\tilde{\mathbf{s}}) = \sum_{p=1}^P \Omega_p(\tilde{\mathbf{s}}) = \|\mathbf{x} - \mathbf{H}\tilde{\mathbf{s}}\|^2 \tag{55}$$

Therefore, the decision rule for the GA-assisted MUD is to find an estimate  $\hat{\mathbf{s}}_{\text{GA}}$  of the  $L \times 1$  transmitted symbol vector such that  $\Omega(\tilde{\mathbf{s}})$  is minimized [3].

Review and analysis of various GA-assisted MUDs is provided in [3] for the SDMA-OFDM uplink consisting of a single transmit antenna at each UE. **Figure 42** shows the schematic diagram of the SDMA-OFDM uplink system based on the concatenated MMSE-GA MUD. The concatenated MMSE-GA MUD uses the MMSE estimate  $\hat{\mathbf{s}}_{\text{MMSE}} \in \mathbb{C}^{L \times 1}$  of the transmitted symbol vector of the  $L$  users as initial information for the GA.  $\hat{\mathbf{s}}_{\text{MMSE}}$  is given by

$$\hat{\mathbf{s}}_{\text{MMSE}} = \mathbf{W}_{\text{MMSE}}^H \mathbf{x} \tag{56}$$

where  $\mathbf{W}_{\text{MMSE}} \in \mathbb{C}^{P \times L}$  is the MMSE MUD weight matrix, expressed as

$$\mathbf{W}_{\text{MMSE}} = (\mathbf{H}\mathbf{H}^H + \sigma_n^2 \mathbf{I})^{-1} \mathbf{H} \tag{57}$$

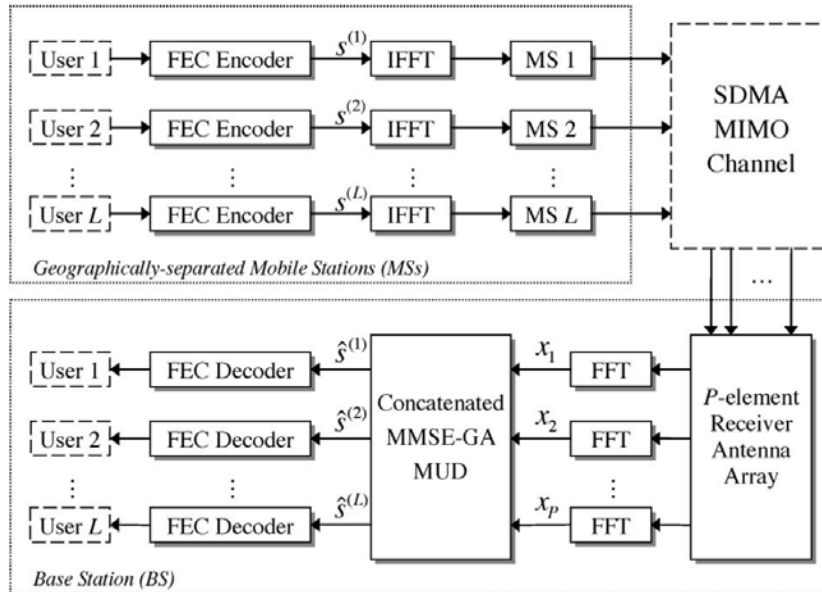


**Figure 42.** SDMA-OFDM uplink system based on concatenated MMSE-GA MUD [3].

Using this MMSE estimate, the 1<sup>st</sup> GA generation,  $y = 1$  containing a population of  $X$  individuals, is created. The  $x$ -th individual is a symbol vector denoted as

$$\tilde{\mathbf{s}}_{(y,x)} = \left[ \tilde{s}_{(y,x)}^{(1)}, \tilde{s}_{(y,x)}^{(2)}, \dots, \tilde{s}_{(y,x)}^{(L)} \right], \quad x = 1, \dots, X \quad (58)$$

$$y = 1, \dots, Y$$

where each element  $\tilde{s}_{(y,x)}^{(l)}$  called a *gene*, belongs to the set of complex-valued modulation symbols corresponding to the particular modulation scheme used.

The GA search procedure shown in **Figure 43** is then initiated, which involves several GA operations like *mating, mutation, elitism* etc. leading to the next generation. This process is repeated for  $Y$  generations and the individual with the highest *fitness value* is considered to be the detected  $L \times 1$  multiuser symbol vector for the

corresponding OFDM subcarrier. All users are jointly detected by the concatenated MMSE-GA MUD and therefore, no error propagation exists between the detected users.

Enhanced GA MUDs, utilizing an advanced mutation technique called biased Q-function-based mutation (BQM) instead of the conventional uniform mutation (UM), and incorporating the iterative turbo trellis coded modulation (TTCM) scheme for FEC decoding, are also discussed in [3]. **Figure 44** shows the schematic diagram of an MMSE-initialized iterative GA (IGA) MUD incorporating TTCM. The  $P \times 1$  received symbol vector  $\mathbf{x}$  is detected by the MMSE MUD to get the estimated symbol vector  $\hat{\mathbf{s}}_{\text{MMSE}}$  of the  $L$  users consisting of the symbols  $\hat{s}_{\text{MMSE}}^{(l)}$ ,  $l = 1, \dots, L$ . Each of these symbols are then

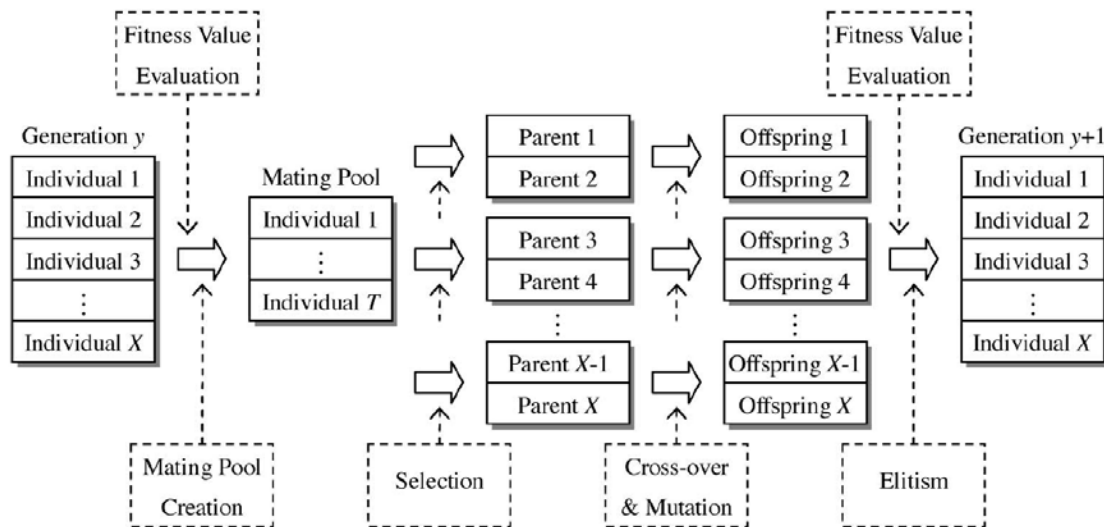


Figure 43. GA search procedure for one generation [3].

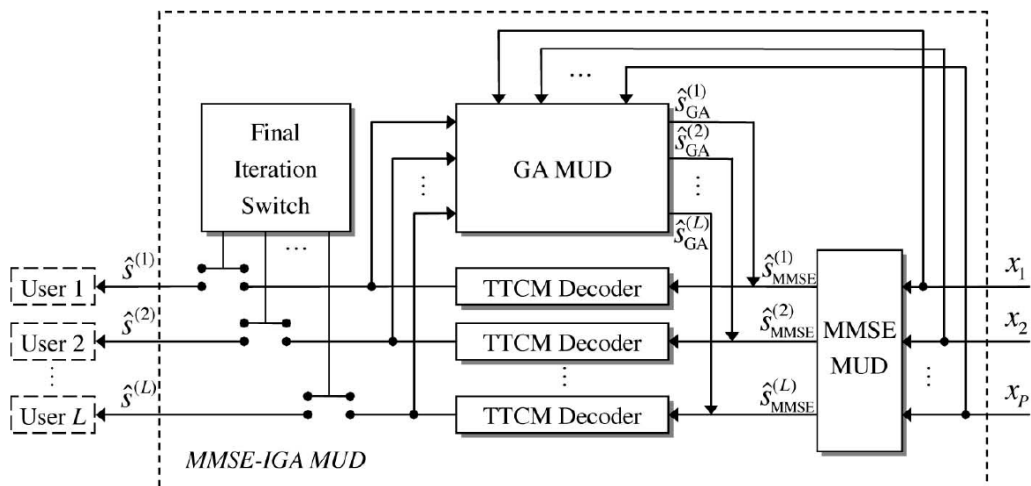


Figure 44. Schematic diagram of an IGA MUD [3].

decoded by a TTCM decoder to get a more reliable estimate. The resulting symbol vector is then used as the initial information for the GA MUD. The GA-estimated symbol vector  $\hat{s}_{GA}$  is then fed back to the TTCM decoders for further improvement of the estimate. This optimization process involving the GA MUD and the TTCM decoders is continued for a desired no. of iterations. The final estimates  $\hat{s}^{(l)}$  of the  $L$  users' symbols are then obtained at the output after the final iteration.

Figure 45 shows the BER performance comparison of various MMSE-initialized TTCM-assisted GA and IGA MUD based SDMA-OFDM systems consisting of  $L = 6$  (single-antenna) users and  $P = 6$  BS antennas. 4-QAM modulation and SWATM channel model is used. GA population size of  $X = 20$  (also  $X = 10$  for TTCM, MMSE-IGA (2)) and a total of  $Y = 5$  generations are considered. UM and BQM mutation schemes are employed. Performance curves for  $1 \times 1$  SISO AWGN,  $1 \times 6$  MRC AWGN, TTCM-MMSE SDMA-OFDM and TTCM-ML SDMA-OFDM systems are also provided for reference. The TTCM-MMSE-GA MUDs and the IGA MUDs in particular provide exceptionally good BER performance. The performance of the TTCM-MMSE-IGA scheme with 2 iterations and  $X = 20$  (represented as TTCM, MMSE-IGA (2) in the figure), is in fact identical to the optimum TTCM-ML MUD.

The BER performance comparison for rank-deficient scenarios where the no. of users exceeds the no. of BS antennas resulting in insufficient degrees of freedom for separating the users, is given in Figure 46. Performance curves for  $L = 6, 7$  and  $8$  users and  $P = 6$  BS antennas are provided. The IGA MUD schemes still perform reasonably good with relatively small performance degradation.

Figure 47 compares the complexity of the TTCM-MMSE-GA and TTCM-ML MUDs in terms of the no. of

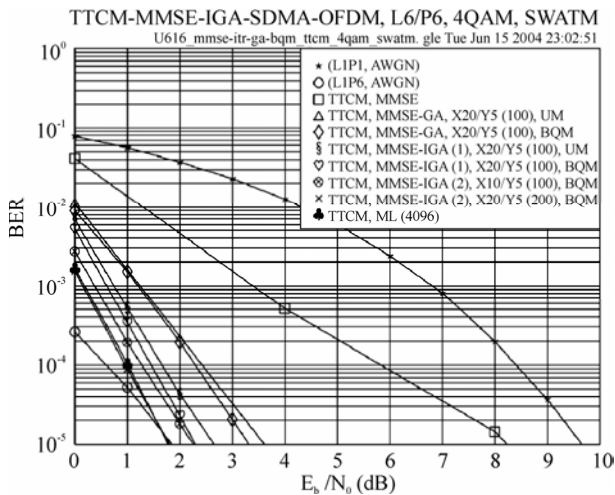


Figure 45. BER performance of TTCM-MMSE-GA/IGA SDMA-OFDM systems,  $L = 6, P = 6$  [3].

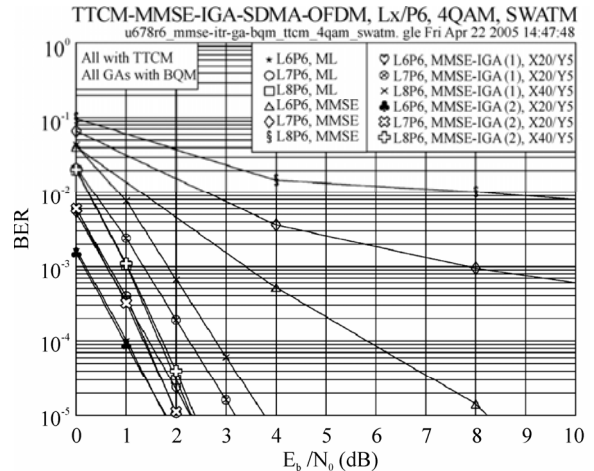


Figure 46. BER performance of TTCM-MMSE-GA/IGA SDMA-OFDM systems,  $L = 6, 7, 8$  and  $P = 6$  [3].

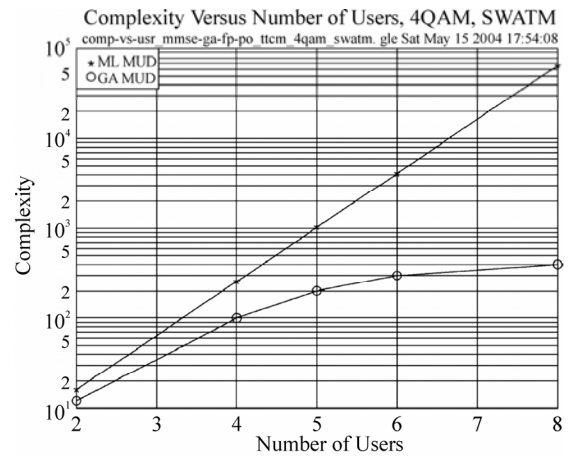


Figure 47. Complexity of TTCM-MMSE-GA and TTCM-ML SDMA-OFDM systems vs. no. of users,  $L = P$  [3].

OF calculations, as the no. of users increase. The no. of BS antennas is kept equal to the no. of users i.e.  $L = P$ . The complexity of the GA MUD increases very slowly with the number of users as compared to the ML MUD, resulting in a huge difference as more users are added to the system.

### 4.2. The MU-MIMO Downlink

The MU-MIMO downlink channel is referred to as the MIMO broadcast channel (MIMO-BC) [49] where the BS equipped with multiple antennas, simultaneously transmits data to multiple UEs consisting of one or more antennas each, as shown in Figure 48. The multiuser interference (MUI) (also called multiple access interference, MAI) can be suppressed by means of transmit beamforming or "dirty paper" coding. Therefore, CSI

feedback from each user is required for precoding at the BS. Various linear and nonlinear precoding techniques for MU-MIMO downlink systems are discussed in the following text.

**4.2.1. Channel Inversion**

Channel inversion is a linear precoding technique for MU-MIMO downlink systems where each UE is equipped with a single receive antenna. As the name suggests, channel inversion uses the inverse of the channel matrix for precoding to remove the MUI, as illustrated in **Figure 49**.

Assuming that the no. of receive antennas  $M_R \leq M_T$ , the no. of transmit antennas, ZF precoding can be used for this purpose. The  $M_T \times 1$  transmitted signal vector is then given by

$$\begin{aligned} \mathbf{x} &= \mathbf{H}^+ \mathbf{d} \\ &= \mathbf{H}^H (\mathbf{H}\mathbf{H}^H)^{-1} \mathbf{d} \end{aligned} \tag{59}$$

where  $\mathbf{d}$  is the vector of data symbols to be precoded and  $\mathbf{H}^+$  is the pseudoinverse of the  $M_R \times M_T$  channel matrix  $\mathbf{H}$ . Vector  $\mathbf{d}$  can have any dimension up to the rank of  $\mathbf{H}$  [48]. The  $i$ -th column of the prefiltering or precoding matrix  $\mathbf{P}_{ZF}$  is given by [49]

$$\mathbf{p}_{ZF,i} = \frac{\mathbf{h}_i^{(+)}}{\sqrt{\|\mathbf{h}_i^{(+)}\|^2}} \tag{60}$$

where  $\mathbf{h}_i^{(+)}$  is the  $i$ -th column of  $\mathbf{H}^+$ . The combined received signal vector can be expressed as

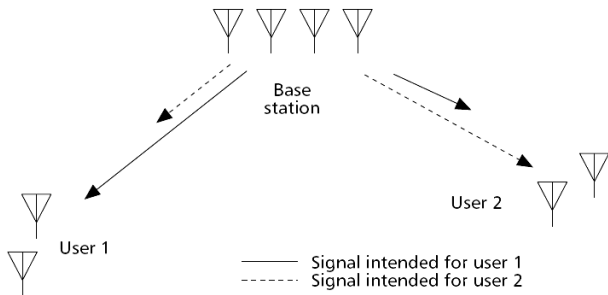


**Figure 48. The MU-MIMO downlink [48].**

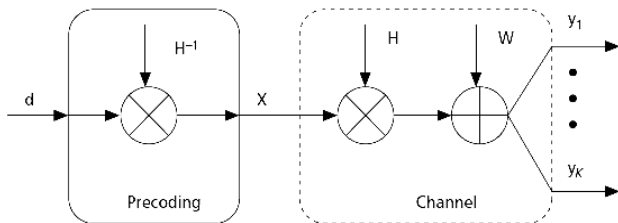


**Figure 49. Channel inversion [48].**

$$\mathbf{y} = \mathbf{d} + \mathbf{w} \tag{61}$$

where  $\mathbf{w}$  is the noise vector. Therefore, ZF precoding is only suitable for low-noise or high transmit power scenarios [48].

MMSE precoding, also called “regularized” channel inversion provides a better alternative. In this case, the transmitted signal vector is given by

$$\mathbf{x} = \mathbf{H}^H (\mathbf{H}\mathbf{H}^H + \alpha\mathbf{I})^{-1} \mathbf{d} \tag{62}$$

where  $\alpha$  is the loading factor. For a MU-MIMO downlink system with total transmit power  $P_T$  and  $K$  simultaneous users,  $\alpha = K / P_T$  maximizes the SINR at the receivers [48].

**4.2.2. Block Diagonalization**

Block diagonalization (BD) or block channel inversion, which was first proposed in [54], is a generalization of channel inversion to multi-antenna UEs [48]. BD also requires the total no. of receive antennas  $M_R$  to be less than or equal to the no. of transmit antennas  $M_T$  i.e.  $M_R \leq M_T$ .

Consider the system model of **Figure 50**. The system consists of  $K$  simultaneous users each having  $M_{R_i}$  receive antennas for  $i = 1, \dots, K$  such that the total no. of receive antennas  $M_R = \sum_{i=1}^K M_{R_i}$ . The combined channel matrix  $\mathbf{H} \in \mathbb{C}^{M_R \times M_T}$  is given by

$$\mathbf{H} = [\mathbf{H}_1^T \ \mathbf{H}_2^T \ \dots \ \mathbf{H}_K^T]^T \tag{63}$$

where  $\mathbf{H}_i \in \mathbb{C}^{M_{R_i} \times M_T}$  represents the MIMO channel from the  $M_T$  BS antennas to user  $i$ . The combined precoding matrix  $\mathbf{P} \in \mathbb{C}^{M_T \times S}$  can be expressed as

$$\mathbf{P} = [\mathbf{P}_1 \ \mathbf{P}_2 \ \dots \ \mathbf{P}_K] \tag{64}$$

where  $\mathbf{P}_i \in \mathbb{C}^{M_T \times S_i}$  is the precoding matrix for the  $i$ -th user,  $S \leq M_R$  is the total no. of transmitted data streams and  $S_i \leq M_{R_i}$  is the no. of data streams transmitted to user  $i$ .  $\mathbf{P}$  needs to be selected in such a way that  $\mathbf{H}\mathbf{P}$  becomes block diagonal. To this end, a matrix  $\tilde{\mathbf{H}}_i$  is defined as

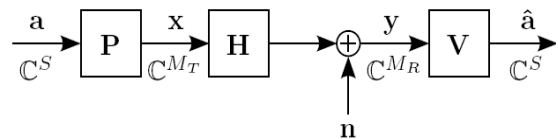


**Figure 50. System model for MU-MIMO downlink transmission [55].**

$$\tilde{\mathbf{H}}_i = [\mathbf{H}_1^T \cdots \mathbf{H}_{i-1}^T \mathbf{H}_{i+1}^T \cdots \mathbf{H}_K^T]^T \quad (65)$$

which contains all but the  $i$ -th user's channel matrix. Therefore,  $\mathbf{P}_i$  lies in the null space of  $\tilde{\mathbf{H}}_i$  and consists of unitary column vectors which are obtained by the SVD of  $\tilde{\mathbf{H}}_i$ , given by

$$\tilde{\mathbf{H}}_i = \tilde{\mathbf{U}}_i \tilde{\mathbf{D}}_i [\tilde{\mathbf{V}}_i^{(1)} \quad \tilde{\mathbf{V}}_i^{(0)}]^H \quad (66)$$

The rightmost  $M_T - \tilde{L}_i$  singular vectors  $\tilde{\mathbf{V}}_i^{(0)} \in \mathbb{C}^{M_T \times M_T - \tilde{L}_i}$  form an orthogonal basis for the null space of  $\tilde{\mathbf{H}}_i$  where  $\tilde{L}_i$  is the rank of  $\tilde{\mathbf{H}}_i$ . The product  $\mathbf{H}_i \tilde{\mathbf{V}}_i^{(0)}$  with dimensions  $M_{R_i} \times (M_T - \tilde{L}_i)$  represents the equivalent channel matrix for user  $i$  after eliminating the MUI. Thus, BD transforms the MU-MIMO downlink system into a set of  $K$  parallel  $(M_T - \tilde{L}_i) \times M_{R_i}$  SU-MIMO systems. Using SVD,  $\mathbf{H}_i \tilde{\mathbf{V}}_i^{(0)}$  can be expressed as

$$\mathbf{H}_i \tilde{\mathbf{V}}_i^{(0)} = \mathbf{U}_i \begin{bmatrix} \mathbf{D}_i & \mathbf{0} \\ \mathbf{0} & \mathbf{0} \end{bmatrix} [\mathbf{V}_i^{(1)} \quad \mathbf{V}_i^{(0)}]^H \quad (67)$$

where  $\mathbf{D}_i$  is an  $L_i \times L_i$  diagonal matrix, assuming  $L_i$  to be the rank of  $\mathbf{H}_i \tilde{\mathbf{V}}_i^{(0)}$ . The product of  $\tilde{\mathbf{V}}_i^{(0)}$  and the first  $L_i$  singular vectors  $\mathbf{V}_i^{(1)}$  produces an orthogonal basis of dimension  $L_i$  and represent the transmission vectors which maximize the information rate for the  $i$ -th user while eliminating the MUI. Therefore, the precoding matrix  $\mathbf{P}_i$  for user  $i$  consists of  $\tilde{\mathbf{V}}_i^{(0)} \mathbf{V}_i^{(1)}$  with appropriate power scaling. Optimal power allocation is achieved by water-filling, using the diagonal elements of the matrices  $\mathbf{D}_i$  and can either be implemented globally to maximize the overall information rate of the system or on a per-user basis [54,56,57].

#### 4.2.3. Successive Optimization

Successive optimization (SO) [54,56,57] is a successive precoding algorithm which addresses the power control problem in BD where capacity loss occurs due to the nulling of overlapping subspaces of different users. First, an optimum ordering of the users is determined like in case of V-BLAST detection. The precoding matrix for each user is then designed in a successive manner so that it lies in the null space of the channel matrices of the previous users only. In other words, the transmit power of user  $i$  is optimized in such a manner that it does not interfere with users  $1, \dots, i-1$ . However, interference with the successive users is allowed. The combined channel matrix for the previous  $i-1$  users can be written as

$$\hat{\mathbf{H}}_i = [\mathbf{H}_1^T \quad \mathbf{H}_2^T \quad \cdots \quad \mathbf{H}_{i-1}^T]^T \quad (68)$$

and its SVD is given by

$$\hat{\mathbf{H}}_i = \hat{\mathbf{U}}_i \hat{\mathbf{D}}_i [\hat{\mathbf{V}}_i^{(1)} \quad \hat{\mathbf{V}}_i^{(0)}]^H \quad (69)$$

$\hat{\mathbf{V}}_i^{(0)}$  contains the  $M_T - \hat{L}_i$  rightmost singular vectors where  $\hat{L}_i$  is the rank of  $\hat{\mathbf{H}}_i$ . The precoding matrix  $\mathbf{P}_i$  that lies in the null space of  $\hat{\mathbf{H}}_i$  is then determined as  $\mathbf{P}_i = \hat{\mathbf{V}}_i^{(0)} \mathbf{P}_i'$  for some choice of  $\mathbf{P}_i'$ .

#### 4.2.4. Dirty Paper Coding

Dirty paper coding is a nonlinear precoding technique and is based on the concept introduced by Costa [58] where the AWGN channel is modified by adding interference which is known at the transmitter. This concept is analogous to "writing on dirty paper" where the writing is the desired signal and the dirt represents the interference. Since the transmitter knows where the "dirt" or interference is, writing on dirty paper is the same as writing on clean paper [48].

In addition to SU-MIMO systems, e.g. the GMD-ZFDP scheme mentioned in Subsection 3.4, dirty paper coding is also applicable to MU-MIMO downlink transmission. In a MU-MIMO downlink system, CSI feedback from the users is available at the BS and it can figure out the interference produced at a particular user by the signals meant for other users. Therefore, dirty paper coding can be applied to each user's signal at the BS so that the known interference from other users is avoided.

Various dirty paper coding techniques for the MU-MIMO downlink are discussed in [48]. A well-known approach is to use QR decomposition of the channel matrix, given by  $\mathbf{H} = \mathbf{L}\mathbf{Q}$ , where  $\mathbf{L}$  is a lower triangular matrix and  $\mathbf{Q}$  is a unitary matrix.  $\mathbf{Q}^H$  is then used for transmit precoding which results in the effective channel  $\mathbf{L}$ . Therefore, the first user does not see any interference from the other users and no further processing of its signal is required at the BS. However, each of the subsequent users sees interference from the preceding users and dirty paper coding is applied to eliminate this known interference.

Another technique called *vector precoding* jointly precodes the users' signals rather than applying dirty paper coding to the users' signals individually. The vector precoding technique is shown in **Figure 51**. The desired signal vector  $\mathbf{d}$  is offset by a vector  $\mathbf{l}$  of integer values and this operation is followed by channel inversion, resulting in the transmitted signal  $\mathbf{x}$ , given by

$$\mathbf{x} = \mathbf{H}^{-1} (\mathbf{d} + \tau \mathbf{l}) \quad (70)$$

where the vector  $\mathbf{l}$  is chosen to minimize the power of  $\mathbf{x}$ , i.e.

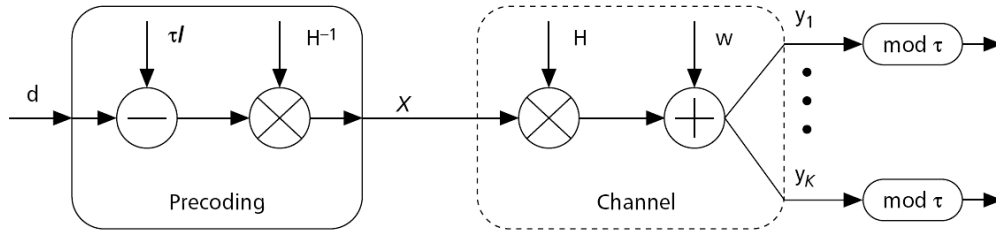


Figure 51. Vector precoding [48].

$$l = \arg \min_l \| \mathbf{H}^{-1} (\mathbf{d} + \tau l) \| \quad (71)$$

The signal received at the  $k$ -th user is expressed as

$$y_k = d_k + \tau l_k + w_k \quad (72)$$

where  $w_k$  represents the Gaussian noise. A modulo operation is then applied to remove the offset  $l_k$ , as given by

$$\begin{aligned} (y_k) \bmod \tau &= (d_k + \tau l_k + w_k) \bmod \tau \\ &= (d_k + w_k) \bmod \tau \end{aligned} \quad (73)$$

Regularized vector precoding is a modification of vector precoding which uses regularized (MMSE) channel inversion in place of simple channel inversion. The transmitted signal vector is then given by

$$\mathbf{x} = \mathbf{H}^H (\mathbf{H}\mathbf{H}^H + \alpha \mathbf{I})^{-1} (\mathbf{d} + \tau \mathbf{l}) \quad (74)$$

where the vector  $\mathbf{l}$  is chosen to minimize the norm of  $\mathbf{x}$  and  $\alpha = K / P_T$ . Dirty paper coding techniques based on vector precoding approach the *sum capacity* of the MU-MIMO downlink channel, which is defined as the maximum system throughput achieved by maximizing the sum of the information rates of all the users [48].

Figure 52 shows the performance comparison of vari-

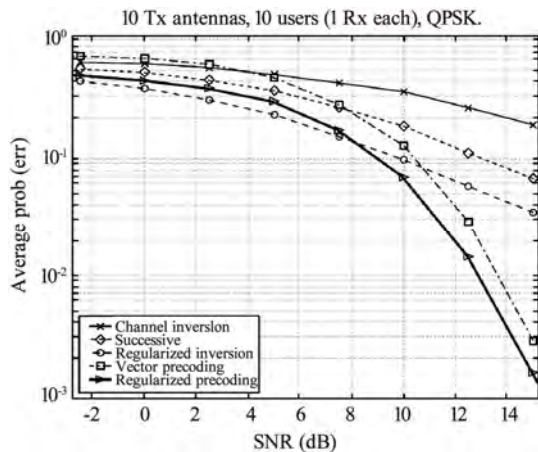


Figure 52. Performance comparison of various channel inversion and dirty paper coding techniques [48].

ous channel inversion and dirty paper coding techniques for uncoded MU-MIMO downlink transmission with  $M_T = 10$  BS transmit antennas and  $M_R = 10$  single-antenna UEs, using QPSK modulation. The vector precoding techniques clearly outperform the others at high SNR. However, regularized channel inversion performs even better than regularized vector precoding in the low SNR region. A possible reason for the performance loss of regularized vector precoding at low SNR is the use of a finite cubical lattice in this algorithm [48]. Use of different lattice strategies may result in improved performance.

#### 4.2.5. Tomlinson-Harashima Precoding

Tomlinson-Harashima precoding (THP) is a nonlinear precoding technique originally developed for SISO systems for temporal pre-equalization of ISI and is equivalent to moving the decision feedback part of the decision feedback equalizer (DFE) to the transmitter [59]. However, THP can also be applied to MU-MIMO downlink systems for MUI mitigation in the spatial domain.

Two MU-MIMO downlink transmission schemes utilizing THP are described in [57]. The first one called SO THP combines SO and THP to improve performance by eliminating residual MUI. SO THP involves successive BD, reordering of the users and finally, THP. Figure 53 shows the block diagram of the SO THP system (taken from [57] with a slight notational change). Here  $\mathbf{P}$  represents the combined precoding matrix for all users generated by SO, given by Equation 64.  $\mathbf{H}$  is the channel matrix and  $\mathbf{D}$  represents the combined demodulation (receive filtering) matrix. The lower triangular feedback matrix  $\mathbf{B}$  is generated in the last step and is used for THP. In order to generate matrix  $\mathbf{B}$ , the users are first arranged in the reverse order of precoding and then the lower diagonal

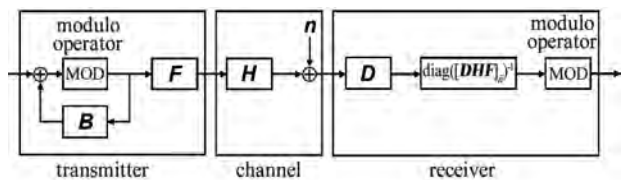


Figure 53. SO THP system block diagram [57].

equivalent combined channel matrix (which includes precoding and demodulation) is calculated, with singular values on the main diagonal. The elements in each row of this matrix are then divided by the corresponding singular values to obtain the feedback matrix  $\mathbf{B}$ . The order in which THP precoding is applied to the users' data streams is opposite to the order in which their precoding matrices are generated. Therefore, THP precoding starts with the data stream of the first user whose precoding matrix  $\mathbf{P}_1$  was generated last.

Use of THP results in increased transmit power and for this reason, a modulo operator is introduced at the transmitter and the receiver so that the constellation points are kept within certain boundaries. At the receiver, each data stream is divided by the corresponding singular value before applying the modulo operator, which ensures that the constellation boundaries remain the same as at the transmitter. Detailed description of SO THP is provided in [60].

The other scheme called MMSE THP [61] combines MMSE precoding and THP to eliminate the MUI below the main diagonal of the equivalent combined channel matrix. MMSE THP is an iterative precoding technique. The users are first arranged according to some optimal ordering criterion and the precoding matrix  $\mathbf{P}$  is calculated column by column starting from the last user  $K$ . The  $i$ -th column of  $\mathbf{P}$  corresponding to the  $i$ -th user is obtained using the corresponding  $i$  rows (first  $i$  rows for user  $K$ ) of the channel matrix  $\mathbf{H}$  according to the MMSE criterion, given by

$$\mathbf{P} = \beta (\mathbf{H}^H \mathbf{H} + \alpha \mathbf{I}_{M_T})^{-1} \mathbf{H}^H \quad (75)$$

where

$$\beta = \sqrt{\frac{P_T}{\text{tr}(\mathbf{P}\mathbf{x}\mathbf{x}^H\mathbf{P}^H)}}, \quad \alpha = \frac{M_R \sigma_n^2}{P_T}$$

$P_T$  represents the total transmit power,  $\mathbf{x}$  is the data vector to be transmitted and  $\sigma_n^2$  represents the variance of the zero-mean circularly symmetric complex Gaussian (ZMCSCG) noise. THP is then applied to eliminate the MUI seen by the  $i$ -th user from the previous  $i-1$  users.

**Figure 54** compares the 10% outage capacity of SO THP and MMSE THP schemes for a MU-MIMO downlink system consisting of 4 single-antenna users and 4 BS transmit antennas, denoted as  $\{1, 1, 1, 1\} \times 4$  antenna configuration. Results for ZF channel inversion and a  $\{2, 2\} \times 4$  TDMA system are also provided.

#### 4.2.6. Successive MMSE Precoding

The Successive MMSE (SMMSE) precoding scheme proposed in [57] addresses the problem of performance degradation associated with MMSE precoding when closely spaced receive antennas are used, like in case of

multi-antenna UEs. SMMSE involves successively calculating the columns of the combined precoding matrix  $\mathbf{P}$ , where each column represents a beamforming vector corresponding to a particular receive antenna.

Consider the system model of Subsection 3.7 where each of the  $K$  users is equipped with  $M_{R_i}$  receive antennas for  $i=1, \dots, K$  and  $\mathbf{P}_i$  represents the precoding matrix for the  $i$ -th user consisting of  $M_{R_i}$  columns, each corresponding to a receive antenna. For the  $j$ -th receive antenna of the  $i$ -th user, the matrix  $\bar{\mathbf{H}}_i^{(j)}$  is defined as

$$\bar{\mathbf{H}}_i^{(j)} = [\mathbf{h}_{i,j} \quad \mathbf{H}_1^T \quad \dots \quad \mathbf{H}_{i-1}^T \quad \mathbf{H}_{i+1}^T \quad \dots \quad \mathbf{H}_K^T] \quad (76)$$

where  $\mathbf{h}_{i,j}^T$  represents the  $j$ -th row of the  $i$ -th user's channel matrix  $\mathbf{H}_i$ . The corresponding column of  $\mathbf{P}_i$  is then calculated using the MMSE criterion and is equal to the first column of the matrix

$$\mathbf{P}_{i,j} = \beta \left( (\bar{\mathbf{H}}_i^{(j)})^H \bar{\mathbf{H}}_i^{(j)} + \alpha \mathbf{I}_{M_T} \right)^{-1} (\bar{\mathbf{H}}_i^{(j)})^H \quad (77)$$

All columns of  $\mathbf{P}_i$  are calculated in this manner and this process is repeated for all users to obtain the combined precoding matrix  $\mathbf{P}$ . After precoding, the equivalent combined channel matrix is given by  $\mathbf{H}\mathbf{P} \in \mathbb{C}^{M_R \times M_R}$  which is block diagonal for high SNR values, resulting in a set of  $K$  SU-MIMO channels. Therefore, any SU-MIMO technique e.g. eigen-beamforming for capacity maximization or DET for maximum diversity and array gain can be applied to the  $i$ -th user's equivalent channel matrix  $\mathbf{H}_i \mathbf{P}_i$ . SMMSE precoding has slightly higher complexity than BD [57]. A reduced complexity version called per-user SMMSE (PU-SMMSE) is proposed in [62].

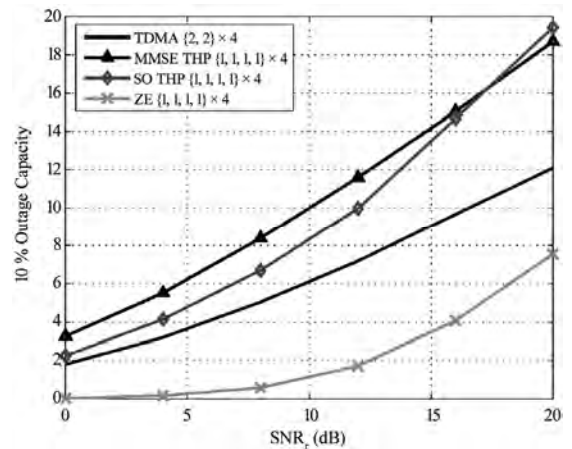


**Figure 54.** 10% outage capacity of SO THP and MMSE THP for  $\{1, 1, 1, 1\} \times 4$  configuration [57].

Figure 55 shows the BER performance comparison of SMMSE, SO THP and BD for  $\{2, 2, 2\} \times 6$  and MMSE THP for  $\{1, 1, 1, 1, 1, 1\} \times 6$  antenna configuration, in a spatially white flat fading channel. These results are based on diversity maximization for the individual users and water-filling is used for power allocation. SMMSE provides the best performance for the case of multi-antenna users while BD surpasses SO THP. Figure 56 shows the BER performance of SMMSE, SO THP and BD for  $\{1, 1, 2, 2\} \times 6$  and MMSE THP for  $\{1, 1, 1, 1, 1, 1\} \times 6$  configuration. Here SO THP outperforms the others. However, SMMSE performs better than MMSE THP and even SO THP at low SNR.

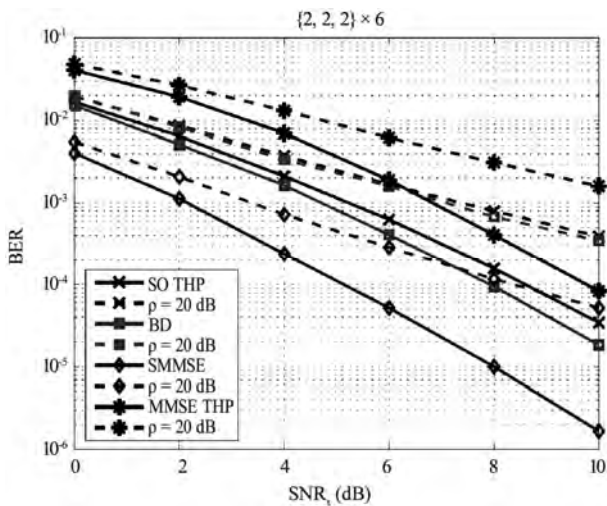


Figure 55. BER performance of SMMSE, SO THP, BD for  $\{2,2,2\} \times 6$  and MMSE THP for  $\{1,1,1,1,1,1\} \times 6$  configuration [57].

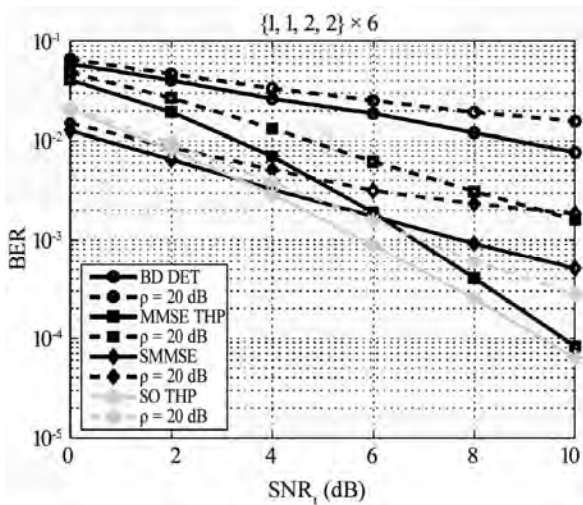


Figure 56. BER performance of SMMSE, SO THP, BD for  $\{1,1,2,2\} \times 6$  and MMSE THP for  $\{1,1,1,1,1,1\} \times 6$  configuration [57].

#### 4.2.7. Iterative Linear MMSE Precoding

Two iterative linear MMSE precoding schemes are discussed in [55] for users with multiple antennas. Consider the system model of Figure 50 where  $\mathbf{P}$  is the combined precoding matrix at the BS and  $\mathbf{V}$  is the block-diagonal combined decoding matrix consisting of the decoding matrices  $\mathbf{V}_i$  of all the users. In case of linear MMSE precoding which minimizes the MSE between  $\hat{\mathbf{a}}$  and  $\mathbf{a}$ ,  $\mathbf{V}_i$  is the linear MMSE receiver for user  $i$  and can be estimated locally at the corresponding UE. The first scheme called *direct optimization*, iteratively computes the MMSE solution using a numerical method. The SMMSE solution can be used as an initial guess for the free variables  $\mathbf{V}_i$  with  $\lambda=1$  for the free variable  $\lambda \in \mathbb{R}$ . An iterative process is then used which can lead to a true MMSE solution but not in all cases. The BD solution can also be used as an initial guess but that would result in slower convergence. The other scheme exploits the uplink/downlink duality [63] to obtain the true MMSE solution using an iterative algorithm. The resulting objective function is convex in this case. Detailed description as well as a practically implementable algorithm for this *duality-based* scheme is presented in [64].

The uncoded BER performance of BD, SMMSE, direct optimization and the duality-based scheme is compared in Figure 57 for  $\{1, 2, 3\} \times 6$  antenna configuration. The bit error rates are averaged over all users. DET is applied for BD and SMMSE while single stream (SS) transmission (consisting of a single data stream per user) is used for direct optimization and the duality-based scheme based on the algorithm from [64]. Independent Rayleigh fading channel perturbed by complex Gaussian noise is considered and QPSK modulation is used for transmission. Both iterative linear MMSE schemes outperform the other two by a large margin. The duality-based scheme shows slightly better performance than

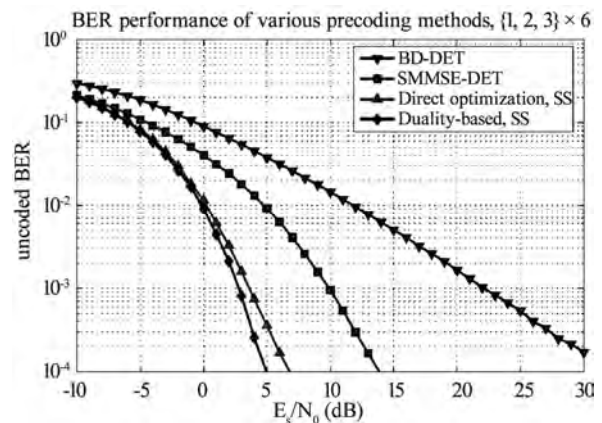


Figure 57. Uncoded BER performance of BD, SMMSE, direct optimization and duality-based scheme [55].

direct optimization. This difference is due to the non-convex objective function used for direct optimization which occasionally causes the optimization routine to undesired minima. BD provides the worst performance because of the zero-forcing constraint.

Figure 58 shows the coded BER performance of these precoding schemes. A rate 1/2 turbo code is used for error correction. OFDM based transmission is considered where the precoding is applied on a per-subcarrier basis. The ITU Vehicular A channel model is used. Direct optimization and the duality-based scheme provide almost identical performance in this case, far better than BD and SMMSE.

#### 4.2.8. Partial CSI Feedback

Transmit precoding for downlink MU-MIMO transmission requires CSI feedback from the users. However, feedback information consisting entirely of the current state of the channel may not be accurate enough in case of rapidly varying channels. Downlink transmission schemes that utilize partial CSI consisting of long-term channel statistics along with some instantaneous channel information like SNR, SINR etc. provide a solution to this problem while reducing the feedback overhead. An interesting MU-MIMO downlink transmission scheme based solely on instantaneous channel norm feedback is proposed in [65]. MU-MIMO configuration with multiple base station (BS) antennas and a single antenna at each UE is considered. The proposed scheme can provide high multiuser diversity gain by optimizing resource allocation at the BS while simply utilizing the instantaneous channel norm feedback from the UEs.

Figure 59 shows the operation of the proposed system at the transmitter (BS). The BS initially transmits orthogonal pilot signals on all transmit antennas which are used by each UE to estimate the received signal energy i.e. the squared norm of the channel vector given by

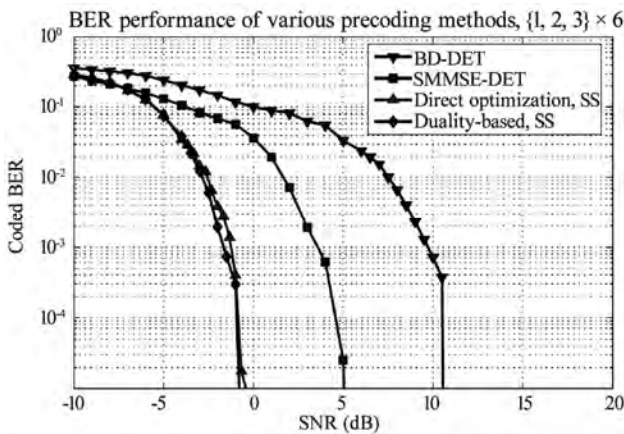


Figure 58. Coded BER performance of BD, SMMSE, direct optimization and duality-based scheme [55].

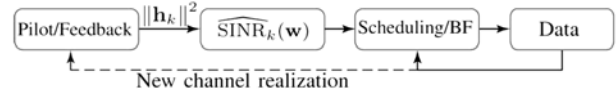


Figure 59. System operation at the transmitter [65].

$$\rho_k \triangleq \|\mathbf{h}_k\|^2 \quad (78)$$

where  $\mathbf{h}_k$  represents the channel vector for the  $k$ -th UE from the  $\mathcal{I}$  UEs scheduled for transmission.  $\rho_k$  is categorized as channel gain information (CGI) in [65]. This quantity is then fed back to the BS. The BS estimates the long-term channel statistics including the channel mean and the channel covariance matrix, defined as

$$\hat{\mathbf{h}}_k \triangleq \mathbb{E}\{\mathbf{h}_k | \rho_k\} \quad (79)$$

$$\hat{\mathbf{Q}}_k \triangleq \mathbb{E}\{\mathbf{h}_k \mathbf{h}_k^H | \rho_k\} \quad (80)$$

This slow varying statistical information is referred to as channel distribution information (CDI). The CGI feedback along with the CDI is used to estimate the SINR and the optimized beamforming weight vectors for each of the UEs scheduled for transmission. The SINR for user  $k$  is estimated as

$$\widehat{\text{SINR}}_k = \frac{\mathbf{w}_k^H \hat{\mathbf{Q}}_k \mathbf{w}_k}{\sum_{i \in \mathcal{I} \setminus \{k\}} \mathbf{w}_i^H \hat{\mathbf{Q}}_k \mathbf{w}_i + \sigma_k^2} \quad (81)$$

where  $\mathbf{w}_k$  is the corresponding beamforming vector,  $\hat{\Gamma}_{ki} = \mathbf{w}_i^H \hat{\mathbf{Q}}_k \mathbf{w}_i$  is the MMSE estimate of the signal-to-interference power ratio (SIR)  $\Gamma_{ki} = \mathbf{w}_i^H \mathbf{h}_k \mathbf{h}_k^H \mathbf{w}_i$  and  $\sigma_k$  is the AWGN power.

The actual data transmission to the scheduled users then begins. Another set of users can later be scheduled to achieve better fairness and this process goes on until the CGI becomes outdated. At this point, BS transmits the pilot signals again and the whole process is repeated.

#### 4.2.9. Multiuser Scheduling

The BS can only support a limited no. of simultaneous users for MU-MIMO downlink transmission with acceptable performance. The performance degrades in rank-deficient scenarios and also when the users are spatially correlated. In case of multi-antenna users, the no. of users that can be supported simultaneously becomes even lesser. In practical situations, the BS would generally serve a larger no. of users than it can simultaneously support. Therefore, an efficient scheduling algorithm is required to select the group of users that will be spatially multiplexed by the BS at a certain time and frequency. The scheduling algorithm should avoid grouping spatially correlated users and maximize system performance while maintaining fairness toward all users. Fairness

ensures that all users are served including those with weak channels. Otherwise, the BS will transmit to the strong users only and the weaker ones will be ignored [59]. A fair scheduling scheme called the strongest-weakest-normalized-subchannel-first (SWNSF) scheduling proposed in [66] enhances the coverage and capacity of MU-MIMO systems while requiring only a limited amount of feedback.

### 4.3. MU-MIMO Capacity

The maximum capacity of a MU-MIMO system is expressed in terms of the sum capacity (or sum-rate capacity) of the broadcast channel. As mentioned earlier, the sum capacity represents the maximum achievable system throughput and is defined as the maximum sum of the downlink information rates of all the users [48]. **Figure 60** illustrates the capacity region and the sum capacity of a MU-MIMO channel with two users. Clearly, achieving the sum capacity requires some tradeoff between the capacities of the individual users, depending on the shape of the capacity region.

It has been shown in [67] that the sum capacity of a Gaussian MIMO broadcast channel with an arbitrary no. of BS transmit antennas and multi-antenna users, is the saddle-point of a minimax problem and (assuming real-valued signals) is given by [49,67]

$$C_{BC} = \min_{\mathbf{R}_{nn} > 0, [\mathbf{R}_{nn}]_{k,k} = \sigma_n^2} \max_{\text{Tr}(\mathbf{R}_{xx}) = P} \frac{1}{2} \log \frac{\det(\mathbf{H}\mathbf{R}_{xx}\mathbf{H}^H + \mathbf{R}_{nn})}{\det(\mathbf{R}_{nn})} \quad (82)$$

$$C_{MAC}(\mathbf{P}; \mathbf{H}^H) \triangleq \bigcup_{\{\mathbf{Q}_i \geq 0, \text{Tr}(\mathbf{Q}_i) \leq P_i \forall i\}} \left\{ (R_1, \dots, R_K) : \sum_{i \in S} R_i \leq \frac{1}{2} \log \left| \mathbf{I} + \sum_{i \in S} \mathbf{H}_i^H \mathbf{Q}_i \mathbf{H}_i \right| \quad \forall S \subseteq \{1, \dots, K\} \right\} \quad (83)$$

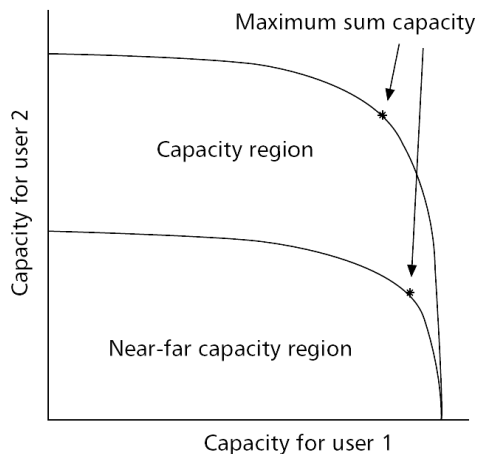


**Figure 60.** The capacity region and sum capacity of a two-user MU-MIMO channel [48].

where  $\mathbf{H}$  is the channel matrix,  $\mathbf{R}_{xx}$  is the transmit signal covariance matrix,  $\mathbf{R}_{nn}$  is covariance matrix of the additive ZMCSCG noise with variance  $\sigma_n^2$  and  $P$  represents the total transmit power. The sum capacity is obtained by iteratively computing the best transmit covariance matrix  $\mathbf{R}_{xx}$  for a given noise covariance and then computing the least favorable noise covariance matrix  $\mathbf{R}_{nn}$  for the given transmit covariance. It is also shown that decision-feedback precoding or dirty paper coding is the optimal precoding strategy capable of achieving the sum capacity. In [68], it has been proved that the capacity region of the Gaussian MIMO-BC with single-antenna users is equivalent to the dirty paper coding (DPC) rate region under a certain total transmit power constraint. The DPC achievable rate region for the case of multi-antenna users is formulated in [67] and is also discussed in [69]. Further research work is required on the capacity of fading MIMO broadcast channels.

The capacity of MIMO-MAC channels constitutes a relatively simple problem. The capacity of any MAC is given as the convex closure of the union of rate regions corresponding to every product input distribution  $p(u_1) \dots p(u_K)$  satisfying certain user-by-user power constraints, where  $\mathbf{u}_k \in \mathbb{C}^{N \times 1}$  is the  $k$ -th user's transmitted signal. However, the convex hull operation is not required for the Gaussian MIMO-MAC and only the Gaussian inputs need to be considered. This can be written as [69]

where  $\mathbf{P} = (P_1, \dots, P_K)$  represents the set of transmit powers corresponding to each of the  $K$  users,  $|\cdot|$  denotes the determinant and  $R_i$ ,  $\mathbf{Q}_i$  and  $\mathbf{H}_i$  represent the rate vector, spatial covariance matrix and the channel matrix respectively for the  $i$ -th user. A general expression for the capacity regions of fading MAC channels is also given in [69].

### 5. Convex Optimization

Convex optimization methods provide a powerful set of tools for solving optimization problems expressed in convex form. However, most engineering problems are not convex when directly formulated and need to be reformulated in a convex form in order to apply convex optimization. Two methods are commonly used for this reformulation. The first method is to use a change of

variables to obtain an equivalent convex form. The other is to remove some of the constraints so that the problem becomes convex, in such a way that the optimal solution also satisfies the removed constraints. Any problem, once expressed in convex form, can be optimally solved either in closed form using the optimality conditions derived from Lagrange duality theory e.g. Karush-Kuhn-Tucker (KKT) conditions or numerically using iterative algorithms like the interior-point, cutting-plane and ellipsoid methods [70].

In recent years, convex optimization has gained significant importance in optimal joint transceiver design (transmit-receive beamforming) of MIMO systems based on linear precoding and equalization. Various design methods for linear multicarrier SU-MIMO transmit-receive beamformers, based on convex optimization are given in [71]. Two novel low-complexity multilevel water-filling solutions for the MAX-MSE and HARM-SINR criteria are also proposed. The MAX-MSE method minimizes the maximum of the MSEs corresponding to the different substreams whereas HARM-SINR maximizes the harmonic mean of the SINRs. The ARITH-BER method which minimizes the arithmetic mean of the BERs, provides the best average BER performance and is considered as a benchmark in [71]. It is shown that when cooperation among different subcarriers is allowed to improve performance, an exact optimal closed-form solution is obtained in terms of minimizing the average BER which unifies all three optimization criteria mentioned above. In other words, MAX-MSE, HARM-SINR and ARITH-BER provide the same optimal solution for carrier-cooperative schemes.

**Figure 61** shows the average BER performance (at 5% outage probability) of ARITH-MSE, HARM-SINR, MAX-MSE and ARITH-BER for  $2 \times 2$  MIMO configuration using a single substream [71].

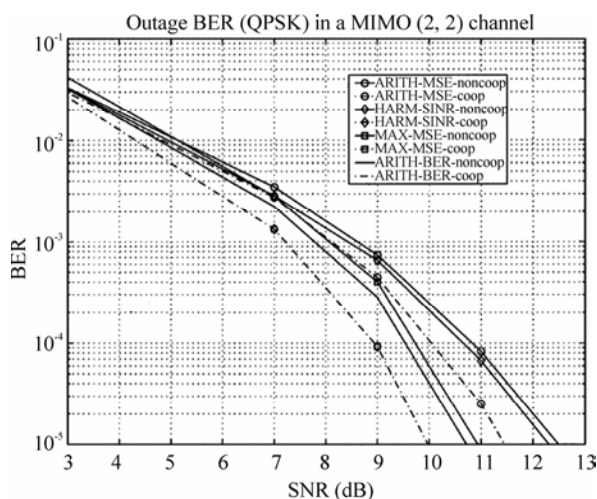


**Figure 61.** BER performance of ARITH-MSE, HARM-SINR, MAX-MSE and ARITH-BER for  $2 \times 2$  MIMO configuration using a single substream [71].

ration. The HIPERLAN/2 standard based on OFDM is used for the simulations with frequency selective fading in an indoor NLOS scenario. QPSK modulation is employed and perfect CSI is assumed at the transmitter and the receiver. In the absence of subcarrier cooperation, ARITH-BER provides the best performance followed by MAX-MSE and HARM-SINR respectively. With subcarrier cooperation ARITH-BER, MAX-MSE and HARM-SINR have identical performance which is optimal in the minimum average BER sense. A joint transceiver optimization scheme based on multiplicative Schur-convexity is proposed in [72] for THP precoded MIMO-OFDM systems. This scheme provides better BER performance than the aforementioned linear precoding schemes when the objective function is multiplicatively Schur-convex like in case of ARITH-BER, MAX-MSE or HARM-SINR, and becomes equivalent to the optimal UCD scheme proposed in [37].

Convex optimization is also applicable to downlink beamforming in MU-MIMO systems as mentioned in [70] for the case of single-antenna users. The duality-based iterative MMSE precoding scheme proposed in [64] supports multi-antenna users and uses an iterative algorithm to solve the KKT optimality conditions.

## 6. Conclusions and Future Research

Open-loop MIMO techniques provide a low-complexity solution for MIMO diversity and SM. STC or SFC e.g. STBC, orthogonal STBC (OSTBC), STTC, SFBC etc. can be used for diversity maximization. These schemes are also well-suited for transmission over high-speed mobile channels where link reliability is the primary concern rather than throughput maximization. Open-loop SM can be implemented by means of a simple V-BLAST system but at the cost of low BER performance. JDM MIMO systems like the CDA-SM-OFDM system which combines CDD and SM, provide better performance. Further research may be carried out to optimize the achievable diversity and multiplexing gain for enhancing system throughput while considering the impact of transmit and receive antenna correlations. The iterative turbo-MIMO systems are also capable of achieving high capacity but are more complex to implement. Turbo-MIMO systems may be improved further by using improved turbo codes and signal constellation shaping [73], improved code interleavers, and stratified processing [74].

Closed-loop MIMO systems like the SVD-based linear transceivers, are capable of achieving the SU-MIMO capacity by transmitting over the channel eigenmodes with optimal water-filling power allocation, provided perfect CSI is available at the transmitter and the receiver. Alternatively, DET can be employed to achieve the maximum diversity and array gain. Closed-loop STC like the closed-loop STBC schemes proposed in [75] which

support more than two transmit antennas, also provide diversity maximization. The GMD-MIMO scheme decomposes the MIMO channel into identical subchannels and attempts to combine MIMO diversity and SM in an optimal manner. MAX-MSE, HARM-SINR and ARITH-BER methods based on convex optimization provide optimal average BER performance for multi-stream transmission when subcarrier cooperation is allowed. However, the GMD and convex optimization approaches assume the availability of full CSI at the transmitter and the receiver which is not always the case e.g. in rapidly changing mobile channels. Therefore, the performance of these schemes with imperfect feedback needs to be evaluated for practical implementation. Use of convex optimization methods for designing optimal linear transceivers utilizing partial CSI also need to be investigated.

For the MU-MIMO uplink, the LAST-MUD scheme based on V-BLAST detection provides good performance for CDMA systems. The SMMSE MUD provides acceptable performance for MIMO-OFDM systems. The higher complexity Turbo-MUD scheme achieves better performance and can jointly detect the transmit antennas of each multi-antenna user. Use of different turbo detection strategies, joint detection of all users and extension to multicarrier systems may be investigated in future. The GA-assisted MUDs, particularly the TTCM-assisted IGA-MUD provide near-ML detection performance for SDMA-OFDM systems and also perform reasonably well in certain rank-deficient scenarios. The complexity is high but increases slowly with the no. of users as compared to the ML-MUD. GA-assisted MUDs can also incorporate joint channel estimation and symbol detection. Future research work may include extending the GA-assisted MUD schemes to support multi-antenna users and development of more efficient GAs to reduce system complexity. Use of artificial intelligence (AI) techniques like the radial basis function (RBF) based artificial neural networks (ANNs) should also be explored for multiuser detection.

Coming to the MU-MIMO downlink, SMMSE precoding performs reasonably well with manageable complexity. The nonlinear dirty paper coding techniques are capable of achieving the sum capacity of Gaussian multiuser channels with single-antenna users. The iterative linear MMSE techniques like direct optimization and the duality-based scheme which uses convex optimization, provide excellent uncoded and coded BER performance for single stream transmission. Further research is required to develop MU-MIMO downlink transmission schemes capable of supporting SM for individual multi-antenna mobile users. Transmission schemes based on partial CSI which require minimal CSI feedback from the users represent the most suitable choice for practical implementation. Convex optimization tools might be

useful in designing joint transmit-receive beamforming systems less prone to errors resulting from imperfect CSI. Research efforts are also needed for developing efficient multiuser scheduling schemes that maintain fairness to the users while minimizing the loss of system capacity. Determining the sum capacity and capacity regions for fading MU-MIMO downlink channels with multi-antenna users is also an area for future research.

Accurate channel estimation is of prime importance in MIMO communications. Channel estimation errors may result in severe performance degradation. Therefore, research efforts are continuing for further improvements in this domain. A broadband wireless transmission technique called orthogonal frequency- and code-division multiplexing (OFCDM) [76] has recently gained prominence as a better alternative to OFDM. OFCDM readily supports MIMO techniques and extensive research would be required to realize the full potential of MIMO-OFCDM systems.

## 7. References

- [1] D. Gesbert, M. Shafi, D.-S. Shiu, P. J. Smith, and A. Naguib, "From theory to practice: An overview of MIMO space-time coded wireless systems," *IEEE Journal on Selected Areas in Communications*, Vol. 21, No. 3, pp. 281–302, April 2003.
- [2] Y. Jiang, J. Li, and W. W. Hager, "Joint transceiver design for MIMO communications using geometric mean decomposition," *IEEE Transactions on Signal Processing*, Vol. 53, No. 10, pp. 3791–3803, October 2005.
- [3] M. Jiang and L. Hanzo, "Multiuser MIMO-OFDM for next-generation wireless systems," *Proceedings of the IEEE*, Vol. 95, No. 7, pp. 1430–1469, July 2007.
- [4] K. W. Park, E. S. Choi, K. H. Chang, and Y. S. Cho, "An MIMO-OFDM technique for high-speed mobile channels," in *Proceedings of Vehicular Technology Conference*, Vol. 2, pp. 980–983, April 2003.
- [5] M. S. Gast, "802.11 wireless networks: The definitive guide," 2nd edition, O'Reilly, April 2005.
- [6] Wi-Fi Alliance, "WiFi CERTIFIED™ 802.11n draft 2.0: Longer-range, faster-throughput, multimedia grade WiFi@ networks," 2007. [http://wi-fi.org/whitepaper\\_80211n\\_draft2\\_technical.php](http://wi-fi.org/whitepaper_80211n_draft2_technical.php).
- [7] FierceBroadbandWireless, "IEEE approves EWC 802.11n as first draft," 24 January 2006. <http://www.fiercebroadbandwireless.com/story/ieee-approves-ewc-802-11n-as-first-draft/2006-01-25>.
- [8] Y. Sun, M. Karkooti, and J. Cavallaro, "High throughput, parallel, scalable LDPC encoder/decoder architecture for OFDM systems," in *Proceedings of IEEE Workshop on Circuits and Systems*, pp. 225–228, October 2006.
- [9] H. N. Niu and C. Ngo, "Diversity and multiplexing switching in 802.11n MIMO systems," in *Proceedings of 40th Asilomar Conference on Signals, Systems and Com-*

- puters (ACSSC '06), pp. 1644–1648, 29 October–1 November 2006.
- [10] P. Kim and K. M. Chugg, “Capacity for suboptimal receivers for coded multiple-input multiple-output systems,” Vol. 6, No. 9, pp. 3306–3314, September 2007.
- [11] S. Abraham, A. Meylan, S. Nanda, “802.11n MAC design and system performance,” in Proceedings of IEEE International Conference on Communications (ICC 2005), Vol. 5, pp. 2957–2961, 16–20 May 2005.
- [12] Cisco Aironet 1250 Series Access Point Q&A. [http://www.cisco.com/en/US/prod/collateral/wireless/ps5678/ps6973/ps8382/prod\\_qas0900aecd806b7c82.html](http://www.cisco.com/en/US/prod/collateral/wireless/ps5678/ps6973/ps8382/prod_qas0900aecd806b7c82.html).
- [13] S. Kim, S.-J. Lee, and S. Choi, “The impact of IEEE 802.11 MAC strategies on multi-hop wireless mesh networks,” Wireless Mesh Networks, in Proceedings of 2nd IEEE Workshop on Wireless Mesh Networks (WiMesh 2006), pp. 38–47, 25–28 September 2006.
- [14] IEEE Std 802.16e™-2005 and IEEE Std 802.16™-2004/Cor 1-2005 (Amendment and Corrigendum to IEEE Std 802.16-2004), “IEEE standard for local and metropolitan area networks Part 16: Air Interface for fixed and mobile broadband wireless access systems amendment 2: Physical and medium access control layers for combined fixed and mobile operation in licensed bands and Corrigendum 1,” 28 February 2006.
- [15] IEEE Std 802.16™-2004, “IEEE standard for local and metropolitan area networks Part 16: Air interface for fixed broadband wireless access systems,” 1 October 2004.
- [16] J. G. Andrews, A. Ghosh, and R. Muhamed, “Fundamentals of WiMAX: Understanding broad-band wireless networking,” Prentice Hall, 2007.
- [17] I. Kambourov, “MIMO aspects in 802.16e WiMAX OFDMA,” WiMAX Tutorial, Siemens PSE MCS RA 2, 22 November 2006.
- [18] Nokia Siemens Networks, “Advanced antenna systems for WiMAX.” <http://www.nokiasiemensnetworks.com>.
- [19] S. Nanda, R. Walton, J. Ketchum, M. Wallace, and S. Howard, “A high-performance MIMO OFDM wireless LAN,” IEEE Communications Magazine, Vol. 43, No. 2, pp. 101–109, February 2005.
- [20] Agilent Technologies, “Mobile WiMAX 802.16 Wave 2 Features.” <http://www.home.agilent.com/agilent/editorial.jsp?action=download&cc=US&lc=eng&ckey=1213544&nid=-536902344.536910932.00&id=1213544>.
- [21] IEEE C802.16m-07/069, “Draft IEEE 802.16m evaluation methodology document,” IEEE 802.16 Broadband Wireless Access Working Group, 2007.
- [22] WiMAX Forum®, “Deployment of Mobile WiMAX™ Networks by Operators with Existing 2G & 3G Networks,” 2008. [http://www.wimaxforum.org/technology/downloads/deployment\\_of\\_mobile\\_wimax.pdf](http://www.wimaxforum.org/technology/downloads/deployment_of_mobile_wimax.pdf).
- [23] C. Ribeiro, “Bringing wireless access to the automobile: A comparison of Wi-Fi, WiMAX, MBWA, and 3G,” 21st Computer Science Seminar, 2005.
- [24] B. M. Bakmaz, Z. S. Bojković, D. A. Milovanović, and M. R. Bakmaz, “Mobile broadband networking based on IEEE 802.20 standard,” in Proceedings of 8th International Conference Telecommunications in Modern Satellite, Cable and Broadcasting Services (TELSIKS 2007), pp. 243–246, 26–28 September 2007.
- [25] IEEE Std 802.20™-2008, “IEEE standard for local and metropolitan area networks Part 20: Air interface for mobile broadband wireless access systems supporting vehicular mobility—physical and media access control layer specification,” 29 August 2008.
- [26] 3GPP TS 36.201 V8.1.0 (2007-11), “LTE physical layer – general description (Release 8),” 3GPP TSG RAN, 2007.
- [27] J. Zyren, “Overview of the 3GPP long term evolution physical layer,” White Paper, Freescale Semiconductor, Inc., 2007.
- [28] 3GPP TR 25.913 V7.3.0 (2006-03), “Requirements for evolved UTRA (E-UTRA) and evolved UTRAN (E-UTRAN) (Release 7),” 3GPP TSG RAN, 2006.
- [29] 3GPP TS 36.300 V8.4.0 (2008-03), “Evolved universal terrestrial radio access (E-UTRA) and evolved universal terrestrial radio access network (E-UTRAN); Overall description; Stage 2 (Release 8),” 3GPP TSG RAN, 2008.
- [30] 3GPP TS 36.211 V8.1.0 (2007-11), “Evolved universal terrestrial radio access (E-UTRA); Physical channels and modulation (Release 8),” 3GPP TSG RAN, 2007.
- [31] P. W. Wolniansky, G. J. Foschini, G. D. Golden, and R. A. Valenzuela, “V-BLAST: An architecture for realizing very high data rates over the rich-scattering wireless channel,” in Proceedings of 1998 URSI International Symposium Signals, Systems, and Electronics, pp. 295–300, 29 September–2 October 1998.
- [32] S. T. Chung, A. Lozano, and H. C. Huang, “Approaching eigenmode BLAST channel capacity using V-BLAST with rate and power feedback,” in Proceedings of IEEE VTC 2001 Fall, Vol. 2, pp. 915–919, 7–11 October 2001.
- [33] Q. P. Cai, A. Wilzeck, C. Schindler, S. Paul, and T. Kaiser, “An exemplary comparison of per antenna rate control based MIMO-HSDPA receivers,” in Proceedings of 13th European Signal Processing Conference (EUSIPCO 2005), 4–8 September, 2005.
- [34] R. Gowrishankar, M. F. Demirkol, and Z. Q. Yun, “Adaptive modulation for MIMO systems and throughput evaluation with realistic channel model,” in Proceedings of 2005 International Conference on Wireless Networks, Communications and Mobile Computing, Vol. 2, pp. 851–856, 13–16 June 2005.
- [35] M. I. Rahman, S. S. Das, E. de Carvalho, and R. Prasad, “Spatial multiplexing in OFDM systems with cyclic delay diversity,” in Proceedings of IEEE Vehicular Technology Conference, pp. 1491–1495, 22–25 April 2007.
- [36] H. Busche, A. Vanaev, and H. Rohling, “SVD based MIMO precoding and equalization schemes for realistic channel estimation procedures,” Frequenz Journal of RF-Engineering and Telecommunications, Vol. 61, No.

- 7–8, pp. 146–151, July–August 2007.
- [37] Y. Jiang and J. Li, “Uniform channel decomposition for MIMO communications,” in Proceedings of 38th Asilomar Conference on Signals, System, and Computers, 7–10 November 2004.
- [38] S. Haykin, M. Sellathurai, Y. de Jong, and T. Willink, “Turbo-MIMO for wireless communications,” *IEEE Communications Magazine*, Vol. 42, No. 10, pp. 48–53, October 2004.
- [39] M. Sellathurai and S. Haykin, “Turbo-BLAST for wireless communications: Theory and experiments,” *IEEE Transactions on Signal Processing*, Vol. 50, No. 10, pp. 2538–2546, October 2002.
- [40] D. J. Love, R. W. Heath Jr., W. Santipach, and M. L. Honig, “What is the value of limited feedback for MIMO channels,” *IEEE Communications Magazine*, Vol. 42, No. 10, pp. 54–59, October 2004.
- [41] Y. Yuda, K. Hiramatsu, M. Hoshino, and K. Homma, “A study on link adaptation scheme with multiple code words for spectral efficiency improvement on OFDM-MIMO systems,” *IEICE Transactions on Fundamentals*, Vol. E90A, No. 11, pp. 2413–2422, November 2007.
- [42] Z. G. Zhou, H. Y. Yi, H. Y. Guo, and J. T. Zhou, “A partial feedback scheme for MIMO systems,” in Proceedings of WiCom 2007, pp. 361–364, 21–25 September 2007.
- [43] A. Heidari, F. Lahouti, and A. K. Khandani, “Enhancing closed-loop wireless systems through efficient feedback reconstruction,” *IEEE Transactions on Vehicular Technology*, Vol. 56, No. 5, pp. 2941–2953, September 2007.
- [44] H. R. Bahrami and T. Le-Ngoc, “MIMO precoding structures for frequency-flat and frequency-selective fading channels,” in Proceedings of 1st International Conference on Communications and Electronics (ICCE '06), pp. 193–197, 10–11 October 2006.
- [45] M. Tsutsui and H. Seki, “Throughput performance of downlink MIMO transmission with multi-beam selection using a novel codebook,” in Proceedings of IEEE VTC 2007-Spring, pp. 476–480, 22–25 April 2007.
- [46] K. W. Park and Y. S. Cho, “An MIMO-OFDM technique for high-speed mobile channels,” *IEEE Communications Letters*, Vol. 9, No. 7, pp. 604–606, July 2005.
- [47] A. A. Hutter, S. Mekrazi, B. N. Getu, and F. Platbrood, “Alamouti-based space-frequency coding for OFDM,” *Wireless Personal Communications: An International Journal*, Vol. 35, No. 1–2, pp. 173–185, October 2005.
- [48] Q. H. Spencer, C. B. Peel, A. L. Swindlehurst, and M. Haardt, “An introduction to the multi-user MIMO downlink,” *IEEE Communications Magazine*, Vol. 42, No. 10, pp. 60–67, October 2004.
- [49] A. Paulraj, R. Nabar, and D. Gore, “Introduction to space-time wireless communications,” Cambridge, UK, Cambridge University Press, 2003.
- [50] S. Sfar, R. D. Murch, and K. B. Letaief, “Layered space-time multiuser detection over wireless uplink systems,” *IEEE Transactions on Wireless Communications*, Vol. 2, No. 4, July 2003.
- [51] V. Stankovic and M. Haardt, “Improved diversity on the uplink of multi-user MIMO systems,” in Proceedings of European Conference on Wireless Technology '05, pp. 113–116, 3–4 October 2005.
- [52] I. Santamaria, V. Elvira, J. Via, D. Ramirez, J. Perez, J. Ibanez, R. Eickoff, and F. Ellinger, “Optimal MIMO transmission schemes with adaptive antenna combining in the RF path,” in Proceedings of 16th European Signal Processing Conference (EUSIPCO 2008), 25–29 August 2008.
- [53] N. Veselinovic, T. Matsumoto, and M. Juntti, “Iterative MIMO turbo multiuser detection and equalization for STTrC-coded systems with unknown interference,” *EURASIP Journal on Wireless Communications and Networking*, Vol. 2004, No. 2, pp. 309–321, 2004.
- [54] Q. Spencer and M. Haardt, “Capacity and downlink transmission algorithms for a multi-user MIMO channel,” in Proceedings of 36th Asilomar Conference on Signals, Systems, and Computers, pp. 1384–1388, November 2002.
- [55] B. Bandemer, M. Haardt, and S. Visuri, “Linear MMSE multi-user MIMO downlink precoding for users with multiple antennas,” in Proceedings of IEEE 17th International Symposium on Personal, Indoor and Mobile Radio Communications (PIMRC'06), pp. 1–5, 11–14 September 2006.
- [56] Q. H. Spencer, A. L. Swindlehurst, and M. Haardt, “Zero-forcing methods for downlink spatial multiplexing in multiuser MIMO channels,” *IEEE Transactions on Signal Processing*, Vol. 52, No. 2, pp. 461–471, February 2004.
- [57] V. Stankovic and M. Haardt, “Multi-user MIMO downlink precoding for users with multiple antennas,” in Proceedings of 12th Wireless World Research Forum (WWRF), Toronto, ON, Canada, November 2004.
- [58] M. Costa, “Writing on dirty paper,” *IEEE Transactions on Information Theory*, Vol. 29, pp. 439–441, May 1983.
- [59] V. Stankovic, M. Haardt, and G. D. Galdo, “Efficient multi-user MIMO downlink precoding and scheduling,” in Proceedings of 1st IEEE International Workshop on Computational Advances in Multi-Sensor Adaptive Processing, pp. 237–240, 13–15 December 2005.
- [60] V. Stankovic and M. Haardt, “Successive optimization Tomlinson-Harashima precoding (SO THP) for multi-user MIMO systems,” in Proceedings of IEEE International Conference on Acoustics, Speech, and Signal Processing (ICASSP), Philadelphia, PA, USA, March 2005.
- [61] M. Joham, J. Brehmer, and W. Utschick, “MMSE approaches to multiuser spatio-temporal Tomlinson-Harashima precoding,” in Proceedings of 5th International ITG Conference on Source and Channel Coding (ITG SCC'04), pp. 387–394, January 2004.
- [62] M. Lee and S. K. Oh, “A per-user successive MMSE precoding technique in multiuser MIMO systems,” in Proceedings of IEEE VTC 2007-Spring, pp. 2374–2378, 22–25 April 2007.

- [63] M. Schubert, S. Shi, E. A. Jorswieck, and H. Boche, "Downlink sum-MSE transceiver optimization for linear multi-user MIMO systems," in Proceedings of 39th Asilomar Conference on Signals, Systems, and Computers, pp. 1424–1428, October 2005.
- [64] A. Mezghani, M. Joham, R. Hunger, and W. Utschick, "Transceiver design for multi-user MIMO systems," in Proceedings of ITG/IEEE Workshop on Smart Antennas (WSA 2006), March 2006.
- [65] D. Hammarwall, M. Bengtsson, and B. Ottersten, "Acquiring partial CSI for spatially selective transmission by instantaneous channel norm feedback," *IEEE Transactions on Signal Processing*, Vol. 56, No. 3, March 2008.
- [66] C.-J. Chen and L.-C. Wang, "Enhancing coverage and capacity for multiuser MIMO systems by utilizing scheduling," *IEEE Transactions on Wireless Communications*, Vol. 5, No. 5, May 2006.
- [67] W. Yu and J. M. Cioffi, "Sum capacity of Gaussian vector broadcast channels," *IEEE Transactions on Information Theory*, Vol. 50, No. 9, September 2004.
- [68] H. Weingarten, Y. Steinberg, and S. Shamai, "The capacity region of the Gaussian MIMO broadcast channel," in Proceedings of ISIT 2004, 27 June–2 July 2004.
- [69] A. Goldsmith, S. A. Jafar, N. Jindal, and S. Vishwanath, "Capacity limits of MIMO channels," *IEEE Journal on Selected Areas in Communications*, Vol. 21, No. 5, pp. 684–702, June 2003.
- [70] D. P. Palomar, A. Pascual-Iserte, J. M. Cioffi, and M. A. Lagunas, "Convex optimization theory applied to joint transmitter-receiver design in MIMO channels," *Space-Time Processing for MIMO Communications*, edited by A. B. Gershman and N. D. Sidiropoulos, Chichester, England, Wiley, 2005.
- [71] D. P. Palomar, J. M. Cioffi, and M. A. Lagunas, "Joint tx-rx beamforming design for multicarrier MIMO channels: A unified framework for convex optimization," *IEEE Transactions on Signal Processing*, Vol. 51, No. 9, September 2003.
- [72] A. A. D'Amico, "Tomlinson-Harashima precoding in MIMO systems: A unified approach to transceiver optimization based on multiplicative Schur-convexity," *IEEE Transactions on Signal Processing*, Vol. 56, No. 8, August 2008.
- [73] B. M. Hochwald and S. ten Brink, "Achieving near-capacity on a multiple-antenna channel," *IEEE Transactions on Communications*, Vol. 51, No. 3, pp. 389–399, March 2003.
- [74] M. Sellathurai and G. Foschini, "A stratified diagonal layered space-time architecture: Information theoretic and signal processing aspects," *IEEE Transactions on Signal Processing*, Vol. 51, No. 11, pp. 2943–2954, November 2003.
- [75] S. Lambotharan and C. Toker, "Closed-loop space time block coding techniques for OFDM broadband wireless access systems," *IEEE Transactions on Consumer Electronics*, Vol. 51, No. 3, pp. 765–769, August 2005.
- [76] Y. Zhou, T.-S. Ng, J. Wang, K. Higuchi, and M. Sawahashi, "OFCDM: A promising broadband wireless access technique," *IEEE Communications Magazine*, Vol. 46, No. 3, March 2008.

# Complex Domain Wavelet-Based Denoising of Measured UHF Wireless Channel Power Delay Profiles

Maurício Henrique Costa Dias<sup>1</sup>, Gláucio Lima Siqueira<sup>2</sup>

<sup>1</sup>Department of Electrical Engineering, Military Institute of Engineering, Rio de Janeiro, Brazil

<sup>2</sup>Center for Telecommunications Studies, Pontifical Catholic University of Rio de Janeiro, Rio de Janeiro, Brazil

Email: [mhcdias@ime.eb.br](mailto:mhcdias@ime.eb.br), [glaucio@cetuc.puc-rio.br](mailto:glaucio@cetuc.puc-rio.br)

Received December 29, 2009; revised January 31, 2010; accepted February 25, 2010

## Abstract

This work extends the use of wavelet-based denoising as an alternative processing scheme to improve measured mobile-radio channel power delay profiles. It has already been reported that, when applied on real domain data (amplitude only), denoising provides mainly a qualitative improvement. Here, phase content was also considered, leading to significant qualitative and quantitative improvement of the processed profiles. Signal-to-noise ratios and dynamic ranges improvements as high as 50 dB have been observed.

**Keywords:** Wireless Propagation Channel, Wideband Channel Sounding, UHF Measurements, Wavelets, Denoising

## 1. Introduction

In wireless wideband propagation channel characterization, time dispersion statistical analysis may be carried out on measurements of the channel impulse response. Local ensemble averages of the time-variant channel responses are very useful in that sense, and are commonly referred to as power delay profiles (PDP) [1]. However, noise, interference and sounder setup imperfections are also present as spurious contributions to the actual PDP, distorting its statistical moments, like mean delay and rms delay spread. In order to minimize those effects to the channel statistics, thresholding procedures are usually adopted. The basic approach consists in establishing a noise threshold, below which the response is simply cut off. The threshold may be determined by a visual inspection or may be guided by noise level estimation [1]. Some additional refinements may also be included, as in [2].

Recently, wavelet-based denoising has been proposed as an alternative cleaning processing scheme. Tests on measured PDP from both outdoor and indoor surveys at UHF frequencies have pointed out qualitative improvement, with smoother noise floors, and also small increases on signal-to-noise ratios (SNR) of the profiles [3]. In the present work, wavelet-based denoising is adopted once again to clean delay profiles, this time taking advantage of the phase content of measured impulse responses, available when frequency domain sounding [1]

is carried out, to further improve the data processing.

The rest of this text is organized as follows. Section 2 briefly describes the measured channel data processed in this work. The denoising procedure adopted is addressed in Section 3. The next section presents and discusses some results of this processing technique. Section 5 concludes this work.

## 2. Available Measured Data Description

The available data used to test this processing technique have been measured with the frequency domain channel sounder described in [4], depicted in **Figure 1**. The sounder was basically a vector network analyzer (VNA) with the propagation channel taken as its *device under test* (DUT). The sounder operated with a 200 MHz band centred on 1.8 GHz. Each recorded impulse response was sampled at a 1/801 rate.

The whole survey has been carried out in two different indoor scenarios: one within the corridors of a university building and the other within a little mall, as described in details in [3]. Both line-of-sight and out-of-sight conditions have been tested. The experiment tried to simulate a pedestrian's walk, so the mobile unit had a speed close to 0.3 m/s. Considering the whole processing time of the sounder, around two impulse responses per second could be stored. In the overall, more than 3500 channel responses have been measured, from 13 different routes.

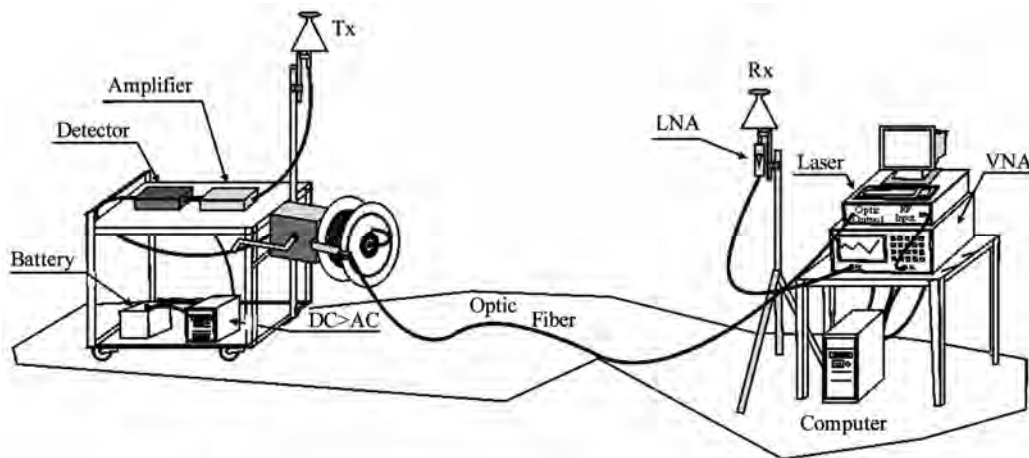


Figure 1. Soudner setup.

The available PDP presented SNR ranging from 21 to 61 dB, and dynamic ranges (DR) within 24 to 61 dB. More information on the survey is found in [3].

### 3. Denoising Procedure

The software tool used to test the proposed technique was Matlab™, including its wavelet toolbox and functions libraries. Matlab has an automated denoising function based on a dyadic discrete decomposition, with a few user-defined parameters, such as the wavelet function and the number of decomposition levels. Another important user-defined parameter is threshold rescaling as a function of noise level. Actually, two practical options are available: one adopts a white noise assumption, while the other assumes coloured noise.

In [3], the denoising function was applied only on the amplitude of the impulse responses, that is, it was a unidimensional (1D) operator. However, the soudner output was actually complex, rather than real, that is, both amplitude and phase variations of the channel were recorded. In fact, the first approach adopted in [3] disregarded the available relevant phase information. A better approach that tries to benefit from the channel phase content is denoising both real and imaginary projections of the complex channel impulse response (or its counterpart, the power delay profile). Each projection should be independently denoised just like in [3]. Such procedure has been applied to the available indoor data ensemble previously described, and will be referred to as “2D denoising” from this point on.

### 4. Results

The trials carried out in [3] provided some insights regarding the best combination of parameters to be chosen

for the denoising processing. Since the data ensemble to be 2D denoised was the same, only the options that led to the best results in [3] have been chosen. In special, the Symlet8 wavelet function has been adopted, as well as Donoho’s VisuShrink soft thresholder [5]. 2D denoising has been applied on the delay domain, in the linear scale, and the noise level rescaling method adopted was the one that considered a coloured noise assumption.

As in the 1D approach, 2D denoising has been computed to all available individual channel responses. In order to better assess the results, average power delay profiles have also been generated for each route. **Figure 2** illustrates the performance of the 2D denoising procedure on a single channel response. As it can be seen, the noise floor drops more than 40 dB, and the noise oscillations almost fade away.

1D denoising presented mainly qualitative improvements, as already thoroughly discussed in [3]. The

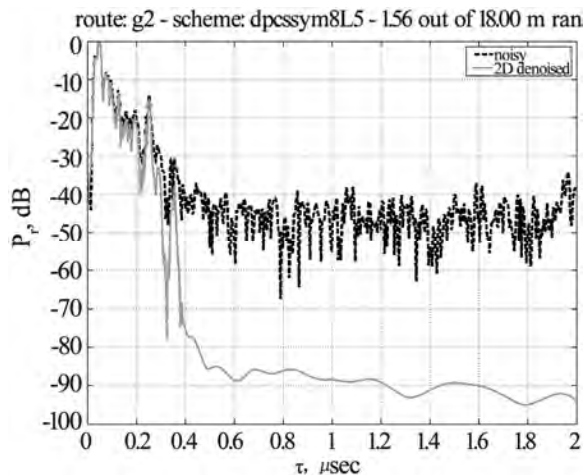


Figure 2. Noisy and 2D denoised channel response sample from G2 route.

performance of the 2D denoising was much better, as illustrated in **Figures 3** and **4**, which also present the widely adopted flat thresholding technique [1], just for comparison. Not only was the noise floor flattened, but also significantly lowered, leading to much higher SNR and DR - as high as 50 dB improvements have been

achieved, against 3 to 6 dB provided by 1D denoising. Some potential hidden peaks were even identified, though no theoretical or simulation based procedure has been tested to confirm such peaks as valid ones.

## 5. Conclusions

This work presented an improved version of the wavelet-based denoising scheme proposed in [3] to process wireless channel power delay profiles. While in [3] only the amplitude content of the profiles was processed (1D denoising), in the present work the phase content was also considered (2D denoising).

In order to show how this complementary approach could improve the profiles even more, the same wide-band 1.8 GHz indoor measurements described in [3] were considered in the present work. Indeed, while 1D denoising provided mostly a qualitative contribution, with a clear noise floor flattening, 2D denoising led also to significant quantitative improvement. The noise floor was lowered up to 50 dB in some cases, against no more than 6 dB when 1D denoising was adopted.

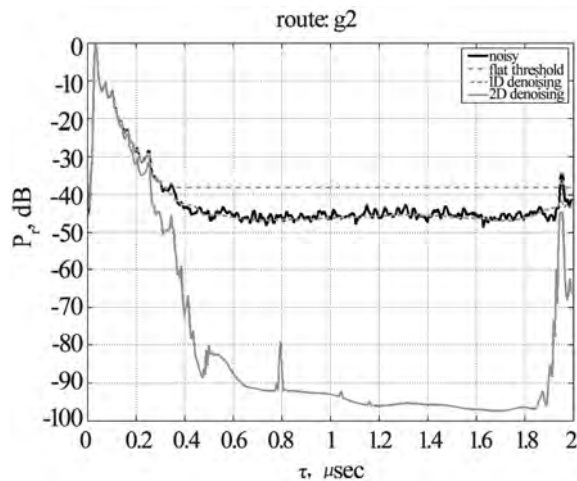


**Figure 3.** Noisy, denoised (1D and 2D) and flat noise thresholded (10 dB above the mean noise floor) average PDP from G2 route.

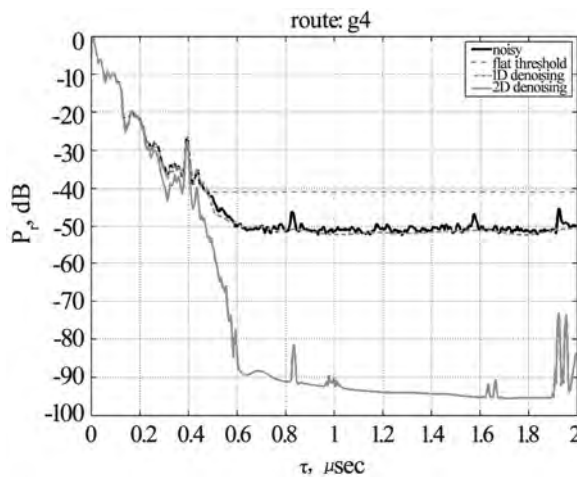


**Figure 4.** Noisy, denoised (1D and 2D) and flat noise thresholded (10 dB above the mean noise floor) average PDP from G4 route.

## 6. References

- [1] T. S. Rappaport, "Wireless communications – Principles & practice," 2nd Edition, Upper Saddle River, Prentice Hall, 2002.
- [2] E. S. Sousa, V. M. Jovanovic, and C. Daigneault, "Delay spread measurements for the digital cellular in Toronto," *IEEE Transactions on Vehicular Technology*, Vol. 43, No. 4, pp. 837–847, November 1994.
- [3] M. H. C. Dias and G. L. Siqueira, "On the use of wavelet-based denoising to improve power delay profile estimates from 1.8 GHz indoor wideband measurements," *Wireless Personal Communications*, Vol. 32, No. 2, pp. 153–175, January 2005.
- [4] L. H. Macedo, M. H. C. Dias, R. D. Vieira, J. F. Macedo, and G. L. Siqueira, "Mobile indoor wide-band 1.8 GHz sounding: measurement-based time dispersion analysis," in *Proceedings of the IEEE 55th Vehicular Technology Conference - VTC Spring 2002*, Birmingham - AL, USA, Vol. 1, pp. 375–379, May 2002.
- [5] D. L. Donoho, "De-noising by soft-thresholding," *IEEE Transactions on Information Theory*, Vol. 41, No. 3, pp. 613–627, May 1995.

# On Cross-Layer Design of AMC Based on Rate Compatible Punctured Turbo Codes

**Fotis Foukalas, Evangelos Zervas**

*Department of Informatics and Telecommunications, University of Athens, Athens, Greece*

*Email: {foukalas, zervas}@di.uoa.gr*

*Received December 24, 2009; revised January 27, 2010; accepted February 28, 2010*

## Abstract

This paper extends the work on cross-layer design which combines adaptive modulation and coding at the physical layer and hybrid automatic repeat request protocol at the data link layer. By contrast with previous works on this topic, the present development and the performance analysis as well, is based on rate compatible punctured turbo codes. Rate compatibility provides incremental redundancy in transmission of parity bits for error correction at the data link layer. Turbo coding and iterative decoding gives lower packet error rate values in low signal-to-noise ratio regions of the adaptive modulation and coding (AMC) schemes. Thus, the applied cross-layer design results in AMC schemes can achieve better spectral efficiency than convolutional one while it retains the QoS requirements at the application layer. Numerical results in terms of spectral efficiency for both turbo and convolutional rate compatible punctured codes are presented. For a more comprehensive presentation, the performance of rate compatible LDPC is contrasted with turbo case as well as the performance complexity is discussed for each of the above codes.

**Keywords:** Cross-Layer Design, Adaptive Modulation and Coding, Rate-Compatible Punctured Turbo Codes, Hybrid ARQ, Codes Complexity

## 1. Introduction

The success of current standard such as 3GPP HSPA and IEEE 802.11/16 in terms of high data rates provision and quality of service (QoS) requirements satisfaction is principally owed to Adaptive Modulation and Coding (AMC), hybrid automatic repeat-request (HARQ) and fast scheduling [1,2]. The AMC realization uses different constellation orders and coding rates according to the signal strength [3]. By this way, when instantaneous channel conditions are proper, link adaptation offers high data rates at the physical layer. The proper usage of each constellation order and coding rate, i.e., mode is specified by the SNR regions in which each separate mode is active.

Enhancement of AMC performance can be achieved by using different channel coding techniques. Particularly, in case of turbo-coding implementation, an AMC scheme can achieve the highest spectral efficiency even if low SNR regions are met [4]. The original rate of a turbo code could be  $1/3$ ; nevertheless by using puncturing techniques greater code rates can be used for each modulated symbol. Incorporating also rate compatibility in punctured turbo codes, by which all of the code sym-

bols of a high rate punctured code are used by the lower rate codes, an enhanced spectral efficiency is reached. This gain is actually provided by Rate-Compatible Punctured Turbo (RCPT) codes [5]. RCPT codes have been employed for HARQ implementations due to the fact that no received information is discarded [6]. Such ARQ schemes are well-known as Incremental Redundancy (IR) HARQ schemes that improves the channel use efficiency since parity bits for error correction are transmitted only if this is required [7].

The aforementioned description is basically a cross-layer combination of AMC at the physical layer and HARQ at the data link layer for QoS provisioning in wireless communication networks [8,9]. It has been shown that such a cross-layer design outperforms in terms of spectral efficiency, the case of AMC use only at the physical layer or the combination of typical ARQ with a single modulation and coding scheme [8]. Moreover, it has been proved that IR HARQ based on convolutional codes has much improvement in spectral efficiency than that with type-I HARQ [9]. To this direction and since a lot of research work has been done on turbo codes as well as turbo coding and decoding is applied to all

known standards of wireless communications [2,10], we extend this study by employing the aforementioned cross-layer design (CLD) that combines AMC and HARQ based on RCPT codes.

The rest of this paper is organized as follows. Section 2 presents the system model and its components in details. In Section 3, the cross-layer design of the system is presented with its assumptions and constraints. In Section 4, system performance is evaluated for both turbo and convolutional rate compatible codes and LDPC as well. Besides, the complexity performance is evaluated for each coded system. Finally, Section 5 provides the concluding remarks and gives some directions for further investigation in this topic.

## 2. System Model

The model of the adopted cross-layer design system is illustrated in **Figure 1**. It shows the layer structure of the system as well as the implementation details of the AMC scheme (i.e. physical layer). In the following text, we first describe concisely the functionality of each layer and in sequel we go into details for each of layers' components.

### 2.1. Turbo Encoding and Decoding

First, confirm that you have the correct template for your paper size. This template has been tailored for output on the A4 paper size. If you are using US letter-sized paper,

please close this file and download the file for "MSW US ltr format". Turbo coding and decoding achieves performances on error probability near to Shannon limit [11]. In its main form, turbo coding is a channel coding type that combines two simple convolutional codes in parallel linked by an interleaver (i.e. Parallel Concatenated Convolutional Codes-PCCC) [12]. It had been studied that recursive systematic convolutional codes (RSC) are superior to nonrecursive counterparts for concatenated implementations [13]. The codewords of such schemes consist of one information bit followed by two parity check bits which both parallel encoders produce. Thus, the rate code of a PCCC scheme with two RSC constituent codes is  $R_c = 1/3$ .

On the other side, the decoding process of concatenated codes is performed by a suboptimum decoding scheme that uses a posteriori probability (APP) algorithms instead of using Viterbi algorithms. Such a scheme is constructed by "soft-in/soft-out" decoders that exchange bit-by-bit or symbol-by-symbol APPs as soft information that depends on the bit or symbol decoding technique [14]. The input soft-information represents the log-likelihoods of encoder input bits and code bits. This is actually the input of the Soft-Input Soft-Output (SISO) "Maximum A Posteriori" (MAP) module presented in [15]. The output soft-information of this module is updated versions of input based on the information of the constituent RSC of the turbo encoder.

More specific, turbo decoding based on a PCCC scheme is constructed by two SISO modules that linked with

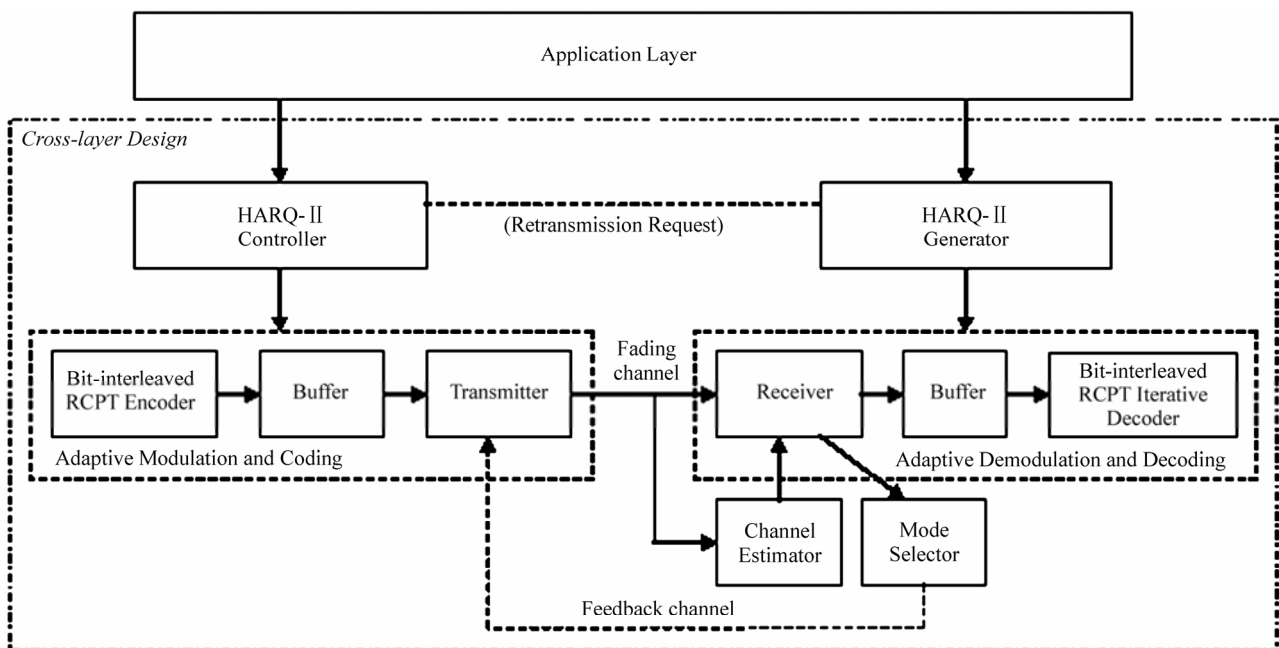


Figure 1. Cross-layer system model combining AMC and HARQ based on RCPT codes.

a deinterleaver (**Figure 2**). In addition to that, iterative decoding is accomplished in order to improve the decoding performance. Henceforth, a feedback loop between the two constituent SISO decoders is established that actually presents the turbo decoding principle [11]. This feedback loop appears an interleaver that gives interleaved inputs to the first parallel decoder required for the first iteration and so on. Multiple iterations between these two decoders exchanging soft information give near to Shannon limit results. Turbo codes and iterative turbo decoders has been extensively studied for implementation purposes in current standards like 3GPP HSPDA (High Speed Data packet Access) [16].

### 2.2. RCPT Codes

In general, a RCPT encoder consists of a turbo encoder as described above followed by a puncturing block with puncturing matrix  $P$ . The puncturing matrix  $P$  is known as the puncturing rule or pattern and indicates the coded bits that should be punctured [17]. Puncturing can be applied both to information or/and parity bits. However, the way of puncturing affects the coding scheme performance and the coded-modulation scheme in general [18]. Assuming only the impact of puncturing on turbo coding scheme, one can realize that without puncturing systematic bits, the code performance decrease is reasonable. In addition to that, by puncturing periodically the parity bits produced by two RSC codes, a better performance of the coding scheme can be achieved.

The rate compatibility offered by a RCPT code has been considered as the enabling technique for incremental redundancy (IR) HARQ schemes [6]. IR HARQ based protocols are major components of HSDPA offering rate matching capabilities [19]. During the rate matching process, the transmitter sends only supplemental coded bits indicated by the aforementioned puncturing rule. A representative example of IR HARQ scheme for HSDPA with turbo encoder as mother code is presented in [20]. The RCPT encoder in particular is constructed by a turbo mother code with a rate code  $R = 1/M$  resulted by  $M - 1$  RSC encoders. The puncturing matrix  $P$  indicates the puncturing period and actually the bits being punctured during the HARQ scheme operation [6,18]. Therefore, the resultant family of rate codes is:

$$R_\ell = \frac{P}{P + \ell}, \quad \ell = 0, 1, \dots, (M - 1)P \quad (1)$$

An example of RCPT encoder dedicated to ARQ mechanisms with  $M = 3$  and  $P = 3$  is illustrated in **Figure 3** which is constructed from two constituent RSC encoders with rate  $1/2$  and offers a family of RCPT code rates  $R_{c_1} > R_{c_2} > \dots > R_{c_M}$  with the following decreasing order  $\{(1), (3/4), (3/5), (1/2), (3/7), (3/8), (1/3)\}$ .

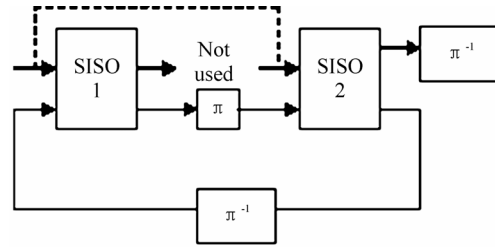


Figure 2. PCCC (i.e. turbo) decoding with SISO modules.

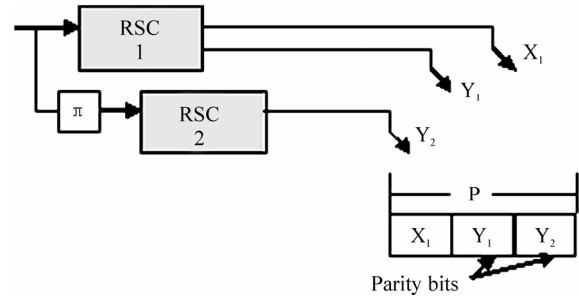


Figure 3. RCPT-ARQ encoder.

### 2.3. RCPT-ARQ Protocol

By puncturing the bits that will be transmitted in the current and future transmission attempts, the HARQ scheme (i.e. RCPT-ARQ) brakes the packet unit with size  $L$  into blocks of bits with size  $L_i$ . The number of transmitted bits  $L_i$  of the RCPT-ARQ protocol at the  $i$ th transmission attempt can be expressed as [10]

$$L_i = \begin{cases} L \cdot \left( \frac{1}{R_{c_1}} \right) & i = 1, \\ L \cdot \left( \frac{1}{R_{c_i}} - \frac{1}{R_{c_{i-1}}} \right) & 1 < i \leq C \end{cases} \quad (2)$$

where  $R_{c_i}$  with  $i = 1, \dots, C$  denotes the  $C$  rates produced by the RCPT encoder. Going into further details, we assume a single stop-and-wait ARQ strategy of RCPT-ARQ protocol (i.e. hybrid ARQ) described by the following step-by-step functionality:

- Depending on previous channel condition the adaptive scheme operates on mode  $n$ .
- The  $L$ -long packet size is encoded by the turbo mother code. The coded packet is stored at the transmitter and is broken into blocks with size of  $L_i = L\{1/R_{c_i}\}$  bits with  $i = 1, \dots, C$ . Bits selection is performed for each transmission attempt according to the puncturing rule.
- Constituent blocks' transmission with size  $L_i$  is initialized according to the puncturing matrix.
- At the receiver, iterative decoding is performed for each separate transmission block  $L_i$ . If decoding is not

successful after the number of maximum transmissions  $N_t^{\max}$  is reached, then a NAK is sent to the transmitter and the adaptive scheme updates to the corresponding mode according to the channel condition.

- Otherwise, an ACK is sent to the transmitter and the adaptive scheme continues to the current mode  $n$ .

### 3. Cross-layer Design

The cross-layer system structure described above is relied on the following assumptions:

- Channel SNR estimation is perfect and in consequence the channel state information (CSI) that is available at the receiver as well, although the impact of errors in SNR estimation on adaptive modulation is negligible [21]. In our implementation, the channel estimator is implemented using the Error Vector Magnitude (EVM) algorithm for AWGN channel [22].

- Feedback channel dedicated to mode selection process is error free and without latency. The mode selection is performed in a packet-by-packet basis i.e. the AMC scheme is updated after  $N_t^{\max}$  transmission attempts. Alternative update policies with e.g. updates for every transmission attempt (i.e. block-by-block basis), will be left for further investigation [10].

- System updates are based on received SNR denoted as  $\gamma$  that is actually the estimated channel SNR at the receiver. It is assumed that the received SNR  $\gamma$  values per packet is described statistically as i.i.d random variables with a Rayleigh probability density function (pdf):

$$p_\gamma(\gamma) = \frac{1}{\bar{\gamma}} \exp\left(-\frac{\gamma}{\bar{\gamma}}\right) \quad (3)$$

where  $\bar{\gamma} = E\{\gamma\}$  is the average received SNR.

#### 3.1. Cross-Layer Design of AMC and HARQ

A cross-layer design approach that combines the AMC at the physical layer with a hybrid ARQ at the data link layer could follow the procedure presented both in [9] and [10]. Applying this method, the following constraints must be imposed in order to keep a particular QoS level at the application layer:

Constraint1 (C1): The maximum allowable number of transmissions per information packet is  $N_t^{\max}$ .

Constraint2 (C2): The probability of unsuccessful reception after  $N_t^{\max}$  transmissions is no greater than  $\Pr_{loss}$ .

C1 is calculated by dividing the maximum allowable delay at the application layer and the round trip time required for each transmission at the physical layer. For

example, assuming the QoS concept of 3GPP, the audio and video media streams for MPEG-4 video payload allows a maximum delay value equal to 400 ms [23]. In addition to that the round trip delay between the terminal and the Node B for retransmissions in case of HSDPA could be approximated less than 100 ms [23]. Thereafter, in such a context, the  $N_t^{\max}$  should be 4. On the other hand, C2 is related to the bit-error rate (BER) at the physical layer and the packet size at the data link layer. Hence, if the BER imposed by the QoS requirements at the application layer is equal to  $10^{-6}$  and the information packet size is  $L = 1000$  then the  $\Pr_{loss}$  should be  $10^{-3}$  [23].

It is obvious that the aforementioned cross-layer design (CLD) dictates the code rates that will be used for each transmission at the data link layer and therefore specifies the AMC switching thresholds at the physical layer. Moreover, the proposed CLD scheme will be affected by constituent encoders (i.e. RSC encoders) of turbo code as well the puncturing rules [6,18]. However, in current investigation, we present the results derived using one of the optimal RCPT code and puncturing rule presented in [6], and we will present the RCPT codes and puncturing impact on our CLD in our future work.

#### 3.2. AMC Schemes

The design of AMC schemes is the process by which the switching thresholds are specified. The switching thresholds of an AMC scheme at the physical layer are specified by a given target BER ( $BER_{target}$ ) [3,4]. The switching thresholds are boundary points of the total SNR range denoted as  $\{\gamma_n\}_{n=0}^{N+1}$  specifying nonoverlapping consecutive intervals  $\gamma \in [\gamma_n, \gamma_{n+1})$ . Afterwards, each mode is selected in accordance to the switching thresholds derived from the  $BER_{target}$ .

However, in a combined system in which the unit of interest is the packet at the data link layer, the AMC design follows the  $PER_{target}$  value. More specific, in order to satisfy the aforementioned constraints of the proposed combination, the switching thresholds should be derived from the following inequality:

$$\Pr^{N_t} \leq \Pr_{loss} := \Pr_{target} \quad (4)$$

where  $\Pr^{N_t}$  is the packet error probability (i.e. packet error rate) after  $N_t$  transmissions at the data link layer. In the following paragraphs, we derive the boundary points  $\{\gamma_n\}_{n=0}^{N+1}$  for each modulation and coding scheme (MCS).

The packet error probability can be expressed in rela-

tion to BER by the following equation

$$Pr = 1 - (1 - BER)^L \tag{5}$$

only if each demodulated and decoded bit inside the packet has the same BER and bit-errors are uncorrelated [9,10]. On the other hand, known closed form expressions for the PER<sup>1</sup> and BER is not available in the literature and closed-form expressions for the BER of turbo-coded modulations in AWGN channel is not available either [8]. All the same, one can use the union bound for turbo-coded modulation system using the bounding technique introduced in [24]. However, this technique is applied for 16QAM system and indeed needs more investigation in case of turbo-coded AMC schemes with multiple modulation modes. Thereafter and since further investigation on union bounds of turbo-coded modulation is not the aim of our current work, we take BER and PER values through simulations. Finally, the simulated PER values are compared with those derived from fitting the curves and those derived from Equation (5).

**Figure 4** shows the PER values versus received SNR of each mode in coding step with  $Rc_i$ , where  $i = 1, 2, 3$  number of transmissions. We use the 1/2 QPSK, 3/4 QPSK, 1/2 16QAM and 3/4 16QAM modulations with RCPT code rates 1, 1/2 and 1/3 for each transmission respectively. The packet size is  $L = 1536$  length and the puncturing follows the optimal rules according to [6] (**Table 1**). The constituent RSC encoders of PCCC turbo codec is the optimal encoder B proposed by [6] with rate 1/2, memory  $\nu = 4$  (i.e. 16 states) and generator matrix  $(1, g_b / g_a)$ , where the generator polynomial  $g_a$  and  $g_b$  have octal representations  $(15)_{octal}$  and  $(13)_{octal}$  respectively. The number of iterations is 8. The figures depict the simulated PER, the fitting curves and the values derived from Equation (5).

In order to have a more clear view on RCPT performance combining with AMC, we should compare it with the other types of rate compatible codes. To this end, we implement also the aforementioned CLD first using RCPC (Rate Compatible Convolutional Code) and second using RC-LDPC (Rate Compatible Low-density Parity-check codes). We use the same rates for both two RC codes. Specifically, the RCPC is a convolutional encoder with rate 1/2, generator polynomial  $(171, 133)$

**Table 1. The block size and the puncturing matrix (in octoal) of applied rcpt codes.**

Block size	Family of Code Rates		
	1	2/3	1/2
$L = 1536$	00	01	05
	00	01	05
	00	01	05

<sup>1</sup>For the rest of this document the packet error probability Pr will be replaced with PER notation.

and constraint length 7 [9]. For LDPC, we employ the same codes as in [25] with rate 1/2 (1008,504) and a variable node degree equal to 3. The corresponding performance of these modulation and coding schemes (MCS) is depicted separately for each code in **Figure 4**.

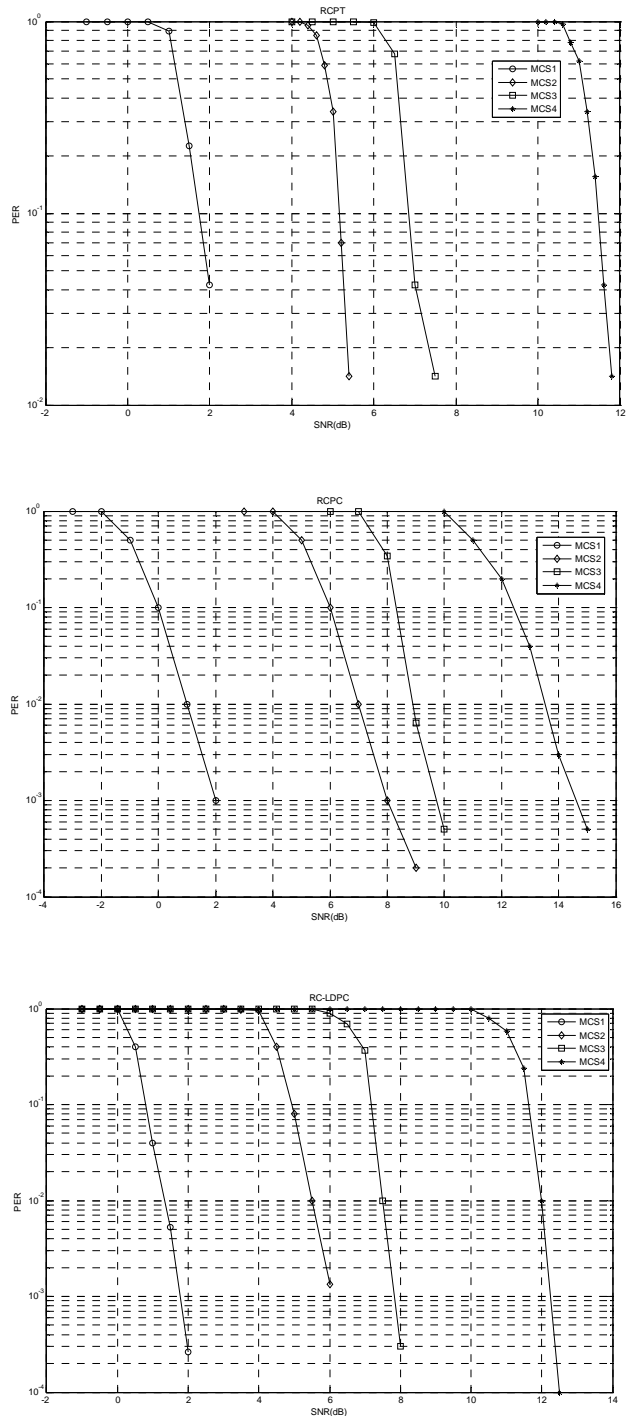


**Figure 4. PER simulation performance of 4 AMC modes using RCPT, RCPC and RC-LDPC.**

## 4. Performance Analysis and Numerical Results

### 4.1. System Performance

In case of a general type-II HARQ that uses punctured codes, the probability of unsuccessful reception after  $N_t$  transmissions represents the event of decoding failure with code  $Rc_i$  after  $i$  transmissions [10]. In case of limited transmissions, the packet error probability of this using AMC mode  $n = 1, \dots, N$  under channel states  $\gamma_n^i = \{\gamma_n^{(1)}, \gamma_n^{(2)}, \dots, \gamma_n^{(N_t)}\}$  is given by [26]

$$PER_n(\gamma) = \prod_{i=1}^{N_t} PER_i(\gamma_n^i) \quad (6)$$

By using (6) over  $PER_i$  for each retransmission and for each mode  $n = 1, \dots, N$  the packet error rates after  $i$  transmissions are resulted. The  $\gamma_n^i$  denotes the region boundaries for each MCS and obtained as follows

$$\begin{aligned} \gamma_1^{(i)} &= 0, \\ \gamma_n^{(i)} &= \frac{1}{g_n} \ln\left(\frac{a_n}{PER_i^{target}}\right), \quad n = 2, \dots, N, \\ \gamma_{N+1}^{(i)} &= +\infty \end{aligned} \quad (7)$$

The  $PER_i^{target}$  is reached using the corresponding decoder  $Rc_i$  when the imposed  $N_t$  transmission attempts is reached either. Assuming  $N_t^{max} = 3$  and  $PER_{loss} = 10^{-2}$ , the derived switching thresholds are listed in **Table 2**. **Table 2** includes also the parameters of MCSs for convolutional and LDPC codes.

We next evaluate the system performance in terms of spectral efficiency when the AMC scheme is combined with type II HARQ (i.e. IR HARQ). In each  $i$  transmission attempt, the number of transmitted bits  $L_i$  is specified according to RCPT code rates  $Rc_1 > Rc_2 > \dots > Rc_M$  as mentioned in Section 2. In addition to that, when mode  $n$  is used, each transmitted symbol carry  $Rn_i = Rc_i \cdot \log_2(M_n)$  information bits where  $M_n$  derived from  $M$ -ary modulation scheme. As in [9], we assume a Nyquist pulse shaping filter with bandwidth  $B = 1/T_s$ , where  $T_s$  is the symbol rate. Afterwards, the spectral efficiency  $S_e$  gives the bit rate in bits per symbol that can be transmitted per unit bandwidth and is given by

$$S_e = \frac{L}{\bar{L}} \quad (8)$$

In (7), where  $L$  is the input information packet size and  $\bar{L}$  is the average of transmitted symbols in order to

**Table 2.** the parameters of each rc-coded modulation at the physical layer.

<i>RCPT</i>	MCS1	MCS2	MCS3	MCS4
Modulation	QPSK	QPSK	16-QAM	16-QAM
Coding rate $R_c$	1/2	3/4	1/2	3/4
Rate (bits/symbol)	1.0	1.5	2.0	3.0
$a_n$	4.4111	4.0152	3.9111	3.7011
$g_n$	5.4355	3.3311	2.7151	1.9461
(dB) $\gamma_n^{(1)}$	3.0103	5.9989	9.9663	11.9224
(dB) $\gamma_n^{(2)}$	-1.9230	1.7144	4.9422	7.11145
(dB) $\gamma_n^{(3)}$	-3.0312	-0.3161	3.1221	5.3121

<i>RCPC</i>	MCS1	MCS2	MCS3	MCS4
Modulation	QPSK	QPSK	16-QAM	16-QAM
Coding rate $R_c$	1/2	3/4	1/2	3/4
Rate (bits/symbol)	1.0	1.5	2.0	3.0
$a_n$	0.3351	0.2197	0.2081	0.1936
$g_n$	3.2543	1.5244	0.6250	0.3484
(dB) $\gamma_n^{(1)}$	4.3617	7.4442	11.2882	13.7883
(dB) $\gamma_n^{(2)}$	0.1150	2.8227	6.6132	9.0399
(dB) $\gamma_n^{(3)}$	-1.6532	0.7272	4.4662	6.8206

<i>RC-LDPC</i>	MCS1	MCS2	MCS3	MCS4
Modulation	QPSK	QPSK	16-QAM	16-QAM
Coding rate $R_c$	1/2	3/4	1/2	3/4
Rate (bits/symbol)	1.0	1.5	2.0	3.0
$a_n$	4.1352	3.9164	3.7071	3.5916
$g_n$	5.1441	3.1233	2.5152	1.7373
(dB) $\gamma_n^{(1)}$	2.9311	5.9222	9.6772	11.4211
(dB) $\gamma_n^{(2)}$	-1.5140	1.4237	5.0131	7.33188
(dB) $\gamma_n^{(3)}$	-3.0312	-0.6161	3.0331	5.1235

transmit an information packet. The average of transmitted symbols for each mode  $n$  is given by

$$\bar{L}_n(\gamma) = \frac{L_1}{R_{n_1}} + \sum_{i=2}^{N_t} \frac{L_i}{R_{n_i}} \cdot P_n(\gamma_n^{(i-1)}) \quad (9)$$

For cross-layer designed AMC schemes with  $n = 1, \dots, N$  modes, the average spectral efficiency needs to be calculated in order to evaluate system performance. By averaging the  $\bar{L}_n$  values in the range of  $(\gamma^{(1)}, \dots, \gamma^{(N_t)})$  for over all  $n = 1, \dots, N$  modes, the average number of transmitted symbols in order to transmit an information packet is

$$\bar{L} = \sum_{n=1}^N \int_{\gamma_n}^{\gamma_{n+1}} \frac{L_1}{Rn_i} \cdot p(\gamma_n^{(i)}) d\gamma_n^{(i)} + \sum_{i=2}^{N_i} \sum_{n=1}^N \int_{\gamma_n}^{\gamma_{n+1}} \frac{L_1}{Rn_i} \cdot PER_n(\gamma_n^{(i-1)}) p(\gamma_n^{(i)}) d\gamma_n^{(i)} \quad (10)$$

Figure 5 depicts the average spectral efficiency of the combination of AMC and type-II HARQ relied on constraints  $N_t = 3$  and  $PER_{loss} = 0.01$ . In this figure, it is shown the performance of AMC at physical layer when

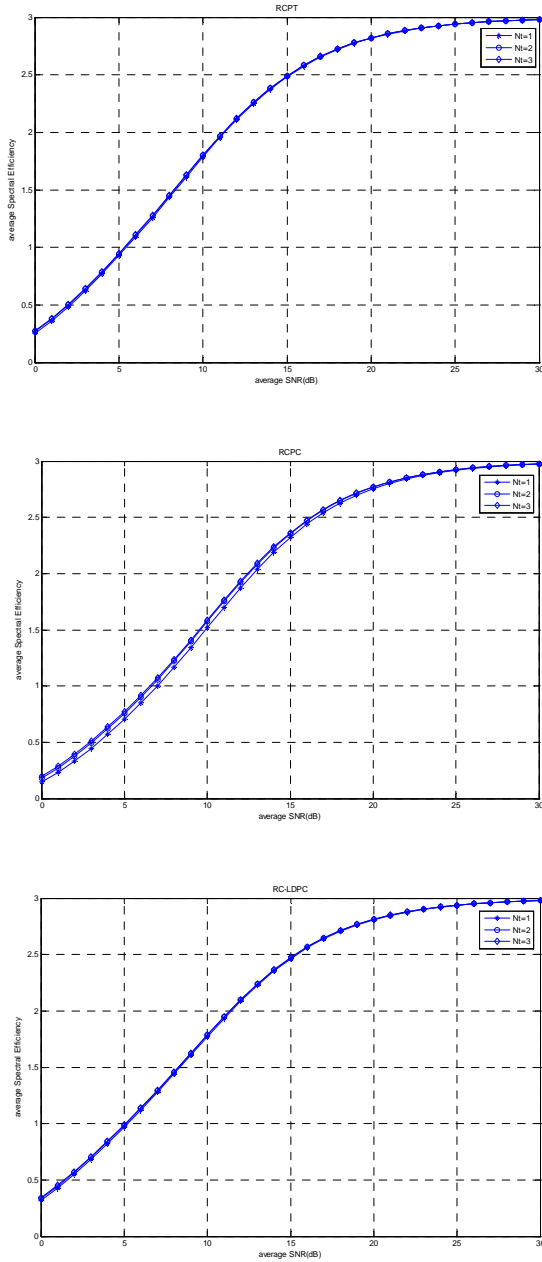


Figure 5. The average spectral efficiency of each RC-coded modulation based on CLD design.

rate compatible punctured codes are employed under the constraints of the previous described cross-layer design. The parameters of each MCS are those listed in Table 2 considering a channel with Rayleigh fading phenomena as described above.

In Figure 6, we make contrast of the average spectral efficiency derived for each rate compatible punctured code. We illustrate the values of third transmission (i.e.  $N_t = 3$ ). Figure 6 shows the performance merit of RCPT against RCPC. This corroborates the benefit of turbo scheme against convolutional one in terms of communication performance as it is well known. Indeed, this performance benefit is more evident in low regions of average SNR than in high regions. Moreover, it is obvious that RC-LDPC achieves performance close to RCPT code. This is a useful outcome considering these two families of codes since LDPC codes are used in several standards and especially in space communications. The fact that turbo and LDPC codes show identical performance has also concluded both in [27] and [28]. [27] has focused on performance in terms of PER values at the physical layer both in AWGN and multipath Rayleigh fading channel. [28] has proposed the PEG (Progressive Edge-Growth) construction method for LDPC codes and has concluded that turbo coding is identical of LDPC in terms of bit-level performance. To this direction, we evaluate the system performance under the aforementioned cross-layer design and we have also concluded in the same result.

### 4.2. Comparison Complexity

However, the comparison between different codes should not be considered only in terms of performance related to communication efficiency. It should be also studied in terms of complexity even when the achieved system performance is identical between different codes (e.g. turbo and LDPC). Most of code complexity issues are

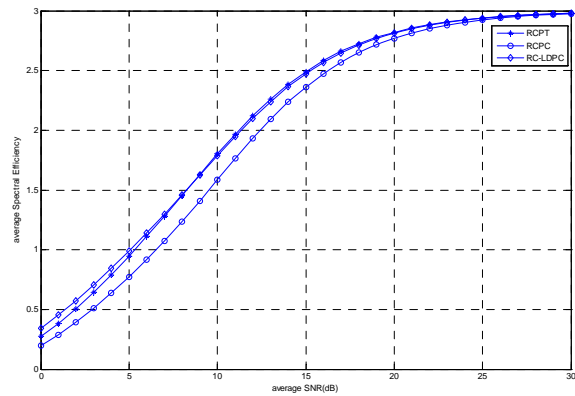


Figure 6. Comparison of RC codes in terms of average spectral efficiency under the constraints of CLD design.

related to computational complexity measuring the additional operations required by each code. Another important aspect of code complexity relies on architectural issues introduced by code design. [29] studies the complexity of decoding algorithms that is measured in terms of computational operations such as multiplications, divisions and additions. In **Table 3** is listed the number of operations (i.e. additions, divisions, etc.) needed for each decoding procedure using the max-log MAP (Maximum A Posteriori) algorithm and the Viterbi algorithm in case of turbo and convolutional decoder respectively. These are actually the decoding algorithms that we have implemented in the RCPT and RCPC decoding procedure. In **Table 3**,  $M$  is the constraint length used by each encoder at the transmitter side.

**Figure 7** shows the complexity of each decoding procedure (i.e. turbo and convolutional) in terms of number of operations vs. the number of iterations and code constraint length respectively. It is obvious from this figure that the decoding complexity in case of convolutional scheme is noticeably less than turbo case. In our case, the convolutional decoding procedure uses Viterbi decoder with constraint length equal to seven. On the other hand, turbo decoding uses max-log MAP with iterations equal to eight. The declension of turbo decoding complexity is close to two times the complexity of convolutional one since convolutional decoding scheme exhibits 1200 number of operations while turbo one exhibits approximately 2400 number of operations.

**Table 3. Complexity of turbo and convolutional decoders.**

	Number of Equivalent Operations
Turbo (Max-log MAP algorithm)	$28 \times 2M - 3$
Convolutional (Viterbi algorithm)	$10 \times 2M - 3$

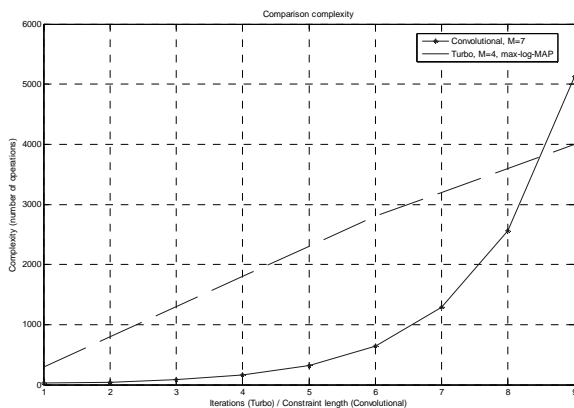


**Figure 7. Complexity comparison between Turbo and Convolutional decoders.**

On the other hand, performance comparisons between turbo and LDPC codes in terms of decoding complexity have shown that when both codes achieve an identical performance then the decoding complexity remains approximately the same. For instance, [28] have claimed that 80 iterations using the belief propagation algorithm produces the same decoding complexity as a turbo code does with 12 iterations using the BCJR decoding algorithm. [27] has studied the performance comparison between turbo and LDPC codes in more details considering computational complexity. The authors have measured the computational complexity in terms of number of operations per iteration per information bit that they could be additions or comparisons. **Table 4** shows the computational complexity per information bit of the sub-optimum decoding algorithm for code rate  $R = 1/3$ . The complexity is expressed in relation to number of iterations  $N_{itr}$  and it is illustrated in **Figure 8**.

Assuming the same configuration as in [27] the turbo decoding with 8 iterations when a max-log-MAP algorithm is used exhibits approximately the same complexity in terms of number of additions with the LDPC decoding scheme that uses the BP algorithm. In our comparative study, we use the decoding schemes from [28] that consist of a turbo decoder with max-log-MAP plus 8 iterations and LDPC decoder with PEG decoding graphs plus 80 iterations. Henceforth, it could be claimed that both turbo and LDPC decoders show the same computational complexity.

**Table 4. Complexity of turbo and LDPC decoding algorithms.**

	Number of Operations per information bit
Turbo (max-log MAP algorithm)	$N_{itr} 106$
LDPC (Belief Propagation algorithm)	$N_{itr} 26.9$

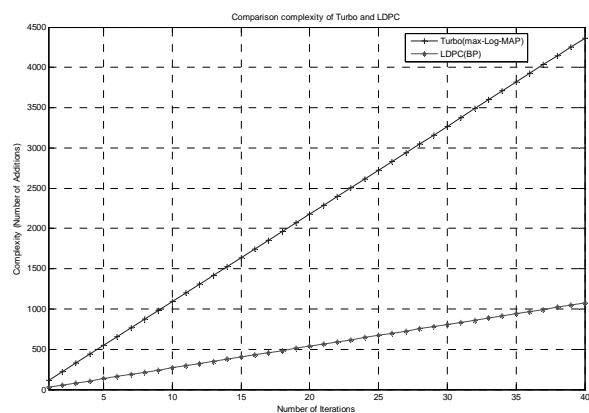


**Figure 8. Complexity comparison between Turbo and LDPC decoders.**

## 5. Conclusions and Future Work

In this paper, we have extended the cross-layer design combining AMC with HARQ using RCPT codes. To this end, a hybrid FEC/ARQ based on RCPT codes has been assumed. In previous works, the proposed CLD was introduced with uncoded modulations, convolutional and rate-compatible convolutional coded modulations dedicated to AMC schemes. In addition to that, we have implemented a CLD approach using puncturing techniques for rate compatibility purposes. The system performance has been evaluated for type-II hybrid ARQ mechanism. Moreover, we have illustrated comparative results of system performance of other rate compatible codes as convolutional and LDPC as well. In order to have a more comprehensive view of coding and decoding schemes we also discuss the computational complexity of each code separately, in terms of the required number of operations either in each iteration attempt or for each memory length. However, since turbo coding and indeed punctured turbo codes are able to accomplish better performance with different RSC encoders and puncturing rules namely optimal encoding and puncturing [26], a future work should be the performance evaluation of AMC and HARQ combination implementing different encoders and puncturing rules using RCPT-ARQ.

## 6. References

- [1] 3GPP TR 25.848 V4.0.0, "Physical layer aspects of UTRA high speed downlink packet access," March 2001.
- [2] IEEE Std 802.16 – 2004, "IEEE standard for metropolitan area networks - Part 16: Air interface for fixed broadband wireless systems".
- [3] A. J. Goldsmith and S.-G. Chua, "Adaptive coded modulation for fading channels," IEEE Transactions on Communications, Vol. 46, pp. 595–602, May 1998.
- [4] S. Vishwanath and A. Goldsmith, "Adaptive turbo-coded modulation for flat-fading channels," IEEE Transactions on Communications, Vol. 51, No. 6, pp. 964–972, June 2003.
- [5] F. Babich, G. Montorsi, and F. Vatta, "On rate-compatible punctured turbo codes design," EURASIP Journal on Applied Signal Processing, Vol. 2005, No. 6, pp. 784–794, May 2005.
- [6] D. N. Rowitch and L. B. Milstein, "On the performance of hybrid FEC/ARQ systems using rate compatible punctured turbo (RCPT) codes," IEEE Transactions on Communications, Vol. 48, No. 6, pp. 948–959, 2000.
- [7] "Performance comparison of hybrid-ARQ schemes," 3rd Generation Partnership Project (3GPP) Technical Specification TSGR1#17(00)1396, October 2000.
- [8] Q. Liu, S. Zhou, and G. Giannakis, "Cross-layer combining of adaptive modulation and coding with truncated ARQ over wireless links," IEEE Transactions on Wireless Communications, Vol. 3, pp. 1746–1755, September 2004.
- [9] D. L. Wu and C. Song, "Cross-layer combination of hybrid ARQ and adaptive modulation and coding for QoS provisioning in wireless data networks," IEEE/ACM QShine, 2006.
- [10] "Multiplexing and channel coding (FDD)," 3rd Generation Partnership Project (3GPP) Technical Specification TS 25.212, Review 7.5.0, May 2007.
- [11] C. Berrou, A. Glavieux, and P. Thitimajshima, "Near Shannon limit error-correcting coding and decoding: Turbo codes," ICC, pp. 1064–1070, 1993.
- [12] S. Benedetto and G. Montorsi, "Design of parallel concatenated convolutional codes," IEEE Transactions on Communications, Vol. 44, No. 5, pp. 591–600, May 1996.
- [13] S. Benedetto and G. Montorsi, "Unveiling turbo codes: Some results on parallel concatenated coding schemes," IEEE Transactions on Information Theory, pp. 409–428, March 1996.
- [14] S. Benedetto, D. Divsalar, G. Montorsi, and F. Pollara, "Soft-output decoding algorithms in iterative decoding of turbo codes," TDA Progress Report 42–124, Jet Propulsion Lab, NASA, 15 February 1996.
- [15] S. Benedetto, D. Divsalar, G. Montorsi, and F. Pollara, "A soft-input soft-output maximum a posteriori (MAP) module to decode parallel and serial concatenated codes," TDA Progress Report 42–127, Jet Propulsion Lab, NASA, 15 November 1996.
- [16] T. Maru, "A turbo decoder for high speed downlink packet access," Vehicular Technology Conference, VTC 2003-Fall, Vol. 1, pp. 332–336, 6–9 October 2003.
- [17] F. Babich, G. Montorsi, and F. Vatta, "Design of rate-compatible punctured turbo (RCPT) codes," ICC 2002, New York, Vol. 3, pp. 1701–1705, 2002.
- [18] M. A. Kousa and A. H. Mugaibel, "Puncturing effects on turbo codes," IEEE Proceedings of Communications, Vol. 149, No. 3, pp. 132–138, June 2002.
- [19] M. Döttling, T. Grundler, and A. Seeger, "Incremental redundancy and bit-mapping techniques for high speed downlink packet access," in Proceedings of the Global Telecommunications Conference, pp. 908–912, December 2003.
- [20] S. Bliudze, N. Billy, D. Krob, "On optimal hybrid ARQ control schemes for HSDPA with 16QAM," WiMob' 2005, August 2005.
- [21] M. Mohammad and R. M. Buehrer, "On the impact of SNR estimation error on adaptive modulation," IEEE Communications Letters, Vol. 9, No. 6, pp. 490–492, June 2005.
- [22] D. Athanasios and K. Grigorios, "Error vector magnitude SNR estimation algorithm for HiperLAN/2 transceiver in AWGN channel," TELSIKS '05, Vol. 2, pp. 415–418, 2005.
- [23] 3GPP TS 23.107 V 5.10.0, "Technical specification group services and systems aspects, service aspects; QoS concept

- and architecture (Release 5),” September 2003.
- [24] T. Duman and M. Salehi, “Performance bounds for turbo-coded modulation systems,” *IEEE Transactions on Communications*, Vol. 47, No. 4, pp. 511–521, April 1999.
- [25] Y. L. Zhang and D. F. Yuan, “Rate-compatible LDPC codes for cross-layer design combining of AMC with HARQ,” 2006 6th International Conference on ITS Telecommunications Proceedings, pp. 537–540, June 2006.
- [26] D. L. Wu and C. Song, “Cross-layer design for combining adaptive modulation and coding with hybrid ARQ,” *IWCMC '06*, Vancouver, British Columbia, pp. 147–152, 2006.
- [27] N. Ohkubo, N. Miki, Y. Kishiyama, K. Higuchi, M. Sawahashi, “Performance comparison between turbo code and rate-compatible LDPC code for evolved UTRA downlink OFDM radio access,” *MILCOM '06*, Washington DC, 2006.
- [28] X. Y. Hu, E. Eleftheriou, and D. M. Arnold, “Regular and irregular progressive edge growth tanner graphs,” *IEEE Transactions on Information Theory*, Vol. 51, pp. 386–398, January 2005.
- [29] A. Chatzigeorgiou, M. R. D. Rodrigues, I. J. Wassell, and R. A. Carrasco, “Comparison of convolutional and turbo coding for Broadband FWA Systems,” *IEEE Transactions on Broadcasting*, 2007.

# Performance of Block Diagonalization Broadcasting Scheme for Multiuser MIMO System Operating in Presence of Spatial Correlation and Mutual Coupling

Feng Wang, Marek E. Bialkowski, Xia Liu

*School of Information Technology & Electrical Engineering, University of Queensland, Brisbane, Australia*

*Email: {fwang, meb, xialiu}@itee.uq.edu.au*

*Received December 31, 2009; revised January 30, 2010; accepted February 27, 2010*

## Abstract

In this paper, the capacity of a multiuser Multiple Input Multiple Output (MIMO) system employing the block diagonalization broadcasting scheme in presence of spatial correlation and mutual coupling is investigated. It is shown by computer simulations that, in general, the presence of spatial correlation decreases the capacity of a multiuser MIMO system. However, for some particular antenna element spacing mutual coupling decreases the spatial correlation rendering an increased capacity. The optimized diagonalization broadcasting technique with a two-stage power allocation scheme is proposed and verified. The presented simulations results confirm the advantage of the proposed broadcasting scheme.

**Keywords:** Multiuser MIMO, Block Diagonalization, Mutual Coupling, Dirty Paper Coding

## 1. Introduction

It has been shown via theoretical derivations as well as by experiment that using multiple element antennas with a suitable signal transmission scheme in a rich scattering propagation environment can enhance peer-to-peer communication without the use of extra frequency bandwidth [1,2]. This potential of multiple input multiple output (MIMO) communication systems can be used to advantage using two alternative approaches. In one approach, the signal transmission quality via diversity can be improved. Alternatively for a chosen quality factor such as bit error rate (BER), the data rate can be increased by a stream multiplexing transmission.

Most recent studies on MIMO focus on multiuser systems. For a multiuser MIMO system, allocation of the channel resources among independent users either in the form of multiple accesses (uplink) or broadcasting (downlink) is considered. The information theory hints that the broadcasting case is by far the most challenging. In this case, an inter-user interference occurs due to the spatially multiplexed transmitted signals at a base station (BS). For the Gaussian MIMO broadcasting channels, it has been proved that dirty paper coding (DPC) [3] can achieve the available capacity [4]. However, to deploy DPC in a real system is challenging due to the high complexity and computational burden on successive encod-

ing and decoding. An alternative strategy is the block diagonalization (BD) [5,6]. Compared with DPC scheme, BD is a suboptimal technique with much reduced complexity. Using this technique, signals are transmitted only to desired users. In turn, null steering is applied to other users by decomposing the multiuser channel into a group of parallel single user MIMO channels. To achieve such decomposition, BS needs to select a suitable beamforming matrix for each user. The matrix is vertical to the space spanned by other users' channels matrices. If the channel matrices of all the scheduled users are perfectly known at the transmitter, the inter-user interference can be eliminated by BD, rendering a simple receiver structure.

Because of its simplicity and good performance, BD is under constant research. In [7], the imperfect channel state information (CSI) assumption was used while investigating BD. The effect of outdated CSI at transmitter on multiuser MIMO system with BD was reported. In [8], a BD algorithm that accounts for the presence of other-cell interferences was proposed under the assumption that the transmitter has full CSI and the information about the interference plus noise covariance matrix for in-cell users. Most of the research on BD for multiuser MIMO systems was done by neglecting interactions within the transmitting and receiving array antennas and between the array antennas and scatterers. When a

MIMO transceiver has to be of compact size interactions within the transmitting or receiving array antennas have to be taken into account. The small inter-element spacing in the antenna array in such transceivers renders mutual coupling. The effect of mutual coupling on a point-to-point MIMO system has been investigated in many works, such as [9,10,11]. In this paper, a BD algorithm that accounts for the effect of spatial correlation and mutual coupling in array antennas is presented and its performance is evaluated with respect to the overall system capacity.

The paper is organized as follows. Section 2 describes a multiuser MIMO system model including the channel model with spatial correlation. Section 3 describes interactions between the array elements and scatterers in the propagation environment in which mutual coupling effects cannot be neglected. Section 4 gives details of the BD algorithm that accounts for the effect of mutual coupling. Section 5 quantifies the effect of mutual coupling by presenting numerical results. Section 6 summarizes the findings of the undertaken research.

## 2. System Model

### 2.1. Signal Model

A narrowband multiuser system is assumed. It is postulated that it is created around a base station (BS) with  $L$  downlink mobile users. The base station includes  $N$  transmitting antennas. At time  $t$ ,  $K$  mobile stations (MS) from  $L$  available users are scheduled to be serviced by BS. The  $k$ -th mobile station (MS) employs  $M_k$  antennas. The transmitted signal intended for the  $k$ -th mobile station is denoted by a  $Q_k \times 1$  dimensional vector  $\mathbf{x}_k$  which is weighted by an  $N \times Q_k$  pre-processing matrix  $\mathbf{W}_k$  before transmission.  $Q_k$  is the number of parallel data symbols transmitted simultaneously to the  $k$ -th MS. The MIMO channel between the BS the  $k$ -th MS is described by the complex matrix  $\mathbf{H}_k$ , whose  $(i,j)$ th entries represent the complex gain between the  $j$ -th transmit antenna at BS and  $i$ -th antenna at  $k$ -th MS. It is assumed that different MS experience independent fading. The received signal at  $k$ -th MS can be presented by

$$\begin{aligned} \mathbf{y}_k &= \mathbf{H}_k \sum_{k=1}^K \mathbf{W}_k \mathbf{E}_k \mathbf{x}_k + \mathbf{n}_k \\ &= \mathbf{H}_k \mathbf{W}_k \mathbf{E}_k \mathbf{x}_k + \sum_{j=1, j \neq k}^K \mathbf{H}_k \mathbf{W}_j \mathbf{E}_j \mathbf{x}_j + \mathbf{n}_k \end{aligned} \quad (1)$$

where  $\text{trace}(\mathbf{E}_k \mathbf{E}_k^\dagger) = p_k$  is the power transmitted to the  $k$ th MS.  $\mathbf{n}_k$  is the additive Gaussian white noise (AWGN) vector, whose elements are independent identical distribution (*i.i.d.*) zero-mean circularly symmetric complex Gaussian random variables with variance  $\sigma_n^2$ .

### 2.2. Channel Model

The channel matrix  $\mathbf{H}_k$  describing the channel properties between BS and the  $k$ th MS is influenced by the transmitting and receiving antenna array configurations and a signal propagation environment. It is assumed that the BS and MSs are equipped with wire dipoles arranged in linear arrays. The length of each dipole element is assumed to be half wavelength. Also, the links between BS and different MSs do not share the same scattering environment. This assumption confirms the earlier assumed independent signal fading for different MSs. For each link, the Kronecker channel model [5,12] is assumed. In this model, the correlations at transmitter and receiver sides are independent and the channel matrix  $\mathbf{H}_k$  is represented as

$$\mathbf{H}_k = (\mathbf{R}_{MS}^k)^{1/2} \mathbf{G}_H \mathbf{R}_{BS}^{1/2} \quad (2)$$

where  $\mathbf{G}_H$  is a matrix with *i.i.d.* Gaussian entries with zero mean and unit variance and  $\mathbf{R}_{MS}^k$  and  $\mathbf{R}_{BS}$  are spatial correlation matrices at the  $k$ th MS and BS, respectively. In a rich scattering environment, the correlation for any pair of dipole element with spacing  $d_{m,n}$  can be obtained using Clark's model and are given by a Bessel function

$$\rho_{m,n} = J_0(kd_{m,n}) \quad (3)$$

Using (3), the correlation matrix for the  $k$ th MS can be generated as

$$\mathbf{R}_{MS}^k = \begin{bmatrix} \rho_{1,1} & \cdots & \rho_{1,M_k} \\ \vdots & \ddots & \vdots \\ \rho_{M_k,1} & \cdots & \rho_{M_k,M_k} \end{bmatrix} \quad (4)$$

In turn, the correlation matrix for BS can be obtained from

$$\mathbf{R}_{BS} = \begin{bmatrix} \rho_{1,1} & \cdots & \rho_{1,N} \\ \vdots & \ddots & \vdots \\ \rho_{N,1} & \cdots & \rho_{N,N} \end{bmatrix} \quad (5)$$

## 3. Mutual Coupling

For the array formed by linear parallel wire dipoles, the mutual coupling matrix can be expressed using electromagnetic and circular theory described in [9]

$$\mathbf{C} = (\mathbf{Z}_A + \mathbf{Z}_T)(\mathbf{Z} + \mathbf{Z}_T \mathbf{I}_M)^{-1} \quad (6)$$

where  $Z_A = 73 + j42.5[\Omega]$  is the element impedance in isolation and  $Z_T$  is impedance of the receiver at each element. It is chosen to be the complex conjugate of  $Z_A$  to obtain the impedance match.  $\mathbf{Z}$  is the mutual impedance

matrix with all the diagonal elements equal to  $Z_A + Z_T$ , its non-diagonal elements  $Z_{nm}$  are decided by the physical parameters including dipole length, the horizontal distance between the two dipoles. For a side-by-side array configuration and dipole length  $l$  equals to  $0.5\lambda$ ,  $Z_{nm}$  is given by [9,10]

$$Z_{nm} = \begin{cases} 30[0.5722 + \ln(2\beta l) - C_i(2\beta l)] \\ \quad + j[30S_i(2\beta l)], & m = n \\ 30[2C_i(u_0) + C_i(u_1) - C_i(u_2)] \\ \quad + j[302S_i(u_0) - S_i(u_1) - S_i(u_2)] & m \neq n \end{cases} \quad (7)$$

where  $\beta = 2\pi/\lambda$  is the wave number and  $C_i(u)$  and  $S_i(u)$  are the cosine and sine integral, respectively, given as

$$C_i(u) = \int_{\infty}^u \frac{\cos(x)}{x} dx \quad (8)$$

$$S_i(u) = \int_0^u \frac{\sin(x)}{x} dx$$

and the constants are given by [10]

$$u_0 = \beta d_h$$

$$u_1 = \beta \left( \sqrt{d_h^2 + l^2} + l \right) \quad (9)$$

$$u_2 = \beta \left( \sqrt{d_h^2 + l^2} - l \right)$$

where  $d_h$  is the horizontal distance between the two dipole antennas.

#### 4. Block Diagonalization with Mutual Coupling

We assume at time  $t$ ,  $K$  mobile stations (MS) from  $L$  available users are scheduled to be serviced by BS. To ensure the sufficient freedom for BS to perform BD over the  $K$  scheduled MSs, it is assumed that

$$\sum_{k=1}^K M_k \leq N \quad (10)$$

With spatial correlation and mutual coupling taken into account, the received signal at  $k$ th MS described by (1) can be rewritten as

$$\begin{aligned} \mathbf{y}_k &= \mathbf{C}_{MS}^k \left( \mathbf{R}_{MS}^k \right)^{1/2} \mathbf{G}_H \mathbf{R}_{BS}^{1/2} \mathbf{C}_{BS} \sum_{k=1}^K \mathbf{W}_k \mathbf{E}_k \mathbf{x}_k + \mathbf{n}_k \\ &= \mathbf{C}_{MS}^k \left( \mathbf{R}_{MS}^k \right)^{1/2} \mathbf{G}_H \mathbf{R}_{BS}^{1/2} \mathbf{C}_{BS} \mathbf{W}_k \mathbf{E}_k \mathbf{x}_k \\ &\quad + \mathbf{C}_{MS}^k \left( \mathbf{R}_{MS}^k \right)^{1/2} \mathbf{G}_H \mathbf{R}_{BS}^{1/2} \mathbf{C}_{BS} \sum_{j=1, j \neq k}^K \mathbf{W}_j \mathbf{E}_j \mathbf{x}_j + \mathbf{n}_k \end{aligned} \quad (11)$$

where,  $\mathbf{C}_{BS}$  and  $\mathbf{C}_{MS}^k$  are the mutual coupling matrices for the dipole element array at BS and the  $k$ th MS, respectively.  $\mathbf{W}_k$  is the beamforming matrix at BS for the

$k$ th MS. To eliminate the interference from the signals transmitted to other MSs, the key idea in the block diagonalization is to zero-force the interference by imposing the following condition

$$\mathbf{C}_{MS}^k \left( \mathbf{R}_{MS}^k \right)^{1/2} \mathbf{G}_H \mathbf{R}_{BS}^{1/2} \mathbf{C}_{BS} \mathbf{W}_j = \mathbf{0} \quad (j \neq k, 1 \leq k, j \leq K) \quad (12)$$

when the mutual coupling and correlation is taken into account,

$$\begin{aligned} \bar{\mathbf{H}}_k &= \mathbf{C}_{MS}^k \left( \mathbf{R}_{MS}^k \right)^{1/2} \mathbf{G}_H \mathbf{R}_{BS}^{1/2} \mathbf{C}_{BS} \\ \tilde{\mathbf{H}} &= [\bar{\mathbf{H}}_1, \bar{\mathbf{H}}_2, \dots, \bar{\mathbf{H}}_K]^T \\ \mathbf{W} &= [\mathbf{W}_1, \mathbf{W}_2, \dots, \mathbf{W}_K] \end{aligned} \quad (13)$$

where  $(\bullet)^T$  donates the matrix transpose operation. By including the condition given by (12), the effective channel matrix for the multiuser MIMO system with  $K$  MSs can be represented by a  $\sum M_k \times \sum M_k$  matrix, given as

$$\begin{aligned} \mathbf{D} &= \tilde{\mathbf{H}} \mathbf{W} \\ &= \begin{bmatrix} \bar{\mathbf{H}}_1 \mathbf{W}_1 & \bar{\mathbf{H}}_1 \mathbf{W}_2 & \dots & \bar{\mathbf{H}}_1 \mathbf{W}_K \\ \bar{\mathbf{H}}_2 \mathbf{W}_1 & \bar{\mathbf{H}}_2 \mathbf{W}_2 & \dots & \bar{\mathbf{H}}_2 \mathbf{W}_K \\ \vdots & \vdots & \ddots & \vdots \\ \bar{\mathbf{H}}_K \mathbf{W}_1 & \dots & \dots & \bar{\mathbf{H}}_K \mathbf{W}_K \end{bmatrix} \end{aligned} \quad (14)$$

By using (12), Equation (14) can be rewritten as

$$\mathbf{D} = \begin{bmatrix} \bar{\mathbf{H}}_1 \mathbf{W}_1 & \mathbf{0} & \mathbf{0} & \mathbf{0} \\ \mathbf{0} & \bar{\mathbf{H}}_2 \mathbf{W}_2 & \mathbf{0} & \mathbf{0} \\ \mathbf{0} & \mathbf{0} & \ddots & \mathbf{0} \\ \mathbf{0} & \mathbf{0} & \mathbf{0} & \bar{\mathbf{H}}_K \mathbf{W}_K \end{bmatrix} \quad (15)$$

At this point it is important to comment whether the condition (12) can be met in practice. From the theory of antennas it is known that an  $N$ -element array antenna is capable of forming  $N-1$  nulls. This means that in the strict sense, the BS having an  $N$ -element array is able only to null up to  $N-1$  MSs. For a larger number of MSs, the condition (12) has to be compromised. In such a case, the BS can direct low sidelobes instead of nulls towards undesired users. In further considerations, it is assumed that the number of MSs served by BS is such that the condition (12) is met.

#### 4.1. Calculation of Beamforming Matrices

In order to transmit a signal only to the desired MS while steering nulls to the remaining MSs, the beamforming matrix for the desired MS should be orthogonal to the space spanned by the channel matrices of the undesired MSs. We define the channel matrix as

$$\tilde{\mathbf{H}}_k = [\bar{\mathbf{H}}_1 \dots \bar{\mathbf{H}}_{k-1}, \bar{\mathbf{H}}_{k+1}, \dots, \bar{\mathbf{H}}_K]^T \quad (16)$$

which is obtained by removing the channel matrix for the  $k$ th MS from  $\tilde{\mathbf{H}}$ . Performing the eigenvalue decomposition (EVD) over the  $N \times N$  non-negative Hermitian Matrix, one obtains

$$\tilde{\mathbf{H}}_k^\dagger \tilde{\mathbf{H}}_k = [\tilde{\mathbf{V}}_k \mathbf{V}_k] \begin{bmatrix} \Sigma & \mathbf{0} \\ \mathbf{0} & \mathbf{0} \end{bmatrix} \begin{bmatrix} \tilde{\mathbf{V}}_k^\dagger \\ \mathbf{V}_k^\dagger \end{bmatrix} \quad (17)$$

where  $(\bullet)^\dagger$  denotes the conjugate transpose operation.

It can be seen that  $\mathbf{V}_k$  is a matrix with the dimension of  $N \times M_k$ . Its columns correspond to those zero eigenvalues. By letting  $\mathbf{W}_k = \mathbf{V}_k$ , a perfect null steering to all the undesired  $K-1$  MSs can be achieved. By repeating the steps represented by Equation (15) and (16), all the  $K$  beamforming matrices can be obtained. In this way, as shown in Equation (14), the multiuser MIMO downlink system is decomposed into  $K$  independent single-user MIMO systems.

#### 4.2. Overall Capacity of Multiuser MIMO Broadcasting with Block Diagonalization

For the case of a multiuser MIMO downlink system which is decomposed into  $K$  independent single-user MIMO systems by block diagonalization, the overall capacity can be obtained as a sum of individual links capacities, as expressed by

$$C_{sum} = \sum_{k=1}^K \log_2 \det \left( \mathbf{I} + \frac{1}{\sigma_n^2} \mathbf{E}_k^\dagger \mathbf{W}_k^\dagger \mathbf{H}_k^\dagger \mathbf{R}_{xx}^k \mathbf{H}_k \mathbf{W}_k \mathbf{E}_k \right) \quad (18)$$

With mutual coupling and spatial correlations taken into account, (18) can be rewritten as

$$C_{sum} = \sum_{k=1}^K \log_2 \det \left( \mathbf{I} + \frac{1}{\sigma_n^2} \mathbf{E}_k^\dagger \mathbf{W}_k^\dagger \tilde{\mathbf{H}}_k^\dagger \mathbf{R}_{xx}^k \tilde{\mathbf{H}}_k \mathbf{W}_k \mathbf{E}_k \right) \quad (19)$$

where  $\mathbf{R}_{xx}^k$  is the  $k$ th MS's input covariance matrix. The capacity for  $k$ th MS is

$$C_k = \log_2 \det \left( \mathbf{I} + \frac{1}{\sigma_n^2} \mathbf{E}_k^\dagger \mathbf{W}_k^\dagger \tilde{\mathbf{H}}_k^\dagger \mathbf{R}_{xx}^k \tilde{\mathbf{H}}_k \mathbf{W}_k \mathbf{E}_k \right) \quad (20)$$

We assume that the signal intended for the  $k$ th MS is a Gaussian signal. As a result, (20) can be simplified to

$$\begin{aligned} C_k &= \log_2 \det \left( \mathbf{I} + \frac{p_k}{\sigma_n^2} \mathbf{W}_k^\dagger \tilde{\mathbf{H}}_k^\dagger \tilde{\mathbf{H}}_k \mathbf{W}_k \right) \\ &= \log_2 \det \left( \mathbf{I} + \frac{p_k}{\sigma_n^2} \mathbf{W}_k^\dagger \mathbf{C}_{BS}^\dagger \mathbf{H}_k^\dagger \mathbf{C}_{MS}^\dagger \mathbf{C}_{MS} \mathbf{H}_k \mathbf{C}_{BS} \mathbf{W}_k \right) \end{aligned} \quad (21)$$

For high SNRs, (21) can be further simplified and given by

$$\begin{aligned} C_k &\approx \log_2 \det \left( \frac{p_k}{\sigma_n^2} \mathbf{W}_k^\dagger \mathbf{C}_{BS}^\dagger \mathbf{H}_k^\dagger \mathbf{C}_{MS}^\dagger \mathbf{C}_{MS} \mathbf{H}_k \mathbf{C}_{BS} \mathbf{W}_k \right) \\ &= \log_2 \det \left( \frac{p_k}{\sigma_n^2} \mathbf{W}_k^\dagger \mathbf{H}_k^\dagger \mathbf{H}_k \mathbf{W}_k \right) \\ &\quad \times \det \left( \mathbf{C}_{MS}^\dagger \mathbf{C}_{MS} \right) \det \left( \mathbf{C}_{BS}^\dagger \mathbf{C}_{BS} \right) \\ &= \log_2 \det \left( \frac{p_k}{\sigma_n^2} \mathbf{W}_k^\dagger \mathbf{H}_k^\dagger \mathbf{H}_k \mathbf{W}_k \right) + \log_2 \det \left( \mathbf{C}_{MS}^\dagger \mathbf{C}_{MS} \right) \\ &\quad + \det \left( \mathbf{C}_{BS}^\dagger \mathbf{C}_{BS} \right) \end{aligned} \quad (22)$$

The last part of Equation (22) shows three terms contributing to the capacity. The first term represents the broadcasting capacity for the  $k$ th MS without the effect of mutual coupling at BS and MS. The second and third terms represent the mutual coupling at  $k$ th MS and BS. The effect of these terms on capacity depends on the coupling matrices at the MS and BS ends. If the product of the determinants of the mutual coupling matrices is larger than one, the effect of mutual coupling on capacity is positive. Otherwise, it is negative.

#### 4.3. Power Allocation Scheme

The most straightforward power allocation scheme from BS to different MSs is accomplished by transmitting equal power to each MS. That is

$$p_k = \text{trace}(\mathbf{E}_k \mathbf{E}_k^\dagger) = \frac{P_T}{K} \quad (23)$$

where  $P_T$  is the total transmitted power at BS and  $p_k$  is the power allocated to the  $k$ th MS.

This power allocation scheme is simple to realize in practice. However, it does not always provide the best performance with respect to capacity. To maximize the capacity, a two-stage power allocation scheme is presented. At the first stage, the power allocation is accomplished according to the objective function at the users' level, as expressed by

$$\begin{aligned} &\text{Max}_{p_1, p_2, \dots, p_K} C_{sum}(p_1, p_2, \dots, p_K) \\ &\text{Subject to } \sum_{k=1}^K p_k = P_T \end{aligned} \quad (24)$$

The result of (24) is the optimized power allocation for different users under service. This is the capacity-greedy power allocation scheme and is non-linear. The solution can be obtained by applying a Lagrange method.

At the second stage, the transmit power for each user can be optimized at an antenna level by using a water-filling scheme. At this stage, the power is allocated to

different transmit antennas according to the objective function, which is described by

$$p_k^i = \left( \mu_k - \frac{\sigma_n^2}{\lambda_k^i} \right)^+, \quad i = 1, 2, \dots, r \quad (25)$$

$$\text{Subject to } \sum_{i=1}^r p_k^i = p_k$$

where  $(z)^+ = \max(0, z)$  and  $\mu_k$  is chosen to obey the power constraint for the  $k$ th MS and  $r$  is the rank of the effective channel matrix between BS and the  $k$ th MS

$$r = \text{rank} \left( \mathbf{C}_{MS}^k \left( \mathbf{R}_{MS}^k \right)^{1/2} \mathbf{G}_H \mathbf{R}_{BS}^{1/2} \mathbf{C}_{BS} \mathbf{W}_k \right) \quad (26)$$

By applying the water-filling scheme, the capacity for  $k$ th MS is

$$C_k = \sum_{i=1}^r \log \left( 1 + \frac{1}{\sigma_n^2} \left( \lambda_k^i \mu_k - \sigma_n^2 \right)^+ \right) \quad (27)$$

### 5. Numerical Results

Using the presented theory, computer simulations are performed for a multi-user MIMO system with 8 transmit antennas at BS and 3 MSs each equipped with 2 receive antennas. It is assumed that the three MSs are scheduled and served by BS at the same time. As a result, this system is referred to as a  $3 \times (2 \times 8)$  system.

**Figure 1** presents the possible impact of spatial correlation and mutual coupling on the broadcasting throughput. In simulations, the dipole spacing at BS and MS is assumed to be fixed at  $1.0\lambda$  and  $0.5\lambda$ , respectively.

As observed from the results presented in **Figure 1**, Dirty Paper Coding, where effects of spatial correlation and mutual coupling are neglected, offers the largest

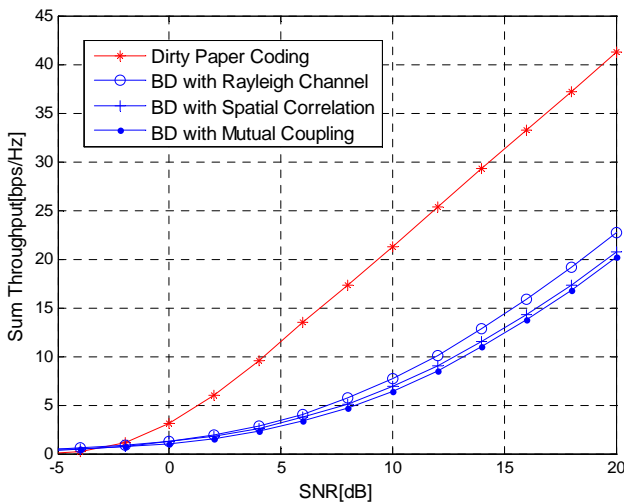


**Figure 1.** Broadcasting throughput for a  $3 \times (2 \times 8)$  system.

scheme in which spatial correlation and mutual coupling are neglected shows a reduced throughput. The throughput for BD with mutual coupling or spatial correlation included in calculations further reduces the system throughput. The differences are most pronounced at larger levels of SNR.

**Figure 2** shows the effect of spatial correlation and mutual coupling on the broadcasting throughput for a  $3 \times (2 \times 8)$  system. The SNR is set to 10 dB and the unit for dipole spacing is the wavelength, represented by  $\lambda$ . The solid lines represent CDF of broadcasting throughput with spatial correlation only and the dotted lines are for the CDF of broadcasting throughput with spatial correlation and mutual coupling combined. It can be seen from **Figure 2** that the presence of spatial correlation and mutual coupling results in a degraded broadcasting throughput in comparison with an idealized Rayleigh channel.

In general, spatial correlation is regarded as a negative factor in a MIMO communication system. However, mutual coupling can be seen as a positive factor at some dipole spacing. As observed in **Figure 2**, for the dipole spacing of  $0.2\lambda$  and  $0.3\lambda$ , the existence of mutual coupling results in a higher capacity. It is interesting to note that the curve of the capacity with and without mutual coupling merge at the point of dipole spacing equal to  $0.4\lambda$ . When the spacing is increased to  $0.6\lambda$ , the plot representing the capacity with mutual coupling is on the left side of the curve for the capacity with correlation only. This is the case for which the presence of mutual coupling leads to a lower capacity.

**Figures 3** and **4** show comparisons between capacity with spatial correlation only, and with spatial correlation plus mutual coupling, as a function of antenna element spacing.

In the presented simulation results, the SNR is set to

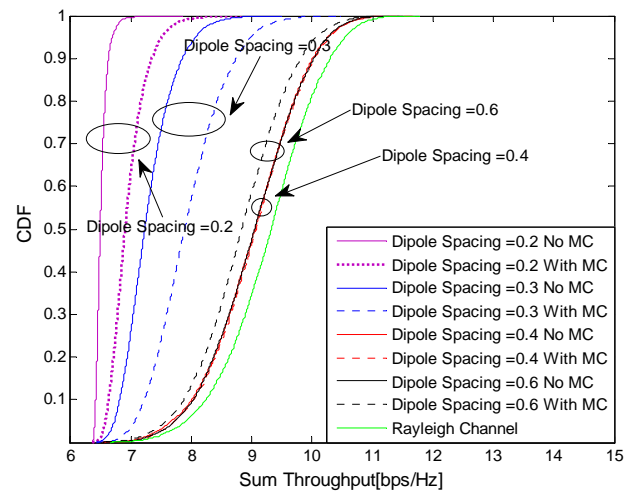


**Figure 2.** Broadcasting throughput CDF for a  $3 \times (2 \times 8)$  system.

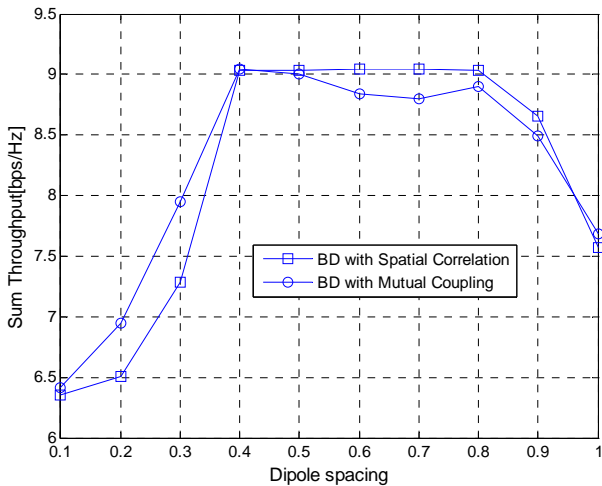


Figure 3. Broadcasting throughput vs. MS array interelement spacing for a  $3 \times (2 \times 8)$  system.

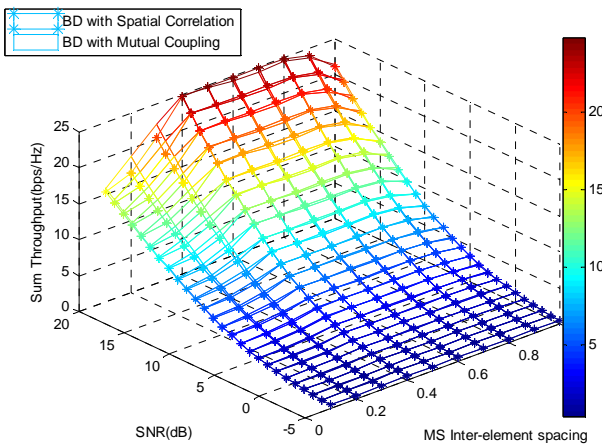


Figure 4. Broadcasting throughput vs. MS array interelement spacing and SNR for a  $3 \times (2 \times 8)$  system.

10 dB and the unit for dipole spacing is the wavelength, as represented by  $\lambda$ . The dipole spacing ranges from  $0.0\lambda$  to  $1.0\lambda$ . We can see that the curves for BD with spatial correlation only and BD with spatial correlation plus mutual coupling cross at  $0.4\lambda$  and  $0.95\lambda$ . For the dipole spacing range from  $0.4\lambda$  to  $0.95\lambda$ , mutual coupling increases the spatial correlation level and results in a decreased capacity. In turn, when the dipole spacing ranges from  $0.1\lambda$  to  $0.4\lambda$ , mutual coupling decreases the spatial correlation level and renders an increased capacity.

The results presented in Figures 5 and 6 verify the two-stage power allocation scheme described in Section 6.

One can see from results presented in Figures 5 and 6 that with or without mutual coupling, the optimized power allocation scheme leads to a higher capacity than the non-optimized one over the SNR range from 5 dB to 20 dB and the antenna spacing from  $0.1\lambda$  to  $1\lambda$ . The

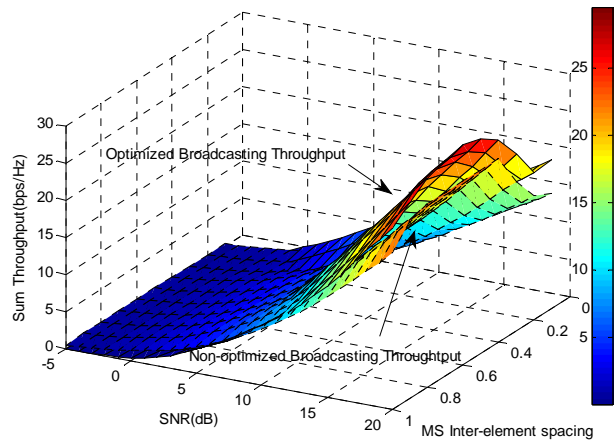


Figure 5. Comparison of optimized and non-optimized broadcasting throughput vs. MS array interelement spacing and SNR for a  $3 \times (2 \times 8)$  system in the presence of spatial correlation only.

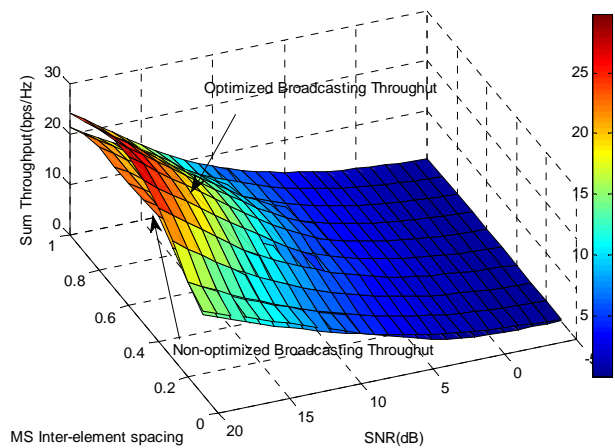


Figure 6. Comparison of optimized and non-optimized broadcasting throughput vs. MS array interelement spacing and SNR for a  $3 \times (2 \times 8)$  system in the presence of spatial correlation and mutual coupling.

optimized scheme improves capacity in the presence of spatial correlation and mutual coupling. This achievement is more apparent at higher values of SNR and larger inter-element antenna spacing.

## 6. Conclusions

In this paper, investigations into the capacity of a multi-user MIMO system with block diagonalization broadcasting scheme in the presence of spatial correlation and mutual coupling have been presented. The effect of spatial correlation and mutual coupling on the broadcasting throughput for block diagonalization broadcasting has been analyzed. It has been shown by the performed computer simulations that the presence of spatial correla-

tion leads to a decreased capacity. However, mutual coupling may have negative or positive influence of capacity. For some particular dipole spacing range, mutual coupling decreases the spatial correlation level, rendering an increased capacity. The optimized diagonalization broadcasting technique with a two-stage power allocation scheme has been proposed and verified. The presented simulations results have demonstrated a positive impact of this optimized BD scheme.

## 7. Acknowledgment

One of the authors (F. Wang) acknowledges the support of the University of Queensland in the form of International Postgraduate Research Scholarship (IPRS).

## 8. References

- [1] G. J. Foschini and M. J. Gans, "On limits of wireless communications in a fading environment when using multiple antennas," *Wireless Personal Communications*, Vol. 6, pp. 311–335, 1998.
- [2] E. Telatar, "Capacity of multi-antenna Gaussian channels," *European Transactions on Telecommunications*, Vol. 10, No. 6, pp. 585–596, November 1999.
- [3] M. Costa, "Writing on dirty paper," *IEEE Transactions on Information Theory*, Vol. 49, No. 3, pp. 439–441, May 1983.
- [4] W. Weingarten, Y. Steinberg, and S. Shamai, "The capacity region of the Gaussian multiple-input multiple-output broadcast channel," *IEEE Transactions on Information Theory*, Vol. 52, No. 9, pp. 3936–3964, September 2006.
- [5] Q. H. Spencer, A. L. Swindlehurst, and M. Haardt, "Zero-forcing methods for downlink spatial multiplexing in multi-user MIMO channels," *IEEE Transactions on Information Theory*, Vol. 42, No. 3, pp. 461–471, February 2004.
- [6] L. U. Choi and R. D. Murch, "A transmit preprocessing technique for multi-user MIMO systems using a decomposition approach," *IEEE Transactions on Wireless Communications*, Vol. 3, No. 1, pp. 20–24, January 2004.
- [7] K. Zhang and Z. Niu, "Multiuser MIMO downlink transmission over time-varying channels," *Proceedings International Conference on Communications*, pp. 5514–5518, June 2007.
- [8] S. Shim, J. S. Kwak, R. W. Heath, and J. Andrews, "Block diagonalization for multi-user MIMO with other-cell interference," *IEEE Transactions on Wireless Communications*, Vol. 7, No. 7, July 2008.
- [9] S. Durrani and M. E. Bialkowski, "Effect of mutual coupling on the interference rejection capabilities of linear and circular arrays in CDMA systems," *IEEE Transactions on Antennas and Propagation*, Vol. 52, No. 4, pp. 1130–1134, April 2004.
- [10] M. E. Bialkowski, P. Uthansakul, K. Bialkowski, and S. Durrani, "Investigating the performance of MIMO systems from an electromagnetic perspective," *Microwave and Optical Technology Letters*, Vol. 48, No. 7, pp. 1233–1238, July 2006.
- [11] F. Wang, M. E. Bialkowski, and X. Liu, "Investigating the effect of mutual coupling on SVD based beamforming over MIMO channels," *International Journal on Signal Processing*, Vol. 3, No. 4, pp. 73–82, July 2009.
- [12] C. N. Chuah, D. N. C. Tse, and J. M. Kahn, "Capacity scaling in MIMO wireless systems under correlated fading," *IEEE Transactions on Information Theory*, Vol. 48, pp. 637–650, March 2002.

# Short-Term Load Forecasting Using Soft Computing Techniques

D. K. Chaturvedi<sup>1</sup>, Sinha Anand Premdayal<sup>1</sup>, Ashish Chandiok<sup>2</sup>

<sup>1</sup>*Department of Electrical Engineering, D. E. I., Deemed University, Agra, India*

<sup>2</sup>*Department of Electronics and Communication, B. M. A. S., Engineering College, Agra, India*

*Email: dkc\_foe@rediffmail.com*

*Received November 10, 2009; revised December 18, 2009; accepted January 21, 2010*

## Abstract

Electric load forecasting is essential for developing a power supply strategy to improve the reliability of the ac power line data network and provide optimal load scheduling for developing countries where the demand is increased with high growth rate. In this paper, a short-term load forecasting realized by a generalized neuron-wavelet method is proposed. The proposed method consists of wavelet transform and soft computing technique. The wavelet transform splits up load time series into coarse and detail components to be the features for soft computing techniques using Generalized Neurons Network (GNN). The soft computing techniques forecast each component separately. The modified GNN performs better than the traditional GNN. At the end all forecasted components is summed up to produce final forecasting load.

**Keywords:** Wavelet Transform, Short Term Load Forecasting, Soft Computing Techniques

## 1. Introduction

Short-term load forecasting (STLF) is an essential technique in power system planning, operation and control, load management and unit commitment. Accurate load forecasting will lead to appropriate scheduling and planning with much lower costs on the operation of power systems [1-6]. Traditional load forecasting methods, such as regression model [7] gray forecasting model [8,9] and time series [10,11] do not consider the influence of all kind of random disturbances into account. At recent years artificial intelligence are introduced for load forecasting [12-17]. Various types of artificial neural network and fuzzy logic have been proposed for short term load forecasting. They enhanced the forecasting accuracy compared with the conventional time series method. The ANN has the ability of self learning and non-linear approximations, but it lacks the inference common in human beings and therefore requires massive amount of training data, which is an intensive time consuming process. On the other hand fuzzy logic can solve uncertainty, but traditional fuzzy system is largely dependent on the knowledge and experiences of experts and operators, and is difficult to obtain a satisfied forecasting result especially when the information is incomplete or insufficient.

This paper aims to find a solution to short term load

forecasting using GNN with wavelet for accurate load forecasting results. This paper is organized as follows: Section 2 discusses various traditional and soft computing based short term load forecasting approaches. Concept of wavelet analysis required for prediction will be discussed in Section 3 while elements of generalized neural architecture needed will be described in Section 4. A prediction procedure using wavelets and soft computing techniques and its application to time series of hourly load forecasting consumption is discussed in Section 5. Section 6 includes discussion and concluding remarks.

## 2. Traditional and Soft Computing Techniques for Short Term Load Forecasting

### 2.1. Traditional Approaches

#### *Time Series Methods*

Traditional short term load forecasting relies on time series analysis technique. In time series approach the model is based on past load data, on the basis of this model the forecasting of future load is done. The techniques used for the analysis of linear time series load signal are:

- 1) *Kalman Filter Method*

The kalman filter is considered as the optimal solution to many data prediction and trend matching. The filter is constructed as a mean square minimization which requires the estimation of the covariance matrix. The role of the filter is to extract the features from the signal and ignore the rest part. As load data are highly non linear and non stationary, it is difficult to estimate the covariance matrix accurately [18].

#### 2) Box Jenkins Method

This model is called as autoregressive integrated moving average model. The Box Jenkins model can be used to represent the process as stationary or non stationary. A stationary process is one whose statistical properties are same over time, which means that they fluctuate over fixed mean value. On other hand non stationary time series have changes in levels, trends or seasonal behavior. In Box Jenkins model the current observation is weighted average of the previous observation plus an error term. The portion of the model involving observation is known as autoregressive part of the model and error term is known as moving average term. A major obstacle here is its slow performance [19].

#### 3) Regression Model

The regression method is widely used statistical technique for load forecasting. This model forms a relationship between load consumptions done in past hour as a linear combination to estimate the current load. A large data is required to obtain correct results, but it requires large computation time.

#### 4) Spectral Expansion Technique

This method is based on Fourier series. The load data is considered as a periodic signal. Periodic signal can be represented as harmonic summation of sinusoids. In the same way electrical load signal is represented as summation of sinusoids with different frequency. The drawback of this method is that electrical load is not perfect periodic. It is a non stationary and non linear signal with abrupt variations caused due to weather changes. This phenomenon results in the variation of high frequency component which may not be represented as periodic spectrum. This method is not suitable and also requires complex equation and large computation time.

## 2.2. Soft Computing Approach

Soft computing is based on approximate models working on approximate reasoning and functional approximation. The basic objective of this method is to exploit the tolerance for imprecision, uncertainty and partial truth to achieve tractability, robustness, low solution cost and best results for real time problems.

#### 1) Artificial Neural Networks (ANN)

An artificial neural network is an efficient information processing system to perform non-linear modeling and adaptation. It is based on training the system with past

and current load data as input and output respectively. The ANN learns from experience and generalizes from previous examples to new ones. It is able to forecast more efficiently the load as the load pattern are non linear and ANN is capable to catch trends more accurately than conventional methods.

#### 2) Rule Based Expert Systems

An expert system is a logical program implemented on computer, to act as a knowledge expert. This means that program has an ability to reason, explain and have its knowledge base improved as more information becomes available to it. The load-forecast model can be built using the knowledge about the load forecast domain from an expert in the field. The knowledge engineer extracts this knowledge from the load domain. This knowledge is represented as facts and rules using the first predicate logic to represent the facts and IF-THEN production rules. Some of the rules do not change over time, some changes very slowly; while others change continuously and hence are to be updated from time to time [20].

#### 3) Fuzzy Systems

Fuzzy sets are good in specialization, fuzzy sets are able to represent and manipulate electrical load pattern which possesses non-statistical uncertainty. Fuzzy sets are a generalization of conventional set theory that was introduced as a new way to represent vagueness in the data with the help of linguistic variable. It introduces vagueness (with the aim of reducing complexity) by eliminating the sharp boundary between the members of the class from nonmembers [21,22].

These approaches are based on specific problems and may represent randomness in convergence or even can diverge. The above mentioned approaches use either regression, frequency component or mean component or the peak component to predict the load. The prediction of the load depends upon both time and frequency component which varies dynamically. In this paper, an attempt is made to predict electrical load that combines the above mentioned features using generalized neurons and wavelet.

## 3. Elements of Wavelet Analysis

Wavelet analysis is a refinement of Fourier analysis [9–15,23–29] which has been used for prediction of time series of oil, meteorological pollution, wind speed, rainfall etc. [28,29]. In this section some important vaults relevant to our work have been described. The underlying mathematical structure for wavelet bases of a function space is a multi-scale decomposition of a signal, known as multi-resolution or multi-scale analysis. It is called the heart of wavelet analysis. Let  $L_2(\mathbb{R})$  be the space of all signals with finite energy. A family  $\{V_j\}$  of subspaces of  $L_2(\mathbb{R})$  is called a multi resolution analysis of this space if

1) intersection of all  $V_j, j = 1, 2, 3, \dots$  be non-empty, that is  $\bigcap_j V_j \neq \emptyset$

2) This family is dense in  $L_2(\mathbb{R})$ , that is,  $\text{span} \{ \psi_{j,k} \} = L_2(\mathbb{R})$

3)  $f(x) \in V_j$  if and only if  $f(2x) \in V_{j+1}$

4)  $V_1 \subseteq V_2 \subseteq \dots \subseteq V_j \subseteq V_{j+1}$

There is a function preferably with compact support of such that translates  $\phi(x-k), k \in \mathbb{Z}$ , span a space  $V_0$ . A finer space  $V_j$  is spanned by the integer translates of the scaled functions for the space  $V_j$  and we have scaling equation

$$\phi(x) = \sum_k a_k \phi(2x-k) \tag{1}$$

with appropriate coefficient  $a_k, k \in \mathbb{Z}$ .  $\phi$  is called a scaling function or father wavelet. The mother wavelet  $\psi$  is obtained by building linear combinations of  $\phi$ . Furthermore  $\phi$  and  $\psi$  should be orthogonal, that is,

$$\langle \phi(-k), \psi(-l) \rangle = 0, l, k \in \mathbb{Z} \tag{2}$$

These two conditions given by (1) and (2) leads to conditions on coefficients  $b_k$  which characterize a mother wavelet as a linear combination of the scaled and dilated father wavelets  $\phi$ :

$$\psi(x) = \sum_{k \in \mathbb{Z}} b_k \phi(2x-k) \tag{3}$$

Haar, Daubechies and Coefmann are some well known wavelets.

Haar wavelet (Haar mother wavelet) denoted by  $\psi$  is given by

$$\psi(x) = \begin{cases} 1, & 0 \leq x \leq 1/2 \\ 1, & 1/2 < x \leq 1 \\ 0, & x < 0, x > 1 \end{cases} \tag{4}$$

Can be obtained from the father wavelet

$$\phi(x) = \begin{cases} 1, & 0 \leq x \leq 1 \\ 0, & x < 0, x > 1 \end{cases} \tag{5}$$

In this case coefficients  $a_k$  in (1) are  $a_0 = a_1 = 1$  and  $a_k = 0$  for  $k \neq 0, 1$ . The Haar wavelets is defined as a linear combination of scaled father wavelets  $\psi(x) = \phi(2x) - \phi(2x-1)$  which means that coefficients  $b_k$  in (3) are  $b_0 = 1, b_1 = -1$  and  $b_k = 0$  otherwise, Haar wavelets can be interpreted as Daubechie's wavelet of order 1 with two coefficients. In general Daubechies' wavelets of order  $N$  are not given analytically but described by  $2N$  coefficients. The higher  $N$ , the smoother the corresponding Daubechies' wavelets are (the smoothness is around  $0-2N$  for greater  $N$ ). Daubechies' wavelets are constructed in a way such that they give rise to orthogonal wavelet bases. It may be verified that orthogonality of translates of  $\phi$  and  $\psi$ , requires that  $\sum_k a_k = 2$  and  $\sum_k b_k = 2$ .

It is quite clear that in the higher case the scaled, translated and normalized versions of  $\psi$  are denoted by

$$\psi_{j,k}(t) = 2^{j/2} \psi(2^j x - k) \tag{6}$$

With orthogonal wavelet  $\psi$  the set  $\{ \psi_{j,k} | j, k \in \mathbb{Z} \}$  is an orthogonal wavelet basis. A function  $f$  can be represented as

$$f = \sum_{j \in \mathbb{Z}} \sum_{k \in \mathbb{Z}} c_{j,k} \psi_{j,k} \quad (\psi, c_{j,k} \rightarrow \langle f \rangle) \tag{7}$$

The Discrete Wavelet Transform (DWT) corresponds to the mapping  $f \rightarrow c_{j,k}$ . DWT provides a mechanism to represent a data or time series  $f$  in terms of coefficients that are associated with particular scales [24,26,27] and therefore is regarded as a family of effective instrument for signal analysis. The decomposition of a given signal  $f$  into different scales of resolution is obtained by the application of the DWT to  $f$ . In real application, we only use a small number of levels  $j$  in our decomposition (for instance  $j = 4$  corresponds to a fairly good level wavelet decomposition of  $f$ ).

The first step of DWT corresponds to the mapping  $f$  to its wavelet coefficients and from these coefficients two components are received namely a smooth version, named approximation and a second component that corresponds to the deviations or the so-called details of the signal. A decomposition of  $f$  into a low frequency part  $a$ , and a high frequency part  $d$ , is represented by  $f = a_1 + d_1$ . The same procedure is performed on  $a_1$  in order to obtain decomposition in finer scales:  $a_1 = a_2 + d_2$ . A recursive decomposition for the low frequency parts follows the directions that are illustrated in **Figure 1**.

The resulting low frequency parts  $a_1, a_2, \dots, a_n$  are approximations of  $f$ , and the high frequency parts  $d_1, d_2, \dots, d_n$  contain the details of  $f$ . This diagram illustrates a wavelet decomposition into  $N$  levels and corresponds to

$$f = d_1 + d_2 + d_3 + \dots + d_{N-1} + d_N + a_N \tag{8}$$

In practical applications, such decomposition is obtained by using a specific wavelet. Several families of wavelets have proven to be especially useful in various applications. They differ with respect to orthogonality, smoothness and other related properties such as vanishing moments or size of the support.

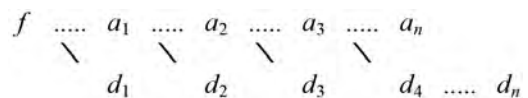


**Figure 1.** Wavelet decomposition in form of coarse and detail coefficients.

### 4. Neuro Theory of Generalized Neuron Model

The following steps are involved in the training of a summation type generalized neuron as shown in **Figure 2**.

#### 4.1. Forward Calculations

Step 1: The output of the  $\sum_1$  part of the summation type generalized neuron is

$$O_\Sigma = \frac{1}{1 + e^{-\lambda s * s\_net}} \tag{9}$$

where  $s\_net = \sum W_{\Sigma i} X_i + X_{o\Sigma}$

Step 2: The output of the  $\pi$  part of the summation type generalized neuron is

$$O_\Pi = e^{-\lambda p * pi\_net^2} \tag{10}$$

where  $pi\_net = \prod W_{\Pi i} X_i * X_{o\Pi}$

Step 3: The output of the summation type generalized neuron can be written as

$$O_{pk} = O_\Pi * (1 - W) + O_\Sigma * W \tag{11}$$

#### 4.2. Reverse Calculation

Step 4: After calculating the output of the summation

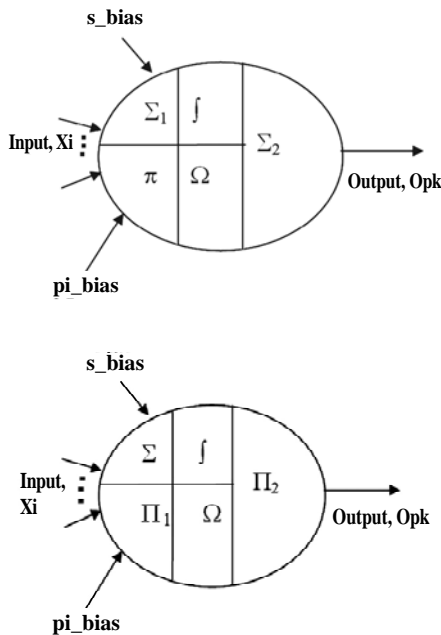


**Figure 2.** Learning algorithm of a summation type generalized neuron.

type generalized neuron in the forward pass, as in the feed-forward neural network, it is compared with the desired output to find the error. Using back-propagation algorithm the summation type GN is trained to minimize the error. In this step, the output of the single flexible summation type generalized neuron is compared with the desired output to get error for the  $i$ th set of inputs:

$$\text{Error } E^i = (Y^i - O^i) \tag{12}$$

Then, the sum-squared error for convergence of all the patterns is

$$E^p = 0.5 \sum E^{i2} \tag{13}$$

A multiplication factor of 0.5 has been taken to simplify the calculations.

Step 5: Reverse pass for modifying the connection strength.

1) Weight associated with the  $\sum_1$  and  $\sum_2$  part of the summation type Generalized Neuron is:

$$W(k) = W(k - 1) + \Delta W \tag{14}$$

where  $\Delta W = \eta \delta_k (O_\Sigma - O_\Pi) X^i + \alpha W(k - 1)$

and  $\delta_k = \sum (Y^i - O^i)$

2) Weights associated with the inputs of the  $\sum_1$  part of the summation type Generalized Neuron are:

$$W_{\Sigma i}(k) = W_{\Sigma i}(k - 1) + \Delta W_{\Sigma i} \tag{15}$$

where  $\Delta W_{\Sigma i} = \eta \delta_{\Sigma j} X_i + \alpha W_{\Sigma i}(k - 1)$

and  $\delta_{\Sigma j} = \sum \delta_k W(1 - O_\Sigma) * O_\Sigma$

3) Weights associated with the input of the  $\pi$  part of the summation type generalized Neuron are:

$$W_{\Pi i}(k) = W_{\Pi i}(k - 1) + \Delta W_{\Pi i} \tag{16}$$

where  $\Delta W_{\Pi i} = \eta \delta_{\Pi j} X_i + \alpha W_{\Pi i}(k - 1)$

and  $\delta_{\Pi j} = \sum \delta_k (1 - W) * (-2 * pi\_net) * O_\Pi$

$\alpha$  – Momentum factor for better convergence.

$\eta$  – Learning rate.

Range of these factors is from 0 to 1 and is determined by experience.

### 5. Generalized Neuron-Wavelet Approach

The Generalized Neuron-Wavelet approach has been used to predict the electrical load. In this approach, Daubechies wavelets Db8 have been applied in the decomposition for the give data pattern. There are four wavelet coefficients are used. All these wavelet coefficients are time dependent (the first three wavelet coefficients from

$d_1$  to  $d_3$  and the coarse approximation  $a_3$ . These coefficients are illustrated in the **Figure 3**. We observe the substantial difference of variability of the signals at different levels. The higher is the wavelet level, the lower variation of the coefficients and easier prediction of them. Our main idea is to substate the prediction task of the original time series of high variability by the prediction of its wavelet coefficients on different levels of lower variability's, and then using Equation (4) for final prediction of the power load at any time instant  $n$ . Since most of the wavelet coefficients are of lower variability we expect the increase of the total prediction accuracy.

The wavelet tool available in Matlab is used for the process of wavelet decomposition of the time series representing average of the power load data for 120 hours. This step involves several different families of wavelets and a detailed comparison of their performance. In our case, The Daubechies wavelets of order 8 are performed. Three level wavelet decomposition of the given time series  $X_N = f$ : is performed

$$f = a_3 + d_3 + d_2 + d_1 \tag{17}$$

The smooth part of  $f$  is stored in  $a_3$ , and details on different levels are captured by  $d_1, d_2, d_3$ . Consequently a decomposition of the time series in three different scales is obtained. **Figure 4** illustrates the decomposition of the original signals. The forecasting procedure methodology explained in Section 4 is used to predict the next value. The basic idea is to use the wavelet transforms and predict the data by soft computing techniques for individual coefficients of wavelet transform represented by  $a_3, d_1, d_2, d_3$ . The input to the architecture to predict the wavelet coefficients is explained in **Figure 5**.

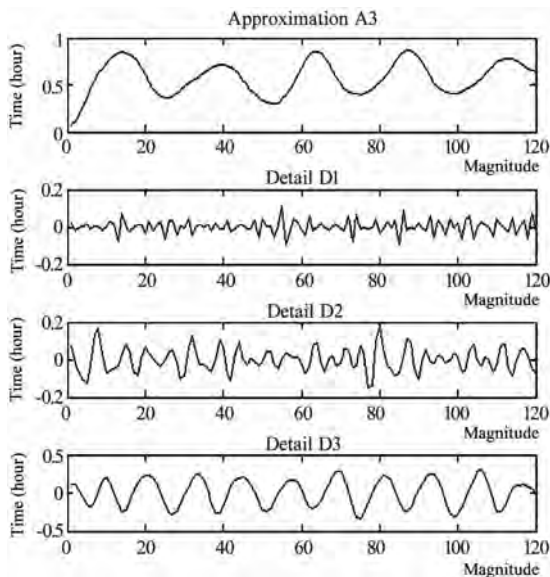


**Figure 3. Wavelet decomposition of hour load data into wavelet coefficient.**

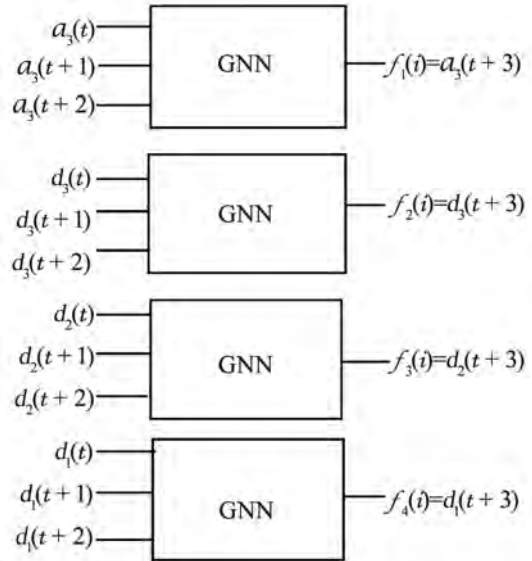


**Figure 4. Mechanism for forecasting Procedure.**

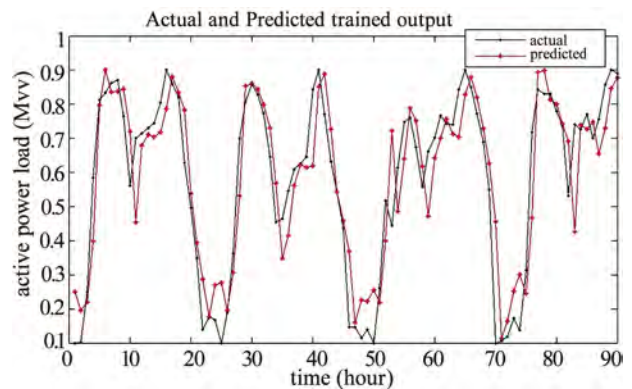


**Figure 5. Actual and predicted training output using generalized neuron model (GNN).**

The total predicted power load at an instant ( $i$ ) is given by

$$F(i) = f_1(i) + f_2(i) + f_3(i) + f_4(i) \tag{18}$$

## 6. Results and Discussions

The electric load data have been collected for 120 hours from Gujarat system and normalized them in the range 0–1. The Daubechies wavelet Db8 is used for decomposition and the wavelet coefficients  $d_1$ – $d_3$  and  $a_3$  have been calculated. The trend of coefficients has been used for GN training and predicting the wavelet coefficients for future loads. So wavelet is used to extract the feature coefficients from data and then GN is implemented to predict the trend of the wavelet coefficient. The results of GN and actual load have been compared and shown in

**Figures 5 and 6.** The root means square error for training and testing results are .1127 and .1152 mega watts (MW) as in **Table 1**. When using generalized neuron and wavelet conjunction model, training each coefficient and combining to get the predicted output, a very high improvement is obtained in both training and testing results as shown in **Figures 7 and 8**. The root means square error for training and testing data are .0554 and .0763 respectively as in **Table 1**. The improvement in the results shows that accuracy of forecasting increases in the combined model and can give correct output for short term load forecasting.

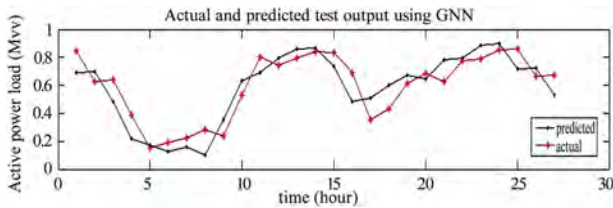


**Figure 6.** Actual and predicted testing output using generalized neuron model (GNN).

**Table 1.** Comparison between GNN and GNN Wavelet technique.

Type	Min. Error (Mw)	Max. Error (Mw)	RMSE (Mw)
GNN (training)	0.0009521	0.3663	0.1127
GNNW(training)	0.002184	0.1706	0.0554
GNN(testing)	0.1306	0.2094	0.1152
GNNW(testing)	0.00462	0.1913	0.0673

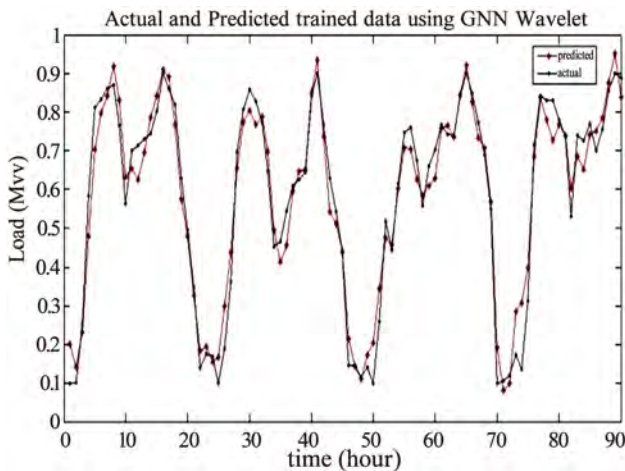


**Figure 7.** Actual and predicted training output using generalized neuron wavelet model (GNNW).

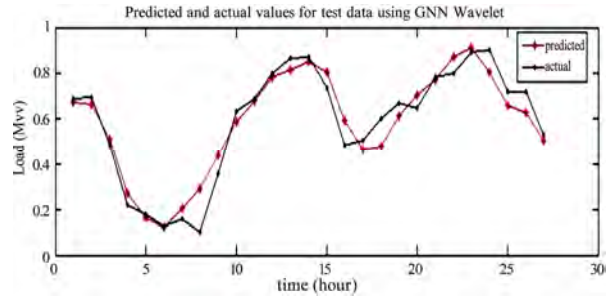


**Figure 8.** Actual and predicted testing output using generalized neuron wavelet model (GNNW).

### 7. References

- [1] S. E. Papadakis, J. B. Theocharis, S. J. Kiartzis, and A. G. Bakirtzis, "A novel approach to short-term load forecasting using fuzzy neuralnetworks," *IEEE Transactions on Power Systems*, Vol. 13, pp. 480–492, 1998.
- [2] D. K. Chaturvedi, P. S. Satsangi, and P. K. Kalra, "Fuzzified neural network approach for load forecasting problems," *International Journal on Engineering Intelligent Systems*, CRL Publishing, U. K., Vol. 9, No. 1, pp. 3–9, March 2001.
- [3] A. A. Eidesouky and M. M. Eikateb, "Hybrid adaptive techniques for electric-load forecast using ANN and ARIMA," *IEE Proceedings–Generation, Transmission and Distribution*, Vol. 147, pp. 213–217, 2000.
- [4] A. G. Bakirtzis, J. B. Theocharis, S. J. Kiartzis, and K. J. Satsios, "Short term load forecasting using fuzzy neural networks," *IEEE Transactions on Power Systems*, Vol. 10, pp. 1518–1524, 1995.
- [5] S. Rahman and O. Hazim, "A generalized knowledge-based short-term load forecasting technique," *IEEE Transactions on Power Systems*, Vol. 8, pp. 508–514, 1993.
- [6] D. K. Chaturvedi, M. Mohan, R. K. Singh, and P. K. Kalra, "Improved generalized neuron model for short term load forecasting," *International Journal on Soft Computing–A Fusion of Foundations, Methodologies and Applications*, Springer–Verlag, Heidelberg, Vol. 8, No. 1, pp. 10–18, April 2004.
- [7] G. Gross and F. D. Galiana, "Short term load forecasting," *Proceedings of the IEEE*, Vol. 75, No. 1212, pp. 1558–1573, December 1987.
- [8] D. K. Chaturvedi, P. S. Satsangi, and P. K. Kalra, "New neuron models for simulating rotating electrical machines and load forecasting problems," *International Journal on Electric Power System Research*, Elsevier Science, Ireland, Vol. 52, pp. 123–131, 1999.
- [9] P. S. Addison, "The illustrated wavelet transform handbook: Introductory theory and applications in science, engineering medicine and finance," IOP Publishing LTD, 2002.
- [10] Z. Can, Z. Aslan, and O. Oguz, "One dimensional wavelet real analysis of gravity waves," *The Arabian Journal*

- for Science and Engineering, Vol. 29, No. 2, pp. 33–42, 2004.
- [11] Z. Can, Z. Aslan, O. Oguz, and A. H. Siddiqi, “Wavelet transform of meteorological parameters and gravity waves,” *Annals Geophysics*, Vol. 23, pp. 650–663, 2005.
- [12] I. Daubechies, “Ten lectures on wavelets,” SIAM, Philadelphia, 1992.
- [13] A. F. Georgiou and P. Kumar, “Wavelet in geophysics,” Academic Press, San Diago, 1994.
- [14] K. M. Furati, M. Z. Nashed, and A. H. Siddiqi, “Mathematical models and methods for real world and systems,” Chapman and Hall/CRC, Taylor and Francis Group, Boca Raton, London, New York, Singapore, 2006.
- [15] Z. Z. Hu and T. Nitta, “Wavelet analysis of summer rainfall over north China and India,” *Journal Meteorological Society of Japan*, Vol. 74, No. 6, 1996.
- [16] J. S. R. Jang and N. Gulley, “Fuzzy logic toolbox,” The Mathworks Inc., 24 Prime Park Way, Natick, Mass, 1995.
- [17] J. S. R. Jang and C. T. Sun, “Neuro-fuzzy modeling and control,” *Proceedings of the IEEE*, Vol. 83, No. 3, pp. 378–406, 1995.
- [18] A. K. Mahalanabis, D. P. Kothari, and S. I. Ahson, “Computer aided power system analysis and control,” Tata McGraw Hill Publishing Company Limited, New Delhi, 1988.
- [19] G. E. Box and G. M. Jenkins, “Time series analysis: Forecasting and control,” Holden-Day, San Fransisco, 1976.
- [20] I. Moghram and S. Rahman “Analysis and evaluation of five short-term load forecasting techniques,” *IEEE Transactions on Power Systems*, Vol. 4, pp. 1484–1491, October 1989.
- [21] C. H. Chen, “Fuzzy logic and neural network handbook,” McGraw Hill Computer Engineering, 1996.
- [22] G. J. Klis and T. A. Folger, “Fuzzy sets uncertainty and information,” Prentice Hall of India Private Limited, 1993.
- [23] P. Kumar and E. Foufoula-Georgiou, “Wavelet analysis for geophysical applications,” *Reviews of Geophysics*, Vol. 33, pp. 385–412, 1997.
- [24] S. Mallat, “A wavelet tour of signal processing,” Academic Press, NewYork, 1998.
- [25] P. Manchanda, J. Kumar, and A. H. Siddiqi, “Mathematical methods for modeling price fluctuations of financial time series,” *Journal of Franklin Institute*, Vol. 344, pp. 613–636, 2007.
- [26] A. H. Siddiqi, “Applied functional analysis,” Maral Dekkar, New York, 2004.
- [27] A. H. Siddiqi, G. Kovin, W. Freeden, U. Mosco, and S. Stephan, “Theme issue on wavelet fractal in science and engineering,” *Arabian Journal for Science and Engineering*, KFUPM.
- [28] O. Stanislaw and K. Garanty, “Forecasting of the daily meteorological pollution using wavelet and support vector machine,” *Engineering Application of Artificial Intelligence*, Vol. 20, pp. 745–755, 2007.
- [29] S. Yousefi, I. Weinrich, and D. Reinartz-Chaos, “Wavelet-based prediction of oil prices,” *Solution and Fractals*, Vol. 25, pp. 265–275, 2005.
- [30] M. V. Wickerhauser, A. K. Peters, and Wellesley, “Adapted analysis from theory to software,” 1994.

# Spectrum Efficiency Improvement Based on the Cognitive Radio Management

**Jamal Raiyn**

*QRC-Qasemi Research Center, Alqasemi College, Baka Alqarbiah, Israel*

*Email: rayan@qsm.ac.il*

*Received November 3, 2009; revised December 5, 2009; accepted January 19, 2010*

## Abstract

Interference and delay are considered as the major reasons limiting the capacity and increasing the new call blocking probability in cellular system. In this paper we introduce a novel strategy based on cognitive radio. Cognitive radio is defined as a radio or system that senses its environment and can dynamically and autonomously change its transmitter parameters based on interaction with the environment in which it operates, such as maximize throughput and reduce interference. The goal of the use of cognitive radio is to improve the spectrum efficiency in cellular system. Spectrum management based on radio cognitive plays thereby an important role to increase the capacity of the radio systems and spectrum utilization, especially in the context of open spectrum.

**Keywords:** Cognitive Radio, Handover, Social Agent

## 1. Introduction

In this paper we introduce cognitive radio approach that is expected to perform more significant role in the view of efficient utilization of the spectrum resources in the future wireless communication networks. The spectrum utilization efficiency is defined as the ratio of information transferred to the amount of spectrum utilization. Our approach is reactive approach, in that it enables, via negotiation, learning, reasoning, prediction, active sense, identification, changes in the base station's parameter to meet the new services requirements in modern wireless networks and future challenges in cellular systems. A major challenge with cognitive radio approach is to be done in near real-time and to keep up with an ever changing RF environment without overly computationally complex. Various resource allocation strategies are proposed to optimize the resource allocation in cellular system by reducing the call blocking probability [2,3,5,6,8] in cellular systems. The call blocking probability is often measured in terms of two blocking probabilities, the arriving call blocking probability, and the handover blocking probability. Analyses and studies in [9–11] show that the call blocking probability in handover is caused by two main parameters, interference and delay. Interference leads to missed and blocked calls due to errors in the digital signaling. Between transmitter (Base Station, BS) and receiver (Mobile Station, MS), the channel is modeled by several key parameters. These pa-

rameters vary significantly with the environment (urban, rural, mountains). There are different type of interference that when not minimized, decreases the ratio of carrier to interference power at the periphery of the cells, causing diminished system capacity, more handover [1,4], and more dropped calls. To reduce the handover blocking probability in cellular systems has been proposed various schemes as, prioritized handover schemes and handover with queueing [4]. In some application fields like real-time communication and industrial automation is needed to ensure a seamless and lossless handoff. Which means the handover latency should be zero. For efficient handover management, Handover is a basic mobile network capability for dynamic support of terminal migration. Handover Management is the process of initiating and ensuring a seamless and lossless handover of a mobile terminal from the region covered by one base station to another base station. In this paper we consider the handover call blocking probability in cellular systems.

The paper is organized as follows: Section 2 introduces the system model and the social agent strategies. Section 3 discuss and analyze the handover call blocking probability based on simulation results and Section 4 concludes the paper.

## 2. Problem Description

Over the last two decades, the demand for mobile host

and multimedia services increased rapidly. One of the biggest challenges in supporting multimedia applications in cellular systems is to fulfill the mobile user demand and satisfy his preferences under the constraint of the limited radio bandwidth, and to utilize the limited *spectrum availability* to meet the increasing demand for mobile service. Some of the most often used methods to increase the spectral efficiency are resource allocation schemes. Various channel allocation schemes have been introduced to provide Quality of Service (QoS) [14,15, 16] and efficient channel utilization in cellular networks. There are many parameters to measure the QoS of a network. These include throughput, latency, service availability etc. The blocking probability is one of the most important QoS parameters. Since users are mobile, the QoS of wireless networks are often measured in terms of two probabilities: the new arriving *call blocking probability* and the *handoff blocking probability*. Hence, this paper deals with the main issue: How to allocate resources (e.g. frequency channels) to radio ports of a wireless system (e.g. cells in a cellular mobile network) that can improve the traffic performance of network (e.g. lower blocking probability in voice networks, lower latency in data networks etc.)?

In the modern data communication systems, we consider the power transmission as the resources. An increase of transmission power enables the increase of data rate and subsequently shorter transmission time. On the other hand, an increased transmission power causes more interference in neighboring cells. One of the physical measures of RF channel quality is the carrier-to-interference or CIR. This ratio is logarithmically proportional to the signal quality enjoyed by the receiver of the signal. The larger the *C/I* ratio, the better the channel quality is. If the measured *C/I* falls below a certain level,  $CIR_{min}$ , which depends on system type and operator requirements, the mobile should be in the coverage region of another cell and a call handoff should be performed. The interior of the cell should provide *C/I* ratio which exceed this level, unless the mobile is located in an RF coverage “hole.” In general, for a feasible solution for the resource managements in the cellular systems must be satisfied four requirements as follows:

- Coverage requirement: each of the MS locations must be able to connect at least to one base station and the received signal strength must exceed a given level  $P_{min}$ .
- Transmitter power requirements: the transmitted power of the mobile stations in the system must not exceed a maximum level  $P_{max}$ .
- Downlink SIR requirement: each downlink SIR must exceed a threshold of  $SIR^{th}$ .
- Uplink SIR's requirement: each uplink SIR must exceed a threshold of  $SIR^{th}$ .

In this case, we consider the problem of minimizing total transmitter power. To minimize the total transmit power, subject to the constraint that each transmitter/

receiver attain a maximum allowed outage probability i.e., a minimum allowed quality of service and subject to limits on the individual transmitter power, we formulate the problem as follows:

$$\begin{aligned} & \text{minimize } P_1 + \dots + P_n \\ & \text{Subject to } P_i^{min} \leq P_i \leq P_i^{max}, i = 1, \dots, n \end{aligned}$$

Here,  $P_i^{min}$  and  $P_i^{max}$  are the minimum and maximum transmitter power for the transmitter  $i$ . To handle the resource allocation problem in cellular systems we introduce the cognitive radio scheme. For the channel allocation problem, the main goal is to bring more distribution of control. In cognitive radio scheme, each cell (base station) is managed by an agent. The resource in the system will be distributed and allocated through interaction between agents and limited to the domain of the agents. In other words, the channel allocation problem can be restricted to one domain, so that the agents can be placed in the base stations.

### 3. Power Control Based on CR

Each cell  $i$  can acquire amount  $i$  while the level in the cell is denoted by  $h_i$  (the demand of channel in each cell depends on the arrival call in the cell). We assume, that the mass flow of resource in the cell  $i$  is proportional to the value position  $u_i$  (call arrival rate). And we consider that the resources in the system are limited. The vector of the required set points of the levels, (to meet the call arrival rate), are given by  $h_s$ . We further assume that the equilibrium point  $(u_0, h_s)$  is known (channel allocation). The control task is the regulation of disturbances (plus the interference) of the resources in the cells. Each cell is considered as a single subsystem and associated with an agent. The input variable of each agent  $i$  is the deviation  $\Delta h_i(k)$  of the resource amount.

$$\Delta h_i(k) = h_i - h_s \tag{1}$$

The output variable is the value position

$$u_i(k) = \Delta u_i(k) + u_0 \tag{2}$$

which is the sum of the deviation  $\Delta u_i(k)$  and the equilibrium position  $u_0$ . Since the equilibrium position is known, the agent only has to compute the output variable  $\Delta u_i(k)$ . Since the amount of the resources that flows into the cell is limited, the absolute Value  $|\Delta u_i(k)|$  is considered as the resource variables. Now each agent can either play the role of the consumer or the producer. A positive deviation  $\Delta h_i(k)$  means that the cell “needs” some more resource to reach the required level (i.e. to allocate all calls).

$$\Delta h_i(k) = h_i - h_s > 0. \text{ i.e., } h_i > h_s \tag{3}$$

Thus, the related agent can be declared as a consumer, which has to acquire a certain amount of the resource. This demand of consumer  $i$  at instance  $k$  is denoted by  $r_{Di}(k)$ . The goal of the consumer is to maximize his utility, (i.e. by reducing the call blocking probability).  $J_{Ci}(k)$  with

$$\frac{J_{Ci}(k)}{r_{Di}(k)} = \Delta h_i(k) - r_{Di}(k) * I(k) \quad (4)$$

The relative utility is a composition of two terms. The first term takes into account that the utility of the cell from getting some resource increases with increasing deviation  $\Delta h_i(k)$ . The second term denotes the consumer's expenditure (allocation) with respect to his interference  $I(k)$ . Its utility decreases with increasing expenditures. The minimization of the call blocking probability  $J_{Ci}(k)$  leads to the consumer's demand:

$$r_{Di}(k) = \Delta h_i(k) * \frac{1}{I(k)} \quad (5)$$

The demand is a function of the interference. An increasing of the interference leads to a decreasing demand. In the case of a negative deviation  $\Delta h_i(k)$ , the cell contains too much free resources. Hence, the related agent is considered as a producer which wants to gift this resource to the consumers with the goal to maximize system capacity/efficiency and its profit  $J_{pi}(k)$ , denoted by

$$\frac{J_{pi}(k)}{r_{Si}(k)} = |\Delta h_i(k)| * I(k) - r_{Si}(k) \quad (6)$$

The relative profit contain two terms; The first term takes into account that the utility of the producer increases with his income and with increasing deviation  $|\Delta h_i(k)|$ . The second term is production costs that are assumed to be proportional to the supply. The maximization of  $J_{pi}(k)$  leads to the supply of producer agent  $i$ :

$$r_{Si}(k) = |\Delta h_i(k)| * I(k) \quad (7)$$

One problem occurs: *If all agents are producers or all agents are consumers.* However, there is always nominal channels/resources in the cells (nominal channel can be used only from own cell). Therefore, obviously have a permanent producer, which is independent of the amount of resource (swapping method). Assuming  $n$  coupled cells, the actual number of producers at the instance  $k$  is  $m$  while the actual number of consumers is  $q$  with  $n = m + q$ . Each consumer agents computes his demand while each producer agents computes his supply. All functions are transmitted to an auctioneer agent using the communication network (the auctioneer could be the distributor agent,  $(D)$ ). The task of the auctioneer is the computation of the equilibrium using the constraint that the sum of all demands has to equal the sum of all supplies:

$$r_{Dp}(k) + \sum_{i=1}^q r_{Di}(k) = r_{Sp}(k) + \sum_{j=1}^m r_{Si}(k) \quad (8)$$

Hence the output variables  $\Delta u_i(k)$  are

$$\Delta u_i(k) = \Delta h_i(k) * \frac{1}{I(k)}, \quad i \text{ consumer.}$$

$$\Delta u_i(k) = \Delta h_i(k) * I(k), \quad i \text{ producer.}$$

#### • Power control

The power control can raise the network capacity. Some power control algorithms [17,18,19,20] based on the idea of balancing the SIR of all radio links have been introduced, but the final SIR achieved by those algorithms may be unsatisfactory for some of the links. Some calls must be dropped in order to keep the SIR of other calls higher than the predefined threshold value. Obviously, the efficiency of radio resource management is dependent on the channel assignment and the power control. The combination of DCA and power control to obtain some substantial capacity gains has been reported in [22], however, because no channel pre-selection is done before the channel probing procedure, inadvertent dropping of calls caused by originating calls can occur so often that all unsuccessful (blocked or dropped) calls are unintentionally dropped calls and not blocked calls. In addition, an exhaustive search and too frequent intra-cell handoff access will decrease the system capacity and make the algorithms difficult to implement in real networks. Here, a cognitive radio algorithm with power control is proposed. The power that is transmitted both from the mobile equipment and from the base station has a far-reaching effect on efficient usage of the spectrum. Power control is an essential feature in mobile networks, in both uplink and downlink. When a mobile transmits high power, there is enough margin in the critical uplink direction. But it can cause interference to other subscriber connections. The power of the signal transmitted by the base station antenna should be kept to a level above the required threshold without causing interference to the mobiles. Mobile stations thus have a feature such that their power of transmission can be controlled. This feature is generally controlled by the BSS. This control is based on an algorithm that computes the power received by the base station and, based on its assessment, it increases or decreases the power transmitted by the mobile station. The signal power at the  $i$ th receiver is given by  $G_{ii}F_{ii}P_k$  [21], and the total interference power is given by  $\sum_{k \neq i} G_{ik}F_{ik}P_k$

The SIR of the  $i$ th receiver (or transmitter) is given by

$$SIR_i = \frac{G_{ii}F_{ii}P_k}{\sum_{k \neq i} G_{ik}F_{ik}P_k} \quad (9)$$

$$SIR_i = \frac{G_{ii}F_{ii}P_i}{I_i} \tag{10}$$

We assume that the QoS requested is provided when the SIR exceeds a given threshold  $SIR^{th}$ . The outage probability of the  $i$ th receiver/transmitter pair is given by

$$O_i = \Pr ob(SIR_i) \leq SIR^{th} \\ = \Pr ob\left(G_{ii}F_{ii}P_i \leq SIR^{th} \sum_{k \neq i} G_{ik}F_{ik}P_k\right) \tag{11}$$

The outage probability  $O_i$  can be interpreted as the fraction of time the  $i$ th transmitter/receiver pair experiences an outage due to fading. Note that in our expression for  $O_i$ , we take into account statistical variation of both received signal power and received interference power. We now consider the market method to regulate the SIR. By ignoring all statistical variation of both signal and noise power, the signal power at the  $i$ th receiver is then  $G_{ii}P_i$  and the interference power at the receiver is given by  $\sum_{k \neq i} G_{ik}P_k$ . Then the SIR at the  $i$ th receiver is given as

$$SIR_i^m = \frac{G_{ii}P_i}{\sum_{k \neq i} G_{ik}P_k} \tag{12}$$

We interpret  $SIR_i^m$  as follows: this is what the signal-to-interference of the  $i$ th transmitter/receiver pair would be, if the fading state of the system where  $F_i = \dots = F_n = 1$ . We also define

$$SIR^m = \min_i SIR_i^m = \min_i \frac{G_{ii}P_i}{\sum_{k \neq i} G_{ik}P_k} \tag{13}$$

which is the minimum SIR of the system over all transmitter/receiver pairs. Like the outage probability  $O$ , the  $SIR^m$  gives a figure of merit for the system and power allocation. We define the market regulation/control method of the system and power allocation as the ratio of the market control SIR to the signal-to-interference reception threshold

$$MCA = \frac{SIR^m}{SIR^{th}} = \min_i \frac{G_{ii}P_i}{SIR^{th} \sum_{k \neq i} G_{ik}P_k} \tag{14}$$

There is a relation between MCA and  $O$ : when MCA is large (which means that the SIR, ignoring statistical variation, is well above the minimum required for reception), we should have small  $O$ . Let

$$\delta_i = \frac{G_{ik}}{I_i} \tag{15}$$

denote the channel variation.  $\delta_i$  will be estimated and predicted in the proposed power control scheme.

$I_i = \sum G_{ik}F_{ik}$  presents the received interference.  $G_{ik}$  is the link gain from mobile station  $k$  to base station  $i$ . Suppose, that the highest transmitted power allowed is  $P^{max}$  and that the lowest transmitted power allowed is  $P^{min}$ . The social agent that SNR oriented uses the following technique to regulate the SNR between the cells. The proposed technique operates in the following way:

- For any cell, two tiers of cells are considered as interfering cells. The channel state information (allocating or releasing) of each cell is locally exchanged to its interfering cells. Every cell maintains a list of the cost for all channels. The cost function is used to decide the cost of a channel. The cost of a channel in a cell is updated (increased or decreased) in real time if a co-channel call is accepted or terminated (dropping and departure) in one of the cell's interfering cells.

- When a call arrives in a cell, the free channel with highest priority (lowest cost) is chosen for call setup and the call power probing process is activated. The procedures of the power probing for a new (or handoff) call are:

- 1) Assigning the minimum transmitted power  $P_{min}$  to the new call  $p$ .

- 2) Measuring the SIR value  $\gamma_p$  of the call.

- 3) If  $\gamma_p < \gamma$ , adjusting the power of the call and going back to step 2; if  $\gamma_p \geq \gamma$ , and  $P^{min} \leq P_p(k) \leq P^{max}$ , this call is admitted into service with this power and the call power probing process is ended.

- 4) If a power cannot be found in the range of  $[P^{min}, P^{max}]$  with which the SIR value  $\gamma_p \geq \gamma$ , or the probing iteration number is larger than a pre-assigned value, the probing is moved to the next highest priority channel. Actually, an exhaustive searching is not allowed in a system. Hence, we prescribe that if four channels have been evaluated, but the SIR requirement is still not satisfied, the call is blocked.

- 5) If a call is in service, the power control algorithm is used to maintain its quality. Each base station monitors its own served calls at some time interval. We assume that all base stations are synchronized (actually the algorithm works asynchronously either). When the SIR of a call falls below the target value, the power control procedure is requested. However, if the maximum transmitted power is requested or the number of iterations of power level adjustment is larger than the allowed value, but the SIR is still below a specified value (e.g., the call dropping threshold value), the handoff procedure is requested. The "call set-up" procedure will begin to search for a channel for handoff. If a channel is found, the call is moved to this channel. Otherwise, the call is dropped.

### 4. System Model

A cellular network consists of an array of cells. We par-

tition the cellular network to clusters. For each cell we set a social agent, as depicted in **Figure 1**. By using radio cognitive approach we aim to achieve an optimal network capacity, minimizing interference to other signals and to reduce messages complexity and channel acquisition delay that are considered the main reasons to block the new calls. A radio cognitive approach may be able to sense the current spectral environment, and have information of past transmitted and received packets along with the power, bandwidth, and modulation. By considering all this, it makes better decisions about how to best optimize for some overall goal. Under heavy traffic load, and if a vacant channel is not found, the social agent then tries to obtain an exclusive channel by optimization of channel distribution based on iterative swapping scheme [23]. In which the social agent changes the channel distribution anew. We partition the set of channels into active and passive channels. The active channels are defined as the channels, which can be used by own cell. Furthermore the active channels can be simultaneously used in different cells without any interference if they are a minimum reuse distance ( $D_{min}$ ) apart from each other [23]. The passive channels are defined as the channels, which can be used by neighbor cells. Furthermore, the free channel will be expressed as 1 and the busy channel will be expressed as 0. The set of channels are classified and assigned uniform to cells in real-time.

### 4.1. Social Agent Negotiation Strategy

Compared to the traditional negotiation strategy that offers high messages complexity, we are interested in ap-

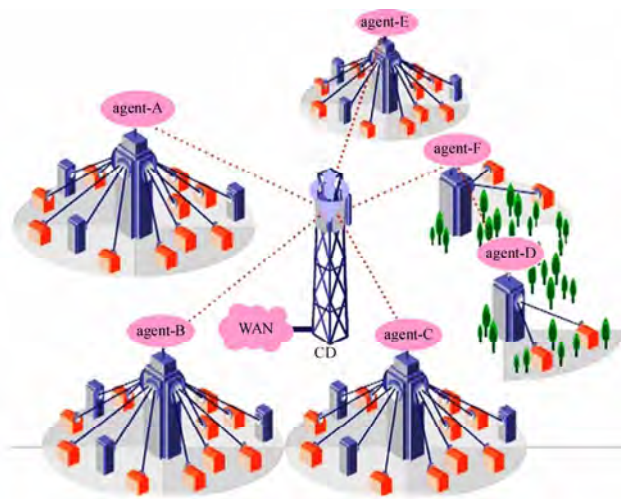


Figure 1. System model.

plications where negotiation between social agents serves to solve the resource allocation problem in cellular systems. Furthermore we anticipate concern the feasibility of reaching an allocation of resources that is optimal from a social point of view. Social agents often need to interact in order to improve their performance. One type of interaction that is gaining an increasing interest is dynamic negotiation. The goal of negotiation is the maximization of the utility of a future decision. In distributed dynamic environment, each cell has an objective that specifies its intention to acquire a free channel for call establishment. That objective should be achieved in a certain amount of time, specified by a deadline. Negotiation stops when this deadline is reached.

### 4.2. Social Agent Decision Strategy

In this phase the agent deals with handover request as illustrates in **Figure 2**. The social agent's decision about the handover process is focused on quality of service requirements (e.g. signal power, signal-to-noise ratio and delay). The signal-to-noise ratio (SNR or S/R) defined as the ratio of a signal power to the noise power corrupting the signal. The social agent estimates the SNR and then determines to carry out the handover or not. Furthermore the agent collects information about the adjacent cells. Based on of the collected information from the adjacent cells, the agent determines the next handover cell. The handover based on SNR can be divided into two main categories:

- 1) The first scenario is based on received SNR from the base station only. This method decides handoff when the SNR from current station is smaller than another station. This kind of method is simple but will take place repeated or unnecessary handoff.
- 2) The second scenario is based on relative SNR with threshold. In this approach, handoff is initiated when the average SNR falls below a certain threshold value. This method can avoid unnecessary handoff when the current station signal is still satisfactory.

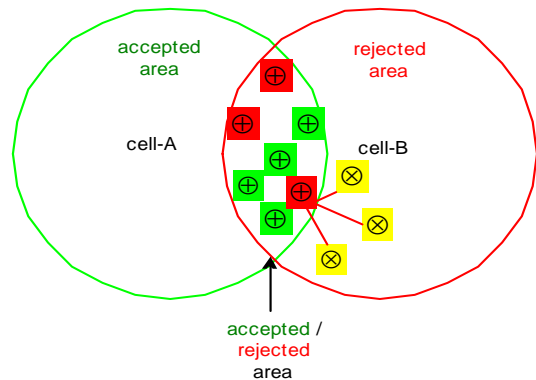


Figure 2. Blocking probability area.

### 4.3. Social Agent Reasoning Strategy

The radio approach draws its decision based on employing a cost function [24]. The resource agent allocates to a request, the channel of which the cost function is minimal. The cost function basically computes the interference level. The cost functions can be collectively expressed in a general expression:

$$J_k = \sum_{i \in I_c} (C_{ki} q_{ki}) \quad (16)$$

where  $J_k$  is the channel interference cost unit for the  $k$ -th channel,  $I_c$  denotes the set of co-channel interference cells related to cell  $C$ .  $C_{ki}$  denotes the binary status of  $I_c$  which signifies that

$$C_{ki} = \begin{cases} 0, & \text{channel } k \text{ causes no interf. in cell } i \\ 1, & \text{channel } k \text{ causes interf. in cell } i \end{cases}$$

$q_{ki}$  is used to reflect the interference between the interfering cell  $i$  and cell  $C$ . Therefore, any available channel having minimum value of  $J_k$  is to be allocated to a new call arising in cell  $C$ . To obtain an optimal reasoning, the social agents consider aggregation rules that enable the social agents to change the currently held reasoning upon acquiring new information. Information and actions that affect the social agent decision in handover process are described below.

- Handover process starts if the mobile station receives a weak SNR.
- Mobile station moves to neighbor cell that have the highest number of free channel to ensure that the call is not blocked.
- Chooses channel with the lowest interference from the set of free channels.  $channel(k) = \arg \min_k I_k$
- Using iterative swapping scheme to avoid high interference.

```

t = 0
FOR i = 1 to k DO r_i(t) = choose (V)
REPEAT
FOR i = 1 to k DO C_i = φ
FOREACH v ∈ V DO
x = arg min_{i: i ∈ {1, ..., k}} d(r_i(t), v)
ENDDO
FOR i = 1 to k DO
r_i(t) = minimize (interf(C_i))
UNTIL (∀ r_i : d(r_i(t), r_i(t-1)) < ε, t > t_max)
RETURN ({r_1(t), ..., r_k(t)})
    
```

### 4.4. Social Agent Beliefs

The new call in cell is blocked when there are no more free channels in the cell or the QoS requested cannot be

provided as the SIR is under a given threshold  $SIR^{tgt}$ . By computing the call blocking probability in handover process, we consider four social agent decision scenarios that are described below.

- 1) Probability (Approve,  $SNR > SNR^{tgt}$ )
- 2) Probability(Reject,  $SNR < SNR^{tgt}$ )
- 3) Probability(Approve,  $SNR < SNR^{tgt}$ )
- 4) Probability(Reject,  $SNR > SNR^{tgt}$ )

### 4.5. Interference Area Identification

In a mobile system, since the mobile stations can move between cells, the number of mobile stations within a cell at a given time can never be known exactly in advance. However, we can estimate roughly the location of the mobile stations. To avoid the call blocking by handover, it is important to identify the interference area. The interference area can be considered as the node of decision to hand over to a new cell. Denote  $P_t$  as the transmitter power of the base station,  $G$  the antenna gain,  $d$  the distance between the transmitter and receiver and  $N_0$  as the thermal noise power. Generally, then, the received signal-to-noise ratio (SNR) at the  $k$ -th user in cell-1 is given by

$$\gamma_{1(d_1)}^1 = \frac{P_t G(d_1)}{N_0}, \gamma_{2(d_2)}^1 = \frac{P_t G(d_2)}{N_0}, \dots, \gamma_{j(d_k)}^1 = \frac{P_t G(d_k)}{N_0} \quad (17)$$

for  $j = 1, \dots, k$ . The signal-to-noise ratio (SNR or S/R)  $\gamma_k$  defined as the ratio of a signal power to the noise power corrupting the signal. Hence, following Markovian analysis, the social agent can predict the average blocking probability of user  $k$  being served by the base station based on calculation of the interference area for cell  $i$ , which is greater than a given target value for cell  $i$ ,  $\gamma_i^{tgt}$ . This blocking probability is:

$$P_b = \frac{1}{n} \sum_{k=1}^n \delta_k \quad (18)$$

$$\text{where } \delta_k = \begin{cases} 1 & (\gamma_k - \gamma_i^{tgt}) < 0 \\ 0 & \text{Otherwise} \end{cases}$$

### 4.6. Active Sense Environment

In sense environment the radio cognitive approach takes in consideration the following parameters, propagation model, traffic model and amount of the information. This represents the maximum amount of information that can be conveyed through a communications channel. From an information theoretic perspective, a communications channel is responsible for passing data between two points, and will likely add some sort of noise to be original signal. In other words, the original signal reception is

possible only when the relation of energy per bit  $E_b$  to noise spectral density  $N_0$  is appropriate. Low value of  $E_b/N_0$  will cause the receiver to be unable to decode the received signal, while a high value of the energy per bit in relation to noise will be perceived as interference for other users of the same radio channel. For example, for CDMA systems, the bit energy-to interference-and-noise-spectral density ( $E_b/N_0$ ) is SINR multiplied by the number of information bits modulated by the spreading code, whereas the carrier-to-interference-and-noise-power ratio ( $CIR$  or  $C/I$ ) is equal to ( $E_b/N_0$ ) divided by the length of the spreading code. The ratio  $E_b/N_0$  is given by

$$E_b / N_0 = G_p (C / I) \tag{19}$$

where  $G_p$  is the processing gain, and the ratio  $C/I$  of the user is given by

$$C / I = \frac{P}{E(I)} \tag{20}$$

To calculate the received signal-to-noise ratio (SNR) at the  $k$ th user is given by

$$\gamma_k(r_k) = \frac{P_t G(r_k)}{N_0} \tag{21}$$

For our purposes we focus on the Shannon Theorem, which states for additive white Gaussian noise (AWGN) channel. The channel capacity is given by

$$C = W \log_2(1 + \xi \gamma_k) \tag{22}$$

where  $\xi$  is the bit error rate.

### 5. Simulation Results

The radio cells treat licensed users, other unlicensed radio networks, interference, and noise all as interference affecting the signal-to-interference ratio (SIR). Higher interference yields lower SIR, which means lower capacity is achievable for a particular signal bandwidth and interference in the radio channel and reduces the quality of the transmission. There are different quantities that measure the quality as signal-to-interference ratio (SIR) and the bit-error rate (BER). SIR, referred to also as signal-to-interference-and-noise ratio (SIR) to emphasize the presence of background noise, is the ratio between the power of the desired signal and the power of the interference (plus noise). In **Figure 3**, two different mobile radio systems are illustrated. Mobile station  $MS_A$  is located at the cell boundaries of system A, however very close to base station BS-B, due different reasons like receiving a weak SNR (finding the mobile station in rural area) or due interference that may occur at base station  $BS_A$  from base station BS-B. To maintain a reliable connection between the user and the base station, the SIR at

the receiver should be no less than some threshold that corresponds to QoS requirement such as the bit error rate. **Figure 4** shows that the received signal to interference ratio varies greatly over the duration of the simulation. **Figure 5** describes the average received power by the

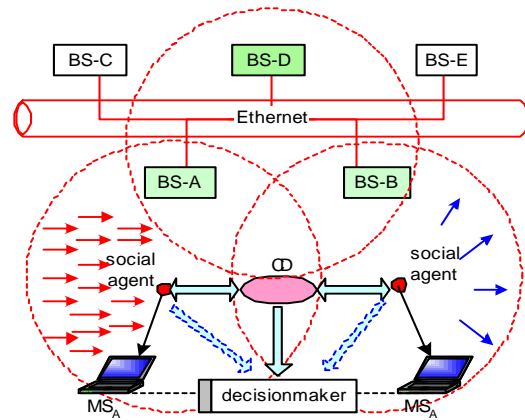


Figure 3. Traffic model.

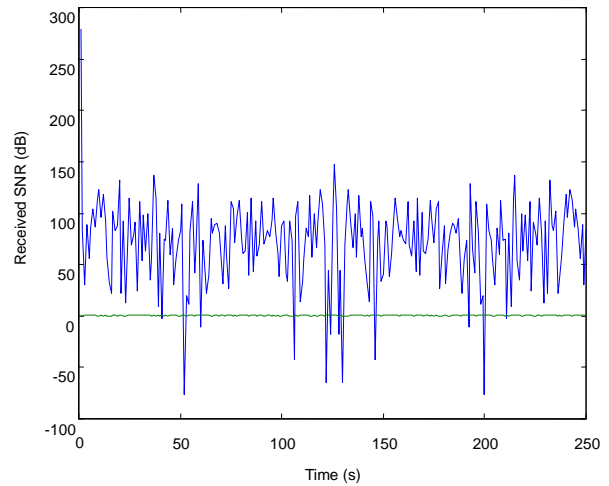


Figure 4. The received SNR.

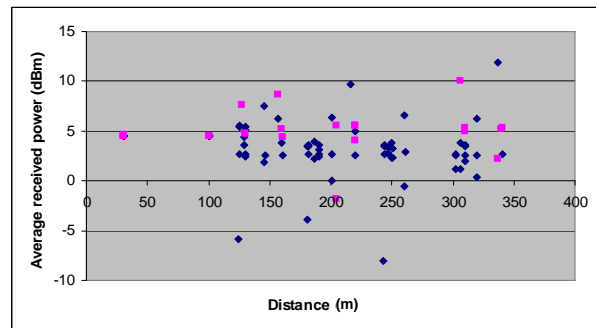
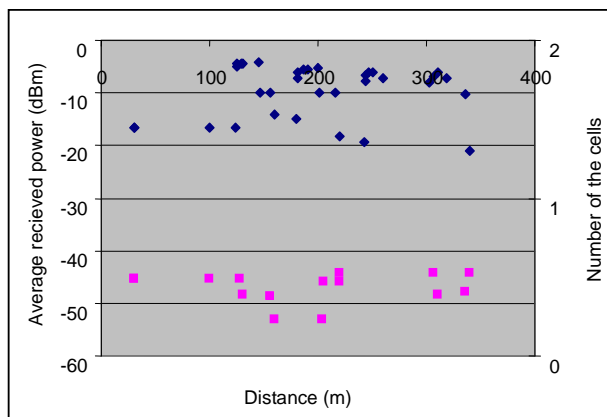
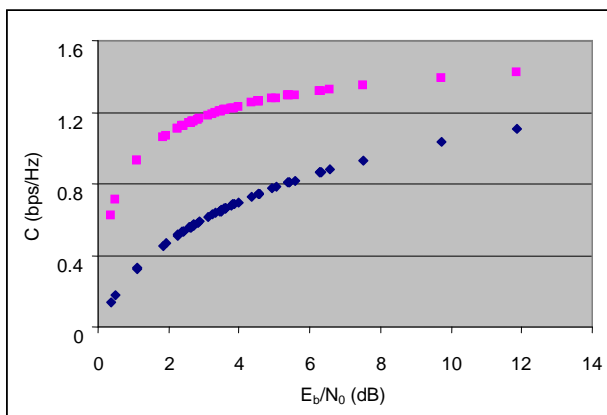


Figure 5. The received power vs. distance.

users. **Figure 6** describes the social agent strategy that may agree on a deal to exchange some of the resources they currently hold, in order to increase the social agent utility. **Figure 7** describes the bandwidth efficiency. **Figure 8** describes the blocking probability related to the SNR.



**Figure 6. Resource distribution.**



**Figure 7. Bandwidth efficiency.**

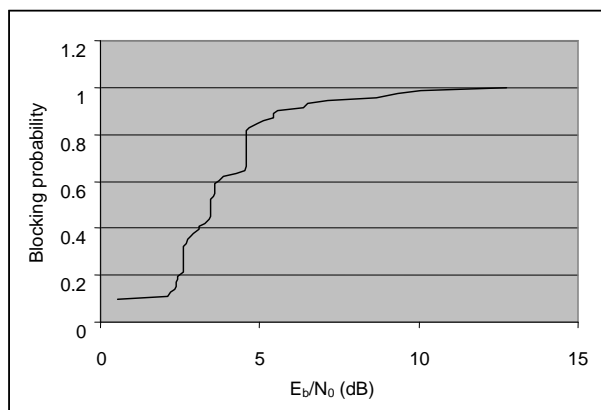


**Figure 8. Blocking probability.**

## 6. Conclusions

In this paper we have presented the principles of handoff procedures and described some of the procedures used in various types of systems. Furthermore we have proposed a radio cognitive for handover management to reduce the interference which is sourced by channel acquisition in cellular system. In general, there are different reasons that caused the interference in cellular system, such as power which is also an important resource. Allocation of power in the proper channels can increase capacity and avoid interference.

## 7. References

- [1] N. D. Tripathi, *et al.*, "Handoff in cellular systems," IEEE Personal Communications, December 1998.
- [2] B. Friedlander and S. Scherzer, "Beamforming versus transmit diversity in the downlink of a cellular communication," IEEE Transactions on Vehicular Technology, Vol. 53, No. 53, July 2004.
- [3] C. W. Leong, W. Zhuang, Y. Cheng, and L. Wang, "Optimal resource allocation and adaptive call admission control for voice/data integrated cellular networks," IEEE Transactions on Vehicular Technology, Vol. 55, No. 2, March 2006.
- [4] L. Cong, *et al.*, "Performance analysis of dynamic channel assignment algorithms in cellular mobile systems with hand-off," International Journal of Communication Systems, July 2002.
- [5] S. S. Manvi and P. Venkataram, "Agent based subsystem for multimedia communications," IEE Proceedings Software, Vol. 153, No.1, February 2006.
- [6] S. Anand, A. Sridharan, and K. N. Sivarajan, "Performance analysis of channlized cellular systems with dynamic channel allocation," IEEE Transactions on Vehicular Technology, Vol. 52, No. 4, July 2003.
- [7] T. Ren and R. J. La, "Downlink beamformig algorithms with inter-cell interference in cellular networks," IEEE Transactions on Wireless Communications, Vol. 5, No.10, October 2006.
- [8] M. Zafer and E. Modiano, "Blocking probability and channel assignment in wireless networks," IEEE Transactions on Wireless Communications, Vol. 5, No. 4, April 2006.
- [9] S. Gupta and P. Srimani, "Distributed dynamic channel allocation in mobile networks: Combining search and update," The Journal Supercomputing, Vol. 17, No. 1, August 2000.
- [10] S. Kandukuri and S. Boyd, "Optimal power control in interference limited fading wireless channels with outage probability specifications," IEEE Transactions on Wireless Communications, Vol. 1, No. 1, January 2002.
- [11] C. J. Chen and L. W. Wang, "Impacts of radio channel

- characteristics, heterogeneous traffic intensity, and near-far effect on rate adaptive scheduling algorithms," *IEEE Transactions on Vehicular Technology*, Vol. 55, No. 5, September 2006.
- [12] J. Raiyn, *et al.*, "Using adaptive agent-based on iterative distributed swapping prediction for interference reduction in cellular systems, international symposium on performance evaluation of computer and telecommunication systems," Edinburgh, U.K., 16–18 June 2008.
- [13] M. Bublin, M. Kongegger, and P. Slanina, "A cost-function-based dynamic channel allocation and its limits," *IEEE Transactions on Vehicular Technology*, Vol. 56, No. 4, July 2007.
- [14] M. S. Do, Y. Park, and J. Y. Lee, "Channel assignment with QoS guarantees for a multiclass multicode CDMA system," *IEEE Transactions on Vehicular Technology*, Vol. 51, pp. 935–948, September 2002.
- [15] A. Seth, H. M. Gupta, and K. Momaya, "Quality of service parameters in cellular mobile communication," *International Journal of Mobile Communications*, Vol. 5, No. 1, pp. 65–93, 2007.
- [16] S. Zhao, Z. Xiong, and X. Wang, "Optimal resource allocation for wireless video over CDMA networks," *IEEE Transaction on Mobile Computing*, Vol. 4, No. 1, pp. 441–424, January–February 2005.
- [17] G. J. Foschini and Z. Miljanic, "A simple distribute autonomous power control algorithm and its convergence," *IEEE Transactions on Vehicular Technology*, Vol. 42, No. 4, pp. 641–646, November 1993.
- [18] S. A. Grandhi, J. Zander, and R. Yates, "Constrained power control," *Wireless Personal Communications*, Vol. 1, No. 4, pp. 257–270, 1995.
- [19] B. C. Jung, Y. J. Hong, D. K. Sung, and S. Y. Chung, "Fixed power allocation with nulling for TDD-based cellular uplink," *IEEE Communications Letters*, Vol. 12, No. 4, April 2008.
- [20] X. Li and D. Wu, "Power control and channel allocation for real time applications in cellular networks," *Wireless Communications and Mobile Computing*, Vol. 8, No. 6, pp. 705–713, 2007.
- [21] J. L. Eaves and E. K. Reely, "Principles of modern radar," Van Nostrand Reinhold Company, New York, 1987.
- [22] G. J. Foschini and Z. Miljanic, "Distributed autonomous wireless channel assignment algorithm with power control," *IEEE Transactions on Vehicular Technology*, Vol. 44, No. 3, pp. 420–429, August 1995.
- [23] D. Beckmann and U. Killat, "A new strategy for the application of genetic algorithms to channel assignment problem," *IEEE Transactions on Vehicular Technology*, Vol. 48, No. 4, pp. 1261–1269, 1999.
- [24] M. Bergounioux and K. Kunisch, "On the structure of Lagrange multipliers for state-constrained optimal control problems," *Optimization and Control of Distributed Systems*, Vol. 48, No. 3–4, pp. 169–176, March 2003.
- [25] S. Hykin, J. D. Thomson, and H. J. Reed, "Spectrum sensing for cognitive radio," *Proceedings of the IEEE*, Vol. 97, No. 5, pp. 849–877, May 2009.

# A Mobile Ad-Hoc Routing Algorithm with Comparative Study of Earlier Proposed Algorithms

**Pawan Kumar Verma, Tarun Gupta, Nitin Rakesh, Nitin Nitin**

*Department of CSE & IT, Jaypee University of Information Technology, Wanknaghat, India*

*E-mail: [nitin.rakesh@gmail.com](mailto:nitin.rakesh@gmail.com), [delnitin@ieee.org](mailto:delnitin@ieee.org)*

*Received December 10, 2009; revised January 12, 2010; accepted February 16, 2010*

## Abstract

A mobile ad-hoc network is an autonomous collection of mobile nodes that communicate over bandwidth constrained wireless links. Due to nodal mobility, the network topology may change rapidly and unpredictably over time. The routing protocols meant for wired network cannot be used for mobile ad-hoc network because of mobility of network. A number of routing protocols like Destination-Sequenced Distance-Vector (DSDV), Ad-Hoc On-Demand Distance Vector (AODV), Dynamic Source Routing (DSR), and Temporally Ordered Routing Algorithm have been implemented. The ad-hoc routing protocols can be divided into two classes; Table-Driven and On-Demand. This paper examines two routing protocols for mobile ad-hoc networks—the Destination Sequenced Distance Vector (DSDV), the table-driven protocol and the Ad-Hoc On-Demand Distance Vector routing (AODV), an on-demand protocol and propose an algorithm that facilitates efficient routing of the packet and failure recovery mechanism.

**Keywords:** AODV, DSDV, Relative Performance

## 1. Introduction and Motivation

Wireless networks are the current field of research as it provides new advancement to the field of mobile network and reliable data transfer. They provide a mechanism to share the information and services via electronic medium without any geographical constraints. As the medium is wireless there is no distance limitations present and the network do not need much maintenance as no physical medium is involved in the actual transmission. Wireless networks can be categorized as-infrastructure network and infrastructure less (ad-hoc) networks. Infrastructure network consists of a network with fixed and wired gateways. A mobile host searches for a bridge in the network in its defined communication radius, if it goes out of the range of the network the search for new base station starts and the communication is established. The approach is called as handoff.

In contrast to infrastructure-based networks, in ad-hoc networks all nodes are mobile and can be connected dynamically in an arbitrary manner. All nodes of these networks behave as routers and take part in discovery and maintenance of routes to other nodes in the network. Ad-hoc networks are very useful in emergency search-and-rescue operations, meetings or conventions in which persons wish to quickly share information, and data ac-

quisition operations in inhospitable terrain. Routing protocols for mobile ad-hoc networks can be classified into two main categories: Proactive or table driven routing protocols and reactive or on-demand routing protocols. In proactive protocols, every node maintains the network topology information in the form of routing tables by periodically exchanging routing information. They include the Destination Sequenced.

Distance Vector (DSDV) [1], the Wireless Routing Protocol (WRP) [2], Source-Tree Adaptive Routing (STAR) [3] and Cluster-head Gateway Switch Routing Protocol (CGSR) [4]. On the other hand, reactive protocols obtain routes only on demand, which include the Dynamic Source Routing (DSR) protocol [5], the Ad-hoc On-demand Distance Vector (AODV) protocol [6], the Temporally Ordered Routing Algorithm (TORA) [7], and the Associativity Based Routing (ABR) protocol [8].

The rest of the paper is organized as follows: Section 2 presents an overview of the two main categories of mobile ad-hoc routing protocols and Section 3 presents a general comparison of the table-driven and on-demand routing protocols. Section 4 provides an overview and general comparison of the routing protocols used in the study. In Section 5, we propose routing algorithm with better performance and failure recovery. Finally, Section 6 concludes the paper and describes the future work of

our paper. Section 7 lists the references used by our research paper.

## 2. Routing Protocols for Mobile Ad-Hoc Network

In Routing, protocols for mobile ad-hoc networks can be classified into two main categories:

- Proactive or table-driven routing protocols and
- Reactive or on-demand routing protocols.

### 2.1. Table-Driven Routing Protocol

In table-driven routing protocols, each node maintains one or more tables containing routing information to every other node in the network. All nodes update these tables to maintain a consistent and up-to-date view of the network. When the network topology changes the nodes propagate update messages throughout the network in order to maintain consistent and up-to-date routing information about the whole network.

- Dynamic Destination Sequenced Distance Vector Routing Protocol (DSDV)
- The Wireless Routing Protocol (WRP)
- Clusterhead Gateway Switch Routing Protocol (CGSR)
- Global State Routing
- Fisheye State Routing
- Hierarchical State Routing
- Zone-Based Hierarchical Link State Routing Protocol

### 2.2. On Demand Routing Protocols

These protocols take a lazy approach to routing. In contrast to table-driven routing protocols not all up-to-date routes are maintained at every node, instead the routes are created as and when required. When a source wants to send to a destination, it invokes the route discovery mechanisms to find the path to the destination. The route remains valid until the destination is reachable or until the route is no longer needed.

- Ad-hoc On-demand Distance Vector Routing (AODV)
- Dynamic Source Routing Protocol (DSR)
- Temporally Ordered Routing Algorithm (TORA)
- Associativity Based Routing (ARB)
- Cluster Based Routing Protocol

## 3. Comparison of Table-Driven and On-Demand Routing Protocols

The table-driven ad-hoc routing approach is similar to the connectionless approach of forwarding packets, with

no regard to when and how frequently such routes are desired. It relies on an underlying routing table update mechanism that involves the constant propagation of routing information. This is not the case, however, for on-demand routing protocols. When a node using an on-demand protocol desires a route to a new destination, it will have to wait until such a route can be discovered. On the other hand, because routing information is constantly propagated and maintained in table-driven routing protocols, a route to every other node in the ad-hoc network is always available, regardless of whether or not it is needed. This feature, although useful for datagram traffic, incurs substantial signaling traffic and power consumption. Since both bandwidth and battery power are scarce resources in mobile computers, this becomes a serious limitation. **Table 1** lists some of the basic differences between the two categories of mobile ad-hoc routing protocols.

## 4. Overview of DSDV and AODV

As each protocol has its own merits and demerits, none of them can be claimed as absolutely better than others. Two mobile ad-hoc routing protocols—the Destination Sequenced Distance Vector (DSDV), the table-driven protocol and the Ad-Hoc On-Demand Distance Vector routing (AODV), an On-Demand protocol are selected for study.

### 4.1. Destination-Sequenced Distance Vector (DSDV)

The Destination-Sequenced Distance-Vector (DSDV)

**Table 1. Comparison of table-driven and on-demand routing protocol.**

Parameters	Table-Driven	On-Demand
<b>Route Availability</b>	Always available irrespective of need	Computed when needed
<b>Routing philosophy</b>	Flat, except for CGSR	Flat, except for CBRP
<b>Periodic updates</b>	Always required	Not required
<b>Handling mobility</b>	Updates occur at regular intervals	Use localized route discovery
<b>Control traffic generated</b>	Usually higher than on-demand	Increases with mobility of active routes
<b>Storage requirements</b>	Higher than on-demand	Depends on the number of routes maintained or needed
<b>Delay</b>	Small as routes are predetermined	High as routes are Computed when needed
<b>Scalability</b>	Usually up to 100 nodes	Usually higher than table driven

Routing Algorithm is based on the idea of the classical Bellman-Ford Routing Algorithm with certain improvements. Every mobile station maintains a routing table that lists all available destinations, the number of hops to reach the destination and the sequence number assigned by the destination node. The sequence number is used to distinguish stale routes from new ones and thus avoid the formation of loops. The stations periodically transmit their routing tables to their immediate neighbors. A station also transmits its routing table if a significant change has occurred in its table from the last update sent. Therefore, the update is both time-driven and event-driven. The routing table updates can be sent in two ways: a “full dump” or an incremental update. A full dump sends the full routing table to the neighbors and could span many packets whereas in an incremental update only those entries from the routing table are sent that has a metric change since the last update and it must fit in a packet. If there is space in the incremental update packet then those entries may be included whose sequence number has changed. When the network is relatively stable, incremental updates are sent to avoid extra traffic and full dump are relatively infrequent. In a fast-changing network, incremental packets can grow big so full dumps will be more frequent. Each route update packet, in addition to the routing table information, also contains a unique sequence number assigned by the transmitter. The route labeled with the highest (i.e. most recent) sequence number is used. If two routes have the same sequence number then the route with the best metric (i.e. shortest route) is used. Based on the history, the stations estimate the settling time of routes. The stations delay the transmission of a routing update by settling time to eliminate those updates that would occur if a better route were found very soon.

**4.2. Ad-Hoc On-Demand Distance Vector Routing (AODV)**

Ad-hoc On-Demand Distance Vector Routing (AODV) is an improvement on the DSDV algorithm discussed in previous section. AODV minimizes the number of broadcasts by creating routes on-demand as opposed to DSDV that maintains the list of all the routes. To find a path to the destination, the source broadcasts a route request packet. The neighbors in turn broadcast the packet to their neighbors until it reaches an intermediate node that has recent route information about the destination or until it reaches the destination (Figure 1(a)). A node discards a route request packet that it has already seen. The route request packet uses sequence numbers to ensure that the routes are loop free and to make sure that if the intermediate nodes reply to route requests, they reply with the latest information only.

When a node forwards a route request packet to its

neighbors, it also records in its tables the node from which the first copy of the request came. This information is used to construct the reverse path for the route reply packet. AODV uses only symmetric links because the route reply packet follows the reverse path of route request packet. As the route reply packet traverses back to the source (Figure 1(b)), the nodes along the path enter the forward route into their tables.

If the source moves then it can reinitiate route discovery to the destination. If one of the intermediate nodes moves then they moved nodes neighbor realizes the link failure and sends a link failure notification to its upstream neighbors and so on till it reaches the source upon which the source can reinitiate route discovery if needed.

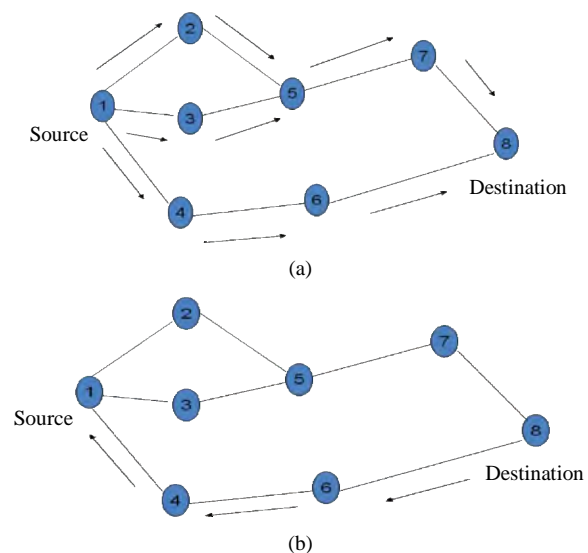


**Figure 1. (a) Propagation of Route Request Packet (RREQ), (b) Path taken by the Route Reply (RREP) Packet.**

**Table 2. AODV v/s DSDV.**

Parameter	DSDV	AODV
<b>Routing structure</b>	Flat	Flat
<b>Frequency of updates</b>	Periodic and as needed	As required
<b>Critical nodes</b>	No	No
<b>Loop-free</b>	Yes	Yes
<b>Multicasting capability</b>	No	Yes
<b>Routing metric</b>	Shortest path	Fastest and shortest path
<b>Utilizes sequence no.</b>	Yes	Yes
<b>Time complexity</b>	O(Diameter of network)	O(2*Diameter of network)
<b>Communication Complexity</b>	O(Number of nodes in n/w)	O(Number of nodes in n/w)
<b>Advantages</b>	Small delays	Adaptable to highly dynamic topology
<b>Disadvantage</b>	Large overhead	Large delays

## 5. Proposed Routing Algorithm

The proposed algorithm involves the computation of efficiency of the given route based on the network historical results and the maintenance of previous route information from source to the current node to handle any failure recovery during the transmission. Other than this the information of the various nodes connected and their distance from the destination is computed and updated after every cycle. Every node in the routing path is assigned a unique sequence number, which is checked after every movement to prevent any loops during the transmission procedure. At every node, a scheduling algorithm is applied based on the priorities of the data packets receiving the nodes. Information contained/processed at every node-

- **Sequence Number:** A unique number assigned to every node for its identification in the network. The unique ID is also used to prevent any loops in the network. The loop in the network are prevented by checking the current node sequence number with the previous node sequence number, if found smaller the routing is moving in a backward direction or will suffer from loop. The unique number is assigned to every node from source to destination.

- **Neighbor Node Table:** The table is maintained at every node that contains the information about every neighbor node in the network with respect to the current node. The search technique searches for the entire connected node in the network and store/update the neighbor node table accordingly. The sequence number of every neighbor node is stored in the table. The distance of every neighbor node from the destination is computed and stored in the table to facilitate shortest path search.

- **Path Information:** The path information contains the path trace from the source node to the current node i.e. the actual routing map with the sequence number stored in the path information. E.g. suppose a route start from a source node with sequence number 1 and move through 3, 6, 7 to the node with sequence number 9 then the path information for the node number becomes 1→3→6→7→9. This path trace helps to know the whole prorogated path from source to destination, which facilitates backtracking. The backtracking is needed when any of the network route fails, in this case the path information can be used to backtrack i.e. moving back in the network and selecting any other optimal path.

- **Efficiency Factor (EF):** This efficiency factor is computed based on the historical records. The network efficiency of the route is monitored every time it sends a data packet through the node. If the route transmits the data packet efficiently, the value of EF increases and vice versa. This factor helps to select the most optimal path as the node for which the EF will be high will result in reliable and speedy data transfer.

- **Data Packet Buffer:** At every node, a buffer is maintained to store the receiving data packets to be transmitted to the destination node. The storing of data packet in the node buffer prevents any packet loss and reduces the network traffic.

- **Scheduling of Data Packet:** A node buffer may receive more than one data packet for routing it to the destination. The selection of the data packet is made in accordance with the priority of the data packets received and the packets are arranged in order of their priorities in the buffer.

When the data packet progress from source to destination the information maintained is viewed. The next node in the network is selected on the basis-

- **Availability of path:** The next node selected must be free to transmit the packet or the buffer of the node should be empty. All the nodes connected are viewed for the buffer position and the one, which is vacant or less busy, is selected.

- **Distance from Destination:** The Neighbor Node Table available at each node is examined for the node with minimum distance from the destination. The node with minimum distance is selected.

- **Efficiency Factor:** The efficiency factor computed at every node that provides the information about the network reliability is looked upon and the node with highest efficiency factor EF is selected.

Based on the commutative result of all the above-described parameters the packet is transmitted to the next node with the condition that the current distance should be less than the distance from the next node. If in case the network path fails the packet is transmitted back to the previous node in the path information and any other path is selected. If there are multiple data packets at any node the scheduling of data packets is done to prevent any collision and data loss. The scheduling is done according to the priority of the data packets. The proposed algorithm provides an efficient way to transmit data over the wireless network reliably and with failure recovery mechanism.

**Table 3** prescribed in the below gives the sequential flow of the routing steps. This algorithm described involves reliable data packet transfer through the best possible path and minimum time latency.

## 6. Conclusions and Future Works

Each earlier proposed protocol has their own merits and demerits, none of them can be claimed as absolutely better than others can. This paper compared the two ad-hoc routing protocols: AODV an on-demand routing protocol, and DSDV a table-driven protocol and proposed a better routing algorithm with historical monitoring of the network and failure recovery to facilitate reliable transmission of data packet over the wireless network.

**Table 3. Proposed algorithm.**

Steps	Task Performed
1	<ul style="list-style-type: none"> <li>- Every node assigned a unique sequence ID;</li> <li>- Neighbour Node Table containing distance from destination;</li> <li>- Path Information is updated;</li> <li>- Efficiency Factor (E.F.) computed based on historical network Efficiency.</li> </ul>
2	The data packed to be sent is selected based on the Scheduling algorithm based on the prioritization.
3	<p>After the packet selection the network is computed on the basis of-</p> <ul style="list-style-type: none"> <li>- Neighbour node table</li> <li>- Each neighbour distance from destination.</li> <li>- Efficiency Factor(E.F.)</li> </ul> <p>The above factors are examined and the next node is selected accordingly.</p>
4	If the network route is efficient the algorithm proceed in forward direction, else the Path Information is used to reverse the path.
5	If data packet reaches Destination Node then algorithm terminates else continue, from step 3.

The future aspect of the system involves the improvement of the scheduling algorithm that facilitates more efficient scheduling of data packets using a data buffer at every node. This will prevent any jam in the network and improve network traffic. The efficiency factor can be computed more precisely to have excellent results during the packet transmission.

## 7. References

- [1] C. E. Perkins and P. Bhagwat, "Highly dynamic destination-sequenced distance-vector routing (DSDV) for mobile computers," In Proceedings of ACM SIGCOMM, pp. 234–244, August 1994.
- [2] S. Murthy and J. J. Garcia-Luna-Aceves, "An efficient routing protocol for wireless networks," ACM Mobile Networks and Applications Journal, Special Issue on Routing in Mobile Communication Networks, Vol. 1, No. 2, pp. 183–197, October 1996.
- [3] J. J. Garcia-Luna-Aceves and M. Spohn, "Source-tree routing in wireless networks," In Proceedings of IEEE ICNP, pp. 273–282, October 1999.
- [4] C. C. Chiang, H. K. Wu, W. Liu, and M. Gerla, "Routing in clustered multi-hop mobile wireless networks with fading channel," In Proceedings of IEEE SICON, pp. 197–211, April, 1997.
- [5] D. B. Johnson and D. A. Malta, "Dynamic source routing in ad hoc wireless networks," Mobile Computing, Kluwer Academic Publishers, Vol. 353, pp. 153–181, 1996.
- [6] T.-W. Chen, J. T. Tsai, and M. Gerla, "QoS routing performance in multihop, multimedia, wireless networks," IEEE 6th ICUPC Record, pp. 557–561, October 1997.
- [7] V. D. Park and M. S. Corson, "A highly adaptive distributed routing algorithm for mobile wireless networks," In Proceedings of IEEE INFOCOM 1997, pp. 1405–1413, April 1997.
- [8] C. K. Toh, "Associativity-based routing for ad hoc mobile networks," Wireless Personal Communications, Vol. 4, No. 2, pp. 1–36, March 1997.
- [9] M. G. Kaosar, M. Hafiz, M. A. Tarek, R. Sheltami, and A. S. H. Mahmoud, "Simulation-based comparative study of on demand routing protocols for MANET," International Conference on Wireless Networking and Mobile Computing (ICWNMC'05), Chennai, India, Vol. 1, pp. 201–206, 28–30 December 2005.
- [10] K. Takahashi, T. Kato, S. Itoh, A. Sugata, F. Kojima, and M. Fujise, "Combining AODV ad hoc routing and conventional IP routing over wireless and wired links," Proceedings of Communication Systems and Networks, 2005.
- [11] Technical report. <http://www.cs.umu.se/education/examina/Rapporter/KrishnaGorantala.pdf>.
- [12] Technical report. <http://en.wikipedia.org/wiki/DSDV>.
- [13] T. Yang, M. Ikeda, G. De Marco, and L. Barolli, "Performance behavior of AODV, DSR and DSDV protocols for different radio models in ad-hoc sensor networks," 2007 International Conference on Parallel Processing Workshops, 10–14 September 2007.
- [14] E. M. Royer and C. K. Toh, "A review of current routing protocols for ad hoc mobile wireless networks," IEEE Personal Communications Magazine, pp. 46–55, April 1999.
- [15] C. E. Perkins and E. M. Royer, "Ad hoc on-demand distance vector routing," Proceedings of IEEE Workshop on Mobile Computing Systems and Applications, pp. 90–100, February 1999.
- [16] Technical report. <http://en.wikipedia.org/wiki/AODV>.
- [17] G. D. Nguyen and S. Kompella "Optimization of transmission schedules in captured-based wireless networks".
- [18] Z. Zhang, S. Moola, and E. K. P. Chong, "Approximate stochastic dynamic programming for opportunistic fair scheduling in wireless networks," Proceedings of the 47th IEEE Conference on Decision and Control Cancun, Mexico, 9–11 December 2008.
- [19] G. Forman and J. Zahorjan, "The challenges of mobile computing," IEEE computer, Vol. 27, No. 4, April 2001.

# A New Global Asymptotic Stability Result of Delayed Neural Networks via Nonsmooth Analysis

Yaning Gu, Deyou Liu, Wenjuan Wu, Jingwen Zhang

College of Science, Yanshan University, Qinhuangdao, China

E-mail: {wwkgogps919, liudeyouysu}@163.com

Received December 28, 2009; revised January 29, 2010; accepted February 26, 2010

## Abstract

In the paper, we obtain new sufficient conditions ensuring existence, uniqueness, and asymptotic stability of the equilibrium point for delayed neural network via nonsmooth analysis, which makes use of the Lipschitz property of the functions. Based on this tool of nonsmooth analysis, we first obtain a couple of general results concerning the existence and uniqueness of the equilibrium point. Then we drive some new sufficient conditions ensuring global asymptotic stability of the equilibrium point. Finally, there are the illustrative examples feasibility and effectiveness of our results. Throughout our paper, the activation function is a more general function which has a wide application.

**Keywords:** Delayed Neural Networks, Global Asymptotic Stability, Nonsmooth Analysis

## 1. Introduction

In recent years, the stability of a unique equilibrium point of delayed neural networks has extensively been discussed by many researchers [1–5]. Several criteria ensuring the global asymptotic stability of the equilibrium point are given by using the comparison method, Lyapunov functional method, M-matrix, diagonal dominance technique and linear matrix inequality approach. In [1–5], some sufficient conditions are given for the global asymptotic stability of delayed neural networks by constructing Lyapunov functions. A new sufficient condition on the global asymptotic stability for delayed neural networks via nonsmooth analysis is derived in this letter. The condition is independent of delay and imposes constraints on both the feedback matrix and delayed feedback matrix. Our results generalize and improve the preciously known works due to expending the activation function of the delay part.

Concerning the global stability of delayed neural networks described by the following differential equations with time delays

$$\dot{x} = -g(x(t)) + Af(x(t)) + A^\tau h(x(t-\tau)) + u \quad (1)$$

where  $x(t) = (x_1(t), \dots, x_n(t))^T \in \mathfrak{R}^n$

$$g(x(t)) = (g_1(x_1(t)), \dots, g_n(x_n(t)))^T \in \mathfrak{R}^n$$

$$f(x(t)) = (f_1(x_1(t)), \dots, f_n(x_n(t)))^T \in \mathfrak{R}^n$$

$$h(x(t-\tau)) = (h_1(x_1(t-\tau)), \dots, h_n(x_n(t-\tau))) \in \mathfrak{R}^n$$

and  $A = (a_{ij})$ ,  $A^\tau = (a^\tau_{ij}) \in \mathfrak{R}^{n \times n}$  are respectively, the feedback matrix and the delayed feedback matrix.  $u = (u_1, u_2, \dots, u_n)^T \in \mathfrak{R}^n$  is a constant input vector and  $\tau$  is the delay parameter. Furthermore, we assume that the function  $g$ , the activation function  $f$  and the activation function  $h$  satisfy the following conditions:

A1) Each function  $g_i : \mathfrak{R} \rightarrow \mathfrak{R}$  is a locally Lipschitz function and there exists  $m_i > 0$  such that  $g'_i(y) \geq m_i$  for all at  $y \in \mathfrak{R}$  which  $g_i$  is differentiable.

A2) Each function  $f_i : \mathfrak{R} \rightarrow \mathfrak{R}$  is a globally Lipschitz function with module  $k_i > 0$ , i.e.,

$$|f_i(y_1) - f_i(y_2)| \leq k_i |y_1 - y_2|$$

$\forall i = 1, \dots, n$  and  $y_1, y_2 \in \mathfrak{R}$

A3) Each function  $h_i : \mathfrak{R} \rightarrow \mathfrak{R}$  is a globally Lipschitz function with module  $l_i > 0$ , i.e.,

$$|h_i(y_1) - h_i(y_2)| \leq l_i |f_i(y_1) - f_i(y_2)|$$

$\forall i = 1, \dots, n$  and  $y_1, y_2 \in \mathfrak{R}$

The paper is organized as follows: Section 2 contains a short introduction to nonsmooth analysis for Lipschitz functions. In particular, the Lipschitzian Hadamard Theorem is explained and a homeomorphism theorem is obtained. Section 3 is to demonstrate how nonsmooth analysis can be carried out on (1) to derive sufficient conditions to ensure the existence and uniqueness of the equilibrium point of (1). In Section 4, we study new sufficient conditions with guarantee the GAS of the (1). In Section 5, we have an illustrative example and its simulations. We conclude in Section 6.

**Notation:** Let  $m_i, k_i, l_i, i = 1, 2, \dots, n$  be the constants given in assumptions (A1), (A2) and (A3), define two diagonal matrices  $M = \text{diag}(m_1, m_2, \dots, m_n)$  and  $K = \text{diag}(k_1, k_2, \dots, k_n)$

Let  $m = \min_i \{m_i\}$ ,  $k = \max_i \{k_i\}$  and  $l = \max_i \{l_i\}$ .

Let  $\|\cdot\|$  denotes the Euclidean norm for vectors and the matrix norm for matrices for any vector  $v = (v_1, v_2, \dots, v_n) \in \mathbb{R}^n$   $|v| = (|v_1|, |v_2|, \dots, |v_n|)^T$  similarly, for any matrix  $B = (b_{ij}) \in \mathbb{R}^{n \times n}$ ,  $|B| = (|b_{ij}|)$ .

Let  $\rho(B)$  denote the spectral radius of  $B$ . It is known that  $\rho(B) \leq \rho(|B|)$ . Moreover,

$$\rho(B) \geq \rho(\tilde{B}) \text{ if } B \geq \tilde{B} \geq 0.$$

$B$  is called a  $P$  matrix ( $P_0$  matrix) if and only if all principal minors of  $B$  are positive (nonnegative) and denoted by  $B \in P(B \in P_0)$ . For any matrix  $B \in \mathbb{R}^{n \times n}$ ,  $\mu_2(B) = (1/2)\lambda_{\max}(B+B^T)$  i.e.,  $\mu_2(B)$  is the largest eigenvalue of the symmetric part of  $B$ . All the mathematical facts concerning the eigenvalues of a matrix used in this paper can be found in the book [6].

## 2. Nonsmooth Analysis on Lipschitz Functions

We first review some concepts which are essential for conducting nonsmooth analysis on Lipschitz function. Then we state the Lipschitzian Hadamard Theorem, which gives conditions for homeomorphism of Lipschitz functions. Finally, we give a sufficient condition which ensures the existence and uniqueness of the equilibrium point of (1) for any input vector  $u \in \mathbb{R}^n$ .

Let the function  $F : \mathbb{R}^n \rightarrow \mathbb{R}^n$  be locally Lipschitzian.

According to Rademacher's theorem [7],  $F$  is differentiable almost everywhere. Let  $D_F$  denote the set of those points where  $F$  is differentiable and  $F'(x)$  denote the Jacobian of  $F$  at  $x \in D_F$ . For any given  $x \in \mathbb{R}^n$ , define the constant

$$Lip_x F := \sup_{\substack{y \rightarrow x \\ x \neq y \in \mathbb{R}^n}} \frac{\|F(y) - F(x)\|}{\|y - x\|}$$

Since  $F$  is locally Lipschitz, the constant  $Lip_x$  is finite and we have

$$\|F'(x)\| \leq Lip_x F \text{ for any } x \in D_F.$$

Now we are ready to define the generalized Jacobian in the sense of Clarke [8]:

For any  $x \in \mathbb{R}^n$ , let  $\partial F$  be the set of the following collection of matrices

$$\partial F(x) = \text{co}\{W \mid \text{there exists a sequence of } \{x^k\} \subset D_F \text{ with } \lim_{x^k \rightarrow x} F'(x^k) = W\}$$

where  $\text{co}\Omega$  denotes the convex hull of the set  $\Omega$ . It is easy to see that the above definition is well defined and  $\|W\| \leq Lip_x F$  for any  $W \in \partial F(x)$ . We say that  $\partial F(x)$  is invertible if every element  $W$  in  $\partial F$  is nonsingular.

For any given  $x, y \in \mathbb{R}^n$ , the Lebourg Theorem [8] states that there exists an element  $W$  in the union  $U_{z \in [x,y]} \partial F(z)$  such that

$$F(y) - F(x) = W(y - x)$$

where  $[x, y]$  denotes the segment connecting  $x$  and  $y$ .

For any two locally Lipschitz functions  $F : \mathbb{R}^n \rightarrow \mathbb{R}^n, \rightarrow \mathbb{R}^n, G : \mathbb{R}^n \rightarrow \mathbb{R}^n$ , we have

$$\partial(F + G) \subseteq \partial F(x) + \partial G(x) \text{ for all } x \in \mathbb{R}^n.$$

Now we are ready to state the Lipschitzian Hadamard Theorem which will lead to our homeomorphism result Theorem 1.

**Lemma 1** [9] (Lipschitzian Hadamard Theorem): Suppose  $F : \mathbb{R}^n \rightarrow \mathbb{R}^n$ , is locally Lipschitzian and let  $\kappa > 0$ . If  $\partial F(x)$  is invertible and  $\|W^{-1}\| \leq \kappa$  for all  $x \in \mathbb{R}^n$  and all  $W \in \partial F(x)$ , then  $F$  is a homeomorphism from  $\mathbb{R}^n$  onto  $\mathbb{R}^n$ .

For more discussions on the generalized Jacobian and its various applications, please refer to books [7,8] as well as to the paper [10,11]. Now, we analyze (1) from the viewpoint of nonsmooth analysis. We first recall that a state  $x^* \in \mathbb{R}^n$  is called an equilibrium point of (1) if it satisfies

$$-g(x^*) + Af(x^*) + A^T h(x^*) + u = 0$$

To study the existence and uniqueness of the equilibrium point for any input vector  $u \in \mathbb{R}^n$ , we define the function  $F : \mathbb{R}^n \rightarrow \mathbb{R}^n$ , by

$$F(x) = g(x) - Af(x) - A^T h(x) - u \tag{2}$$

Naturally,  $F$  is a locally Lipschitz function since  $g, f$  and  $h$  are so. Moreover, the generalised Jacobian of  $F$  at  $x$  is overestimated by (3). If each of the activation function  $f_i, h_i$  is nondecreasing on the real line  $\mathfrak{R}$ , then we have a more accurate estimate of  $\partial F(x)$  as follows (see (4)).

$$\partial F(x) \subseteq \tilde{V} = \left\{ \begin{array}{l} W \in \mathfrak{R}^{n \times n} \mid C - AD - IA^\tau D, \\ C = \text{diag}(c_1, c_2, \dots, c_n), \\ D = \text{diag}(d_1, d_2, \dots, d_n) \\ \text{with } c_i \geq m_i, -k_i \leq d_i \leq k_i, \\ \text{for all } i = 1, 2, \dots, n \end{array} \right\} \quad (3)$$

$$\partial F(x) \subseteq \tilde{V} = \left\{ \begin{array}{l} W \in \mathfrak{R}^{n \times n} \mid C - AD - IA^\tau D, \\ C = \text{diag}(c_1, c_2, \dots, c_n), \\ D = \text{diag}(d_1, d_2, \dots, d_n) \\ \text{with } c_i \geq m_i, 0 \leq d_i \leq k_i, \\ \text{for all } i = 1, 2, \dots, n \end{array} \right\} \quad (4)$$

Clearly,  $\tilde{V} \subset V$ . By applying Theorem 1 to (3) and (4), we have the following.

**Theorem 1:** Suppose functions  $f, g$  and  $h$  satisfy assumptions (A1), (A2) and (A3) and that one of the following two conditions holds.

- 1) Each element  $W \in V$  is nonsingular.
- 2) Each element  $W \in \tilde{V}$  is nonsingular and each activation function  $f_i$  and  $h_i$  is nondecreasing.

Then for each input vector  $u \in \mathfrak{R}^n$ , the function  $F$  in (2) is a homeomorphism from  $\mathfrak{R}^n$  onto  $\mathfrak{R}^n$ .

**Proof:** We only prove the result for the case (i). The case (2) be proved similarly as (1).

To show that  $F$  is a homeomorphism from  $\mathfrak{R}^n$  to  $\mathfrak{R}^n$ , in accordance with Theorem 1 it suffices to prove that the norms of inverses of all elements in  $V$  are uniformly bounded. In other words, we need to show that there exists a positive constant  $\kappa$  such that

$$\|W^{-1}\| \leq \kappa \quad \text{for all } W \in V \quad (5)$$

We prove it by a contradiction. Assume that there exists a sequence of matrices  $\{W^k\} \subset V$  satisfying

$$\|W^{-1}\| \rightarrow \infty \quad (6)$$

Then there exist two sequences of diagonal matrices  $\{C^k\}$  and  $\{D^k\}$ ,  $C^k = \text{diag}(c_1^k, c_2^k, \dots, c_n^k)$ ,  $D^k = \text{diag}(d_1^k, d_2^k, \dots, d_n^k)$  with  $c_i^k \geq m_i$  and  $d_i^k \in [-k_i, k_i]$  for all  $i = 1, \dots, n$  such that

$$W^k = C^k - AD^k - IA^\tau D^k$$

Recall that  $M = \text{diag}(m_1, m_2, \dots, m_n)$  and let  $P^k = M^{-1}C^k = \text{diag}(p_1^k, p_2^k, \dots, p_n^k)$ . It is easy to see that  $p_i^k \geq 1$  for all  $i = 1, \dots, n$

$$\|(P^k)^{-1}\| \leq 1$$

and  $W^k = (M - AD^k(P^k)^{-1} - IA^\tau D^k(P^k)^{-1})P^k$ .

Since both sequences of diagonal matrices  $\{D^k\}$  and  $\{(P^k)^{-1}\}$  are bounded, without loss of generality, we assume that

$$\lim_{k \rightarrow \infty} D^k(P^k)^{-1} = Q = \text{diag}(q_1, q_2, \dots, q_n)$$

For some  $q_i \in [-k_i, k_i]$ ,  $i = 1, \dots, n$ . We observe that the matrix sequence

$$\{M - AD^k(P^k)^{-1} - IA^\tau D^k(P^k)^{-1}\}$$

and the matrix  $\{M - AQ - IA^\tau Q\}$  all belong to the collection  $V$ . Hence, those matrices are nonsingular. Moreover, for all  $k$  sufficiently large, we have

$$\begin{aligned} \|(W^k)^{-1}\| &\leq \|(P^k)^{-1}\| \\ &\|(M - AD^k(P^k)^{-1} - IA^\tau D^k(P^k)^{-1})^{-1}\| \\ &\leq 2\|(M - AQ - IA^\tau Q)^{-1}\| \end{aligned}$$

This contradicts our assumption (6). Hence, there exists a constant  $\kappa > 0$  such that (5) holds. It then follows from Theorem 1 that  $F$  is a Homeomorphism from  $\mathfrak{R}^n$  onto itself.

The above homeomorphism result means that if each element in  $V$  is nonsingular, then the neural network defined by (1) has a unique equilibrium point for any input vector  $u \in \mathfrak{R}^n$ . This result is the starting point of the next two sections where we will consider what practical conditions make the delay neural network stable.

### 3. Existence and Uniqueness of the Equilibrium Point

In this section, based on Theorem 1 we present some new sufficient conditions which ensure the existence and uniqueness of the equilibrium point of (1). As consequences, we further show that the existence assumption on equilibrium point is unnecessary in some existing results for GAS.

**Theorem 2:** Suppose one of the following assumptions holds:

- 1)  $\rho(A + IA^\tau)KM^{-1} < 1$ ;
- 2)  $-(A + IA^\tau) \in P_0$  and each activation function is nondecreasing;

3)  $\mu_2(A+IA^\tau) < m/k$  and each activation function is nondecreasing;

Then for each input vector  $u \in \mathfrak{R}^n$ , the function  $F(\cdot)$  is a homeomorphism from  $\mathfrak{R}^n$  onto  $\mathfrak{R}^n$ .

**Proof:** 1) we first recall the facts that for any matrix  $B \in \mathfrak{R}^{n \times n}$ ,  $\rho(B) \leq \rho(|B|)$ . And that if two nonnegative matrices  $B, \tilde{B} \in \mathfrak{R}^{n \times n}$  satisfy  $B \leq \tilde{B}$ , then we have  $\rho(B) \leq \rho(\tilde{B})$ . It follows from Theorem 1 that we need only to show that each element in  $W$  is nonsingular.

Let  $W$  be an element in  $V$ , then there exist two diagonal matrices  $C = \text{diag}(c_1, c_2, \dots, c_n)$  and  $D = \text{diag}(d_1, d_2, \dots, d_n)$  with  $c_i \geq m_i$  and  $d_i \in [-k_i, k_i]$  for all  $i = 1, 2, \dots, n$  such that

$$W = C - AD - IA^\tau D$$

We have from the assumption i) of the theorem and the mathematical facts listed at the beginning of the proof that

$$\begin{aligned} \rho((A+IA^\tau)DC^{-1}) &\leq \rho(|A+IA^\tau| |D| C^{-1}) \\ &\leq \rho((A+IA^\tau)KM^{-1}) < 1 \end{aligned}$$

This means that the matrix  $I - (A+IA^\tau)DC^{-1}$  is nonsingular. Then the nonsingularity of  $W$  follows from the observation that

$$W^{-1} = C^{-1}(I - (A+IA^\tau)DC^{-1})^{-1}$$

For the remaining two cases, we need only to show that each element in  $V$  is nonsingular. We note the fact  $d_i \geq 0$  for all  $i = 1, \dots, n$  in defining  $\tilde{V}$ .

2) The proof is trivial by noticing the fact that for any three matrices  $B_1, B_2, Q$ , in  $\mathfrak{R}^{n \times n}$  with  $B_1$  being positive diagonal,  $B_2 \in P_0$  and  $Q$  a nonnegative diagonal matrix, then the matrix  $B_1 + B_2Q \in P$ , hence it is nonsingular. Any matrix we encountered in  $\tilde{W}$  has the same structure as of  $B_1 + B_2Q$  and therefore it is nonsingular.

3) As in 2), it suffices to show that any element  $W$  in  $\tilde{V}$  is nonsingular. Then there exist two diagonal matrices  $C = \text{diag}(c_1, c_2, \dots, c_n)$ ,  $D = \text{diag}(d_1, d_2, \dots, d_n)$  with  $c_i \geq m_i$  and  $d_i \in [0, k_i]$  for all  $i = 1, \dots, n$  such that  $W = C - AD - IA^\tau D$ . Since  $C$  is nonsingular, it suffices to show the matrix  $N = I - (A+IA^\tau)DC^{-1}$  is nonsingular. We prove it by a contradiction. Assume that  $N$  is singular, then there exists  $0 \neq x \in \mathfrak{R}^n$  such that  $Nx = 0$ , or equivalently

$$\left(\frac{m}{k}\right)(A+IA^\tau)DC^{-1}x = \left(\frac{m}{k}\right)x \tag{7}$$

Let  $Q = (m/k)DC^{-1} = \text{diag}(q_1, q_2, \dots, q_n)$ , then  $0 < q_i < 1$ , for all  $i = 1, 2, \dots, n$ .

Multiplying  $(Qx)^T$  on both sides of (7), we have

$$(Qx)^T(A+IA^\tau)Qx = \left(\frac{m}{k}\right)x^T Qx$$

which yields that

$$\begin{aligned} \frac{m}{k} \|Qx\|^2 &= \left(\frac{m}{k}\right)x^T Q^2 x \leq \left(\frac{m}{k}\right)x^T Qx \\ &\leq \mu_2(A+IA^\tau) \|Qx\|^2 \end{aligned}$$

That is

$$\left(\frac{m}{k} - \mu_2(A+IA^\tau)\right) \|Qx\|^2 \leq 0$$

Since  $Qx \neq 0$  (otherwise it would follow from (7) that  $x = 0$ ), we have

$$\frac{m}{k} \leq \mu_2(A+IA^\tau)$$

a contradiction to the assumption  $\mu_2(A+IA^\tau) < m/k$ .

Hence any element  $W \in \tilde{V}$  is nonsingular. This completes our proof.

### 4. New Conditions for GAS

In this section, we present new conditions for the GAS of the equilibrium point of (1). We assume that all the activation function are nondecreasing, i.e., the generalized Jacobian of  $F$  at any point  $x \in \mathfrak{R}^n$  is contained in  $\tilde{V}$ .

**Theorem 3:** In addition to assumptions (A1), (A2) and (A3), we assume that each activation function is nondecreasing. Suppose

$$2\mu_2(A+IA^\tau) + \|IA^\tau - I\|^2 < 2\left(\frac{m}{k}\right)$$

Then for each  $u \in \mathfrak{R}^n$ , (1) has a unique equilibrium point which is GAS.

In particular, the DCNN where  $m = k = 1$  has a unique equilibrium point for each input vector  $u \in \mathfrak{R}^n$  and this equilibrium point is GAS if the following condition holds:

$$2\mu_2(A+IA^\tau) + \|IA^\tau - I\|^2 < 2 \tag{8}$$

**Proof:** Since  $2\mu_2(A+IA^\tau) + \|IA^\tau - I\|^2 < 2(m/k)$ , we obviously have  $\mu_2(A+IA^\tau) < (m/k)$ . Then it follows from Theorem 2 3) that (1) has a unique equilibrium

point. Hence it remains to show that this equilibrium point, say  $x^*$ , is GAS. For simplicity, we shift  $x^*$  to this origin through the transformation

$$\begin{aligned} z(t) &= x(t) - x^* \\ z(t - \tau) &= x(t - \tau) - x^* \end{aligned}$$

Equation (1) then can be equivalently written as the following system

$$\dot{z}(t) = -(g(z(t) + x^*) - g(x^*)) + A\Phi(z(t)) + A^\tau\Psi(z(t - \tau)) \tag{9}$$

where  $z(\cdot) = (z_1(\cdot), z_2(\cdot), \dots, z_n(\cdot))^T$

$$\begin{aligned} \Phi(z(\cdot)) &= (\phi_1(z_1(\cdot)), \phi_2(z_2(\cdot)), \dots, \phi_n(z_n(\cdot)))^T \\ \Psi(z(\cdot)) &= (\varphi_1(z_1(\cdot)), \varphi_2(z_2(\cdot)), \dots, \varphi_n(z_n(\cdot)))^T \end{aligned}$$

and  $\phi_i(z_i(\cdot)) = f_i(z_i(\cdot) + x^*) - f_i(x^*)$

$$\varphi_i(z_i(\cdot)) = h_i(z_i(\cdot) + x^*) - h_i(x^*)$$

We now show that the origin is GAS of (9). It is easy to see  $\phi_i(0) = 0, \forall i = 1, 2, \dots, n.$  and

$$\begin{aligned} \|\Phi(z(\cdot))\|^2 &\leq kz^T(\cdot)\Phi(z(\cdot)) \\ \|\Psi(z(\cdot))\| &\leq l\|\Phi(z(\cdot))\| \end{aligned} \tag{10}$$

Let us consider the Lyapunov function:

$$\begin{aligned} V(z(t)) &= \|z(t)\|^2 + 2\alpha \sum_{i=1}^n \int_0^{z_i} \phi_i(s) ds \\ &\quad + \frac{1}{l^2}(\alpha + \beta) \sum_{i=1}^n \int_{t-\tau}^t \psi_i^2(z_i(\xi)) d\xi \end{aligned}$$

with  $\alpha, \beta > 0$  being chosen appropriately later on. We first point out that  $V(z(\cdot))$  is positive except at the origin, and it is radially unbounded in the sense that  $V(z(t)) \rightarrow \infty$  as  $\|z(t)\| \rightarrow \infty$ . Next, evaluating the time derivative of  $V(z)$  along the trajectories of (9), we obtain

$$\begin{aligned} \dot{V}(z(t)) &= 2z^T(t)\dot{z}(t) + 2\alpha\Phi^T(z(t))\dot{z}(t) \\ &\quad + \frac{1}{l^2}(\alpha + \beta)(\|\Psi(z(t))\|^2 - \|\Psi(z(t - \tau))\|^2) \\ &= -2z^T(t)(g(z(t) + x^*) - g(x^*)) \\ &\quad + 2z^T(t)A\Phi(z(t)) + 2z^T(t)A^\tau\Psi(z(t - \tau)) \\ &\quad - 2\alpha\Phi^T(z(t))(g(z(t) + x^*) - g(x^*)) \\ &\quad + 2\alpha\Phi^T(z(t))A\Phi(z(t)) \\ &\quad + 2\alpha\Phi^T(z(t))A^\tau\Psi(z(t - \tau)) \\ &\quad + \frac{1}{l^2}(\alpha + \beta)(\|\Psi(z(t))\|^2 - \|\Psi(z(t - \tau))\|^2) \end{aligned} \tag{11}$$

The Lebourg theorem for Lipschitz functions means that

$$g(z(t) + x^*) - g(x^*) = Dz(t) \tag{12}$$

for some  $D \in \cup_{y \in [x^*, x^* + z(t)]} \partial g(y)$

From the definition of  $g$ , matrix  $D$  is diagonal, and we denote  $D = \text{diag}(d_1, d_2, \dots, d_n)$ . It is obvious to see  $d_i \geq m$  for  $i = 1, 2, \dots, n$ . We then have

$$\begin{aligned} z^T(t)(g(z(t) + x^*) - g(x^*)) &= \sum_{i=1}^n d_i z_i^2(t) \geq m\|z(t)\|^2 \\ \Phi^T(z(t))(g(z(t) + x^*) - g(x^*)) &= \sum_{i=1}^n d_i \phi_i(z_i(t)) z_i(t) \\ &\geq mz^T(t)\Phi(z(t)) \geq \frac{m}{k}\|\Phi(z(t))\|^2 \end{aligned}$$

Putting those inequalities into (11) and using (10), we have

$$\begin{aligned} \dot{V}(z(t)) &\leq -2m\|z(t)\|^2 + 2z^T(t)A\Phi(z(t)) \\ &\quad + 2z^T(t)A^\tau\Psi(z(t - \tau)) - 2\alpha\frac{m}{k}\|\Phi(z(t))\|^2 \\ &\quad + 2\alpha\Phi^T(z(t))A\Phi(z(t)) + 2\alpha\Phi^T(z(t))A^\tau\Psi(z(t - \tau)) \\ &\quad + \frac{1}{l^2}(\alpha + \beta)(\|\Psi(z(t))\|^2 - \|\Psi(z(t - \tau))\|^2) \end{aligned} \tag{13}$$

Noticing that

$$\begin{aligned} &-m\|z(t)\|^2 + 2z^T(t)A\Phi(z(t)) \\ &= -\left\| \sqrt{m}z(t) - \frac{1}{\sqrt{m}}A\Phi(z(t)) \right\|^2 \\ &\quad + \frac{1}{m}\Phi^T(z(t))A^T A\Phi(z(t)) \\ &-m\|z(t)\|^2 + 2z^T(t)A^\tau\Psi(z(t - \tau)) \\ &= -\left\| \sqrt{m}z(t) - \frac{1}{\sqrt{m}}A^\tau\Psi(z(t - \tau)) \right\|^2 \\ &\quad + \frac{1}{m}\Psi^T(z(t - \tau))(A^\tau)^T A^\tau\Psi(z(t - \tau)) \\ &2\alpha\Phi^T(z(t))A^\tau\Psi(z(t - \tau)) + \frac{1}{l^2}\alpha\|\Psi(z(t - \tau))\|^2 \\ &= -\alpha\left\| \frac{1}{l}\Psi(z(t - \tau)) - l(A^\tau)^T\Phi(z(t)) \right\|^2 \\ &\quad + \alpha l^2\Phi^T(z(t))A^\tau(A^\tau)^T\Phi(z(t)) \end{aligned}$$

Rearranging terms in (19) and using above inequalities,

we obtain

$$\begin{aligned} \dot{V}(z(t)) &\leq \frac{1}{m} \Phi^T(z(t)) A^T A \Phi(z(t)) \\ &\quad + \frac{1}{m} \Psi^T(z(t-\tau)) (A^\tau)^T A^\tau \Psi(z(t-\tau)) \\ &\quad - 2\alpha \frac{m}{k} \|\Phi(z(t))\|^2 + 2\alpha \Phi^T(z(t)) A \Phi(z(t)) \\ &\quad + \alpha l^2 \Phi^T(z(t)) A^\tau (A^\tau)^T \Phi(z(t)) + \frac{1}{l^2} \alpha \|\Psi(z(t))\|^2 \\ &\quad + \frac{1}{l^2} \beta \|\Psi(z(t))\|^2 - \frac{1}{l^2} \beta \|\Psi(z(t-\tau))\|^2 \\ &\leq \frac{1}{m} \lambda_{\max}(A^T A) \|\Phi(z(t))\|^2 + \frac{1}{m} \lambda_{\max}((A^\tau)^T A^\tau) \cdot \\ &\quad \|\Psi(z(t-\tau))\|^2 - 2\alpha \frac{m}{k} \|\Phi(z(t))\|^2 \\ &\quad + 2\alpha \Phi^T(z(t)) A \Phi(z(t)) \\ &\quad + \alpha l^2 \Phi^T(z(t)) A^\tau (A^\tau)^T \Phi(z(t)) + \frac{1}{l^2} \alpha \|\Psi(z(t))\|^2 \\ &\quad + \frac{1}{l^2} \beta \|\Psi(z(t))\|^2 - \frac{1}{l^2} \beta \|\Psi(z(t-\tau))\|^2 \end{aligned}$$

Let  $\beta = (l^2/m) \lambda_{\max}((A^\tau)^T A^\tau)$ , we have

$$\begin{aligned} \dot{V}(z(t)) &\leq \frac{1}{m} (\lambda_{\max}(A^T A) \\ &\quad + l^2 \lambda_{\max}((A^\tau)^T A^\tau)) \|\Phi(z(t))\|^2 \\ &\quad - 2\alpha \frac{m}{k} \|\Phi(z(t))\|^2 + 2\alpha \Phi^T(z(t)) A \Phi(z(t)) \\ &\quad + \alpha l^2 \Phi^T(z(t)) A^\tau (A^\tau)^T \Phi(z(t)) + \frac{1}{l^2} \alpha \|\Psi(z(t))\|^2 \\ &\quad + 2\alpha \Phi^T(z(t)) (A^\tau)^T \Psi(z(t)) \\ &\quad - 2\alpha \Phi^T(z(t)) (A^\tau)^T \Psi(z(t)) - 2\alpha \Phi^T(z(t)) A \Phi(z(t)) \\ &\quad + \alpha l^2 \Phi^T(z(t)) A^\tau (A^\tau)^T \cdot \Phi(z(t)) + \frac{1}{l^2} \alpha \|\Psi(z(t))\|^2 \\ &\quad + \frac{1}{l^2} \beta \|\Psi(z(t))\|^2 - \frac{1}{l^2} \beta \|\Psi(z(t-\tau))\|^2 \end{aligned} \tag{14}$$

Using the fact that

$$\begin{aligned} &\alpha l^2 \Phi^T(z(t)) A^\tau (A^\tau)^T \Phi(z(t)) \\ &\quad - 2\alpha \Phi^T(z(t)) (A^\tau)^T \Psi(z(t)) \\ &= \alpha (l^2 \Phi^T(z(t)) A^\tau (A^\tau)^T \Phi(z(t)) \\ &\quad - 2\Phi^T(z(t)) (A^\tau)^T \Psi(z(t))) \\ &\leq \alpha \left\| l(A^\tau)^T \Phi(z(t)) - \Phi(z(t)) \right\|^2 - \frac{1}{l^2} \alpha \|\Psi(z(t))\|^2 \\ &\leq \alpha \left\| lA^\tau - I \right\|^2 \|\Phi(z(t))\|^2 - \frac{1}{l^2} \alpha \|\Psi(z(t))\|^2 \end{aligned}$$

We have from (14) that

$$\begin{aligned} \dot{V}(z(t)) &\leq \frac{1}{m} (\lambda_{\max}(A^T A) + l^2 \lambda_{\max}((A^\tau)^T A^\tau)) \cdot \\ &\quad \|\Phi(z(t))\|^2 - 2\alpha \frac{m}{k} \|\Phi(z(t))\|^2 - \alpha \left\| lA^\tau - I \right\|^2 \cdot \\ &\quad \|\Phi(z(t))\|^2 - \frac{1}{l^2} \alpha \|\Psi(z(t))\|^2 + \frac{1}{l^2} \alpha \|\Psi(z(t))\|^2 \\ &\quad + 2\alpha \Phi^T(z(t)) (A + A^\tau + lA + lA^\tau) \Phi(z(t)) \\ &\leq \frac{1}{m} (\lambda_{\max}(A^T A) + l^2 \lambda_{\max}((A^\tau)^T A^\tau)) \|\Phi(z(t))\|^2 \\ &\quad + 2\alpha \frac{m}{k} \|\Phi(z(t))\|^2 + 2\mu_2(A + lA^\tau) \|\Phi(z(t))\|^2 \\ &\quad + \alpha \left\| lA^\tau - I \right\|^2 \|\Phi(z(t))\|^2 \\ &\leq \frac{1}{m} (\lambda_{\max}(A^T A) + l^2 \lambda_{\max}((A^\tau)^T A^\tau)) \|\Phi(z(t))\|^2 \\ &\quad - \alpha (2\frac{m}{k} - 2\mu_2(A + lA^\tau) - \left\| lA^\tau - I \right\|^2) \|\Phi(z(t))\|^2 \end{aligned} \tag{15}$$

Now we consider the following three cases.

1)  $\Phi(z(t)) \neq 0$  and  $z(t) \neq 0$ . It then follows from (15)

and  $2\mu_2(A + lA^\tau) + \left\| lA^\tau - I \right\|^2 < 2(m/k)$  that the choice

$$\alpha > \frac{\lambda_{\max}(A^T A) + l^2 \lambda_{\max}((A^\tau)^T A^\tau)}{m(2\frac{m}{k} - 2\mu_2(A + lA^\tau) - \left\| lA^\tau - I \right\|^2)}$$

ensures that  $\dot{V}(z(t))$  is negative.

2)  $\Phi(z(t)) = 0$  but  $z(t) \neq 0$ . Then it follows from (13) that

$$\begin{aligned} \dot{V}(z(t)) &\leq -2m \|z(t)\|^2 + 2z^T(t) A^\tau \Psi(z(t-\tau)) \\ &\quad + \frac{1}{l^2} (\alpha + \beta) (\|\Psi(z(t))\|^2 - \|\Psi(z(t-\tau))\|^2) \\ &= -m \|z(t)\|^2 + 2z^T(t) A^\tau \Psi(z(t-\tau)) - m \|z(t)\|^2 \\ &\quad + \frac{1}{l^2} (\alpha + \beta) (\|\Psi(z(t))\|^2 - \|\Psi(z(t-\tau))\|^2) \\ &\leq \frac{1}{m} \Psi^T(z(t-\tau)) (A^\tau)^T A^\tau \Psi(z(t-\tau)) \\ &\quad + \frac{1}{l^2} (\alpha + \beta) (-\|\Psi(z(t-\tau))\|^2) + (\alpha + \beta) \|\Phi(z(t))\|^2 \\ &\leq -\frac{1}{l^2} (\alpha + \beta) - \frac{1}{m} \lambda_{\max}((A^\tau)^T A^\tau) \|\Psi(z(t-\tau))\|^2 \end{aligned}$$

We recall that  $\beta = (l^2/m) \lambda_{\max}((A^\tau)^T A^\tau)$ , which obviously implies  $\dot{V}(z(t)) < 0$  for this case.

3)  $z(t) = 0$ , clearly,  $\Phi(z(t)) = 0$  due the fact (10). In this case,  $\dot{V}(z(t))$  is given by

$$\begin{aligned} \dot{V}(z(t)) &= \frac{1}{l^2}(\alpha + \beta)(\|\Psi(z(t))\|^2 - \|\Psi(z(t - \tau))\|^2) \\ &\leq (\alpha + \beta)\|\Phi(z(t))\|^2 - \frac{1}{l^2}(\alpha + \beta)\|\Psi(z(t - \tau))\|^2 \\ &\leq -\frac{1}{l^2}(\alpha + \beta)\|\Psi(z(t - \tau))\|^2 \end{aligned}$$

Hence,  $\dot{V}(z(t))$  is negative if  $\Psi(z(t - \tau)) \neq 0$  and  $\dot{V}(z(t)) = 0$  if and only if it happens in the last case where

$$z(t) = \Phi(z(t)) = \Psi(z(t - \tau)) = 0$$

We recall that  $V(z(t))$  is radially unbounded. According to [12] or [13] that the origin of (9) or equivalently the equilibrium point  $x^*$  of (1) is GAS.

The sufficient conditions (8) for DCNNs are direct consequence of the general result proved above.

**Theorem 4:** In addition to assumptions (A1), (A2) and (A3), we assume that all the activation  $f_i$  and  $h_i$  are nondecreasing. Suppose that there exists a positive diagonal matrix  $P = \text{diag}(p_1, p_2, \dots, p_n)$  such that the matrix

$$PA + A^T P + l^2(PA^\tau)(PA^\tau)^T - 2MK^{-1}P + I \quad (16)$$

is negative definite. Then for each  $u \in \mathfrak{R}^n$ , (1) has a unique equilibrium point which is GAS.

**Proof:** We first prove the existence and uniqueness of the equilibrium point by using Theorem 1.

Let  $C = \text{diag}(c_1, c_2, \dots, c_n)$  be a diagonal matrix with  $c_i \geq m_i$  for all  $i = 1, 2, \dots, n$ . Since both  $K$  and  $P$  are diagonally positive, the negative definiteness of the matrix in (16) implies that the matrix

$$PA + A^T P + l^2(PA^\tau)(PA^\tau)^T - 2CK^{-1}P + I$$

is also negative definite. By using positive semi definiteness of the matrix  $XX^T + I - (X + X^T)$ , we have that the matrix

$$PA + A^T P + l^2(PA^\tau + (PA^\tau)^T) - 2CK^{-1}P \quad (17)$$

is negative definite. In the other word, the matrix  $-(A + lA^\tau - CK^{-1})$  is Lyapunov diagonally stable under (16). Consequently, it is a  $P$  matrix. Then it follows from [9] that for any diagonal matrix  $D$  such that  $0 \leq D \leq K$ ,  $\det(C - (A + lA^\tau)D) \neq 0$ ; that is, the matrix  $C - (A + lA^\tau)D$  is nonsingular for the above choice of  $C$  and  $D$ . This fact in turn means that any element in  $V$  is nonsingular. Now the existence and uniqueness of the equilibrium point follows from Theorem 1.

Next we prove the GAS of the equilibrium point, say

$x^*$ , of (1). Through the transformation as in the proof of Theorem 3, we consider the GAS of the system (9) at the origin. Define a Lyapunov function as [10] follows:

$$\begin{aligned} V(z(t)) &= \|z(t)\|^2 + 2\alpha \sum_{i=1}^n p_i \int_0^{z_i} \varphi_i(s) ds \\ &\quad + (\alpha + \beta) \sum_{i=1}^n \int_{t-\tau}^t \varphi_i^2(z_i(\xi)) d\xi \end{aligned}$$

with  $\alpha, \beta > 0$ , being selected later on. It is easy to see that  $V(z(\cdot))$  is positive except at the origin and it is radially unbounded. Evaluating its time derivative along the trajectory of (9), we obtain that

$$\begin{aligned} \dot{V}(z(t)) &= -2z^T(t)(g(z(t) + x^*) - g(x^*)) \\ &\quad + 2z^T(t)A\Phi(z(t)) + 2z^T(t)A^\tau\Psi(z(t)) \\ &\quad - 2\alpha\Phi^T(z(t))P(g(z(t) + x^*) \\ &\quad + 2\alpha\Phi^T(z(t))PA\Phi(z(t)) \\ &\quad + 2\alpha\Phi^T(z(t))PA^\tau\Psi(z(t - \tau)) \\ &\quad + \frac{1}{l^2}(\alpha + \beta)(\|\Psi(z(t))\|^2 - \|\Psi(z(t - \tau))\|^2) \end{aligned}$$

Using the Lebourg theorem of (12) and as of deriving (13), we obtain

$$\begin{aligned} \dot{V}(z(t)) &= -2m\|z(t)\|^2 + 2z^T(t)A\Phi(z(t)) \\ &\quad + 2z^T(t)A^\tau\Psi(z(t)) - 2\alpha\Phi^T(z(t))PMK^{-1}\Phi(z(t)) \\ &\quad + 2\alpha\Phi^T(z(t))PA\Phi(z(t)) \\ &\quad + 2\alpha\Phi^T(z(t))PA^\tau\Psi(z(t - \tau)) \\ &\quad + \frac{1}{l^2}(\alpha + \beta)(\|\Psi(z(t))\|^2 - \|\Psi(z(t - \tau))\|^2) \end{aligned}$$

Let  $\beta = (l^2/m)\lambda_{\max}((A^\tau)^T A^\tau)$ , we obtain similarly as of (22) that

$$\begin{aligned} \dot{V}(z(t)) &= \frac{1}{m}(\lambda_{\max}((A)^T A + l^2\lambda_{\max}((A^\tau)^T A^\tau)) \\ &\quad \times \|z(t)\|^2 + 2\alpha\Phi^T(z(t))PA\Phi(z(t)) \\ &\quad - \alpha\Phi^T(z(t))(2PMK^{-1} - I)\Phi(z(t)) \\ &\quad + \alpha l^2\Phi^T(z(t))PA^\tau(PA^\tau)^T\Phi(z(t)) \\ &= \frac{1}{m}(\lambda_{\max}((A)^T A + l^2\lambda_{\max}((A^\tau)^T A^\tau)) \times \|z(t)\|^2 \\ &\quad + \alpha\Phi^T(z(t))(PA + A^T P + l^2PA^\tau(PA^\tau)^T \\ &\quad - 2PMK^{-1} + I)\Phi(z(t)) \end{aligned}$$

Since the matrix in (16) is assumed to be negative definite, we can prove that the origin is GAS of (9) by following the very similar way of 1)–3) in the last part of the proof of Theorem 3. This accomplishes our proof.

### 5. Illustrative Examples

**Example 1:** Consider the following model:

$$\begin{cases} \dot{x}_1(t) = -g(x_1(t)) + Af(x_1(t)) + A^\tau h(x_1(t-\tau)) + u_1 \\ \dot{x}_2(t) = -g(x_2(t)) + Af(x_2(t)) + A^\tau h(x_2(t-\tau)) + u_2 \\ \dot{x}_3(t) = -g(x_3(t)) + Af(x_3(t)) + A^\tau h(x_3(t-\tau)) + u_3 \end{cases}$$

where  $g(x) = 0.3x$ ,  $f(x) = 0.2x$ ,  $h(x) = 0.1(x - \sin x)$ , obviously,  $g(x), f(x), h(x)$  satisfied the assumption (A1), (A2) and (A3), we obtain

$$m = 0.3, \quad k = 0.2, \quad l = 0.1$$

Let 
$$A = \begin{bmatrix} 0.2 & -0.1 & 0 \\ 0.1 & 0.3 & -0.2 \\ -0.2 & 0.1 & 0.2 \end{bmatrix}$$

$$A^\tau = \begin{bmatrix} 0.1 & 1 & 0.2 \\ -0.1 & 0.2 & 0.1 \\ 0.2 & -0.1 & 0.4 \end{bmatrix} \quad u = \begin{bmatrix} 0.1 \\ 0.2 \\ 0.1 \end{bmatrix}$$

It is easy to check that the model satisfied the condition of Theorem 3. Using the Matlab, we have made graphics of the solution as the time in the system with initial conditions  $[-0.5 \ 0.6 \ -0.8]$  and the delay  $\tau = 0$ , as follow: (**Figure 1**)

From the figure, we can easily see the system has a unique equilibrium point, and is GAS.

**Example 2:** In order to demonstrate the validity of our criterion of the Theorem 4, we consider a delayed neural network in (5) with parameters as

$$A = \begin{bmatrix} 0.2 & 0.1 \\ -0.1 & 0.2 \end{bmatrix} \quad A^\tau = \begin{bmatrix} 0.4 & 0.1 \\ 0.5 & 0.5 \end{bmatrix} \quad u = \begin{bmatrix} 1 \\ 0.5 \end{bmatrix}$$

$$g(x) = \begin{pmatrix} 0.2x_1 \\ 0.1x_2 \end{pmatrix} \quad f(x) = \begin{pmatrix} 0.4x_1 \\ 0.4x_2 \end{pmatrix}$$

$$h_j(x_j) = \begin{pmatrix} 0.2(x_1 - \sin x_1) \\ 0.2(x_2 - \sin x_2) \end{pmatrix}$$

obviously, (A1), (A2) and (A3) hold.

$$M = \begin{bmatrix} 0.2 & 0 \\ 0 & 0.1 \end{bmatrix} \quad K = \begin{bmatrix} 0.4 & 0 \\ 0 & 0.4 \end{bmatrix} \quad l = 0.1$$

Using the Matlab LMI toolbox, we prove that the ma-

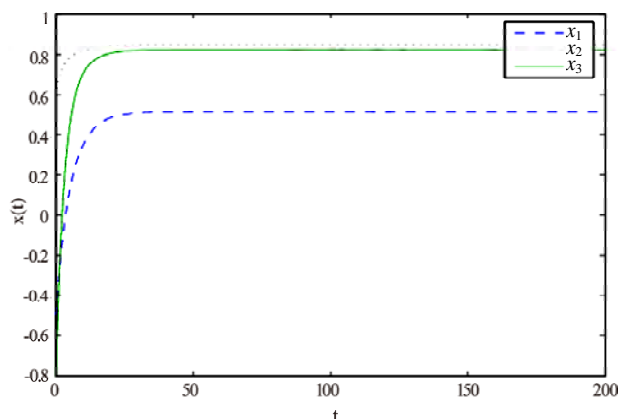


**Figure 1.** State trajectories of  $x_1, x_2, x_3$ .

trix inequality (17) is feasible. Also, we obtain the matrix

$$P = \begin{bmatrix} 1.169 & 0.000 \\ 0.000 & 1.2765 \end{bmatrix}$$

### 6. Conclusions

In this paper, we present new conditions for the existence, uniqueness, and GAS of the equilibrium point of DNNs. Our study is based on a thorough nonsmooth analysis on functions defining DNNs. The general Theorem 1 on existence and uniqueness of the equilibrium point is proved easy to apply. This general result, allows us to study sufficient conditions for GAS in which the spectral properties of the matrix  $(A + lA^\tau)$  play an important role. Advantages of our results are illustrated by examples and also given a graph of the GAS. It would be very interesting to see how our approach can be used to study conditions which do not enjoy symmetric properties.

### 7. References

- [1] S. Arik, "An improved global stability result for delayed cellular neural networks," *IEEE Transactions on Circuits and Systems Part I*, Vol. 49, pp. 1211–1214, 2002.
- [2] T. L. Liao and F. C. Wang, "Global stability for cellular neural networks with time delay," *IEEE Transactions on Neural Networks*, Vol. 11, pp. 1481–1484, 2000.
- [3] Q. Zhang, X. Wei, and J. Xu, "Global asymptotic stability analysis of neural networks with time-varying delays," *Neural Processing Letters*, Vol. 21, pp. 61–71, 2005.
- [4] Q. Zhang, X. Wei, and J. Xu, "Global asymptotic stability of cellular neural networks with infinite delay," *Neural Network World*, Vol. 15, pp. 579–589, 2005.
- [5] Q. Zhang, X. Wei, and J. Xu, "Stability analysis for cellular neural networks with variable delays," *Chaos, Solitons Fractals*, Vol. 28, pp. 331–336, 2006.

- [6] R. A. Horn and C. A. Johnson, "Matrix analysis," U. K. Cambridge University Press, Cambridge, 1985.
- [7] R. T. Rockafellar and R. J. B. Wets, "Variational analysis," Springer-Verlag, Berlin Heidelberg, Germany, 1998.
- [8] F. H. Clarke, "Optimization and nonsmooth analysis," Wiley, New York, 1983.
- [9] B. H. Pourciau, "Hadamard theorem for locally Lipschitzian maps," *Journal of Mathematical Analysis and Applications*, Vol. 85, pp. 279–285, 1982.
- [10] A. L. Dontchev, H.-D. Qi, and L. Qi, "Convergence of Newton's method for convex best interpolation," *Numerical Mathematik*, Vol. 87, pp. 435–456, 2001.
- [11] L. Qi and J. Sun, "A nonsmooth version of Newton's method," *Mathematical Programming*, Vol. 58, pp. 353–367, 1993.
- [12] H. K. Khalil, "Nonlinear systems," Macmillan, New York, 1988.
- [13] R. M. Lewis and B. O. Anderson, "Intensitivity of a class of nonlinear compartmental systems to the introduction of arbitrary time delays," *IEEE Transactions on Circuits and Systems Part I*, Vol. CAS-27, pp. 604–612, 1980.

# Self-Organized Detection of Relationships in a Network

**Qurban A. Memon**

*EE Department, College of Engineering, UAE University, Al Ain, UAE*

*Email: qurban.memon@uaeu.ac.ae*

*Received December 20, 2009; revised January 24, 2010; accepted February 26, 2010*

## Abstract

Multistate operations within a network result in high-dimensional, multivariate temporal data, and are useful for systems, which monitor access to network entities like resources, objects, etc. Efficient self organization of such multi-state network operations stored in databases with respect to relationships amongst users or between a user and a data object is an important and a challenging problem. In this work, a layer is proposed where discovered relationship patterns amongst users are classified as clusters. This information along with attributes of involved users is used to monitor and extract existing and growing relationships. The correlation is used to help generate alerts in advance due to internal user-object interactions or collaboration of internal as well as external entities. Using an experimental setup, the evolving relationships are monitored, and clustered in the database.

**Keywords:** Relationship Network, Network Access, Self-Organization in Networks, Relationship Clustering

## 1. Introduction

Communication started to grow due to several factors in nineties, firstly, due to privatization and deregulation; secondly, due to penetration of mobile phones into the society; thirdly due to emergence of wavelength division multiplexing; and fourthly due to private companies entering into Internet business [1]. This growth has been hit by Internet bubble burst that took place during 2001 to 2002. As recovery in telecommunication industry has recently been witnessed, a new paradigm of ubiquitous networking has emerged that is expected to change the scene of computing. This concept is creating new network topologies and relationship networks.

The network of the future can also be visualized as we see the industry transitions today like from static markets to dynamic fast-paced innovations; low speed to high speed; divergence to convergence; local to global; fixed to mobile; sometimes to always-on; one medium to multimedia; and from distinct to bundled etc. [2]. The intelligence is moving from centers to edges, where key technology developers are surfacing in the area of tagging-things, sensors, smart technologies, and nano-structures. The edges of the market include users, devices at user level and the applications riding on them. The growth of such technologies is going to affect the business and the ways of doing businesses.

The ubiquitous networking, tagging, nano-structures, etc. is also enriching the concept of mobile networking.

A mobile ad hoc network (MANET) [3] provides a communication environment that is characterized by dynamic changes in the topology and in the availability of resources. In chaining partnerships and collaborations within this environment, various access control models have been proposed. The Enterprise Dynamic Access Control (EDAC) model [4] is based on basic principles of role based access control (RBAC) published by National Institute of Standards and Technology (NIST) [5], and accommodates complex and scalable access control situations with pre-configured conditions. The model criterion for resource access is based on user characteristics and environmental factors. As collaborations among the participants of an ad hoc network cannot be set up, therefore there is a need for explicit specification of policies for each activity. This accounts only for relationships set within an access control model; but it is natural that users, computing nodes and devices do communicate with other users or objects in a user space or outside their specified domain occasionally and continually.

Thus, new concepts in networking and corresponding access technologies have triggered a great interest in study of possible new forms of relationships in networks. Typical applications include network access detection, frequency of use of each resource, tracking use of resources, user relationships, etc.

In order to model evolving relationships and build relationship clusters from such databases, neural networks can be investigated as they have been reported to be

flexible, fault tolerant, robust, and can solve difficult problems [6]. The learning/training features of neural networks in absence of a supervisory role may be used to model relationship clusters. Unsupervised learning in the neural network helps in finding energy minima and is therefore more efficient with pattern association. Obviously, the disadvantage is that it is then up to the user to interpret the output.

The Self-Organizing Map (SOM) with its related extensions has been the most popular artificial neural algorithm for use in unsupervised learning and data visualization. There are quite a few types of self-organizing networks, like the Instar-Outstar network, the ART-series, and the Kohonen network [7]. The Kohonen network is probably the best example, because it is quite simple and introduces the concepts of self-organization and unsupervised training easily. It provides an ordered display of data to facilitate understanding of the structures in the data and illustrates clustered density in the input space case temporally and sequentially.

In the next section, the related research works found in the literature regarding detection of network accesses are highlighted.

## 2. Related Work

A lot of research work has recently been reported in the area of access control in network operations of field units. The primary target has been detection of intrusions in the form of events and development of computer audit data. In [8], the authors present studies for detecting intrusions into the information system, using frequency property of multiple audit event types for a given sequence of events. In another work [9], the authors present an algorithm for monitoring of frequent items in a distributed data stream environment, with advantages claimed as reduced communication cost and overall quality of output. The human signatures have also been investigated in [10] for intrusion detection. The respective authors consider signature based detection techniques and investigate the ability of various routing protocols to facilitate intrusion detection when attackers are completely known. In the research works [8–9] stated above, the main idea has been to identify the relationship in the form of intrusion after it has taken place.

The authors in [11] present a survey on the state of the art work in intrusion detection in mobile ad hoc network and conclude that schemes that would be distributed and collaborative are more likely to succeed in intrusion detection. In a similar work [12], the authors investigate the placement of modules for misuse detection in ad hoc networks and propose a family of algorithms that approximate the optimal solution, with resource consumption tradeoffs. The Dempster-Shafer theory has also been investigated in [13] in the context of intrusion detection

in networks and respective authors discuss its usefulness in distributed networked environment. In the research works [11–13], the main target has been the distributed environment and the placement of sniffers in order to monitor the data for subsequent analysis.

Regarding data classification and self-organization, a lot of research has been reported in open literature, and many commercial projects employ the SOM as the tool for solving hard real-world problems [14–15]. The authors in [16] suggest a method for clustering time varying data by using self-organizing maps, by introducing dissimilarity measures for capturing the temporal structure of the data in a simple topology preserving model. In another work [17], a temporal extension of the Self-Organizing Map (SOM) is presented by authors, where the network learns local representations of the temporal context associated with a time series, and extends classical properties of SOM to time. The authors in [18] discuss self-organizing models that provide valuable tools for data mining, clustering and visualization. In that, they extend basic vector-based models by recursive computation to process sequential and tree-structured data directly.

In [19], the authors present an approach to build an associative classifier composing consistent rules, and have shown the effectiveness of such classifiers over traditional classifiers in several datasets. The clustering within an application other than network has also been investigated in [20], where the authors discuss knowledge discovery (in melanomas domain) using combination of clustering and generalization to identify groups and build general descriptions of respective clusters.

In summary, many approaches were found in literature for detection of network access (either online or offline), but objectives set for such works were either intrusion detection or subsequent analysis for audit purposes. In this work, the study and analysis of evolving relationships formed during multi-state operations within a network is the main focus.

The Section 3 discusses modeling of relationships and the proposed scheme. In Section 4, experimental setup is discussed to implement the proposed algorithm. For purposes of simplicity and training, the Kohonen network is embedded in the model for developing classification and identifying evolving relationships in a network. The Section 5 presents comparative discussions followed by conclusions in Section 6.

## 3. Proposed Approach

In order to understand relation between participating devices or nodes, it is desirable that a mathematical relation among features or attributes of participating nodes or devices be defined. Let  $X$  be a set of features, and  $R$  be a relation. Then  $x R y$  iff  $x$  and  $y$  satisfy following conditions [21]:

Reflectivity:

$$(\forall x \in X) (x R x) \tag{1}$$

Symmetry:

$$(\forall x, y \in X) (\text{if } x R y, \text{ then } y R x) \tag{2}$$

Transitivity:

$$(\forall x, y \in X) (\text{if } x R y \wedge y R z, \text{ then } x R z) \tag{3}$$

Therefore,  $R$  is called an equivalence on  $X$  iff  $R$  obeys reflectivity, symmetry, and transitivity. In other words, the features of nodes and devices stored in databases may have relation if they satisfy reflectivity, symmetry, and transitivity. Further, equivalence clause of an element may be defined as follows [13]:

$$a \in X, [a] \stackrel{\Delta}{=} \{x \in X \mid x R a\} \tag{4}$$

Properties of Relation  $R$ :

Let  $R$  be an equivalence relation on  $X$ , such that:

$$1) \quad \forall a, b \in X (\text{if } a R b, \text{ then } [a] \cap [b] = \varnothing) \tag{5}$$

$$2) \quad \forall a, b \in X (\text{if } a R b, \text{ iff } [a] = [b]) \tag{6}$$

$$3) \quad X = \bigcup_{i=2}^n [a_i], \tag{7}$$

where  $[a_i]$  and  $[a_j]$  are pair wise disjoint subsets of  $X$ . We can narrate here an example of relation  $R$  on modular arithmetic as follows:

Consider  $X = Z$ , where  $x, y \in Z; n \in N$  (and is fixed),  $n > 1$ . If

$$x R y \text{ iff } n \mid (x - y) \text{ i.e., } n \text{ divides } (x - y) \tag{8}$$

then  $R$  is reflective, symmetric, and transitive. This relationship is examined further in the next section, once sample user activities in the form of attributes of each node are considered for relationship detection.

### 3.1. Relationship Network

Relationship network analysis concerns itself with measuring of relationships and flows among different measurements of attributes [22]. Once a database containing attributes or features of participating devices is developed, relations among attributes can be developed. Thus, it is possible to model such an analysis as a relationship network, as each individual activity measurement of the device is an entity and their interactions or interactions between users and data objects imply relationships and flows. Such relationship networks can provide a mathematical analysis of relationships in an expert system, yet visual representations are often easier to comprehend.

The relationship network can be modelled as a graph, consisting of a set of nodes and edges, where each node represents a device or a data object and an edge repre-

sents a relationship between a pair of such entities, as shown in **Figure 1**. The **Figure 1** represents network relationship among six entities ( $p_1, p_2, \dots, p_6$ ) within a network. Some of them are derived from others, in that some relationships are prerequisite to others which may further be termed as consequence. The connection between any two entities is weighted, and the weighted link may be termed as an edge of the relationship. The edge can be strong or weak depending on the value of corresponding weight. Once this strength is correlated with a threshold, it may be defined as: the higher the value of this weight, the stronger the link and hence stronger the relationship.

Based on correlation, the relationships can be exploited to develop clusters of similar and close attributes. The correlations may further be used to generate triggers or alerts once new instances of relationships are sensed and correlated with these clusters. The question that needs to be addressed is how such a relation is to be inferred and how many such instances are needed for ensuring confidence that a stronger relationship has occurred between users or between a user and a data object. In the following section, this is further investigated.

### 3.2. Modeling Relationship in a Network

Modeling or discovering a new relationship has been an open problem. Generally, a threshold is deemed necessary to trigger an alert before new relationship amongst users or between a user and a data object affects the system. In order to understand this, consider the example of an intrusion detection system where port scan, buffer overflow are considered as attacks and corresponding messages from intrusion detection system are called as alerts. An alert correlation system with a known model database, which uses the correlation technique based on a-priori knowledge, clusters the alerts that act as a pattern defined in the model database. The matching threshold is used to generate an alert. Let us classify this alert typically as Orange\_alert ( $O\_alert$ ). This type of modeling may be illustrated as shown in **Figure 2**.

Since the models in the database are limited to known patterns, hence the new pattern of relationship is different from a-priori knowledge based alert correlation. The

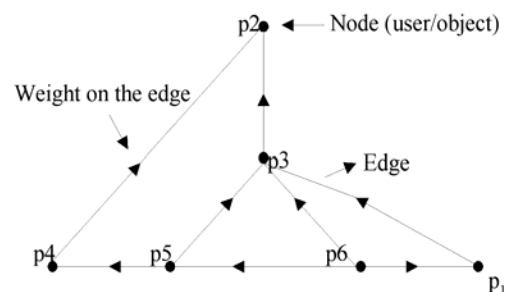


Figure 1. A simple relationship network.

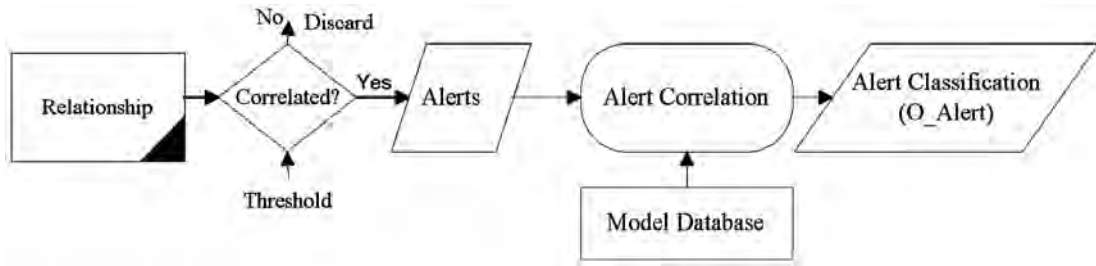


Figure 2. Alert correlation based on known patterns.

alerts based on discovery of new relationships can help to solve this problem. For this, the strength and rising process of the new relationship may be used to define the threshold for triggering the tolerance mechanism of the Relationship Detection System (RDS). This seems rationale as the rising process of achieving new strengths in relationships on the network increases the vulnerability of the targeted system.

In order to model this rising process of achieving new strength in relationship, consider a node/device which is trying to access an object in a network. The capability of the developing relationship may be described as a six-tuple, as follows:

$$Capability = \{src, trgt, actn, srvc, prprty, crdnrls\} \quad (9)$$

where capability describes the initiator (source  $\sim src$ ) of the relationship to perform an action ( $\sim actn$ ) on the property ( $\sim prprty$ ) of the service ( $\sim srvc$ ) with given credentials ( $\sim crdnrls$ ) on the target ( $\sim trgt$ ) destination. In order to illustrate this, a state transition diagram can be used where edges are new relationships and nodes are new capabilities. This is shown in **Figure 3**, where  $C_0$  is the initial capability state. After a relationship  $R_i$  is formed, a new strength  $S_i$  is achieved. Looking at **Figure 3** as an example, the union of  $C_1$ ,  $C_2$  and  $C_3$  is the pre-requisite to new relationship  $R_4$ . After  $R_4$  is formed, a new strength is achieved and reaches capability state  $C_4$ . Thus, a capability state has a prerequisite before a new relationship can be formed. This gives rise to new relationships and capability states. Thus, this may form a chain of relationships, one derived from the preceding one and so on, in a temporal fashion.

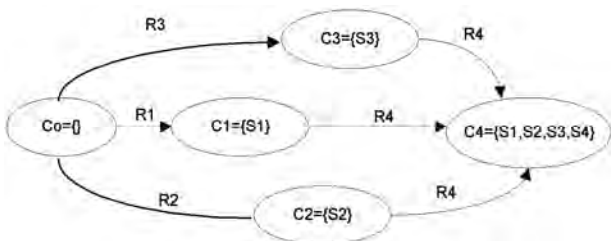


Figure 3. State transition based on new relationships and strengths.

To understand this further, an example of an unauthorized file access may be phrased as: getting knowledge of the service  $\rightarrow$  port of the address  $\rightarrow$  getting the root access  $\rightarrow$  installing the components to access the file  $\rightarrow$  get the file. There is a logical relationship between two capability states. For example, if  $C_0 = \{src, trgt, sniff, address, content, Anne\}$  and  $C_1 = \{src, trgt, sniff, all addresses, content, [Anne, Bill]\}$ , this means  $C_0$  can be logically inferred from  $C_1$ .

It can be inferred that every relationship is related to two capability states: one is prerequisite state providing the necessary strength for a new relationship, and the other the consequence state, which includes the new achieved strengths. This, in turn, raises a new concept of an alert which embeds existing alert level, prerequisite state and the consequence state. This new alert may be classified as Yellow alert (Y\_Alert), and defined as a three-tuple:

$$Y\_Alert (YA) = (Alert, Prerequisite, Consequence) \quad (10)$$

where *Alert* is a four-tuple message from RDS and it carries four information components: *name*, *time*, *source*, *target*. The *name* is name of the relationship that triggers this alert, *time* = (*begin*, *end*) of the relationship, *source* and *target* are net addresses of the relationship entities; *Prerequisite* includes prerequisite capability of the alert, and *Consequence* is the current capability state after alert is finished. To find new relationship patterns, alerts are transformed into Y\_Alerts, then correlated into a new relationship incident to uncover logic relations. The Y\_Alerts can be listed along with their capabilities states and corresponding timing ranges. This helps in correlating Y\_Alerts with Meta-Relationship (R), and thus new relationships can be discovered and ultimately stored in the database. This Meta-relationship triggers another level alert, say Red\_Alert (RA), and is defined as a three-tuple:

$$R\_Alert 'RA' = \{set\_R, set\_C, Time\} \quad (11)$$

where *set\_R* is the set of correlated Y\_Alert, *set\_C* is the set of the capabilities of all consequences of the Y\_alert, *Time* is *begin\_time* and *end\_time* of these Y\_Alerts. Meta relationship R resulting in R\_Alert can be easily proved that it is a partial relationship. For this, it can be

easily seen that they do not follow Equation (1) and (2). For reflectivity, it can be easily verified that  $\text{end\_time of } YA_1 > \text{begin\_time of } YA_2$  and the reverse is not true, if  $YA_1 \in R$ . For symmetry, it is also easy to see that  $YA_2$  is derived from the other  $YA_1$  and the converse is not true.

Based on these Y\_Alerts and Meta-relationship “R”, an experimental model for alert correlation and generating Red Alert ‘RA’ is depicted as shown in **Figure 4**. The **Figure 4** shows a self-evolving model for relationship correlation and detection. The alerts are correlated and the ones which exist in the database are reported as existing relationship incidence. This step reduces a greater number of alerts for modeling of relationships in the network. In the second step, the isolated alerts are correlated with Meta-relationship ‘R’. If correlated, the Meta-relationship is reported as R\_Alert and termed as a new relationship. After that, it is described in the database. The setup illustrated in **Figure 4** may be summarized in an algorithm as follows:

**Relationship Detection Algorithm:** After an alert is sensed, the following sequence of events takes place:

1) If there is an existing Red\_Alert ‘RA’, whose set\_C contains consequence of new YA, go to step “g”, else go to step “b”.

2) If prerequisite of ‘YA’ is empty go to step “e”, else go to step “c”.

3) If there is a Red\_Alert ‘RA’ and union of capability of RA’s set\_C implies prerequisite of ‘YA’, go to step “e”, else go to step “d”.

4) If there are some meta-relationships existing and the union of the set\_C of these meta-attacks implies the prerequisite of YA, then combine these meta-relationship to a new Red\_Alert RA, go to step “e”, else go to step “f”.

5) If the union of set\_C of the newly combined meta-relationship ‘R’ implies consequence of YA, go to step “g”, else go to step “f”.

6) Let YA join the red\_alert ‘RA’, put YA into RA’s set\_R and let consequence of RA join set\_C, determine RA’s time stamp. Break

7) Discard false alert YA; go to ‘a’ to deal with next yellow alert ‘YA’.

In the next section, an experimental setup is described to simulate the discovery and clustering of relationships developed in a local area network.

## 4. Experimental Setup

A typical local area network was selected with about five hundred and fifty user accounts. The accounts were grouped into five categories of access (i.e. credentials) on the network. These categories were ‘administration’, ‘faculty’, ‘student’, ‘staff’, and ‘public’. The actions supposed to be carried through these accounts during network access involved five different types of actions on twelve different target hosts or servers. The actions involved were ‘create’, ‘modify’, ‘read’, ‘delete’, and ‘not available/unauthorized’. The target hosts were centrally placed in a room. The service available on different target hosts contained files and programs. The objective was to examine the network setup vis-à-vis **Figure 4**, using the procedure outlined in the algorithm described in the previous section.

Based on this information, six-tuple data was generated using Equation (9) for any user access. A data mapping followed that converts these tuples to numerical values to train the network. The time stamp was added to make it to seven-tuple data to show evolution of the relationships during run time. These data values enable self-organizing feature of Kohonen network to allow data values to be mapped onto a two-dimensional plane with similar data residing in closer proximity.

The architecture of such a network can be reduced to two key issues: input layer and output layer [14]. The number of input nodes (say 7 based on source address, time stamp, target, service, property, action, credentials) equals the dimension of the input vector. The output layer processes the input data and gives an output. The number of output nodes determines the maximum number of

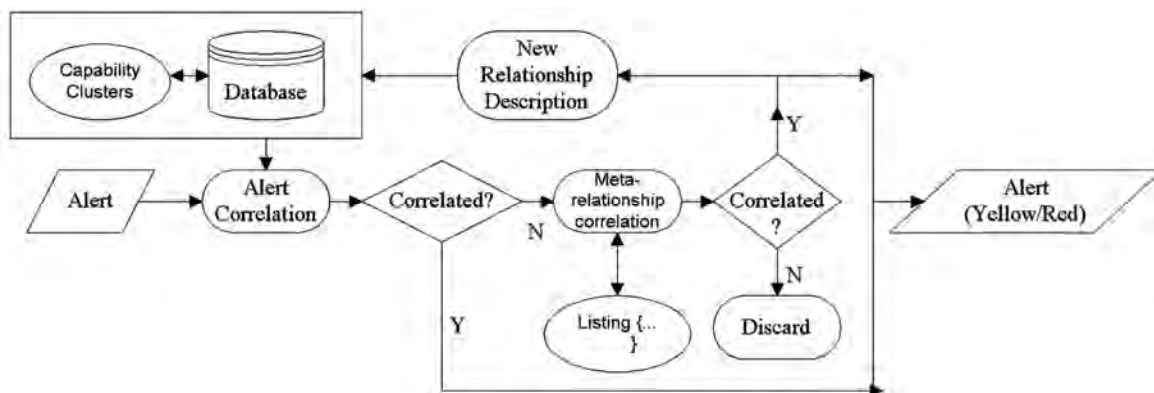


**Figure 4.** Relationship measurement & description model.

clusters to be found. Each neuron (node) in the output sheet has a location in the configuration and represents a cluster, or alternatively a set of common features.

The proposed system uses Kohonen Self Organizing Maps (SOM) to plot a matrix of the available data. This is a two dimensional plane containing 1024 cells (32x32 plot). The size of 32x32 clusters is arbitrary (although above than required number of clusters adequate for possible relationship clusters in a typical local area network) and has been selected only for experimental purposes.

Activity on the network was monitored for users on a full working day. The period of network activity for a typical user ranged from few minutes to less than seventy minutes. Out of five hundred and fifty user accounts, one hundred and eighty-five users accessed the network at different times. The mapped values for these users accumulated in a database were processed to train the SOM network to generate capability clusters.

Once built, the SOM takes the data from the database and decides the position of a user entity or the source of activity in the network based on the attributes attached to it. It contains  $32 \times 32$  output nodes along with input nodes, hence total of  $(7 \times 32 \times 32 \approx) 7168$  weights of the network were updated each time an input pattern (i.e., seven-tuple data) was presented for training. This process continued till convergence of its training algorithm. The algorithm used for training of the network typically undergoes the following steps [14]:

- Define input value range
- Present an input pattern (i.e., twenty data values)
- Compute distance between input and weight, and sum them
- Select the output node with minimum distance – this is the node that is closest to the input vector
- Alter weights for the closest node (and its neighbours) so that it is even nearer to the input vector.
- Go to step 2 until convergence is achieved.

Effectively, this training algorithm is very simple, following a familiar equation:

$$\Delta w_{ij} = k (x_i - w_{ij}) \quad (12)$$

where  $k$  is the learning coefficient,  $x$  is input pattern,  $w_{ij}$  is weight in two dimensions, and  $\Delta w_{ij}$  is the change in the weight. So all neurons in neighbourhood (say  $N$ ) to neuron  $x_{d0}$  (i.e., the one with minimum distance) have their weights adjusted. The adjustment of  $k$  and  $N$  is an area of much research, but Kohonen suggested splitting the training up into two phases. Phase 1 reduces down the learning coefficient from 0.9 to 0.1 (or similar values), and the neighbourhood reduces from half the diameter of the network down to the immediately surrounding cells ( $N = 1$ ). Following that, phase 2 reduces the learning coefficient from perhaps 0.1 to 0.0 but over double or more the number of iterations in phase 1. The

neighbourhood value is fixed at 1. It was seen that the two phases allow firstly the network to quickly ‘fill out the space’ with the second phase fine-tuning the network to a more accurate representation of the space. The resulting output diagram may be visualized showing clusters, evolving as time progresses. The examples of typical clusters include each user accessing the network, each object to be accessed on the network, each targeted host, each action, each service, and each credential of the user, etc.

This part of the experiment did not involve any correlation as there were previously, in fact no capability clusters present in the database. Rather, this activity filled up the database with relationship description, to the extent of entering second part of the activity where correlation is to be examined and database is to be enriched with new relationships. This part of the experiment is also considered equivalently as setting threshold for correlation.

For the second part of the experiment, the network was monitored for second and third day of the experiment. This enabled to see most of the users accessing the similar objects on the network, thus generating an alert. In this part of the experiment, a total of seventy (70) new users were identified, and thus relationships were described in the database, and clusters created onto the map.

A visualization application was added to the network (with the database) to enable analysis of emerging information from these activities, as access to the network evolves. The double click, for example on an object cluster shows data from the database, about how many users accessed it with respective credentials and actions with respect to time. Though, it was visualized in real time through alerts. In another example, a user access along with its credential was monitored in real time with a range of objects accessed on a particular host with respective actions. In each instance, respective alert generated was observed.

## 5. Comparative Discussion

The clustering approach proposed in this work is simple and addresses the objectives for real time notification of (registered) alerts and enriches the database with evolving relationships.

An important component of network policy in many commercial environments is separation of duty and monitoring of network traffic for network management purposes. Nowadays, many networks deploy policy based access to the network to implement separation of duty. The role based access control (RBAC) model [5] provides a conceptual framework for implementing a role based activity in a policy. However, it does not detect an evolving capability of the user growing beyond its legitimate strength or access limits. This weakness is

generally found in networks, when the status of a (private & secured) object on the network that is being accessed, modified or deleted by a user exceeding one's role. The approach in this work identifies the relationships while they are evolving or in other words the object contents are to be accessed. Such a weakness in the system deploying only RBAC may be addressed using the proposed approach by setting role of the respective account with objects on the targeted hosts. The threshold is set accordingly to generate alert. Thus, the system gets added capability.

In fact, the proposed model provides a self-adaptable approach to trigger the tolerance level of the system. The six-tuple capability data is user-defined and may replace source with an IP address by its role; or capability may even be increased beyond six-tuple by adding role of the user entity to existing six-tuple data. This tends to increase the number of clusters and in turn strengthens the correlation process of the system.

The other examples of undetected activities include access to the object by interaction of (internal or external) users, etc. This situation may be addressed using our approach, as described in Equation (10), and outlined in the algorithm. In other words, the evolving relationship between the user and the object is alerted during the correlation stage, earlier than it takes place.

The proposed approach is independent of many constraints. At a centralized place, it provides a real time discovery of evolving relationships amongst users or between users and network object. The proposed approach can also be easily embedded in distributed environments to trigger alerts before systems become vulnerable to attacks. In that case, a modification may be suggested such that the six-tuple capability data would be provided by distributed sniffers rather than a set of closely and fixed-placed sniffers.

There are many correlation algorithms available in the literature like [19,20], which may be used in conjunction with our proposed approach.

## 6. Conclusions and Future Work

The proposed model for detecting relationships is highly customizable as it is dependent on capability model which is user defined. The approach may be independently deployed or used in conjunction with existing approaches, for example, intrusion detection. The database evolves with time as new relationships are discovered and capabilities are formed as clusters. The detection of relationships may be done using network sensors or sniffers by reading the network packets. Two stages of correlation are performed; first one detects using cluster knowledge compared with capability of the entity; the second stage meta-correlation enables enriching of network database by identifying new relationships. As more

and more events are registered, lesser becomes the probability of finding new patterns of relationships and easier becomes the job of the network management.

As a future work, we intend to modify some parameters of the clustering: first we want to confirm the relevance of the pattern with role based access and set the threshold to initiation of possible new relationship; secondly we want to develop distributed monitoring of these relationships and observe frequency of such events to discover new associations within the data.

## 7. Acknowledgement

This work was financially supported by the Research Affairs at the UAE University under a contract no. 03-04-7-11/06.

## 8. References

- [1] T. Shinohara, "Ubiquitous network vision for new growth," ITU Telecom Report, 2003.
- [2] L. Srivastava, "The network of the future: What is over the horizon," Billing Asia 2006, Shanghai, China, 13 March 2006.
- [3] Y. Zhang and W. Lee, "An integrated environment for testing mobile ad-hoc networks," Proceedings of 3rd ACM Symposium on Mobile Ad Hoc Networking and Computing (MobiHoc), June 2002.
- [4] R. Fernandez, "Enterprise dynamic access control (EDA C) case study," CS1/06-0078 Project, United States Navy, March 2006.
- [5] National Institute of Standards and Technology-RBAC. <http://csrc.nist.gov/rbac/>.
- [6] D. Hammerstrom, "Neural networks at work," IEEE Spectrum, pp. 26–32, June 1993.
- [7] Aleksander, *et al.*, "An Introduction to neural computing," Chapman and Hall, 1990.
- [8] N. Ye, X. Li, Q. Chen, S. Emran, and M. Xu, "Probabilistic techniques for intrusion detection based on computer audit data," IEEE Transactions on Systems, Man, and Cybernetics-Part A: Systems and Humans, Vol. 31, No. 4, pp. 266–274, 2001.
- [9] R. Fuller and M. Kantardzic, "Distributed monitoring of frequent items," Transactions on Machine Learning and Data Mining, Vol. 1, No. 2, pp. 67–82, 2008.
- [10] F. Anjum, D. Subhadrabandhu, and S. Sarkar, "Signature based intrusion detection for wireless ad hoc networks: A comparative study of various routing protocols," IEEE Vehicular Technology Conference, Orlando, FL, Vol. 58, pp. 2152–2156, 6–9 October 2003.
- [11] A. Mishra, K. Nadkarni, and A. Patcha, "Intrusion detection in wireless ad hoc networks," IEEE Wireless Communications, pp. 48–60, February 2004.

- [12] D. Subhadrabandhu, S. Sarkar, and F. Anjum, "Efficacy of misuse detection in ad hoc networks," Proceedings of the Annual IEEE Communications Society Conference on Sensor and Ad Hoc Communications and Networks, pp. 97–107, 2004.
- [13] T. Chen and V. Venkataramanan, "Dempster-Shafer theory for intrusion detection in ad hoc networks," IEEE Internet Computing, pp. 35–41, December 2005.
- [14] T. Otto, A. Meyer-Baese, M. Hurdal, D. Sumners, D. Auer, and A. Wismuller, "Model-free functional MRI analysis using cluster-based methods," Proceedings of SPIE, Vol. 5103, pp. 17–24, August 2003.
- [15] S. Przylucki, W. Wojcik, K. Plachecki, and T. Golec, "An analysis of self-organization process for data classification in multisensor systems," Proceedings of SPIE, Vol. 5124, pp. 325–332, September 2003.
- [16] P. D'Urso and L. Giovanni, "Temporal self-organizing maps for telecommunications market segmentation," Neurocomputing, Vol. 71, pp. 2880–2892, 2008.
- [17] T. Voegtlin and P. Dominey, "Recursive self-organizing maps," Neural Networks, Vol. 15, No. 8–9, pp. 979–991, 2002.
- [18] B. Hammer, A. Micheli, A. Sperduti, and M. Strickert, "Recursive self-organizing network models," Neural Networks, Vol. 17, No. 8–9, pp. 1061–1085, 2004.
- [19] Y. Shidara, M. Mineichi Kudo, and A. Nakamura, "Classification based on consistent itemset rules," Transactions on Machine Learning and Data Mining, Vol. 1, No. 1, pp. 17–30, 2008.
- [20] A. Fornells, E. Armengol, E. Golobardes, S. Puig, and J. Malveyh, "Experiences using clustering and generalizations for knowledge discovery in melanomas domain," Transactions on Machine Learning and Data Mining, Vol. 1, No. 2, pp. 49–65, 2008.
- [21] K. Rosen, "Discrete mathematics and its applications," 4th Edition, McGraw-Hill Publishers, 2000.
- [22] V. Krebs, "Introduction to social network analysis," 15 January 2007. <http://www.orgnet.com/sna.html>.

# Scheduling Mobile Data Services in a Bluetooth Based Platform

Xiaoyu Liu, Kin Choong Yow

*School of Computer Engineering, Nanyang Technological University, Singapore City, Singapore*

*Email: liu.xiaoyu.mac@gmail.com, kcyow@ntu.edu.sg*

*Received November 4, 2009; revised December 10, 2009; accepted January 8, 2010*

## Abstract

Public buses play an important role in public transportation in most parts of the world and it is still the dominant public transportation mode in some regions. Nowadays, as people switch to a mobile lifestyle, they spend significant amount of time on the traveling to work, back and forth. However, not much research has been done on how to provide some on-board service for those commuters in the public bus. This paper presents a Bluetooth-based system which is inexpensive, yet flexible, and scalable to serve commuters in a personalized manner using Bluetooth enabled mobile phones. However, from the Bluetooth specification, one Bluetooth dongle can connect to at most seven other Bluetooth devices. As we expect more than 7 users to use the services provided in the Bluetooth-based system (a full double-deck bus can carry around 100 passengers), we need to work out an effective scheduler to schedule all the private services on the Bluetooth servers in the bus. This paper also describes a scheduling algorithm that exploits the park mode feature of the Bluetooth specification to allow more users to have access to the Bluetooth services on the bus.

**Keywords:** Mobile Device, Bluetooth, Public Bus, Data Service

## 1. Introduction

We have transited into the Information era, and most people are eager to get various kinds of information in convenient ways. However, due to the increasingly mobile and busy lifestyle, people are having lesser time for some daily activities e.g. reading the newspaper, checking online news, enriching themselves by casual chat or relax themselves with games. Moreover, due to the large distances and the increasing of mobile lifestyle, people are using public transportation very frequently. After an observation on the public bus or MRT in Singapore, we found that many passengers are killing time by playing some casual game or reading some text content with their cell phones or PDAs during the journey. Quite few people will use GPRS to browse news, download some audio or video clips or go for online chatting due to the cost consideration. We can see that the on-board information and entertainment system in the public transportation system is required.

Several proposed systems exist in providing integrated support for commuters in using a public transportation system, such as e-ticketing and navigating through the complex metro system through mobile phones in Japan [1], and bus routes and schedules information display in

bus stations in Mexico (EMI system [2]). Some others extend the public transportation routes and scheduling information to be included on a travel planner application on mobile phones, such as TramMate [3] in Australia and Buster [4] in Denmark. These systems, although helpful for commuters, do not address the 'idle-ty' of commuters while on the ride.

Some other systems address this issue by providing infotainment experience on-board the public transportation, such as the system proposed by Lin and Chang [5], ALSTOM [6], and the system deployed on French TGV trains [7]. These systems include a LAN on-board the public transportation. This LAN is connected to the outside world through either cellular networks or satellite connection. Although these systems are able to provide data live from the Internet while on the move, the requirement of direct connection to the cellular networks (3G/3.5G) or satellite network is still considered expensive nowadays.

This paper presents the BlueBus System, a system which is inexpensive, yet flexible, and scalable to serve commuters in a personalized manner using Bluetooth enabled mobile phones. However, from the Bluetooth specification, one Bluetooth dongle can connect to seven other Bluetooth devices at most. In order to serve more

than 7 users simultaneously, as a full double-deck bus can carry around 100 passengers, we need to work out an effective scheduler to schedule all the private services on the BlueBox side. This paper also proposes a scheduling algorithm that exploits the park mode feature of the Bluetooth specification to allow more users to have access to the BlueBus services.

## 2. System Design

### 2.1. Overview

We aim to design an inexpensive and flexible system to serve the passenger at a personalized level in the bus, so we would like to develop the client system on the Bluetooth enabled mobile phone. The project is named as “BlueBus” which indicate the bus is Bluetooth signal covered, passengers can use their Bluetooth enabled mobile phone as the interface to get the kinds of information. Beside the client side, BlueBus consists the other two parts that are base station on the bus and the administration server at the bus terminal. The overall system architecture is shown in **Figure 1**. The Mac mini will be installed on the bus as the base station, which should be able to support multiple users on the BlueBus platform. The Mac mini will communicate with mobile phone through Bluetooth while it will communicate with server via Wi-Fi.

**Administration server** is connected to the base station, BlueBox, through the Wireless LAN connection. BlueBus end user, mobile phones are connected to BlueBox via Bluetooth connection.

Function of the Administration server is to manage all BlueBox in the public buses parked in its located bus terminal. It is able to push updates and content synchronization to all BlueBox through Wi-Fi. Administration server located in the bus terminal office must have a stable broadband Internet connection, in order to function well.



Figure 1. Overall system architecture.

**BlueBox** serves as the bridge in the overall system. It retrieves all contents from the Administration server and stores all contents in its local storage waiting for BlueBus commuters to browse or download. It also has to handheld all service requests from client application. The BlueBox must communicate with the Administration server periodically to ensure that it always carries the most recent content and services. In the scenario of the bus, the synchronization takes place when the bus arrives at the bus interchange terminal. The BlueBox will detect the availability of Administration server network and automatically start the service or content synchronization with Administration server.

**Client application** is a Java application installed in commuters’ mobile phones or PDAs. Users in the bus will use this application to choose and enjoy the services in the system.

**Figure 2** is the flow-chart on how to distribute the content to every single end user.

### 2.2. Hardware Selection

#### 2.2.1. Administration Server

For Administration server, it must able to create a wireless network or join the wireless network in the bus terminal in order to synchronize the content and do some administrative control to all BlueBox. It also needs a broadband Internet connection to download new contents

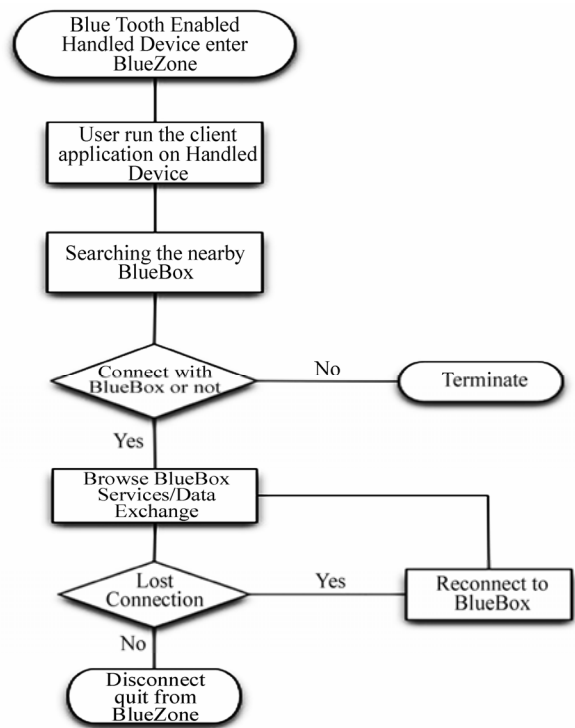


Figure 2. Flow chat of overall system.

and synchronize end user’s upload content with all Administration servers in different bus terminals. It must be preinstalled Windows OS because Server side is developed using SyncML under Windows platform, Windows XP would be preferred. Any hard disk which capacity is larger than 20GB should cater for this system.

**2.2.2. BlueBox**

The BlueBox serves as the access point to this BlueBus system. The domain of each of these BlueBox is the range of Bluetooth i.e. a circle radius 10–100 meters, depending on the power of Bluetooth dongle. So the BlueBox should have little processing power, certain storage capacity and both Bluetooth and wireless LAN capability, certainly, small physical size will be a bonus point. Based on a preliminary analysis, we chose Mac mini as the BlueBox whose specifications are shown in **Table 2** below.

The Mac mini has a built in Mac OS X which provides a stable Bluetooth framework for system implementation. **Figure 3** shows the Bluetooth profiles available in Mac OS X [8]. We will use OBEX and RFCOMM for system development.

**Table 1. Recommended specifications for administration server.**

Specifications for a Administration Server	
Processor	1.5 GHz
Memory	512 MB
Hard Disk	20 GB(min)
Local Area Network	802.11b/g (11 Mbps/54 Mbps)

**Table 2. Recommended specifications for BlueBox.**

Specifications for BlueBox	
Processor	Core Solo 1.5 GHz
Memory	512 MB
Hard Disk	60 GB
Personal Area Network	Bluetooth v2.0+EDR
Wireless LAN Network	802.11g (54 Mbps)
Battery life	1 hour (min)
Physical dimensions	6.5” × 6.5” × 2” (L*W*H)

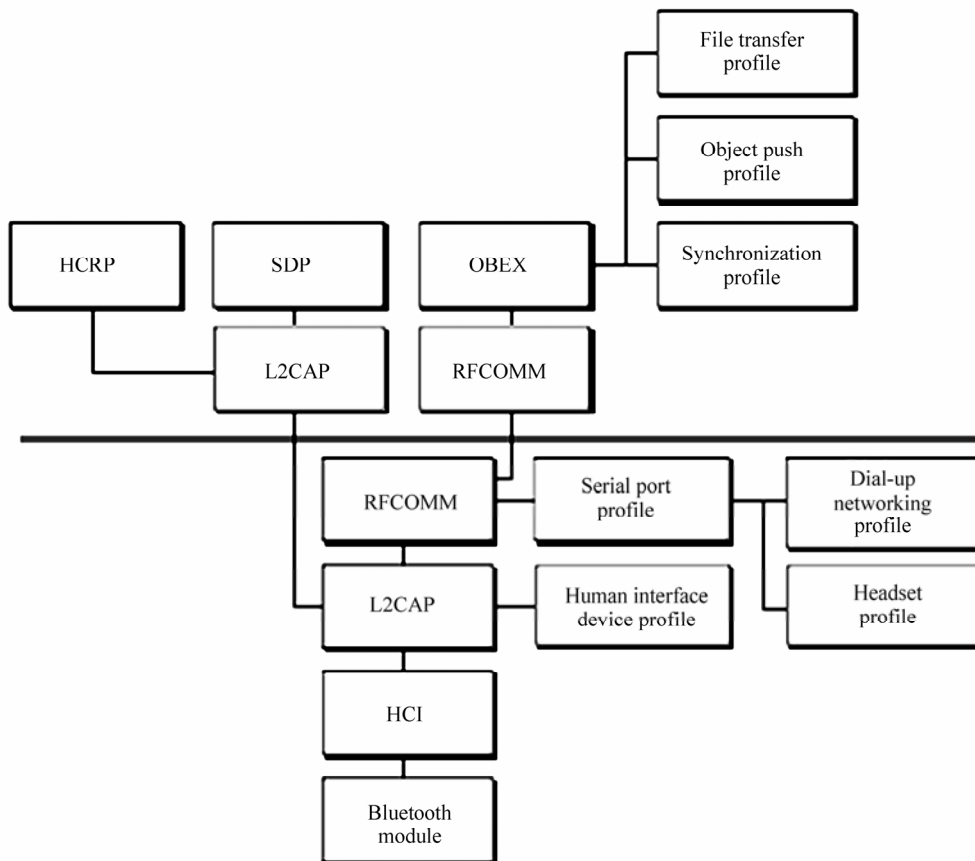


**Figure 3. Mac OS X Bluetooth profiles.**

**2.2.3. J2ME Client Application**

The J2ME client application can run on any handheld device which is Java enabled and built in JSR82 Bluetooth API.

According to our study in the market, there are more than 90 mobile phone models satisfied the hardware requirement that indicates that we really got a large potential user base.

**2.3. System Requirements**

As described in the previous section, BlueBus serves as the platform for mobile data services that can be delivered to users over Bluetooth. The requirements of the system are as follows:

The system must be able to detect new users who are running the client application with Bluetooth enabled handhelds.

- The BlueBus client application must provide a friendly, interactive interface for users to connect to the system and use the services provided.
- The Administration server must provide an effective interface for content providers to add new content to existing services.
- The system must be scalable and must provide an easy method for the system administrator to add new BlueBox to the system.
- The BlueBox must be able to simultaneously support several users accessing the services provided.
- The BlueBox must be easily deployable in static as well as mobile application scenarios, with occasional as well as continuous connectivity.
- The Administration server must ensure automatic synchronization of content and services on all connected BlueBox. If a BlueBox is temporarily disconnected, it must be updated as soon as connectivity restored.

**2.4. BlueBox Design**

BlueBox is developed in Apple Mac OS X platform. The programming language we used is Cocoa which is a famous programming language in Mac OS. Because we expect an automatic working style of BlueBox (no user interference involved) it is implemented using IOBluetooth framework in Cocoa.

**Table 3. Recommended specifications for handheld device.**

Specifications for Handheld Device	
Display Resolution	176*208 pixels
Free Device Memory	2 MB (min)
Phone External Storage	16 MB
Personal Area Network	Bluetooth v1.1(min)
JAVA	JAVA MIDP 1.0 or 2.0

When the server started, it will register a new Bluetooth service provided to Bluetooth stack and start accepting a new connection. The system will automatically create the input stream and output stream when there is a new client wants to connect to the service.

Communication is mostly built in request-reply model where client send the request to server first then server response to the client accordingly.

When server receives a request message, the function associated with that service is called. Each service would have separate function to handle data from client. After some processing, BlueBox will send the reply to client.

**3. Bluebus Scheduling Design**

**3.1. Bluetooth Network Topology**

Bluetooth enabled devices are organized in groups called Piconet [9]. The Piconet consists of a master and up to seven active slaves. A master and a single slave use point-to-point communication; if there are multiple slaves, point-to-multipoint communication is used. The master unit is the device that initiates the communication. A device in one Piconet can communicate to another device in another Piconet, forming a scatternet, as depicted in **Figure 4**. Notice that a master in one Piconet maybe a slave in another Piconet:

**3.2. Constraints on Bluetooth**

From the Bluetooth specifications we know that one Bluetooth dongle can connect to seven other Bluetooth devices at most. However, we expect more users can use the services provided in BlueBus because a full double-deck bus can carry around 100 passengers. We consider add more Bluetooth dongles on the Mac mini, but after

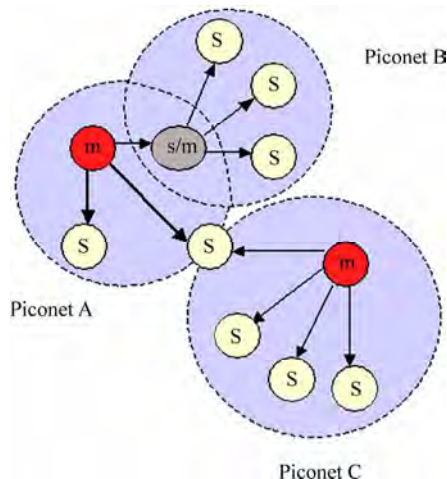


**Figure 4. Scatternet comprising three piconets.**

trying, we found that the seven slaves limitation cannot be solved by simply adding USB powered Bluetooth dongles. This is because the Bluetooth stack currently does not support multiple Bluetooth dongle connections. Although multiple Bluetooth dongle connection is possible in theory, so far, there is no Bluetooth stack in any other platform that support this feature.

### 3.3. Scheduling Algorithm Design

We want to create the Piconet which can serve all the Bluetooth end users. However, the Bluetooth master only can support seven active channels simultaneously which means only seven passengers can enjoy the services we provided in the BlueBus system. The addition of the Bluetooth dongle will not help in solving this issue as previous section discussed.

In order to serve more users simultaneously, we need to work out an effective scheduler to schedule all the private services on the BlueBox side.

#### 3.3.1. Power Mode of Bluetooth Device

Every Bluetooth device has four different power modes [10] shown below:

- **Active Mode:** The slave actively participates in the Piconet by listening, transmitting and receiving packets. The master periodically transmits to the slaves to maintain synchronization.
- **Sniff Mode:** The slave listens on specified slots for its messages. It can operate in a reduced-power status the rest of the time. The master designates a reduced number of time slots for transmitting to a specific slave.
- **Hold Mode:** The device can participate only in SCO packet exchanging and runs in reduced-power status. While it is not active, the device can participate in another Piconet.
- **Park Mode:** It is a low power mode with very little activity. Used when a slave does not need to participate in a Piconet, but still is retain as part of it. The device is changing Active Mode Address (AM\_ADDR) to Park Mode Address (PM\_ADDR). With this mode, a Piconet may have more than seven slaves.

As we see from the properties of the four different power modes, we need to switch the slaves between Active mode and Park mode, in order to achieve our goal supporting more than seven devices simultaneously.

#### 3.3.2. How to Switch between Active Mode and Park Mode

The Bluetooth enabled device has an Active Mode Address (AM\_ADDR) when it is in active status while it has a Park Mode Address (PM\_ADDR) when it is in park/inactive status. The length of AM\_ADDR is 3 bits while the length of PM\_ADDR is 8 bits. So theoretically

one Bluetooth master can support  $2^3-1 = 7$  active Bluetooth devices and  $2^8=256$  parked devices.

Before a Bluetooth device entering Park mode, the master will give the device a PM\_ADDR. Then this Bluetooth slave will give up the active member address, AM\_ADDR if it already got one and listen to the broadcast traffic in regular intervals. The park mode timing parameters should be negotiated with the master using Link Manager Protocol (LMP). Master also can send message to parked device to wake up the parked the device and reassign the AM\_ADDR to it [11].

*(In present devices on the market, the master will do the mode switching automatically instead of user controlling. So we don't know how to control the mode switching in the API level or Stack Level. If we can do that, the following will be the scheduling algorithm.)*

#### 3.3.3. Scheduling Algorithm – First Version

##### Define Service Priority

The Schedule Algorithm design is divided into two parts, one is the active Bluetooth devices scheduling (the number of Bluetooth devices is less than or equal to 7) and the other part is overall scheduling (the number of Bluetooth devices is greater than 7).

##### Active Devices only Scheduling Algorithm

We had done a Bluetooth data transmitting speed test. First, connect individual Bluetooth enabled cell phone to Mac mini which served as the Bluetooth master in the Piconet and trying to download a 3.3MB size file from Mac mini. Second, connect 6 cell phones to Mac mini and try to download the same 3.3MB size file from Mac mini simultaneously. We took the records of the data transmitting speed and consolidate into the table shown below.

From the table, we can easily see that the data transmitting speed drop a lot when there are multiple connections existing. Generally speaking, the data transmission rate in single connection is two to three times of the rate in multiple connections in the cell phone.

**Table 4. Bluetooth data transmission rate of different mobile phones.**

Cell Phone Model	Single connection (4-5m)	6 connections (4-5m)
Nokia N-Gage QD	5 Kbps	5 Kbps
Nokia 6280	104 Kbps	20-30 Kbps
Nokia 3230	41 Kbps	15-18 Kbps
O2 Xphone-11m	16 Kbps	10 Kbps
SonyEricsson K750i	40 Kbps	15 Kbps
SonyEricsson P910i	20 Kbps	10 Kbps
Motorola L7	3-10 Kbps	N/A (always disconnect)

In the BlueBus, we provide four basic services which are listed based on the priority, 1) indicates the highest priority.

- 1) *Bus Stop Alert*
- 2) *Blue Bubble Chatting*
- 3) *RSS News*
- 4) *Entertainment Download*

Only the Entertainment download will involve a large size file which requires fast data transmitting speed. In this case, we will schedule the download process into serial order instead of parallel order because it can save the total data transmitting time.

**Active Queue**

- A0 Chatting Service
- A1 Chatting Service
- A2 RSS News Service
- A3 Download Service
- A4 Bus Stop Alert Service
- A5 Download Service 2
- A6 Bus Stop Alert Service

**After the Scheduling**

- A0 Bus Stop Alert Service → A4
- A1 Bus Stop Alert Service → A6
- A2 Chatting Service → A0
- A3 Chatting Service → A1
- A4 RSS News Service → A2
- A5 Download Service → A3
- A6 Download Service2 → A5

The actual service order is:

- A0 Bus Stop Alert Service
  - A1 Bus Stop Alert Service
  - A2 Chatting Service
  - A3 Chatting Service
  - A4 RSS News Service
  - A5 Download Service
- } Been processed simultaneously



A6 Download Service 2

In the Active queue, if there are no download services or only one download service be found, all the rest services will being processed simultaneously due to the low requirement of the data rate. However, if there are more than two download services in the Active queue, considering them as d1 and d2, we will get the files' size of each download service and current data transmitting rate of each channel. We can calculate the consuming time left to download the specific file. The less the downloading time the higher the processing priority. We assume

d1 got the higher priority, so d2 will start once the d1 finished the downloading. During d1 is in downloading status, d2 is in waiting status, it is possible that d2 will be swap into Park queue if there is another device parked with higher priority. We will talk about it in later section.

**Active and Parked Devices Scheduling**

There is a case which more than seven Bluetooth enabled devices are willing to connect to the Bluetooth master. We will put the first seven devices into the Active queue, the eighth device and followings will be put into Park queue, PM\_ADDR of them will be set.

```

sort Active queue 0-6 based on the priority level
Priority high → low
sort Park queue 0-n (n<256) based on the priority level
Priority high → low
compare (AQ [6], PQ [0])
if priority of AQ [6] >= PQ [0]
    Return;
else if priority of AQ [6] < PQ [0]
    //swap (AQ [6], PQ [0]);
    set AQ [6] PM_ADDR;
    set PQ [0] AM_ADDR;
    add AQ [6] to Park queue, resort the Park queue;
    add PQ [0] to Active queue, resort the Active queue;
    compare( AQ[6], PQ [0]);
    
```

**3.3.4. Improved Version of Scheduling Algorithm**

**3.3.4.1. Reserve Channel for a Certain Service**

Bus Stop Alert service is not a time consuming service, we just need to record the user's registration and save the destination in the BlueBox database. After that, we are able to put it into the Park queue. We only need to wake up this user one stop before the customized destination by sending an alert message.

There is an alternative way to implement the Chat service. The design is shown below.

Figure 5 shows the data structure of a chat service user. It got two buffers which is used to send message while the other buffer is used to receive message from chat server.

We reserve one active channel for the Chat service, each time only one sender can send the message to chat server (BlueBox), after it deposit message to the server, server begin to broadcast this new message to every connected user who are online by swapping them one by

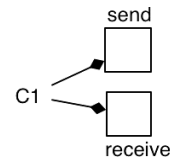


Figure 5. Send and receive buffer of C1.

one from Park queue to Active Queue. After that, the second sender will deposit its composed message to chat server, then server will do the same thing to broadcast this new message to all online users. Certainly, the server is also able to send the message to the specific recipient. We will limit the message length to 160 English characters which is as the same as the normal SMS length. Assume the average Bluetooth data transmitting rate is 5Kbps, then the average time to transmit one message will cost:  $160\text{bytes} / 5\text{Kbps} = 0.03\text{s}$

If there are 20 users using the Chat service, the server can finish the “swap broadcasting” in around 0.6s, within one second which should be acceptable for the users.

We take an example of three users are using the public chat service. We use C1, C2 and C3 to indicate the three users.

From **Figure 6**, we can see that C1 and C3 want to send a message to others. They take the active channel and communicate with server in a serial manner. C1 deposits the message to server, then the server will broadcast the message to C2 and C3 when they are taking the channel. C3 will not send its own message to server in this server swap broadcasting round. So after 3), everyone got the message from C1. Message 1 will be displayed on every users’ screens, and the message one will be cleared from receive buffer.

Then it goes to next message deposit round, it is same as round 1. Chat server will keep all the messages. Chat

server will broadcast the message based on the time stamp of message itself which will ensure the accuracy of the message received by users.

As for the RSS News service, we also can use the similar mechanism, reserve one channel for RSS News service use only. We can do a calculation that, normally the size of one RSS News thread should be within 2KB which equal to 300 to 400 English words. It will cost the user less than 2 minutes to finish the reading on 176\*208 sized cell phone screen, one minute is needed at least. Within 1 minute the server can send at 60 RSS News threads to users that mean it can support up to 60 users to read RSS News with one channel used (**Figure 7**).

Download service must be processed one by one unless the download file size is small.

With the above statement, we can reserve the 7 active channels for different services. Download and Bus Stop Alert services only reserve one channel for each while both Chatting and RSS News service can reserve 2 channels for each, because they are more timing issue is more critical for them.

### 3.3.4.2. Random channel allocation and Sub Queue Algorithm

We also can split the Park Queue to several Park queues based on how many services we provided. In current stage, we can reform 4 Park queues, which are Bus Stop

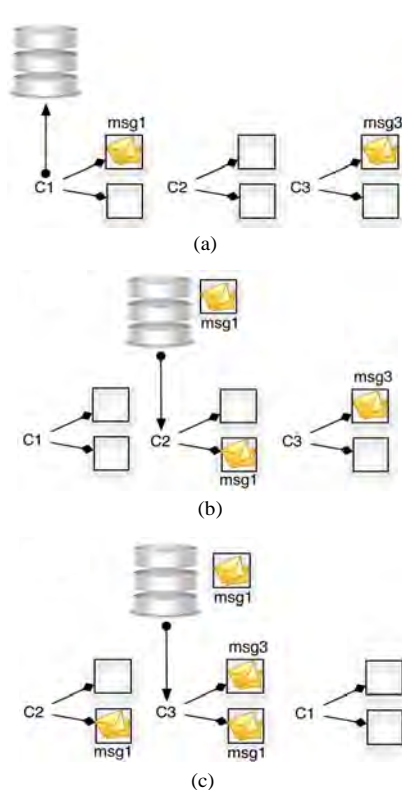


**Figure 6.** Swap-broadcast message from C1.

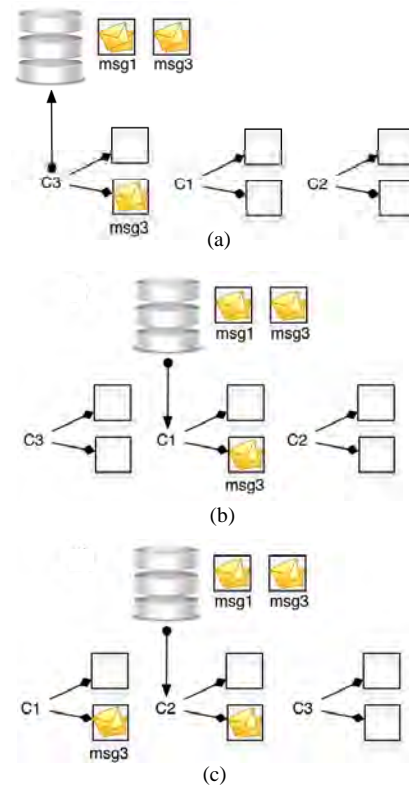


**Figure 7.** Swap-broadcast message from C3.

Alert Queue, Chat Queue, RSS News Queue and Download Queue, listed based on the priority from high to low. Once there is an active channel is free, we will process the service queue based on its priority level. If there are more active channels are free, more service queues will be processed by server.

Because there are 7 active channels while there are only 4 services currently, some service park queue, such as Chat service and RSS News service, can split its park queue equally into 2 sub-park queues. Each sub-park queue will take a channel for processing which may reduce the time consuming for one round “swap broadcasting”.

### 4. System Evaluation

For the system evaluation, eight Bluetooth 2.0 Class 1 + EDR dongles are used. The experiments were conducted to measure the transmission rate and interference that may affect the transmission rate due to co-existing piconets and the effect of obstacles in-between the Bluetooth devices to the transmission rate. Therefore, three test sets were conducted as follows: 1. Single piconet Test, 2. Multiple piconets test, and 3. Obstacle test. For every test, the experiment is conducted five times and the average is taken and plotted to a graph.

#### 4.1. Single Piconet Test

This test was conducted to measure the effect of increasing number of slaves on a Bluetooth master to its transmission rate.

Figure 8 shows the test result. For the transmission to only one slave on a master dongle, it achieved the data rate of 1.6 Mbps, which is fairly close to the theoretical transmission rate of Bluetooth, i.e., 2.0 Mbps. However, as the number of slave increases, the total data rate drops quite significantly. With only one additional slave, the total data rate drops by 400 kbps to 1.2 Mbps. According to the Bluetooth Specification [12], this drop is due to the

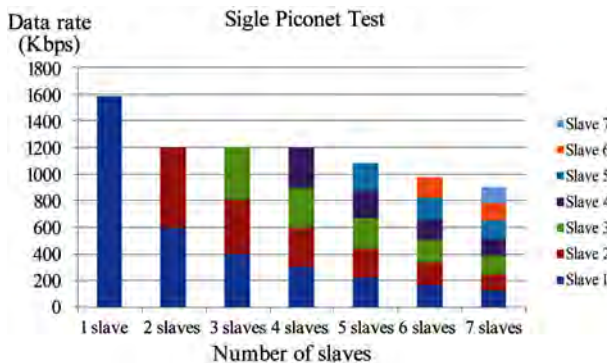


Figure 8. Effect of the number of slave dongles on the data rate in one piconet.

fact that when there is only one slave, the master is able to transport L2CAP (Logical Link Control and Adaptation Protocol) broadcasts over the ACL-U (Asynchronous ConnectionLess – User) logical link rather than over the ASB-U (Active Slave Broadcast – User) or PSB-U (Parked Slave Broadcast – User) logical links. This allows the transmission to be more efficient in terms of bandwidth (if the physical channel quality is not too degraded) for the case of only one slave.

Also, as only one device is allowed to transmit/receive in each 625 μsec time slot of a Bluetooth transmission, the data rate of one of the slaves (in the two-slave case) drops to only 600 kbps (from 1.6 Mbps when there is only one slave) – a very significant reduction. However, on subsequent addition of slaves, the total data rate varies only slightly from the two-slave case, where the total data rate decreases as the number of slaves increases. Although there is a drop in the total data rate, each slave still gets an equal share of bandwidth. At the limit of 7 slaves, each slave achieves a data rate of around 100 Kbps which is considered acceptable for the BlueBus services.

#### 4.2. Multiple Piconets Test

The Bluetooth Class 1 device could reach the range of 100 m, and this is the Bluetooth device planned to be used on the BlueBus. Since the interior area of the bus is less than 100 m, having four server dongles (the dispatcher is not involved in the experiments) may introduce interference problem. Therefore, this test is intended to see the effect of the increasing number of co-existing piconets on the transmission rate.

Figure 9 shows the data rates achieved when multiple piconets co-exist. Here, ‘m’ denotes the master dongle and ‘s’ denotes the slave dongle. In the base experiment of one server and one client (which is essentially the same as the case of only one slave in Figure 8), it can achieve a data rate of 1.6 Mbps. However, if multiple

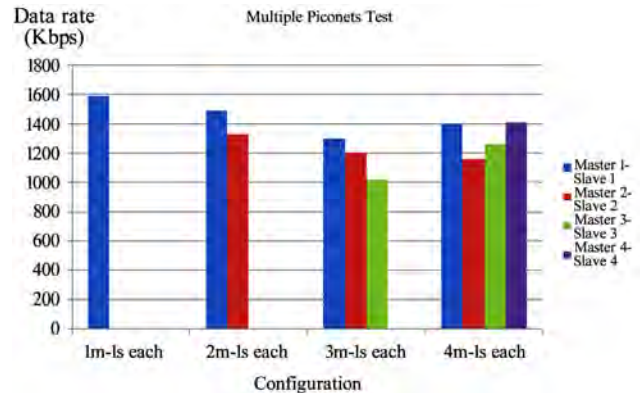


Figure 9. Effect of the number of master dongles on the data rate.

masters exist (i.e. multiple piconets), the performance drops. It can be seen from **Figure 9** that the drop is not very significant, and it is concluded that the multiple piconets interference does not affect the data rate much.

### 4.3. Obstacle Test

Bluetooth is a wireless technology, and as such, its transmission rate may be subjected to the objects that hinder its transmission path. Inside a bus, the obstacles can be the seats or the metal poles, including the people packed inside the bus with the various objects they may carry. Therefore, this test is used to find out the influence of various typical objects in between the Bluetooth transmission path on the Bluetooth's transmission rate. In this test, the master and the slave dongle are separated 1.5 meters apart. The separation is based on the derivation from **Figure 7**. All the obstacles are placed within close proximity to the receiving dongle (around 10 cm). If a user uses his mobile device on a bus, it will be close to the objects that he is currently holding (books, newspapers, etc) or the seat in front of him. In this test, only one master and one slave are used.

**Figure 10** shows the result of putting different obstacles in the Bluetooth transmission path. The obstacles used are representative of the objects that are typically in the bus or the objects that people may carry. The obstacle of human body is obvious, since the bus will be packed by passengers inside. The 3.5 cm thick book used in this test represent any types of printed media of pages bound together such as text books, newspapers, magazines, etc. A thick book is used, since if the transmission rate is good on the thick book, the Bluetooth will perform equally well on thinner books or printed media. The bottle of water represents any liquid that a person may carry. The plastic glass represents materials made up of plastic such as the plastic bottles, and finally the glass represents the windows of the bus.

As **Figure 10** shows, different obstacles of different materials affect the data rate to different extents. How-

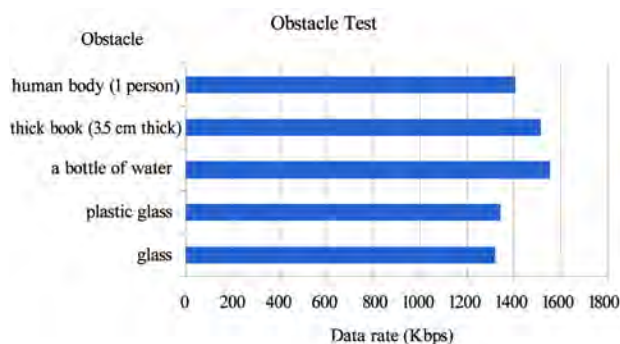


**Figure 10. Influence of different obstacles on the data rate.**

ever, the figure still shows acceptable performance on all the obstacles tested. Nevertheless, to minimize the impact of obstacles inside the bus, the master dongles should be mounted along the ceiling of the bus and connected to the BlueBox by USB cables. As the distance limit of a USB cable is 5 m, additional USB hubs can be used to extend this distance limit.

## 5. Conclusions and Future Development

We had designed and developed the BlueBus system which is able to provide variety information and entertainment services to passengers in a personalized level and give them a good user experience. We have shown that, based on the test on real Bluetooth dongles that even when a Bluetooth device is full with active connections, it can still maintain relatively good data rate for each slave on 100 Kbps. The experiments conducted also shows that the interference of co-existing Bluetooth piconets does not affect the data rate much. This is also true for the obstacle experiment where the Bluetooth data rate does not vary widely when it is presented with different materials.

We are planning to provide more interesting services such as send birthday or greeting cards, share personal Mobile Log (similar with Blog) etc. Apart from this, we also aim to find a way in the Bluetooth stack level or scheduling algorithm to improve the multiple user support feature.

## 6. References

- [1] K. Goto and Y. Kambayashi, "Integration of electronic tickets and personal guide system for public transport using mobile terminals," *Proceedings of the 2003 ACM SIGMOD International Conference on Management of Data*, pp. 642–646, 2003.
- [2] T. Y. Banos, E. Aquino, F. D. Sernas, Y. R. Lopez, and R. C. Mendoza, "EMI: A system to improve and promote the use of public transportation," *Conference on Human Factors in Computing Systems, CHI'07 Extended Abstracts on Human Factors in Computing Systems*, pp. 2037–2042, 2007.
- [3] J. Kjeldskov, S. Howard, J. Murphy, J. Carrol, F. Vetere, and C. Graham, "Designing TramMateña context-aware mobile system supporting use of public transportation," *Proceedings of the 2003 Conference on Designing for User Experiences*, pp. 1–4, 2003.
- [4] J. Kjeldskov, E. Andersen, and L. Hedegaard, "Designing and evaluating buster: An indexical mobile travel planner for public transportation," *Proceedings of 19th Australian Conference on Computer-Human Interaction: Entertaining User Interfaces*, pp. 25–28, 2007.
- [5] K. D. Lin and J. F. Chang, "Communications and enter-

- tainment onboard a high-speed public transport system,” *IEEE Wireless Communications*, Vol. 9, pp. 84–89, February 2002.
- [6] V. Scinteie, “Implementing passenger information, entertainment, and security systems in light rail transit,” *Transportation Research Circular E-C058: 9th National Light Rail Transit Conference*, pp. 528–533, 2003.
- [7] “French railways launch their on-board internet and multimedia connectivity services on TGV high-speed train,” *Appear, the Context Company*, 2007. <http://www.appear-networks.com/French-Railways-launch-their-on.html>.
- [8] “Bluetooth device access guide in Mac OS X.” <http://developer.apple.com/documentation/DeviceDrivers/Conceptual/Bluetooth/index.html>.
- [9] “Bluetooth network topology.” <http://developers.sun.com/techtopics/mobility/midp/articles/bluetooth1>.
- [10] “Bluetooth power mode overview.” [http://72.14.235.104/search?q=cache:4LenKxr14d0J:www.ece.ualberta.ca/~sbates/downloads/Mint702\\_PartSix.ppt+how+to+assign+the+PM\\_ADDR&hl=en&gl=sg&ct=clnk&cd=3](http://72.14.235.104/search?q=cache:4LenKxr14d0J:www.ece.ualberta.ca/~sbates/downloads/Mint702_PartSix.ppt+how+to+assign+the+PM_ADDR&hl=en&gl=sg&ct=clnk&cd=3).
- [11] “Simple differences between Sniff mode and Park mode.” <http://www.palowireless.com/infotooth/knowledge/baseband/78.asp>.
- [12] “Bluetooth core specification V2.1 + EDR,” *Bluetooth SIG*, 2007.

# Time Domain Signal Analysis Using Wavelet Packet Decomposition Approach

M. Y. Gokhale<sup>1</sup>, Daljeet Kaur Khanduja<sup>2</sup>

<sup>1</sup>*Professor and Head of Department of Mathematics, Maharashtra Institute of Technology, Pune, India*

<sup>2</sup>*Assistant Professor Department of Mathematics, Sinhgad Academy of Engineering, Pune, India*

*Email: dkdkhalsa@gmail.com*

*Received November 11, 2009; revised December 17, 2009; accepted January 22, 2010*

## Abstract

This paper explains a study conducted based on wavelet packet transform techniques. In this paper the key idea underlying the construction of wavelet packet analysis (WPA) with various wavelet basis sets is elaborated. Since wavelet packet decomposition can provide more precise frequency resolution than wavelet decomposition the implementation of one dimensional wavelet packet transform and their usefulness in time signal analysis and synthesis is illustrated. A mother or basis wavelet is first chosen for five wavelet filter families such as Haar, Daubechies (Db4), Coiflet, Symlet and dmey. The signal is then decomposed to a set of scaled and translated versions of the mother wavelet also known as time and frequency parameters. Analysis and synthesis of the time signal is performed around 8 seconds to 25 seconds. This was conducted to determine the effect of the choice of mother wavelet on the time signals. Results are also prepared for the comparison of the signal at each decomposition level. The physical changes that are occurred during each decomposition level can be observed from the results. The results show that wavelet filter with WPA are useful for analysis and synthesis purpose. In terms of signal quality and the time required for the analysis and synthesis, the Haar wavelet has been seen to be the best mother wavelet. This is taken from the analysis of the signal to noise ratio (SNR) value which is around 300 dB to 315 dB for the four decomposition levels.

**Keywords:** WPA, Wavelet Packet Decomposition (WPD), SNR, Haar

## 1. Introduction

Over the last decade much work has been done in applying time frequency transforms to the problem of signal representation and classification. Signals possessing non-stationary character are not well suited for detection and classification by traditional Fourier methods. It has been shown that wavelets can approximate time varying non-stationary signals in a better way than the Fourier transform representing the signal on both time and frequency domains [1]. Hence they can easily detect local features in a signal. Furthermore, wavelet decomposition allows analyzing a signal at different resolution levels. The discrete wavelet transform (DWT) provides a very efficient representation for a broad range of real-world signals. This property has been exploited to develop powerful signal de-noising and estimation methods [2] and extremely low-bit-rate compression algorithms [3]. The discrete wavelet transform (DWT) is usually implemented using an octave-band tree structure. This is ac-

complished by dividing each sequence into a component containing its approximated version (low-frequency part) and a component with the residual details (high-frequency part) and then iterating this procedure at each stage only on the low-pass branch of the tree [4,5]. The main drawback of the octave-band tree structure is that it does not provide a good approximation of the critical subband decomposition [6]. An alternate means of analysis is sought, so that valuable time-frequency information is not lost. The Wavelet Packet Transform (WPT) is one such time frequency analysis tools. It is a transform that brings the signal into a domain that contains both time and frequency information (Wickerhauser, 1991). Thus, analysis of the signal can be done simultaneously in frequency and time. The most basic way to do time frequency analysis is by making FFT analysis in short windows. That has the drawback that the window needs to be short to find out fast changes in the signal and long to determine low frequency components. The wavelet packet transform (WPT) offers a great deal of freedom in dealing

with different types of transient signals. Indeed the development of the wavelet transform (WT) [7–9] and wavelet packets [10–12] has sparked considerable activity in signal representation and in transient and non-stationary signal analysis.[13–15].

Wavelet packet decomposition (WPD) (sometimes known as just wavelet packets) is a wavelet transform where the signal is passed through more filters than the DWT. Wavelet packets are the particular linear combination of wavelets. They form bases which retain many of the orthogonality, smoothness, and localization properties of their parent wavelets. The coefficients in the linear combinations are computed by a recursive algorithm making each newly computed wavelet packet coefficient with the result that expansions in wavelet packet bases have low computational complexity. In the DWT, each level is calculated by passing the previous approximation coefficients through high and low pass filters. However, in the WPD, both the detail and approximation coefficients are decomposed. For  $n$  levels of decomposition the WPD produces  $2^n$  different sets of coefficients (or nodes) as opposed to  $(n+1)$  sets for the DWT. However, due to the down sampling process the overall number of coefficients is still the same and there is no redundancy.

The work presented in this paper contributes a new era in wavelet packet analysis and synthesis of time domain signals. Wavelet packet transform techniques have been used to extract feature from time domain signals. Feature extraction involves information retrieval from the time signal [16]. The wavelet packet transform has more important benefits than the discrete wavelet transform. Wavelet packet functions comprise a rich family of building block functions. Wavelet packet functions are still localized in time, but offer more flexibility than wavelets in representing different types of signals. In particular, wavelet packets are better at representing signals that exhibit oscillatory or periodic behavior. Wavelet packets are organized naturally into collections, and each collection is an orthogonal basis for  $L^2(R)$ . It is a simple, but very powerful extension of wavelets and multiresolution analysis (MRA). The wavelet packets allow more flexibility in adapting the basis to the frequency contents of a signal and it is easy to develop a fast wavelet packet transform. The power of wavelet packet lies in the fact that we have much more freedom in deciding which basis function is to be used to represent the given function. It can be computed very fast, it demands only  $O(M \log M)$  time, where  $M$  is the number of data points which is important in particular in real time applications. It also has compact support in time as well as in frequency domain and adapts its support locally to the signal which is important in time varying signals. With wavelet packets we have a much finer resolution of the

signal and a greater variety of options for decomposing it.

The paper is organized as follows. In Section 2, brief background information on Discrete Wavelet transform and wavelet packet decomposition is discussed. In Section 3 the present work is explained. The results are given in Section 4 and Section 5 gives the conclusions.

## 2. Background

### 2.1. Discrete Wavelet Transform

The DWT, which is based on subband coding, is found to yield a fast computation of Wavelet Transform. It is easy to implement and reduces the computation time and resources required. In continuous wavelet transform (CWT), the signals are analyzed using a set of basis functions which relate to each other by simple scaling and translation. In the case of DWT, a time scale representation of the digital signal is obtained using digital filtering techniques. The signal to be analyzed is passed through filters with different cutoff frequencies at different scales. In the discrete wavelet transform, a signal can be analyzed by passing it through an analysis filter bank followed by a decimation operation. When a signal passes through these filters, it is split into two bands. The low pass filter, which corresponds to an averaging operation, extracts the coarse information of the signal. The high pass filter, which corresponds to a differencing operation, extracts the detail information of the signal. The output of the filtering operations is then decimated by two. Filters are one of the most widely used signal processing functions. Wavelets can be realized by iteration of filters with rescaling. The DWT is computed by successive low pass and high pass filtering of the discrete time-domain signal as shown in **Figure 1**. This is called the Mallat algorithm or Mallat-tree decomposition.

At each decomposition level, the half band filters produce signals spanning only half the frequency band. This doubles the frequency resolution as the uncertainty in frequency is reduced by half. In accordance with Nyquist's rule if the original signal has a highest frequency of  $\omega$ , which requires a sampling frequency of  $2\omega$  radians, then it now has a highest frequency of  $\omega/2$  radians. It can now be sampled at a frequency of  $\omega$  radians thus discarding half the samples with no loss of information. This decimation by 2 halves the time resolution as the entire signal is now represented by only half the number of samples. Thus, while the half band low pass filtering removes half of the frequencies and thus halves the resolution, the decimation by 2 doubles the scale. The filtering and decimation process is continued until the desired level is reached. The maximum number of levels depends on the length of the signal. The DWT of the original signal is then obtained by concatenating all the

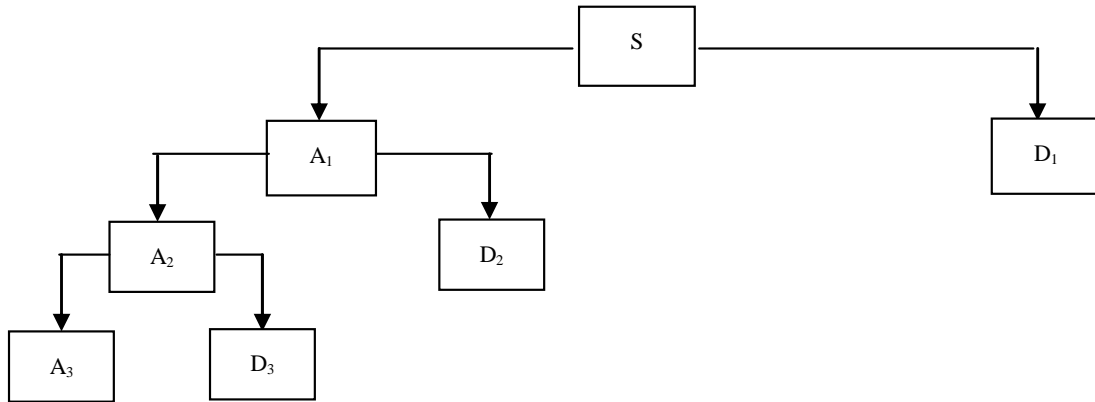


Figure 1. Level 3 decomposition using wavelet transform.

coefficients, approximation and details, starting from the last level of decomposition.

2.2. Multiresolution Analysis

An orthogonal wavelet decomposition of a signal  $x(t) \in L^2(R)$  to coefficients  $\{W_j^k(x)\}_{k,j \in Z^2}$  such that

$$W_j^k(x) \cong \left\langle x(t), 2^{-j/2} \psi(2^{-j}t - k) \right\rangle \cong 2^{-j/2} \int_{-\infty}^{\infty} x(t) \psi^*(2^{-j}t - k) dt \quad (1)$$

where the function  $\psi$  is usually referred to as a mother wavelet and  $*$  stands for the complex conjugation. The orthonormal wavelet basis  $\left\{ 2^{-j/2} \psi(2^{-j}t - k), (k, j) \in Z^2 \right\}$  may be built from a multiresolution analysis of  $L^2(R)$ . In this case, the approximation of the signal at resolution  $2^{-j}$  can be described by the coefficients

$$A_j^k(x) \cong \left\langle x(t), 2^{-j/2} \phi(2^{-j}t - k) \right\rangle, k \in Z \quad (2)$$

where the function  $\phi$  is the scaling function. The mother wavelet and the scaling function then satisfy the so called two-scale equations:

$$2^{-j/2} \phi\left(\frac{t}{2} - k\right) = \sum_{l=-\infty}^{\infty} h_{l-2k} \phi(t-l) \quad (3)$$

$$2^{-j/2} \psi\left(\frac{t}{2} - k\right) = \sum_{l=-\infty}^{\infty} g_{l-2k} \psi(t-l) \quad (4)$$

Where  $\{h_k\}_{k \in Z}$  and  $\{g_k\}_{k \in Z}$  are respectively the impulse response of lowpass and highpass paraunitary Quadrature mirror filters (QMF) [17]. If we denote the vector spaces

$$V_j \cong span\{\phi(2^{-j}t - k), k \in Z\} \text{ and } O_j \cong span\{\psi(2^{-j}t - k), k \in Z\}$$

it results from Equations (3) and (4) that  $V_{j+1} = V_j \oplus O_j^\perp$ . We then find that for every  $j_m \in Z$ ,

$$\left\{ 2^{-j/2} \psi(2^{-j}t - k), k \in Z, j \leq j_m \right\} \cup \left\{ 2^{-j_m/2} \phi(2^{-j_m}t - k), k \in Z \right\}$$

is an orthonormal basis of  $L^2(R)$ .

The interest in the QMF filters lies in the efficient computation of the orthogonal wavelet decomposition via a two channel filter bank structure. The decomposition which is useful in emphasizing the local features of a signal, presents however a limitation, namely its non-variance in time (or space). This implies that the wavelet coefficients of  $T_\tau[x(t)] \cong x(t - \tau), \tau \in R$  are generally not delayed versions of  $\{W_j^k(x)\}_{k \in Z}$ .

2.3. Wavelet Packet Decomposition

The wavelet packet method is a generalization of wavelet decomposition that offers a richer range of possibilities for signal analysis and which allows the best matched analysis to a signal. It provides level by level transformation of a signal from the time domain into the frequency domain. It is calculated using a recursion of filter-decimation operations leading to the decrease in time resolution and increase in frequency resolution. The frequency bins, unlike in wavelet transform, are of equal width, since the WPT divides not only the low, but also the high frequency subband. In wavelet analysis, a signal is split into an approximation and a detail coefficient. The approximation coefficient is then itself split into a second-level approximation coefficients and detail coefficients, and the process is repeated. In wavelet packet

analysis, the details as well as the approximations can be split. This yields more than  $2^{2^{n-1}}$  different ways to encode the signal. When the WT is generalized to the WPT, not only can the lowpass filter output be iterated through further filtering, but the highpass filter can be iterated as well. This ability to iterate the highpass filter outputs means that the WPT allows for more than one basis function (or *wavelet packet*) at a given scale, versus the WT which has one basis function at each scale other than the deepest level, where it has two. The set of *wavelet packets* collectively make up the complete family of possible bases, and many potential bases can be constructed from them. If only the lowpass filter is iterated, the result is the wavelet basis. If all lowpass and highpass filters are iterated, the *complete tree* basis results. The top level of the WPD tree is the time representation of the signal. As each level of the tree is traversed there is an increase in the trade off between time and frequency resolution. The bottom level of a fully decomposed tree is the frequency representation of the signal. **Figure 2** shows the level 3 decomposition using wavelet packet transform.

Based on the above analysis, **Figure 1** and **Figure 2** give the comparison of a three-level wavelet decomposition and wavelet packet decomposition. It can be seen in **Figure 1** that in wavelet analysis only the approximations (represented by capital A in the figure) at each resolution level are decomposed to yield approximation and detail information (represented by capital D in the figure) at a higher level. However, in the wavelet packet analysis [**Figure 2**], both the approximation and details at a certain level are further decomposed into the next level, which means the wavelet packet analysis can provide a more precise frequency resolution than the wavelet analysis.

The wavelet packet decomposition [4,5,18] is an extension of the wavelet representation which allows the best matched analysis to a signal. To define wavelet packets, we introduce functions of  $L^2(R)$ ,  $W_m(t)$ ,  $m \in N$  such that

$$\int_{-\infty}^{\infty} W_0(t) dt = 1 \tag{5}$$

and for all  $k \in Z$ ,

$$2^{-j/2} W_{2^j m} \left( \frac{t}{2^j} - k \right) = \sum_{l=-\infty}^{\infty} h_{l-2^j k} W_m(t-k) \tag{6}$$

$$2^{-j/2} W_{2^j m+1} \left( \frac{t}{2^j} - k \right) = \sum_{l=-\infty}^{\infty} g_{l-2^j k} W_m(t-k) \tag{7}$$

where  $\{h_k\}_{k \in Z}$  and  $\{g_k\}_{k \in Z}$  are the previously defined impulse responses of the QMF filters. If for every  $j \in Z$ , we define the vector space  $\Omega_{j,m} \cong \text{span}\{W_m(2^{-j}t-k), k \in Z\}$  then it can be shown that  $\Omega_{j,m} = \Omega_{j+1,2m} \oplus \Omega_{j+1,2m+1}$ . As a result, if we denote by  $P$  a partition of  $R^+$  into intervals  $I_{j,m} = [2^j m, \dots, 2^j(m+1)]$ ,  $j \in Z$  and  $m \in \{0, 1, \dots, 2^j - 1\}$ , then

$$L^2(R) = \bigoplus_{(j,m)/I_{j,m} \in P} \Omega_{j,m} \tag{8}$$

In an equivalent way,  $\{2^{-j/2} W_m(2^{-j}t-k), k \in Z, (j,m)/I_{j,m} \in P\}$  is an orthonormal basis of  $L^2(R)$ . Such a basis is called a wavelet packet. The coefficients resulting from the decomposition of a signal  $x(t)$  in this basis are

$$C^k_{j,m}(x) \cong \left\langle x(t), 2^{-j/2} W_m(2^{-j}t-k) \right\rangle \tag{9}$$

By varying the partition P, different choices of wavelet packets are possible. While a fixed and dyadic partitioning of time frequency domain is imposed in the case of the wavelet transform, the idea of wavelet packets is to introduce more flexibility making this partitioning adaptive to spectral content of the signal.

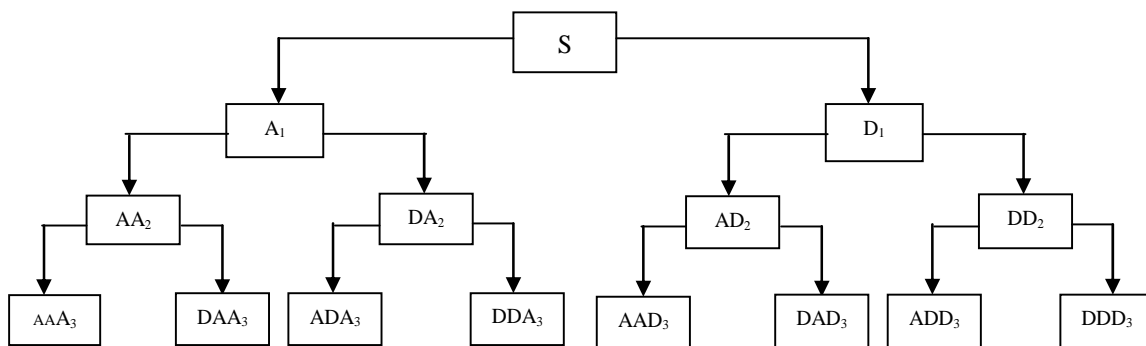


**Figure 2.** Level 3 decomposition using wavelet packet transform.

In wavelet packet analysis, an entropy-based criterion is used to select the most suitable decomposition of a given signal. This means we look at each node of decomposition tree and quantify the information to be gained by performing each split [19]. The wavelets have several families. The most important wavelets families are Haar, Daubechies, Symlets, Coiflets, and biorthogonal.

### 3. Proposed Work

The block diagram shown in **Figure 3** gives the actual implementation of the method proposed in this paper.

#### 1) Input time domain signal

The system described above was simulated on a computer with floating point numbering system. The input time domain wave is pre-emphasized, low pass filtered with sampling frequency 8 K to 44.1 KHz range and 1–10 sec duration samples. The time domain is digitized to 16 bits.

#### Preprocessing:

In this block unwanted noise is removed when the signal gets recorded with the help of various digital filter such as Low pass filter (LPF) with 3.4 KHz, Notch filter to remove the line frequency effect i.e. 50 Hz.

#### Wavelet transforms:

In this block we applied the wavelet filter coefficients as low and high band and filter the input signal to enhance the band energies.

#### Decimation:

As deals with the multi-rate analysis system the decimation factor helps to enhance the band level information from wavelet transform. We consider decimation by 2, 4 etc for our experiments.

#### Analysis Subband Feature Vectors:

From the filtering results obtained with the 2 band system, we have extracted the various features from low pass and high pass band and then re-arranged with the desired format for further analysis part.

#### Interpolation:

Interpolation deals with up sampling the inverse wavelet filtering to reconstruct the original input signal.

#### Inverse Wavelet transforms:

Analysis of interpolated features is reordered with respect to the 2 bands system to extract the original contents from the feature vector for input signal synthesis purpose.

#### Noise Removal:

Input noisy signal is filtered with band stop filter with desired cut off frequency. Filtered output is further applied to post processing.

#### Post Processing:

Final tuning is done in the post processing block.

#### 2) Testing Setup

Matlab programs were written to implement the structure shown in **Figure 3**. Time domain signals in a \*.wav format sampled at 8 KHz were used for all simulations. Results for different setups are given in the next section. Several examples of time domain signals of different sampling frequencies, with five wavelet filter families are given below.

#### 3) Performance Evaluation

Performance evaluation tests can be done by subjective quality measures and objective quality measures. Objective measures provide a measure that can be easily implemented and reliably reproduced. Objective measures are based on mathematical comparison of the original and processed time domain signals. The majority of objective quality measures quantify time domain quality of the signal in terms of a numerical distance measure. The signal to noise ratio is the most widely used method to measure time domain signal quality. It is calculated as the ratio of the signal to noise power in decibels.

$$SNR = 10 \log_{10} \left( \frac{\sum_n s^2(n)}{\sum_n [s(n) - \hat{s}(n)]^2} \right) \quad (10)$$

where  $s(n)$  is the clean time domain signal and  $\hat{s}(n)$  is the processed time domain signal.

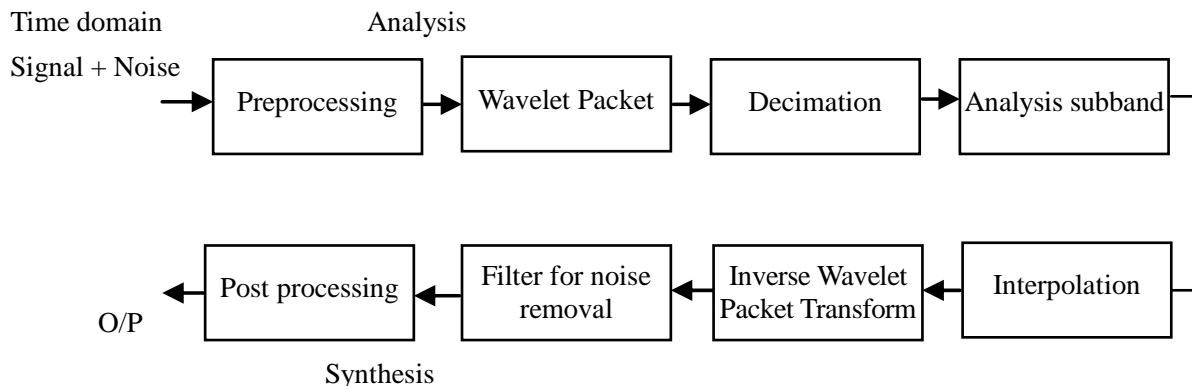


**Figure 3. Block diagram of time domain signal using wavelet packet transform.**

4. Results

We have tested the 10 input samples with sampling frequency of 8 K on various wavelet filtering bank i.e. Haar, Db4, Symlet, dmey, etc. as shown in **Tables 1, 3, 4, 7**. We observe that SNR for wavelet packet analysis and synthesis after filtering is around 120 dB to 320 dB for level 1 decomposition, level 2 decomposition 120 dB to 310 dB, level 3 decomposition 115 dB to 310 dB and level 4 decomposition 115 dB to 305 dB.

From **Tables 2, 4, 6, 8** as per timing consideration the total time for analysis and synthesis is tabulated. We observe that total time for analysis and synthesis using wavelet filtering is around 8 sec to 25 sec.

**Table 1. SNR calculation for various mother wavelet level 1 decomposition.**

Sample	Haar	Db4	Sym5	dmey	Coif5
T1	315.64	244.16	247.86	122.32	165.94
T2	315.58	244.16	247.86	122.28	165.95
T3	315.53	244.16	247.86	122.35	165.94
T4	315.55	244.16	247.86	122.34	165.94
T5	315.55	244.16	247.86	122.34	165.94
T6	315.53	244.16	247.86	122.35	165.94
T7	315.53	244.16	247.86	122.30	165.95
T8	315.53	244.16	247.86	122.35	165.94
T9	315.55	244.17	247.87	122.25	165.95
T10	315.54	244.16	247.86	122.32	165.95

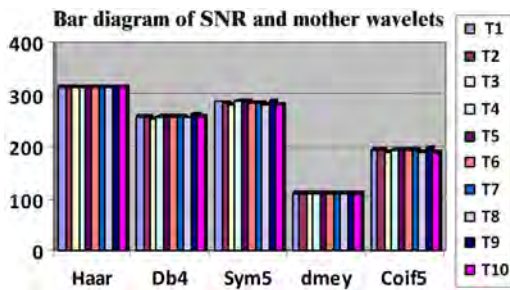


**Figure 4. Graphical presentation of SNR for various mother wavelets.**

**Table 2. Total time calculation (in seconds) for analysis and synthesis using wavelet filtering for level 1.**

Sample	Haar	Db4	Sym5	dmey	Coif5
T1	8.10	8.31	9.15	9.40	8.96
T2	8.90	10.56	9.17	11.01	9.28
T3	8.53	9.43	9.32	13.45	10.40
T4	8.85	9.34	9.06	12.31	10.20
T5	8.39	9.01	8.59	11.90	9.29
T6	10.73	11.37	12.45	13.10	11.90
T7	11.48	12.03	13.07	13.28	13.18
T8	8.65	9.23	10.46	12.57	9.62
T9	9.59	10.65	10.20	11.40	11.26
T10	9.32	9.64	9.67	13.29	10.11

**Table 3. SNR calculation of various mother wavelets for level 2 decomposition.**

Sample	Haar	Db4	Sym5	dmey	Coif5
T1	310.41	232.64	247.31	121.37	165.81
T2	310.41	232.64	247.31	121.34	165.82
T3	310.40	232.64	247.31	121.36	165.81
T4	310.41	232.64	247.31	121.39	165.81
T5	310.38	232.64	247.31	121.36	165.81
T6	310.40	232.64	247.31	121.42	165.81
T7	310.40	232.64	247.31	121.33	165.82
T8	310.39	232.64	247.31	121.42	165.81
T9	310.40	232.65	247.31	121.25	165.82
T10	310.41	232.64	247.31	121.34	165.82

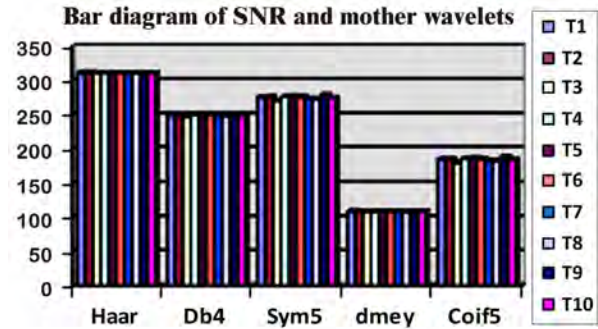


**Figure 5. Graphical presentation of SNR for various mother wavelets.**

**Table 4. Total time calculation (in seconds) for analysis and synthesis using wavelet filtering for level 2.**

Sample	Haar	Db4	Sym5	dmey	Coif5
T1	8.29	8.73	10.11	12.85	9.20
T2	10.10	11.06	11.57	14.64	11.21
T3	9.60	9.56	10.06	12.51	10.43
T4	8.93	10.43	9.48	13.95	11.67
T5	8.42	10.18	8.89	11.92	10.85
T6	11.82	13.51	12.48	15.62	13.00
T7	10.70	12.64	13.11	16.84	13.40
T8	9.45	10.53	9.82	13.28	10.56
T9	9.21	10.09	9.81	12.18	11.04
T10	10.75	10.98	11.09	14.25	10.71

**Table 5. SNR calculation of various mother wavelets for level 3 decomposition.**

Sample	Haar	Db4	Sym5	dmey	Coif5
T1	307.15	230.59	241.56	115.85	159.86
T2	307.15	230.60	241.56	115.84	159.86
T3	307.13	230.59	241.56	115.84	159.86
T4	307.12	230.59	241.56	115.86	159.86
T5	307.14	230.59	241.56	115.85	159.86
T6	307.14	230.59	241.56	115.88	159.86
T7	307.16	230.60	241.56	115.83	159.87
T8	307.15	230.59	241.56	115.87	159.87
T9	307.15	230.60	241.57	115.77	159.87
T10	307.14	230.60	241.56	115.83	159.86

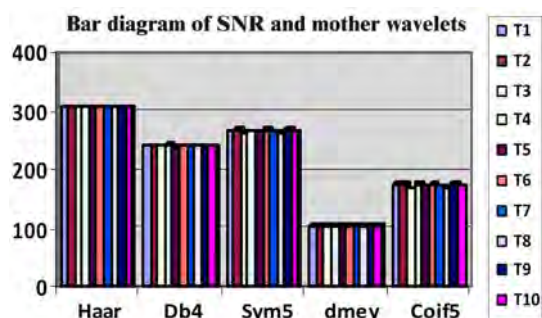


Figure 6. Graphical presentation of SNR for various Mother wavelets.

Table 6. Total time calculation (in seconds) for analysis and synthesis using wavelet filtering for level 3.

Sample	Haar	Db4	Sym5	dmey	Coif5
T1	9.45	9.42	9.76	12.46	9.40
T2	10.35	11.70	10.57	15.64	11.01
T3	10.17	11.53	13.28	14.98	12.07
T4	10.11	11.48	12.21	16.54	12.40
T5	10.00	10.89	10.04	12.89	11.57
T6	11.84	13.73	13.21	18.04	14.68
T7	12.65	12.12	12.76	20.37	13.60
T8	10.53	11.20	10.87	15.43	11.86
T9	9.56	10.00	11.59	14.32	11.96
T10	10.32	10.48	11.96	16.68	13.42

Table 7. SNR calculation of various mother wavelets for level 4 decomposition.

Sample	Haar	Db4	Sym5	dmey	Coif5
T1	304.74	226.62	241.29	115.31	159.79
T2	304.74	226.62	241.29	115.29	159.79
T3	304.74	226.62	241.29	115.33	159.79
T4	304.73	226.62	241.29	115.37	159.79
T5	304.73	226.62	241.29	115.32	159.79
T6	304.73	226.62	241.29	115.37	159.79
T7	304.74	226.62	241.29	115.27	159.80
T8	304.75	226.62	241.29	115.36	159.79
T9	304.74	226.62	241.29	115.21	159.80
T10	304.74	226.62	241.29	115.30	159.80

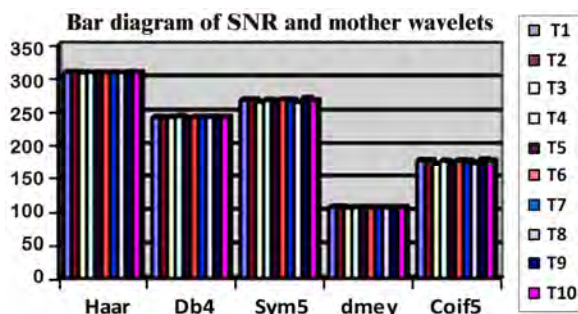


Figure 7. Graphical presentation of SNR for various Mother wavelets.

Table 8. Total time calculation (in seconds) for analysis and synthesis using wavelet filtering for level 4.

Sample	Haar	Db4	Sym5	dmey	Coif5
T1	9.95	10.90	10.76	14.92	12.26
T2	12.01	12.59	13.48	19.46	14.84
T3	12.12	12.81	14.79	22.09	12.53
T4	11.03	12.79	11.98	20.34	14.73
T5	11.34	12.37	12.54	16.79	13.09
T6	13.25	15.59	16.37	25.25	19.20
T7	14.51	15.40	17.39	25.89	17.98
T8	11.90	13.14	11.96	19.57	13.15
T9	12.09	13.17	12.51	20.01	15.48
T10	13.09	13.28	14.57	21.75	15.35

From Table 9, entropy which is a common measure of the efficiency of a signal transform is calculated using wavelet packet analysis is matched before decomposition and reconstruction.

In Table 10, Band stop filtered signal is tabulated which removes the line frequency noise from the signal, it shows a reasonable SNR of 40–46 dB.

Figure 8 shows the tree diagram associated with a depth-3 WPT. It reflects the structure of its corresponding hierarchical filter bank, such as the structure shown in Figure 2. Moving from top to bottom in the diagram

Table 9. Entropy for 4 levels.

Sample	Haar/Db4/Sym5/dmey/Coif5
T1	21937
T2	32511
T3	29809
T4	34655
T5	29145
T6	49058
T7	51218
T8	32971
T9	34857
T10	37040

Table 10. SNR after removing noise.

Sample	Haar/Db4/Sym5/dmey/Coif5
T1	44.16
T2	44.41
T3	41.29
T4	44.52
T5	44.47
T6	44.85
T7	44.58
T8	40.39
T9	46.36
T10	41.89

of **Figure 8**, frequency is divided into ever smaller segments. Each line that emanates down and to the left of a node represents a lowpass filtering operation ( $h_0$ ), and each line emanating down and to the right a highpass filtering operation ( $h_1$ ). The nodes that have no further nodes emanating down from them are referred to as *terminal nodes*, *leaves*, or *subbands*. We refer to the other nodes as *non-terminal*, or *internal* nodes. As such, the tree node labeling scheme provides a simple mechanism for indicating the nodes in the tree that we can work with when imparting modifications on the signal.

For the node  $(j,k)$ ,  $j$  denotes the depth within the transform (tree) and  $k$  the position. For example, at node  $(0,0)$  no filtering has taken place, and we simply have the original sequence of time samples. Lowpass filtering this will produce node  $(1,0)$  and highpass filtering with produces  $(1,1)$ . These filtering operations are equivalent to finding the correlation of the signal with the scaling function for node  $(1,0)$  and the correlation of the signal with the wavelet function for node  $(1,1)$ . Going down the tree to the next depth, we see that  $(2,0)$  and  $(2,1)$  emanate from  $(1,0)$ . From the filter perspective, the samples at  $(1,0)$  are applied to the filters and. Multiresolution is achieved because the coefficients at  $(1,0)$  have been down sampled by two to achieve *critical sampling*. From the wavelet and scaling function perspective, the correlations between both and the samples of  $(1,0)$  are determined through this operation.

**Figure 9** shows how the block diagram wise analysis and synthesis is carried out.

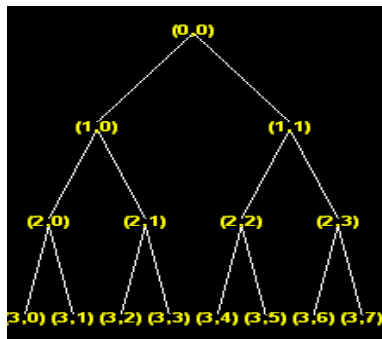
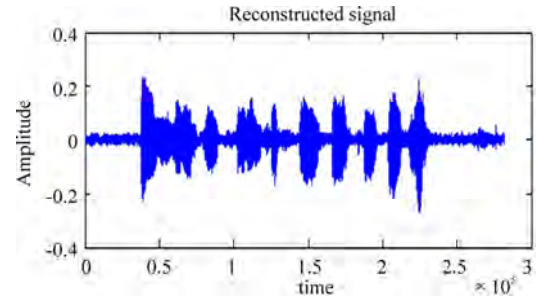
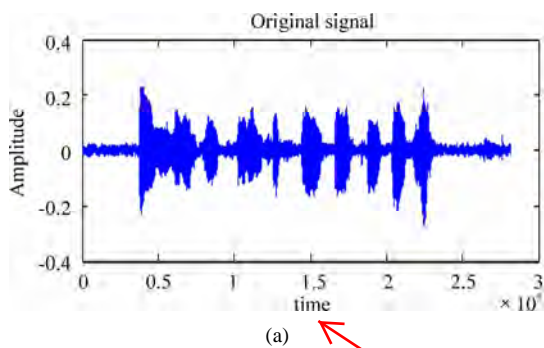
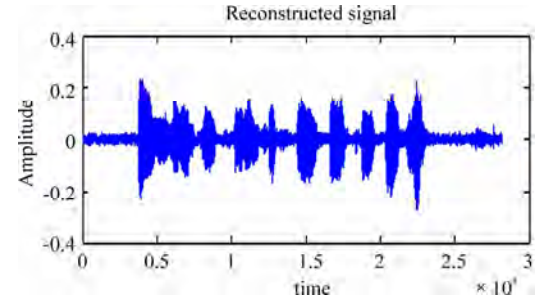


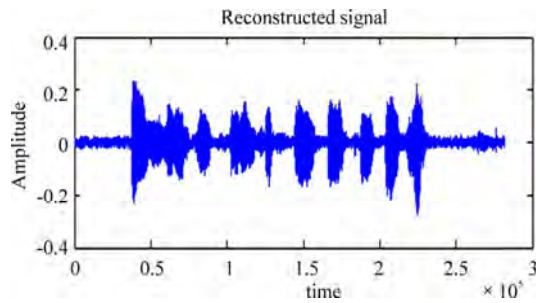
**Figure 8.** Wavelet packet tree for level 3 of decomposition.



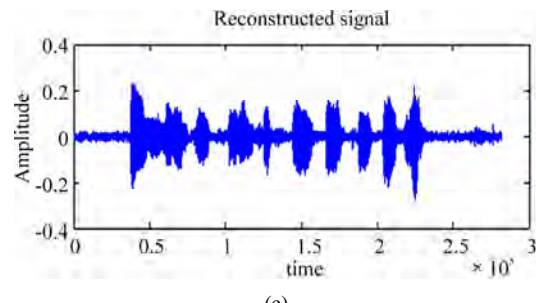
(b)



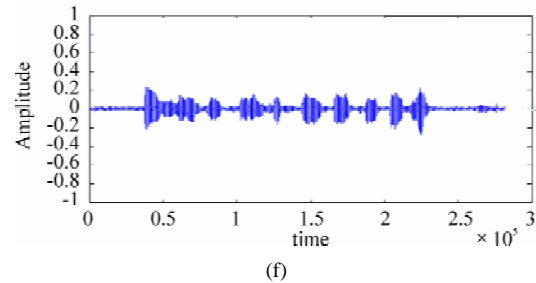
(c)



(d)



(e)



(f)

**Figure 9.** Input sample: (a) t7.wav; (b) For Haar wavelet; (c) For Db4 wavelet; (d) For Sym5 wavelet; (e) For dmey wavelet; (f) line freq filter.

Please add units to Figure 9(a)-(f) -time (sec) or (min) or (hour)?

## 5. Conclusions

We have presented a method for analysis and synthesis of time signals using wavelet packet filtering techniques. From this study we could understand and experience the effectiveness of wavelet packet transform in time signal analysis and synthesis. The performance of wavelet packet is appreciable while comparing with the discrete wavelet transform decomposition technique since wavelet packet analysis can provide a more precise frequency resolution than the wavelet analysis. It also has compact support in time as well as in frequency domain and adapts its support locally to the signal which is important in time varying signal. With wavelet packets we have a greater variety of options for decomposing the signal. The method presented is used for time as well as frequency analysis of time varying signals. From the results we conclude that the wavelet filtering find applications in the time domain analysis and synthesis era. In terms of signal quality, Haar wavelet has been seen to be the best mother wavelet. This is taken from the analysis of the signal to noise ratio (SNR) value around which is quite satisfactory for time varying signals. The system has been tested with various sampling frequencies for time domain samples which gave satisfactory output. Taking into consideration the signal quality and the time for analysis and synthesis it can be concluded that Haar wavelet is the best mother wavelet. Hence we conclude that the system will behave stable with wavelet packet filter and can be used for time signal analysis and synthesis purpose.

## 6. References

- [1] S. Mallat, "A wavelet tour of signal processing," Second Edition, Academic Press, 1998.
- [2] D. Donoho, "De-noising by soft-thresholding," IEEE Transactions on Information Theory, Vol. 41, pp. 613–627, May 1995.
- [3] I. Daubechies, "Ten lectures on wavelets," SIAM, New York, 1992.
- [4] J. W. Seok and K. S. Bae, "Speech enhancement with reduction of noise components in the wavelet domain," IEEE International Conference on Acoustics, Speech and Signal Processing, Vol. 2, pp. 1323–1326, 1997.
- [5] P. V. Tuan and G. Kubin, "DWT-Based classification of acoustic-phonetic classes and phonetic units," International Conference on Spoken Language Processing, 2004.
- [6] E. P. A. Montuori, "Real time performance measures of low delay perceptual audio coding," Journal of Electrical Engineering, Vol. 56, No. 3–4, pp. 100–105, 2005.
- [7] I. Daubechies, "Orthonormal bases of compactly supported wavelets," Communications on Pure and Applied Mathematics, Vol. 41, No. 7, pp. 909–996, November 1998.
- [8] S. Mallat, "A theory for multiresolution signal decomposition: The wavelet representation," IEEE Transactions on Pattern Analysis and Machine Intelligence, Vol. 11, No. 7, pp. 674–693, July 1989.
- [9] A. Grossman and J. Morlet, "Decompositions of Hardy functions into square integrable wavelets of constant shape," SIAM Journals on Mathematical Analysis, Vol. 15, No. 4, pp. 723–736, July 1984.
- [10] R. Coifman and M. Wickerhauser, "Entropy-based algorithms for best basis selection," IEEE Transactions on Information Theory, Vol. 38, No. 2, March 1992.
- [11] R. Learned, "Wavelet packet based transient signal classification," Master's Thesis, Massachusetts Institute of Technology, 1992.
- [12] M. Wickerhauser, "Lectures on wavelet packet algorithms," Technical Report, Department of Mathematics, Washington University, 1992.
- [13] R. Priebe and G. Wilson, "Applications of 'matched' wavelets to identification of metallic transients," Proceedings of the IEEE-SP International Symposium, Victoria, British Columbia, Canada, October 1992.
- [14] E. Serrano and M. Fabio, "The use of the discrete wavelet transform for acoustic emission signal processing," Proceedings of the IEEE-SP International Symposium, Victoria, British Columbia, Canada, October 1992.
- [15] T. Brotherton, T. Pollard, R. Barton, A. Krieger, and L. Marple, "Applications of time frequency and time scale analysis to underwater acoustic transients," Proceedings of the IEEE-SP International Symposium, Victoria, British Columbia, Canada, October 1992.
- [16] K. P. Soman and K. I. Ramachandran, "Insight into wavelets: From theory to practice," 2nd Edition, PHI, 2005.
- [17] P. P. Vaidyanathan, "Multirate systems and filter banks," Prentice Hall, New Jersey, 1992.
- [18] M. V. Wickerhauser, "INRIA lectures on wavelet packet algorithms," Lecture Notes, pp. 31–99, June 1991.
- [19] MATLAB7.0. <http://www.mathworks.com>.

# Indoor Radio Propagation Model Based on Dominant Path

Yongxiang Zhao<sup>1</sup>, Meifang Li<sup>2</sup>, Feng Shi<sup>3</sup>

<sup>1</sup>Wuhan University, State Key Laboratory of Software Engineering, Wuhan, China

<sup>2</sup>Wuhan University of Technology, School of Management, Wuhan, China

<sup>3</sup>Wuhan Academy of Social Sciences, Wuhan, China

Email: zhaosanhe@263.net, poplimeif@126.com, sf196293@163.com

Received November 18, 2009; revised December 22, 2009; accepted January 12, 2010

## Abstract

When there are bigger obstacles in the indoor environment such as elevator, the radio waves basically can not penetrate it. The contribution of received signal strength by transmission and reflection will be greatly reduced, and most of the time, the radio waves will reach the user by bypass diffraction. Therefore, the traditional path loss model is no longer applicable, and the improved model should be proposed. In this paper, we firstly proposed an indoor radio propagation model based on dominant path in which the received signal strength has nothing to do with the direct distance between user and access point, but is related to the length of dominant path. Then on the basis of dominant path model, the NLOS influence is considered in order to further improve the accuracy of dominant path model. Experimental results demonstrated that the proposed dominant path model can improve the accuracy of traditional path loss model remarkably.

**Keywords:** Wireless LANs, Indoor Positioning, Radio Waves, Received Signal Strength, Path Loss Model, Dominant Path

## 1. Introduction

Indoor positioning systems have become very popular in recent years, both the research and commercial products in this area are new, and many people in academia and industry are currently involved in the development of these systems.

It is possible to obtain the position location of a mobile device in two ways: by using a special infrastructure or by improving the existing communications infrastructure. GPS is not suitable for indoor areas because of the lack of coverage. Therefore, it is preferable to employ the existing wireless communications infrastructure to determine the location of users. The wireless communications infrastructure is primarily based on wireless local area networks (WLANs) [1] in indoor areas. Thus, these indoor positioning systems mainly lie on an IEEE 802.11b or 802.11g WLAN.

Owing to the harsh multi-path environment in indoor areas, techniques that use triangulation or direction are not very attractive and often can yield highly erroneous results [2]. Location fingerprinting refers to techniques that match the fingerprint of some characteristic of the signal that is location dependent. In WLANs, an easily available signal characteristic is the received signal

strength (RSS) and this has been used in [3] for fingerprinting.

Due to severe multi-path fading and shadowing present in the indoor environment, there is no accurate indoor radio propagation model. A traditional radio propagation model, named path loss model, is often used to describe the characteristic of indoor environment.

However, when there are bigger obstacles in the indoor environment such as elevator, the radio waves basically can not penetrate it. The contribution of received signal strength by transmission and reflection will be greatly reduced, and most of the time, the radio waves will reach the user by bypass diffraction. Therefore, the traditional path loss model is no longer applicable, and the improved model should be proposed.

This paper is organized as follows. In Section 2, we proposed three indoor radio propagation models, named Path Loss Model, Dominant Path Model 1 and Dominant Path Model 2. Section 3 described experimental testbed which is a typical office building environment. In Section 4, the experimental results of three models were discussed and analyzed. Section 5 depicted field strength simulation results of dominant path model 2 for the experimental access points. Finally, Section 6 summarized the paper and gave possible future research directions.

## 2. Three Indoor Radio Propagation Models

### 2.1. Path Loss Model

In this paper, a path loss model [4] is introduced to describe the characteristic of indoor environment which is as follows:

$$P(d) = P(d_0) - 10 \times n \times \log\left(\frac{d}{d_0}\right) + \zeta \quad (1)$$

In the Equation (1), the  $P(d)$  is the received signal strength of users when the distance between users and access points is  $d$ . And  $P(d_0)$  is the received signal strength of users when the distance between users and access points is  $d_0$  ( $d_0$  is equal to 1 meter). The parameter  $n$  is the path-loss index which depends upon the indoor propagation environment.  $\zeta$  is the shadowing factor which is a random variable.

### 2.2. Dominant Path Model 1

When there are bigger obstacles in the indoor environment such as elevator, the radio waves basically can not penetrate it. The contribution of received signal strength by transmission and reflection will be greatly reduced, and most of the time, the radio waves will reach the user by bypass diffraction. Therefore, the traditional path loss model is no longer applicable because the received signal strength  $P(d)$  has nothing to do with the direct distance  $d$  between user and access point, but is related to the length  $L$  of dominant path which is described in **Figure 1**.

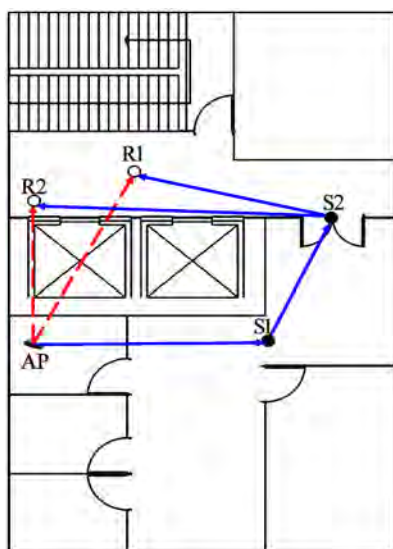


Figure 1. Dominant path model 1 in indoor scenarios.

In **Figure 1**, AP is placed in a small room, sampling points R1 and R2 are close to elevator. The traditional path loss model supposes that the radio waves from AP directly arrive at sampling points R1 and R2 by penetrating the elevator. However, the elevator is bigger obstacle which is made up of metal and concrete materials, and can not be penetrated by radio waves. In fact, the radio waves from AP reach the sampling points R1 and R2 by bypass diffraction, that is, the radio waves firstly reach the point S1, then reach the point S2, and finally arrive at points R1 and R2.

The proposed Dominant Path Model 1 was described as follows:

$$P(L) = P(d_0) - 10n \log\left(\frac{L}{d_0}\right) \quad (2)$$

In the Equation (2), the  $P(L)$  is the received signal strength of users when the length of dominant path is  $L$ . And  $P(d_0)$  is the received signal strength of users when the length of dominant path is  $d_0$  ( $d_0$  is equal to 1 meter). The parameter  $n$  is also the path-loss index which depends upon the indoor propagation environment.

### 2.3. Dominant Path Model 2

However, the received signal strength (RSS) in indoor environment is influenced by Non-line-of-sight (NLOS) propagation, and the attenuation level of signal strength is different when in Line-of-sight (LOS) environment and in Non-line-of-sight (NLOS) environment. Therefore, the LOS propagation and NLOS propagation should be discussed and analyzed separately in order to further improve the accuracy of dominant path model which is depicted in **Figure 2**.

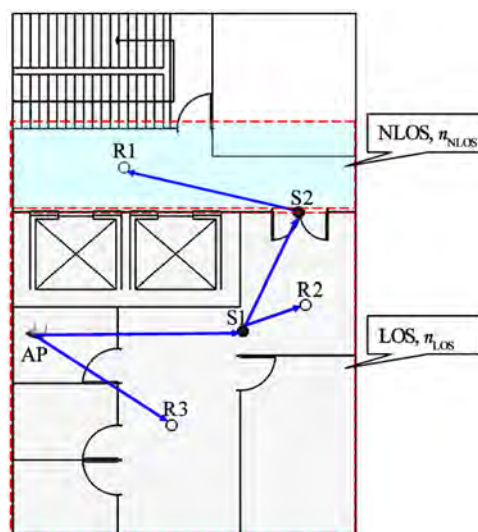


Figure 2. Dominant path model 2 in indoor scenarios.

In **Figure 2**, the whole experimental environment is divided into two separate parts. 1) Room part. It includes three small rooms and three big rooms, so, the Room part is approximate LOS environment in which the path-loss index is  $n_{LOS}$ . 2) Corridor part. All the APs are placed in the Room part, thus, the Corridor part is typical NLOS environment in which the path-loss index is  $n_{NLOS}$  because the radio waves from APs can not penetrate thicker concrete wall.

The proposed Dominant Path Model 2 was described as follows:

$$P(L) = \begin{cases} P(d_0) - 10n_{LOS} \log\left(\frac{L}{d_0}\right) & , \text{Line-of-sight(LOS)} \\ P(d_0) - 10n_{NLOS} \log\left(\frac{L}{d_0}\right) & , \text{Non-Line-of-sight(NLOS)} \end{cases} \quad (3)$$

In the Equation (3), the  $n_{LOS}$  is the path-loss index in LOS environment, and the  $n_{NLOS}$  is the path-loss index in NLOS environment. Other parameters are the same as Dominant Path Model 1.

### 3. Experimental Testbed

The experimental testbed is located in the 11th floor of Cherry Blossom Building. The floor has dimensions of 15 meters by 10 meters and includes 6 rooms which is the typical indoor office environment. In this work, we choose the TP-LINK TL-WA501G as our experimental APs because of its low cost. The WLAN consists of four access points, and the MAC, SSID and operating channel of these access points are listed in **Table 1**.

The survey trail and AP placement of experimental testbed is shown in **Figure 3**. From **Figure 3**, we can see that our experimental testbed is the typical indoor office environment. The AP placement of experimental testbed refers to the conclusion of literature [5], that is, the access points should be scattered asymmetrically and should be placed around the site in a “zigzag” pattern rather than placing several APs close together or placing them on a straight line.

**Table 1.** MAC, SSID and channel of experimental access points.

MAC	SSID	Channel
00:1D:0F:43:CA:7F	AP1	9
00:1D:0F:43:CA:86	AP2	13
00:1D:0F:43:CB:A1	AP3	3
00:1D:0F:43:CB:A8	AP4	1

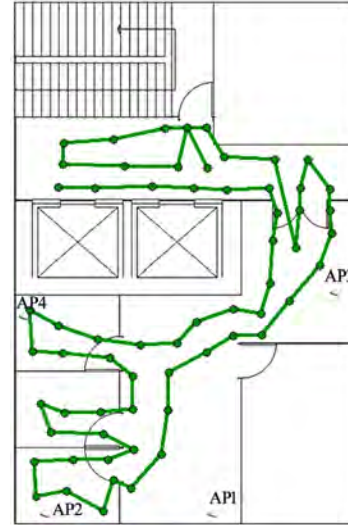


**Figure 3.** The survey trail and AP placement of experimental testbed.

The minimum distance between two locations or grid spacing was fixed at 1.5 meters. At each location, we calculated the average of 50 samples, and it would spend 25 seconds for each location when scanning frequency was set to two times per second.

### 4. Experimental Results and Analysis

In our experiments,  $d_0$  is equal to 1 meter, and  $P(d_0)$  is set to  $-28.0$  dB. The RSS estimation results and RSS estimation error comparison for Path Loss Model, Dominant Path Model 1 and Dominant Path Model 2 are listed as follows.

#### 4.1. The RSS Estimation Results of Three Propagation Models

##### 1) The RSS Estimation Results of Path Loss Model

The RSS Estimation Results of Path Loss Model are shown in **Figure 4**, and the path-loss index of Path Loss Model for four APs is listed in **Table 2**.

From the experimental results of **Figure 4** and **Table 2**,

**Table 2.** The path-loss index of path loss model.

AP Name	Path-loss Index $n$
AP1	3.45
AP2	3.73
AP3	3.20
AP4	4.20

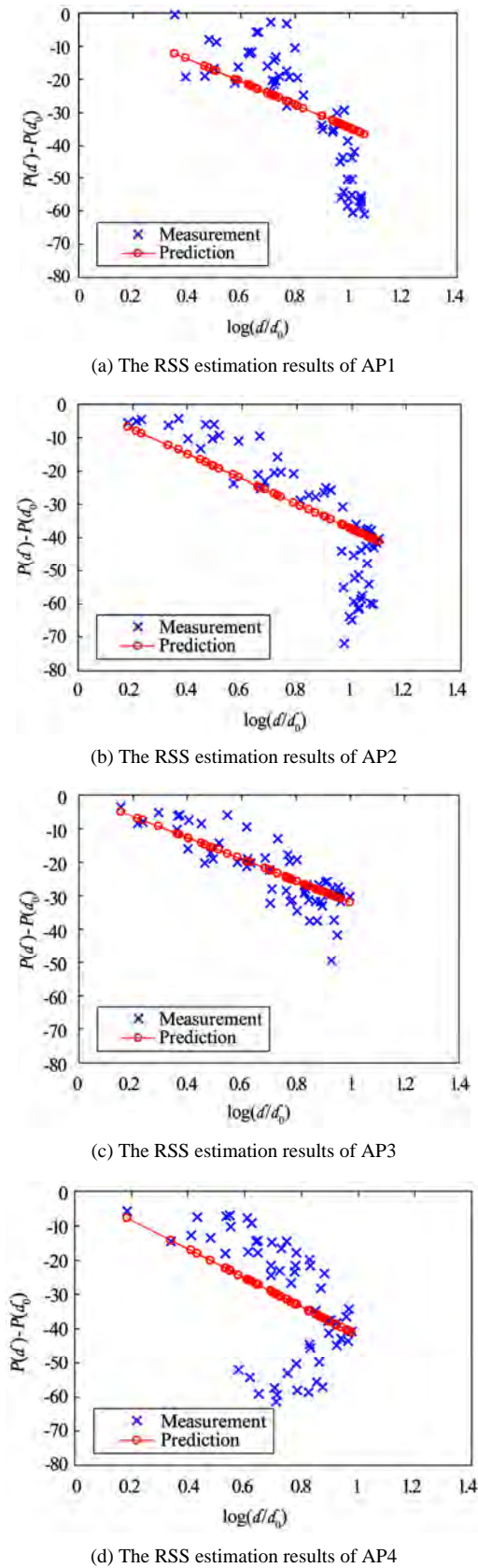


Figure 4. The RSS estimation results of path loss model.

we can see that the RSS estimation result of AP3 is better, and its path-loss index is 3.20. However, the RSS estimation results of AP1, AP2 and AP4 are worse, and the path-loss index are 3.45, 3.73 and 4.20.

The reason is that, the AP3 is placed at the entrance of Room part, thus, the propagation environment of radio waves in Corridor part is close to the propagation environment in Room part which is approximate LOS environment. But the AP1, AP2 and AP4 are placed in the inside room which are farther away from the corridor and elevator, thus, the attenuation level of signal strength in Corridor part is more serious than in Room part.

The most serious situation is that, from **Figure 4(b)** and **Figure 4(d)**, we can see that the radio waves propagation does not match with the Path Loss Model at all in Corridor part because the received signal strength is weaker and weaker when the direct distance between user and AP is closer and closer. Therefore, the traditional path loss model is no longer applicable because the received signal strength has nothing to do with the direct distance between user and access point, but is related to the length of dominant path.

2) The RSS Estimation Results of Dominant Path Model 1

The RSS Estimation Results of Dominant Path Model 1 are shown in **Figure 5**, and the path-loss index of Dominant Path Model 1 for four APs is listed in **Table 3**.

From the experimental results of **Figure 5** and **Table 3**, we can see that the RSS estimation results of AP1, AP2, AP3 and AP4 are all better, and the path-loss index are 3.26, 3.48, 3.10 and 3.43.

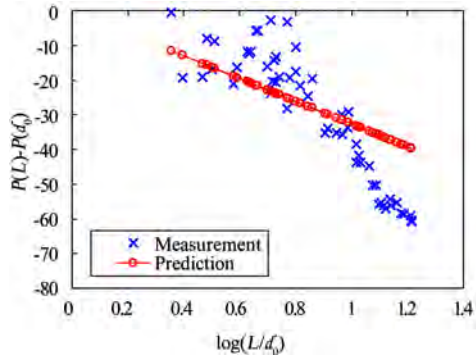
Compared with the result of Path Loss Model, the Dominant Path Model 1 achieves remarkable improvement because the path-loss index of four APs are all decreased, for example, the path-loss index of AP1 decreases to 3.26 from 3.45, the path-loss index of AP2 decreases to 3.48 from 3.73, the path-loss index of AP3 decreases to 3.10 from 3.20, and the path-loss index of AP4 decreases to 3.43 from 4.20. Therefore, the Dominant Path Model 1 is more rational and accurate than the traditional Path Loss Model.

3) The RSS Estimation Results of Dominant Path Model 2

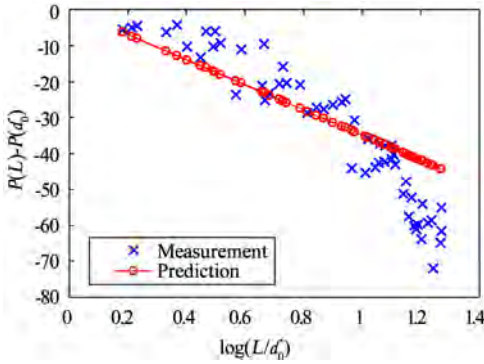
The RSS Estimation Results of Dominant Path Model 2 are shown in **Figure 6**, and the path-loss index of Dominant Path Model 2 for four APs is listed in **Table 4**.

Table 3. The path-loss index of dominant path model 1.

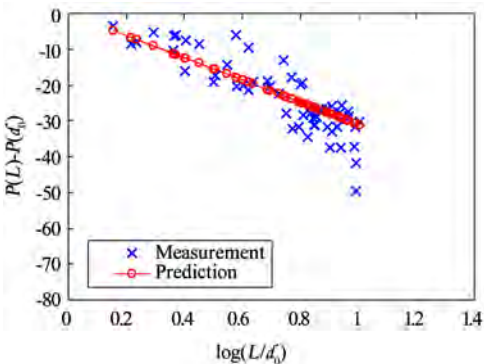
AP Name	Path-loss Index $n$
AP1	3.26
AP2	3.48
AP3	3.10
AP4	3.43



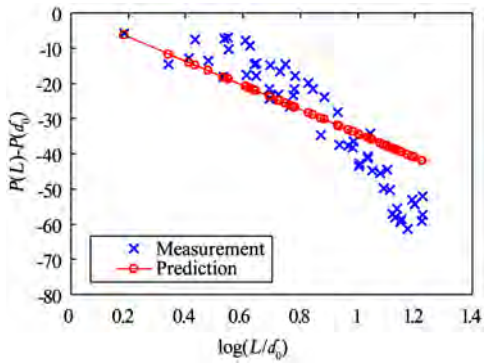
(a) The RSS estimation results of AP1



(b) The RSS estimation results of AP2

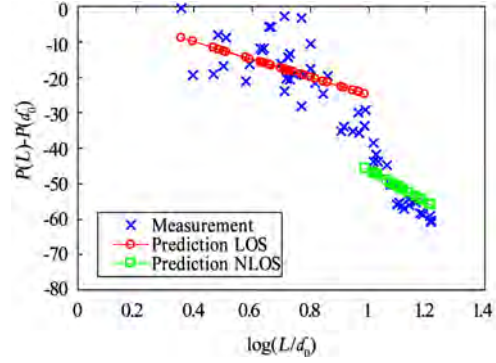


(c) The RSS estimation results of AP3

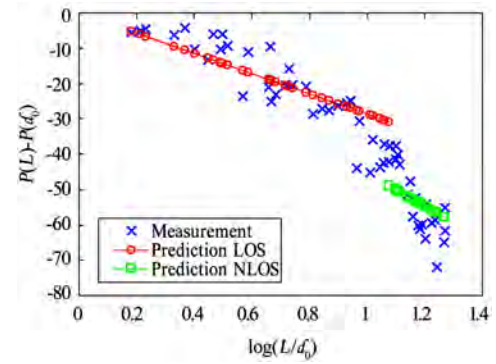


(d) The RSS estimation results of AP4

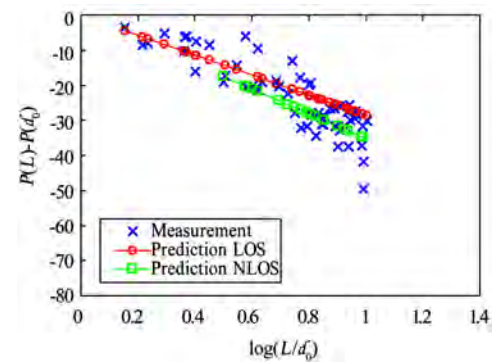
Figure 5. The RSS estimation results of dominant path model 1.



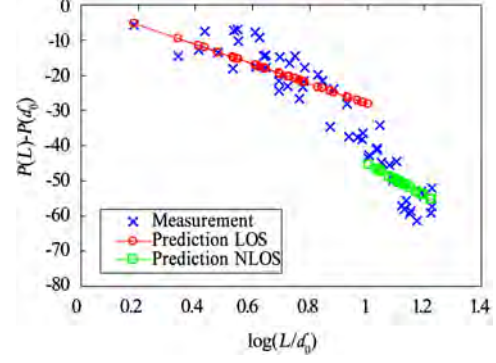
(a) The RSS estimation results of AP1



(b) The RSS estimation results of AP2



(c) The RSS estimation results of AP3



(d) The RSS estimation results of AP4

Figure 6. The RSS estimation results of dominant path model 2.

**Table 4. The path-loss index of dominant path model 2.**

AP Name	Path-loss Index $n_{LOS}$	Path-loss Index $n_{NLOS}$
AP1	2.49	4.62
AP2	2.87	4.56
AP3	2.86	3.52
AP4	2.81	4.52

From the experimental results of **Figure 6** and **Table 4**, we can see that the RSS estimation results of AP1, AP2, AP3 and AP4 achieve further improvement after the LOS propagation and NLOS propagation are analyzed separately.

The path-loss index  $n_{LOS}$  of four APs are 2.49, 2.87, 2.86 and 2.81 which are all less than 3, and the path-loss index  $n_{NLOS}$  of four APs are 4.62, 4.56, 3.52 and 4.52. Therefore, the Dominant Path Model 2 is more rational and accurate than the Dominant Path Model 1.

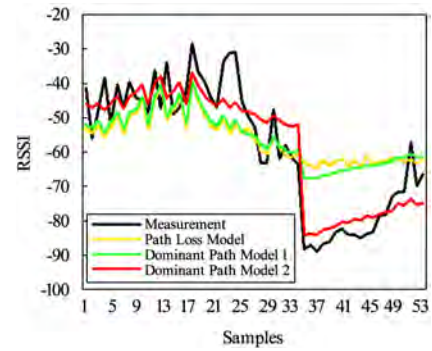
#### 4.2. The RSS Estimation Error Comparison of Three Propagation Model

The RSS estimation error comparison of three propagation model, named Path Loss Model, Dominant Path Model 1 and Dominant Path Model 2, are shown in **Figure 7**, and the RSS estimation error values of three propagation model are listed in **Table 5**.

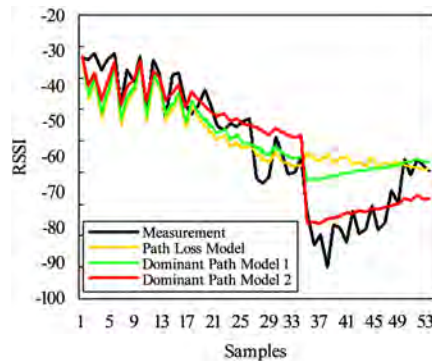
Experimental results of **Figure 7** and **Table 5** demonstrated that the accuracy of Path Loss Mode is worst, and its average mean value for four APs is 9.32, its average

**Table 5. The RSS estimation error values of three propagation model.**

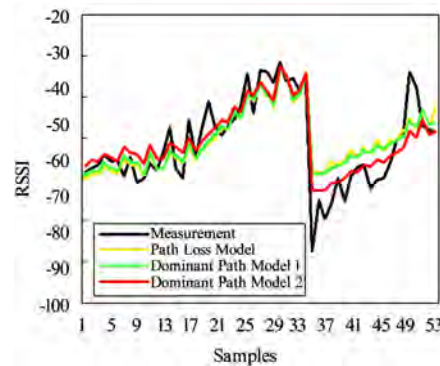
AP Name	Path Loss Model (dB)		Dominant Path Model 1 (dB)		Dominant Path Model 2 (dB)	
	Mean Value	Std. Dev.	Mean value	Std. Dev.	Mean value	Std. Dev.
AP1	11.06	7.78	10.25	6.76	5.64	4.03
AP2	9.57	8.15	8.12	6.68	5.61	4.33
AP3	4.46	3.79	4.19	3.62	3.51	3.22
AP4	12.20	8.77	8.25	5.55	4.76	3.58
Average	9.32	7.12	7.70	5.65	4.88	3.79



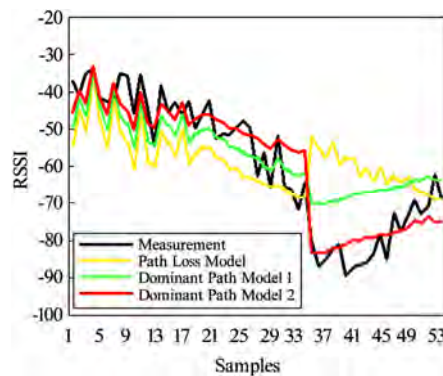
(a) The RSS error comparison of AP1



(b) The RSS error comparison of AP2



(c) The RSS error comparison of AP3



(d) The RSS error comparison of AP4

**Figure 7. The RSS estimation error comparison of three propagation model.**

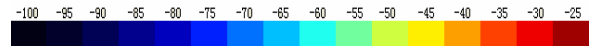
standard deviation is 7.12. The accuracy of Dominant Path Model 1 is better, and its average mean value for four APs is 7.70, its average standard deviation is 5.65. Finally, the accuracy of Dominant Path Model 2 is best, and its average mean value for four APs is only 4.88, its average standard deviation is only 3.79.

Therefore, the proposed dominant path model in this paper can improve the accuracy of traditional path loss model remarkably. When the NLOS influence is further considered, the dominant path model is more rational and accurate, and its average estimation error of received signal strength is only 4.88 dB in the typical indoor office environment.

### 5. The Field Strength Simulation of Dominant Path Model

Finally, we depicted the whole field strength simulation

results of dominant path model 2 for the experimental access points which is shown in **Figure 8**. In this paper, the color indication of received signal strength is as follows:



The field strength simulation of **Figure 8** demonstrated that when there are bigger obstacles in the indoor environment such as elevator, the radio waves basically can not penetrate it. The contribution of received signal strength by transmission and reflection will be greatly reduced, and most of the time, the radio waves will reach the user by bypass diffraction.

In dominant path model 2, the received signal strength has nothing to do with the direct distance between user and access point, but is related to the length of dominant path. Therefore, the proposed dominant path model in

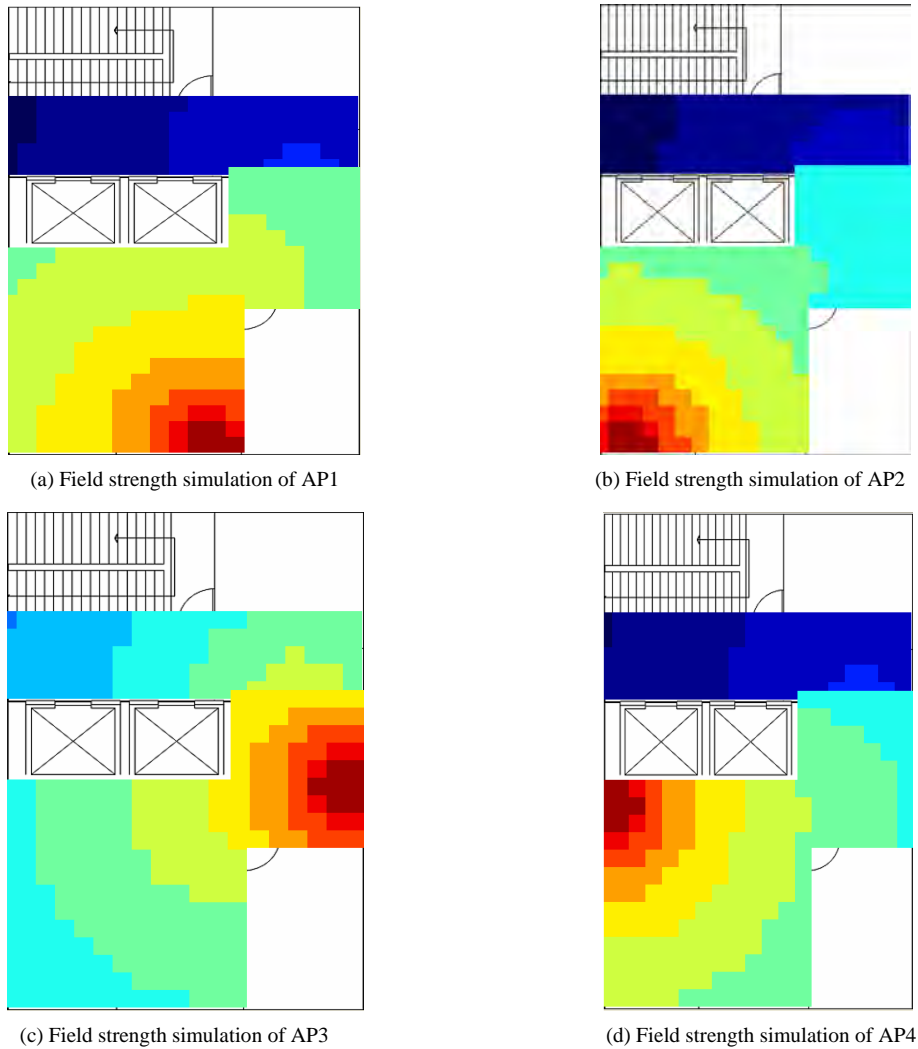


**Figure 8. The field strength simulation of dominant path model 2.**

this paper can improve the accuracy of traditional path loss model remarkably.

## 6. Conclusions and Future Work

In this paper, we firstly proposed an indoor radio propagation model based on dominant path in which the received signal strength has nothing to do with the direct distance between user and access point, but is related to the length of dominant path. Then on the basis of dominant path model, the NLOS influence is considered in order to further improve the accuracy of dominant path model. Experimental results demonstrated that the proposed dominant path model can improve the accuracy of traditional path loss model remarkably.

Future research directions are as follows:

1) Further improve the proposed dominant path model in this paper, for example, the influence factor of wall should be further considered.

2) Study and design intelligent algorithm to automatically search and determine the dominant path of radio propagation in bigger office building environment in order to further improve the applicability and scalability of the proposed dominant path model in this paper.

## 7. Acknowledgment

This work was supported by National 863 project (Grant Nos. 2007AA12Z324, 2009AA12Z324).

## 8. References

- [1] IEEE P802.11 Working Group, "Changes and additions to IEEE 802.11," 1999 Edition, January 2000.
- [2] J. Caffery Jr. and G. Stuber, "Overview of radiolocation in CDMA cellular systems," *IEEE Communications Magazine*, April 1998.
- [3] M. A. Youssef, A. Agrawala, A. U. Shankar, and S. H. Noh, "A probabilistic clustering-based indoor location determination system," Technical Report CS-TR-4350 and UMIACS-TR-20002-30, University of Maryland, 2002.
- [4] T. S. Rappaport, "Wireless communications principles and practices [M]," Second Edition, Publishing House of Electronics Industry, 2004.
- [5] Y. X. Zhao, H. B. Zhou, M. F. Li, "Indoor access points location optimization using differential evolution," In *International Conference on Computer Science and Software Engineering, CSSE '08*, IEEE Computer Society, pp. 382–385, 2008.



## International Journal of **Communications, Network and System Sciences (IJCNS)**

ISSN 1913-3715 (Print)    ISSN 1913-3723 (Online)

<http://www.scirp.org/journal/ijcns/>

IJCNS is an international refereed journal dedicated to the latest advancement of communications and network technologies. The goal of this journal is to keep a record of the state-of-the-art research and promote the research work in these fast moving areas.

### Editors-in-Chief

Prof. Huaibei Zhou  
Prof. Tom Hou

Advanced Research Center for Sci. & Tech., Wuhan University, China  
Department of Electrical and Computer Engineering, Virginia Tech., USA

### Subject Coverage

This journal invites original research and review papers that address the following issues in wireless communications and networks. Topics of interest include, but are not limited to:

MIMO and OFDM technologies

Sensor networks

UWB technologies

Ad Hoc and mesh networks

Wave propagation and antenna design

Network protocol, QoS and congestion control

Signal processing and channel modeling

Efficient MAC and resource management protocols

Coding, detection and modulation

Simulation and optimization tools

3G and 4G technologies

Network security

We are also interested in:

- Short reports—Discussion corner of the journal :  
2-5 page papers where an author can either present an idea with theoretical background but has not yet completed the research needed for a complete paper or preliminary data.
- Book reviews—Comments and critiques.

### Notes for Intending Authors

Submitted papers should not have been previously published nor be currently under consideration for publication elsewhere. Paper submission will be handled electronically through the website. All papers are refereed through a peer review process. For more details about the submissions, please access the website.

### Website and E-Mail

<http://www.scirp.org/journal/ijcns>

[ijcns@scirp.org](mailto:ijcns@scirp.org)

## TABLE OF CONTENTS

**Volume 3 Number 3**

**March 2010**

<b>Advances in MIMO Techniques for Mobile Communications—A Survey</b> F. Khalid, J. Speidel.....	213
<b>Complex Domain Wavelet-Based Denoising of Measured UHF Wireless Channel Power Delay Profiles</b> M. H. C. Dias, G. L. Siqueira.....	253
<b>On Cross-Layer Design of AMC Based on Rate Compatible Punctured Turbo Codes</b> F. Foukalas, E. Zervas.....	256
<b>Performance of Block Diagonalization Broadcasting Scheme for Multiuser MIMO System Operating in Presence of Spatial Correlation and Mutual Coupling</b> F. Wang, M. E. Bialkowski, X. Liu.....	266
<b>Short-Term Load Forecasting Using Soft Computing Techniques</b> D. K. Chaturvedi, S. A. Premdayal, A. Chandio.....	273
<b>Spectrum Efficiency Improvement Based on the Cognitive Radio Management</b> J. Raiyn.....	280
<b>A Mobile Ad-Hoc Routing Algorithm with Comparative Study of Earlier Proposed Algorithms</b> P. K. Verma, T. Gupta, N. Rakesh, N. Nitin.....	289
<b>A New Global Asymptotic Stability Result of Delayed Neural Networks via Nonsmooth Analysis</b> Y. N. Gu, D. Y. Liu, W. J. Wu, J. W. Zhang.....	294
<b>Self-Organized Detection of Relationships in a Network</b> Q. A. Memon.....	303
<b>Scheduling Mobile Data Services in a Bluetooth Based Platform</b> X. Y. Liu, K. C. Yow.....	311
<b>Time Domain Signal Analysis Using Wavelet Packet Decomposition Approach</b> M. Y. Gokhale, D. K. Khanduja.....	321
<b>Indoor Radio Propagation Model Based on Dominant Path</b> Y. X. Zhao, M. F. Li, F. Shi.....	330

